Final Report

Marine Species Density Models for the Mediterranean and Black Seas

Submitted to and prepared for:

Naval Facilities Engineering Systems Command Atlantic, for U.S. Fleet Forces Command, under Contract N62470-20-D-0016 Task Order 21F4096 issued to HDR, Inc.

NAVFAC
Naval Facilities Engineering Systems Command
NAVFAC Atlantic

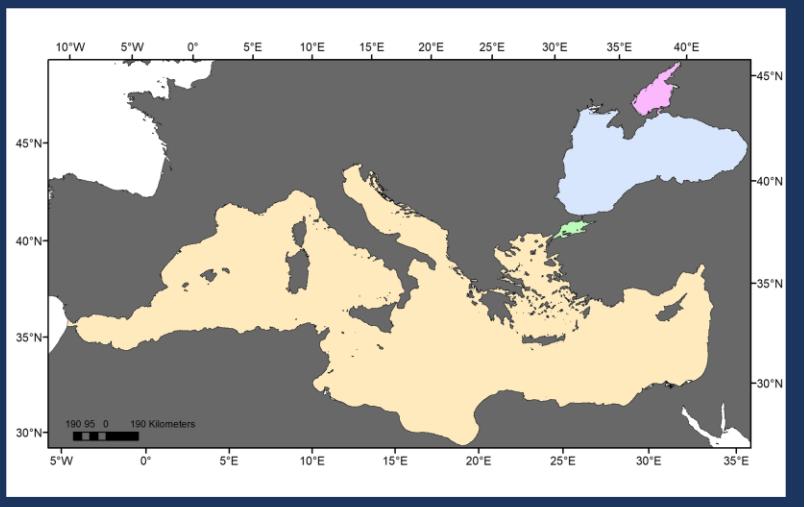

Prepared by:

Marine Geospatial Ecology Lab
Duke University

Ana Cañadas, Jason J. Roberts,
Tina M. Yack, and Patrick N. Halpin
Marine Geospatial Ecology Lab, Duke University

Document version 1.2

Submitted by:

HDR

Virginia Beach, VA

20 December 2024

Suggested Citation:

Cañadas, A., Roberts, J.J., Yack, T., and Halpin, P.N. 2024. *Marine Species Density Models for the Mediterranean and Black Seas.* Final Report. Document version 1.2 Report prepared for Naval Facilities Engineering Systems Command, Atlantic under Contract No. N62470-20-D-0016 Task Order 21F4096 issued to HDR, Inc., by the Duke University Marine Geospatial Ecology Lab, Durham, North Carolina.

Table of Contents

Appendices

Figures

Tables

Acronyms and Abbreviations

â	availability bias
ACCOBAMS	Agreement on the Conservation of Cetaceans of the Black Sea, Mediterranean Sea, and Contiguous Atlantic Area
AFTT	Atlantic Fleet Training and Testing
AIC	Akaike's information criterion
ASI	ACCOBAMS survey initiative
AUC	area under the ROC curve
cdf	cumulative distribution function
CI	Confidence interval
CV	Coefficient of variation
CvM	Cramér–von Mises
edf	empirical distribution function
EMed	eastern Mediterranean Sea
ER	Encounter rate
ESA	Endangered Species Act
esw	Effective strip half-width
GAM	Generalized additive model
g(0)	trackline detection probability
IMMA	Important Marine Mammal Area
IUCN	International Union for the Conservation of Nature
km	kilometer(s)
km²	square kilometer(s)
m	meter(s)
m²	square meter(s)
MCDS	multiple-covariate distance sampling
MGET	Marine Geospatial Ecology Tools
MMPA	Marine Mammal Protection Act
mrds	Mark-Recapture Distance Sampling
NAVEUR	Commander Naval Forces Europe
Navy	U.S. Navy
NMSDD	Navy Marine Species Density Database
p0	perception bias
Q-Q	quantile-quantile
REML	restricted maximum likelihood
ROC	receiver operating characteristic curve
SE	Standard error
SPUE	sightings per unit effort
U.S.	United States
WMed	western Mediterranean Sea

This page intentionally left blank.

1. Introduction

The United States (U.S.) Navy is responsible for compliance with federal laws and regulations that apply to the marine environment and marine species, including but not limited to, the Endangered Species Act (ESA), the Marine Mammal Protection Act (MMPA), the National Environmental Policy Act, and Executive Order 12114. Specifically, and for the purposes of this document, Executive Order 12114 applies to the Global Commons (High Seas), the Foreign Nation Exclusive Economic Zone, and within Foreign Nation Territorial Seas. The ESA and the MMPA also apply to the Global Commons (High Seas). As such, Navy military readiness activities that can occur on the high seas, Foreign Nation Exclusive Economic Zones, and Foreign Nation Territorial Waters throughout the globe necessitate an assessment of risk and potential impact to protected marine mammals and sea turtles.

The Navy Marine Species Density Database (NMSDD) is the authoritative source of marine species density data maintained by the Navy. These data comprise multiple sources and quality levels and are used as inputs to the Navy Acoustic Effects Model to determine the number of potential incidental “takes” of protected species.

To evaluate potential environmental impacts to marine species in regions, the Navy applies a ranking scheme to guide selection of the best density data from those available (**Figure 1**). Where no density estimates exist, the Navy uses global extrapolations (Department of Navy 2012) derived from relative environmental suitability models (Kaschner et al. 2006). The relative environmental suitability models currently supporting risk assessments in the northeast Atlantic are coarsely scaled and data deficient, and are becoming increasingly outdated. There is a need to begin development of spatially explicit density models of marine mammals in the region to support continued risk assessments on a per-exercise basis and for potential future environmental compliance efforts in the region.

In 2018, preliminary habitat-based density estimates of cetaceans in the Mediterranean Sea were developed (Mannocci et al. 2018). Density estimates of cetaceans were produced for the entire Mediterranean Sea, along with maps of uncertainty and of the extent of interpolation versus extrapolation. Roberts et al. (2016, western North Atlantic), Mannocci et al. (2018a, Mediterranean) and Cañadas et al. (2018, Mediterranean; 2021, northeast Atlantic) showed how broad inference can be made over large spatial and temporal scales when disparate datasets are fused together using a “density surface modeling” approach. In the Mediterranean and Black Sea there was a unique opportunity to extend this work, thereby affording a broader understanding of the distributions, and drivers of distributions, for marine mammals across the two basins. By fusing datasets collected across this geographic space, and therefore borrowing strength from each individual dataset, we can have a better and more accurate understanding of where marine mammals are distributed and therefore most vulnerable to disturbance. The studies mentioned above are good examples of what a broad large-scale collaboration among many parties can achieve in this sense.

Given that the Mediterranean and the Black Sea are two distinct basins, and the marine mammals populations inhabiting them in principle do not mix (Natoli et al. 2005, 2008), and as such, they were modeled separately.

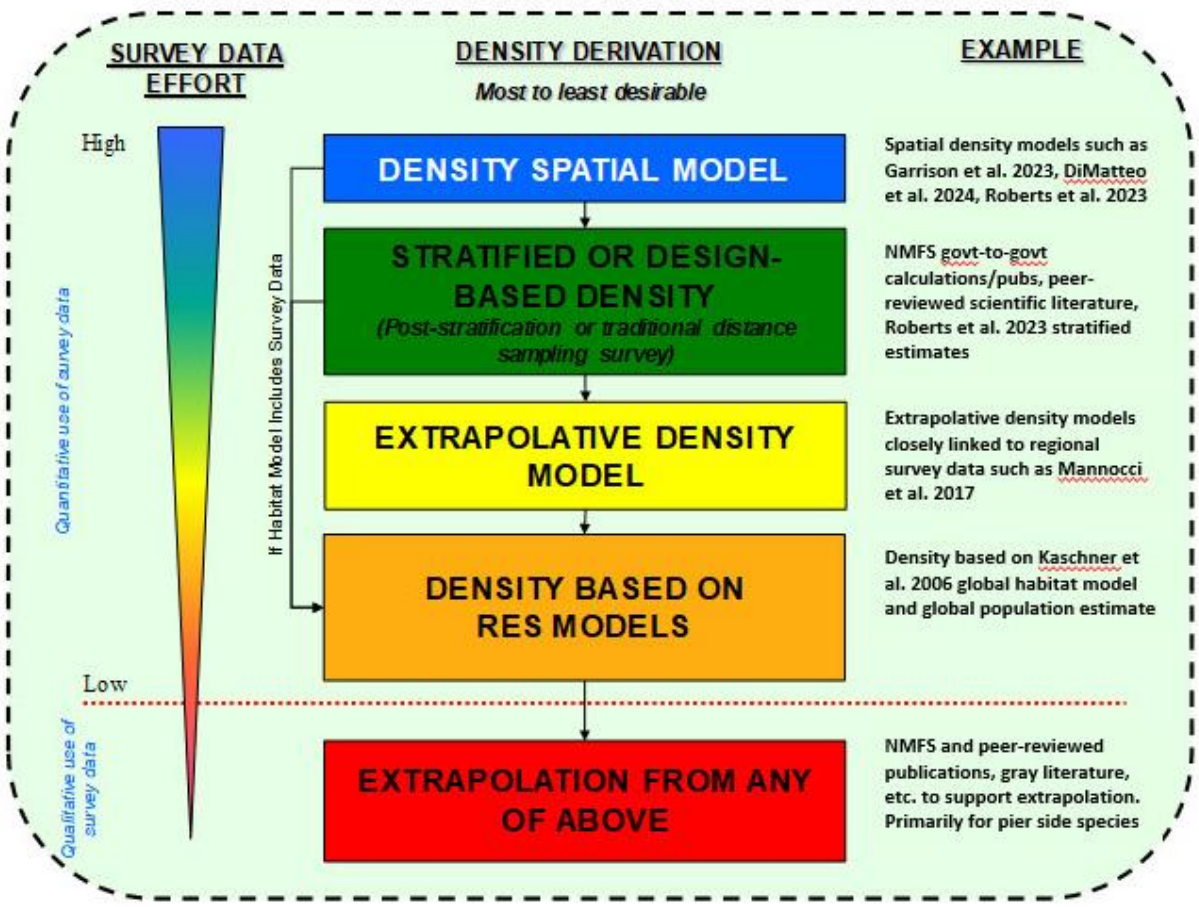

Figure 1. Phase IV NMSDD hierarchy for data inclusion.

2. Materials and Methods

2.1. Study Area 1: the Black Sea

The Black Sea is a semi-enclosed sea, connected to the Mediterranean Sea only via the narrow Istanbul Strait, and the world´s largest meromictic water body with an oxygen-depleted deep layer, known as a unicum *hidrobiologicum* due to its unique physio-chemical properties (Vespremeanu 2007; Bologa 2015) and highly vulnerable marine ecosystem (Zaitsev and Mamaev 1997; Daskalov 2003). The maximum depth is around 2,200 meters (m) and it is characterized by a low salinity (much lower than the Mediterranean) (Shapiro 2009); the surface circulation is dominated by a large cyclonic gyre (**Figure 2**), influenced by wind and freshwater inflows (Özsoy and Ünlüata 1997). In the north, the Crimean Peninsula separates the Black Sea from the shallow Sea of Azov, which is connected through the narrow Kerch Strait.

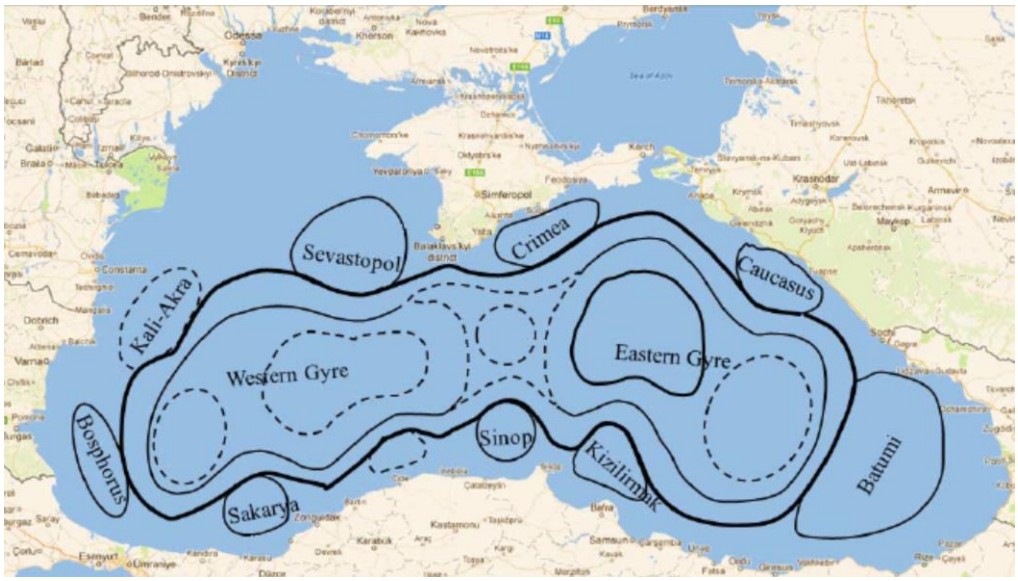

Figure 2. Black Sea circulation (Toderascu and Rusu 2013).

For modeling purposes, the Black Sea region was divided into three sub-basins (**Figure 3**): the Black Sea proper, the Azov Sea including the narrow Kerch Strait that separates it from the Black Sea proper, and the Marmara Sea, separated from the Black Sea proper through the Bosphorus Strait and from the Mediterranean through the Dardanelles.

Figure 3. Black Sea sub-basins: Azov Sea, Black Sea proper, and Marmara Sea.

2.2. Study Area 2: the Mediterranean Sea

The Mediterranean Sea (**Figure 4**) is a semi-enclosed water body connected to the Atlantic Ocean by the Strait of Gibraltar, to the Black Sea by the Bosphorus Strait, and since 1869 to the Red Sea by the Suez Canal. It is divided into a western and an eastern basin by a central ridge between Sicily and the Tunisian-Libyan Coast. The Mediterranean Sea is mainly characterized by narrow continental shelves, steep slopes, and extensive abyssal plains. It includes a variety of submarine canyons, mostly located along the continental slopes in the north. It also includes approximately one hundred seamounts, known to affect the distribution of pelagic species, including cetaceans (Mussi et al. 2014; Tepsich et al. 2014; Fiori et al. 2014). The Mediterranean is an oligotrophic sea characterized by salty and nutrient-poor waters (Longhurst 2007).

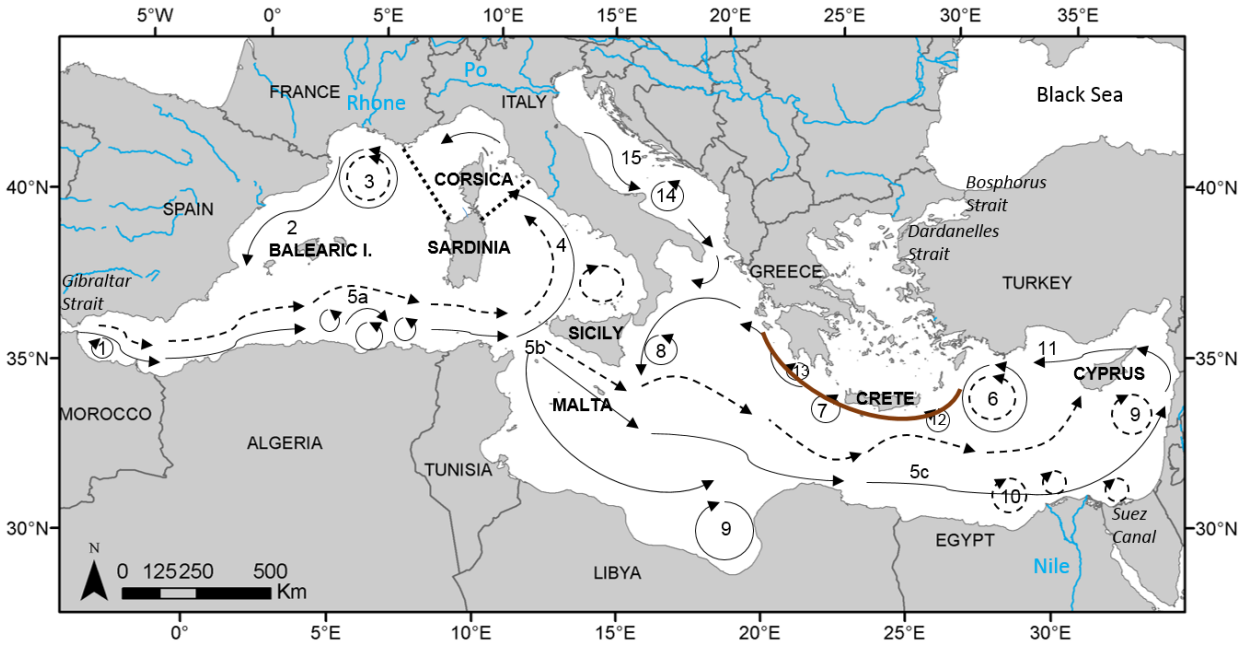

Figure 4. Map of main surface currents and gyres in the Mediterranean Sea.

Dashed arrows represent summer circulation; plain arrows represent winter circulation. (1: western Alboran gyre ; 2: Ligurian-Provençal current; 3: Lions Gyre; 4: Tyrrhenian cyclonic circulation with summer weakening and eastern anticyclone; 5a: Algerian current and eddies, 5b: Atlantic Ionian stream and 5c: mid-Mediterranean jet; 6: Rhodes gyres; 7: western Cretan gyre; 8: Western Ionian gyre; 9: Gulf of Sirte anticyclone; 10: Shikmona and Mers a-Matruh gyres; 11: Cicilian and Asia Minor current; 12: Iera-Petra gyre; 13: Pelops gyre; 14: Southern Adriatic gyre; 15: western Adriatic coastal current.) This figure was adapted from Pinardi and Masseti (2000). The extent of the Pelagos Sanctuary is represented by black dotted lines. The location of the Hellenic trench is represented by a brown line.

Circulation in the Mediterranean Sea is mainly driven by water flow through the Strait of Gibraltar, freshwater inputs from the main rivers (Nile, and to a lesser extent, Po, Rhone, and Ebro), wind stress, and thermohaline and topographic features (Pinardi and Masetti 2000). Atlantic Surface Water flows into the Mediterranean Sea through the Strait of Gibraltar and circulates in a cyclonic (counterclockwise) direction (**Figure 4**). Water flow along the southern coasts generates short-lived mesoscale anticyclonic eddies (e.g., the eddy field off Algeria). To the north, water flow creates persistent cyclonic gyres (e.g., the Lions gyre) associated with upwelling of nutrient-rich waters that result in enhanced primary productivity (Pinardi and Masetti 2000). As it moves eastward, surface water evaporates and becomes saltier, warmer, and poorer in nutrients, resulting in a gradual decline in phytoplankton biomass and productivity from west to east (Bethoux and Gentili 1999; Bethoux et al. 1999). As it becomes saltier and denser, the Atlantic Surface Water sinks in the Levantine Sea, returning westward as Levantine Intermediate Water before exiting into the Atlantic through the Strait of Gibraltar. During winter, water sinks in the Aegean, Adriatic, and Ligurian Seas and goes to the bottom, creating the Mediterranean Deep Water (Pinardi and Masetti 2000).

Phytoplankton biomass and primary production have marked seasonal cycles in the Mediterranean Sea (Bosc et al. 2004; D'Ortenzio and Ribera d'Alcalà 2009). Phytoplankton blooms are primarily initiated in winter and spring by wind stress, causing mixing and nutrient

upwelling to surface layers. Upwelling of nutrients also occurs at cyclonic eddies. While blooms are markedly seasonal and intense in the northwestern basin (e.g., in the Gulf of Lions), they are often sporadic and subject to significant inter-annual variability in the eastern basin. Stratification occurs in summer, resulting in a lower and more homogeneous phytoplankton biomass across the Mediterranean Sea.

The Mediterranean basin was divided into seven sub-basins for comparison purposes (**Figure 5**).

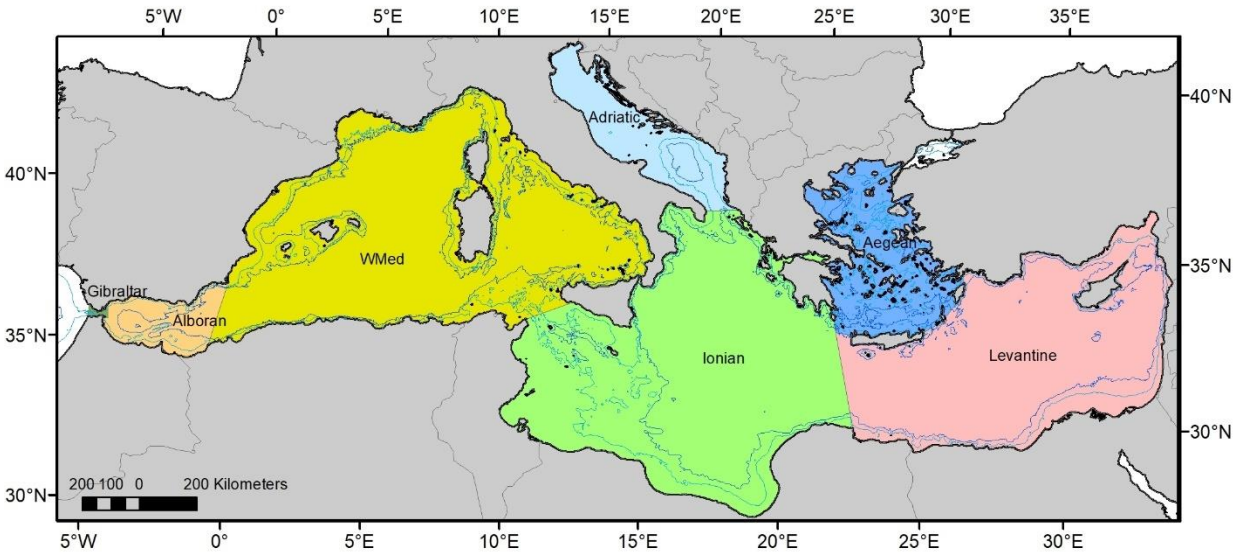

Figure 5. Division of blocks in the Mediterranean Sea: Strait of Gibraltar, Alboran Sea; western Mediterranean (WMed), Adriatic Sea, Ionian Sea, Aegean Sea, and Levantine Sea.

2.2.1. Definition of the Spatial Extent of the Study Area

At the project's inception, the U.S. Navy provided a shapefile that delineated the extent of the Mediterranean Sea and the Black Sea and defined a polygon representing the desired study area for the project.

We manually edited the study area polygon to split off gulfs, estuaries, and other inshore areas where the literature (or our expert judgment, when no literature was available) suggested that marine mammals were absent.

We projected the study area to ETRS_1989_LAEA coordinate system and gridded it into 5 x 5 kilometers (km) square cells. The parameters of this coordinate system are as follows:

ETRS_1989_LAEA
WKID: 3035 Authority: EPSG
Projection: Lambert_Azimuthal_Equal_Area
False_Easting: 4321000.0
False_Northing: 3210000.0

Central_Meridian: 10.0
Latitude_Of_Origin: 52.0
Linear Unit: Meter (1.0)
Geographic Coordinate System: GCS_ETRS_1989
Angular Unit: Degree (0.0174532925199433)
Prime Meridian: Greenwich (0.0)
Datum: D_ETRS_1989

This 5 km spatial resolution represented a compromise between resolutions of available covariate products, which ranged from 30 arc seconds (approximately 500 m) to 0.25° (approximately 25 km).

2.3. Mediterranean and Black Sea Marine Mammal Species

Three species of small odontocetes inhabit the Black Sea and adjoining Marmara and Azov Seas, which include the Black Sea common dolphin (*Delphinus delphis ponticus,* Barabasch 1935), the Black Sea common bottlenose dolphin (*Tursiops truncatus ponticus,* Barabash-Nikiforov 1940), and the Black Sea harbor porpoise (*Phocoena phocoena relicta,* Abel 1905).

It is likely that the Black Sea common dolphin (*Delphinus delphis ponticus*) and the Black Sea bottlenose dolphin (*Tursiops truncatus ponticus*) do not regularly enter the Mediterranean Sea, as the Turkish Straits System forms a strong ecological barrier that precludes gene flow between Black Sea and Mediterranean populations (Natoli et al. 2005, 2008). All these species form Mediterranean subpopulations that are genetically distinct from their North Atlantic relatives. The Mediterranean subpopulations of four species (sperm whale, short-beaked common dolphin, the Black Sea harbor porpoise, and Mediterranean monk seal) are currently listed as endangered by the International Union of Conservation of Nature (IUCN).

Eleven cetacean species and one pinniped species are known to regularly occur in the Mediterranean Sea (Notarbartolo di Sciara 2016). These species are fin whale *Balaenoptera physalus*, sperm whale *Physeter macrocephalus*, Cuvier's beaked whale *Ziphius cavirostris*, common dolphin *Delphinus delphis*, long-finned pilot whale *Globicephala melas*, Risso's dolphin *Grampus griseus*, killer whale *Orcinus orca*, striped dolphin *Stenella coeruleoalba*, rough-toothed dolphin *Steno bredanensis*, common bottlenose dolphin *Tursiops truncatus*, the Black Sea harbor porpoise *Phocoena phocoena relicta*, and the Mediterranean monk seal *Monachus monachus*.

2.4. Survey Data Processing

From now on we only refer to on-effort tracks in adequate conditions (Beaufort sea state <=4 and SubjectiveCode—subjective detectability conditions usually based on sea state, glare, visibility, etc.—not "poor" or "unacceptable"). The study identified 1,643,048 km of tracklines on Beaufort sea state less than or equal to 4 conducted in the Mediterranean and 42,292 km in the Black Sea by many teams under the auspices of 52 surveyor organizations with whom we established collaborations (see **Table 1** for the Black Sea and **Table 2** for the Mediterranean Sea).

Starting from collaborator-specific text files, spreadsheets, and databases, we transformed all survey data into a common format, imported it into Excel spreadsheets, and manually reviewed and cleaned each day of survey effort. While all collaborators utilized generally similar survey protocols, the data collected by, and format used by, each collaborator differed, requiring collaborator-specific treatments in all cases. All collaborators utilized satellite global positioning systems, so we were able to reconstruct survey tracklines, but the degree of precision depended on how frequently data collaborators reported positions. In general, most aerial surveys reported positions several times per minute, with some as frequently as every 4 seconds. Most shipboard surveys reported positions several times per hour, with some as frequently as once per minute. However, there were some studies in the Black Sea that were extracted from published papers (some Russian surveys in the early 2000s in the northern part of the basin), for which we did not have the data. In these few cases, the tracks and the observations were georeferenced in ArcMap and added to the database.

Most collaborators reported the minimum information necessary to estimate density via distance sampling methodology (Buckland et al. 2001), including the time, location, species, and group size of the sighting, as well as the perpendicular distance to the animal(s) from the trackline or the information needed to calculate this distance. Some surveys did not have recorded angles and/or distances, but they were kept in the database and an effective strip half-width (esw) was applied to them according to the covariates, from the most similar platforms (see **Section 2.7**, Detection Modeling). Most collaborators also reported one or more covariates related to the probability of making a sighting, such as an assessment of the sea state, presence of sun glare, water turbidity, and so on. When such covariates were reliably recorded, we retained them and utilized them in detection modeling (described in **Section 2.7**, Detection Modeling).

After all surveys were processed, we aggregated all survey transects where observers were reported to be “on effort” and split them into segments. We sought to obtain segments of 5 km in length, matching the spatial resolution of the analysis. We first split the tracklines wherever the detection covariates changed, and then split each resulting section using the approach of Roberts et al. (2016). That is, for each survey, we first iterated through the sequence of points that defined the transects, finding sections of continuous survey effort, defined as a sequence of effort points for which there were no off-effort gaps of 1 hour or more and no stretch of 7.5 km for which one-third or more was off-effort. We then split each continuous section into equal-length on-effort segments, as follows.

First, we computed the number of segments, n, for the continuous section by dividing its length by 5 km using integer division. Then, if the remainder was less than 2.5 km, we split the continuous section into n equal-length segments slightly longer than 5 km. Otherwise, we increased the number of segments by 1, resulting in n+1 equal-length segments slightly shorter than 5 km. For example, an 11 km continuous section would be split into 2 segments of 5.5 km, while a 13 km continuous section would be split into 3 segments of 4.3 km.

For the period for which data were available (1991–2022), this segmenting procedure was applied to all surveys, resulting in 380,596 segments with a mean length of 4.4 km (SD = 1.8 km, min = 0.05, max = 7.7) for the Mediterranean and 8,644 segments with a mean of 4.9 km

(SD = 0.7 km, min = 0.07, max = 7.7) for the Black Sea. Of these, 33,169 segments were less than 1 km long in the Mediterranean (8.7%), and 75 segments were less than 1 km long in the Black Sea (0.9%).

2.5. Survey Data Summary

2.5.1. Overview of Effort Data

We incorporated line-transect surveys from 52 survey organizations (**Table 1** and **Table 2**). In the Black Sea, 22,758 km of survey effort were collected by shipboard surveys (**Figure 6**) and 19,535 km by aerial surveys (**Figure 7**) between 2001 and 2022 (**Table 1**), and it was concentrated mainly in the western and southern portions of the basin, with very little survey effort in the center. In the Mediterranean, 1,203,685 km of survey effort were collected by shipboard surveys (**Figure 8**) and 439,363 km by aerial surveys (**Figure 9**) between 1991 and 2022 (**Table 2**), and it was concentrated in the northwestern and central Mediterranean, being patchy in the eastern and southern Mediterranean. This totals 1,643,048 km of tracks in the Mediterranean, around 10 times more than in the previous analysis (Mannocci et al. 2018), when there were 166,333 km of tracks available.

Table 1. Area covered, years, and effort covered by the collaborators, in the Black Sea.

Collaborator	Area covered	Platform	Range of years	Effort (km)
ACCOBAMS	Russia, West & South Black Sea	Plane	2018–2019	8,439
Brema	Kerch Strait, Central & NW Black Sea	Ship	2003–2005	1,388
Green Balkans	Bulgaria	Ship	2015–2021	7,063
Ilia State University	Georgia	Ship	2014–2019	2,745
IO-BAS	Bulgaria	Ship	2015–2017	2,119
Istanbul University	Turkey, Marmara Sea	Ship	2005–2019	959
MareNostrum	Romania	Plane, Ship	2013	7,358
Moscow State University	Azov Sea, Georgia, Russia & Ukraine	Plane, Ship	2001–2005	9,118
Sinop University	Sinop peninsula (Turkey)	Ship	2019–2020	745
TCR	Turkey	Ship	2005–2008	521
TUDAV	W Turkey	Ship	2019–2021	1,019
Zonguldak Bülent Ecevit University	Turkey	Ship	2019–2022	820
			TOTAL	**42,292**

Table 2. Area covered, years, and effort covered by the collaborators, in the Mediterranean Sea.

Collaborator	Area covered	Platform	Range of years	Effort (km)
Accademia del Leviatano	Western Med	Ship	2012–2018	73,540
ACCOBAMS	All Mediterranean	Plane	2018–2019	73,151
Acquario di Genova	Gulf of Genova (Italy)	Ship	2001–2021	76,808
Alnilam	Alboran Sea	Ship	2011	472
AlnitakAlnilam	Alboran Sea & SE Spain	Ship	1992–2010	74,980
ANSE	SE Spain	Ship	2003–2009	9,246
Archipelago	Greece	Ship	2017–2021	14,482
Association BREACH	Gulf of Lyon	Ship	2013–2016	3,723
Association Nereide	Strait of Gibraltar	Ship	2018	1,239
BDRI	Sardinia	Ship	2004–2013	12,638
BWI	Adriatic Sea	Plane, Ship	2004–2022	173,771
Capo Carbonara Marine Protected Area	Western Med	Ship	2013–2019	14,552
Caterina Fortuna	Italy	Ship	2004–2007	1,708
CE.TU.S	Tyrrhenian Sea	Ship	2003–2019	24,773
CIMA Research Foundations	Ligurian Sea	Ship	2008–2020	84,339
CIRCE	Strait of Gibraltar	Ship	2001–2014	27,715
CNRS	Western Med	Ship	2006–2007	7,324
EcoOcean	Gulf of Lyon	Ship	1998–2015	33,025
Gaia Research Institute & University of Torino	Eastern Med	Ship	2014–2016	15,772
IAMC	Italy	Ship	2011–2017	1,448
Ibrahem Benamer	Libya, Tunisia	Ship	2014–2016	2,377
ICCAT	All Mediterranean	Plane	2011–2021	163,603
IMMRAC	Israel	Ship	1999–2020	45,312
ISPRA	Italy	Plane	2002–2020	11,350
Istanbul University	Turkey	Ship	2005–2015	1,232
Ketos	Tyrrhenian Sea	Ship	2013–2015	7,405
MCR	All Mediterranean	Ship	1994–2017	32,661
MERIS	Italy	Ship	2016–2018	1,455
MIRACETI	France	Ship	2004–2018	44,173
Morigenos	Slovenia	Ship	2008–2017	21,865
NURC	All Mediterranean	Ship	1999–2011	19,135
Oceanomare	Tyrrhenian Sea	Ship	2001–2020	70,462
Pelagis	Gulf of Lyon	Plane	2011–2012	31,272
Pelagos	Greece	Ship	1999–2021	30,828
Stazione Zoologica di Napoli	Tyrrhenian Sea	Ship	2019–2021	1,952
SUBMON	NE Spain	Ship	2009–2021	5,899
TCR	Turkey	Ship	2005–2008	6,277
Tethys	Central Med, Ionian Sea	Plane, Ship	1991–2021	324,693
Tursiops	Balearic Islands	Ship	2003–2019	30,102
University of Valencia	East Spain	Plane	2000–2021	40,481
Università di Palermo	Tyrrhenian Sea	Ship	2016–2019	16,626
University of Barcelona	Western Med	Ship	2018–2020	7,585
University of Pisa	Tyrrhenian Sea	Ship	2020–2022	1,598
			TOTAL	**1,643,048**

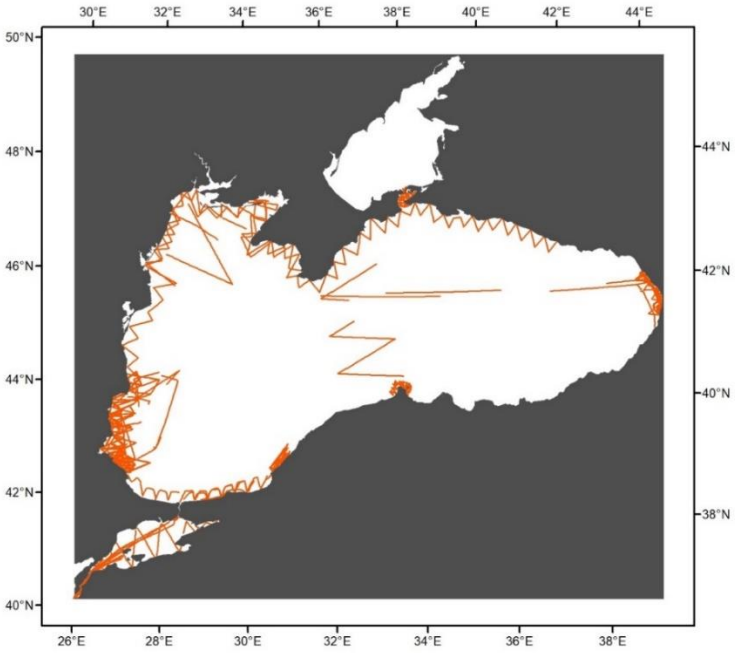

Figure 6. Shipboard survey tracks in the Black Sea.

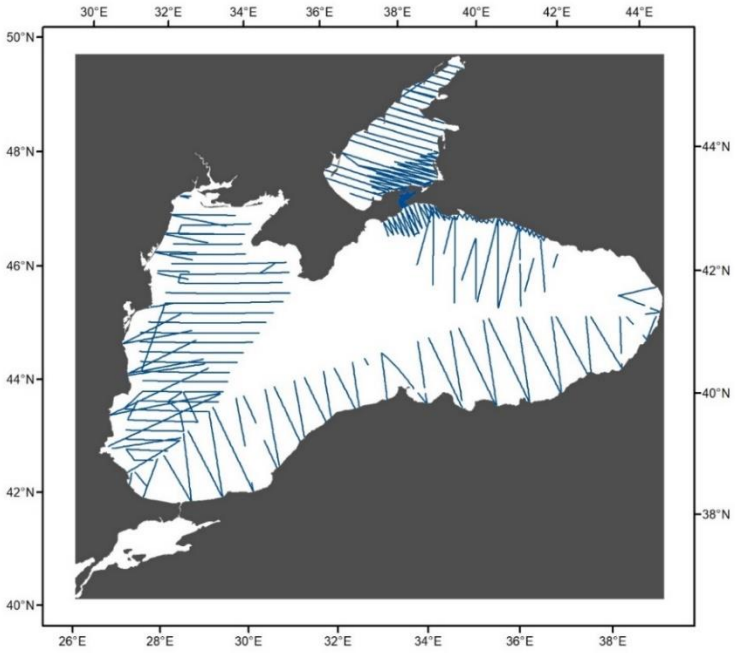

Figure 7. Aerial survey tracks in the Black Sea.

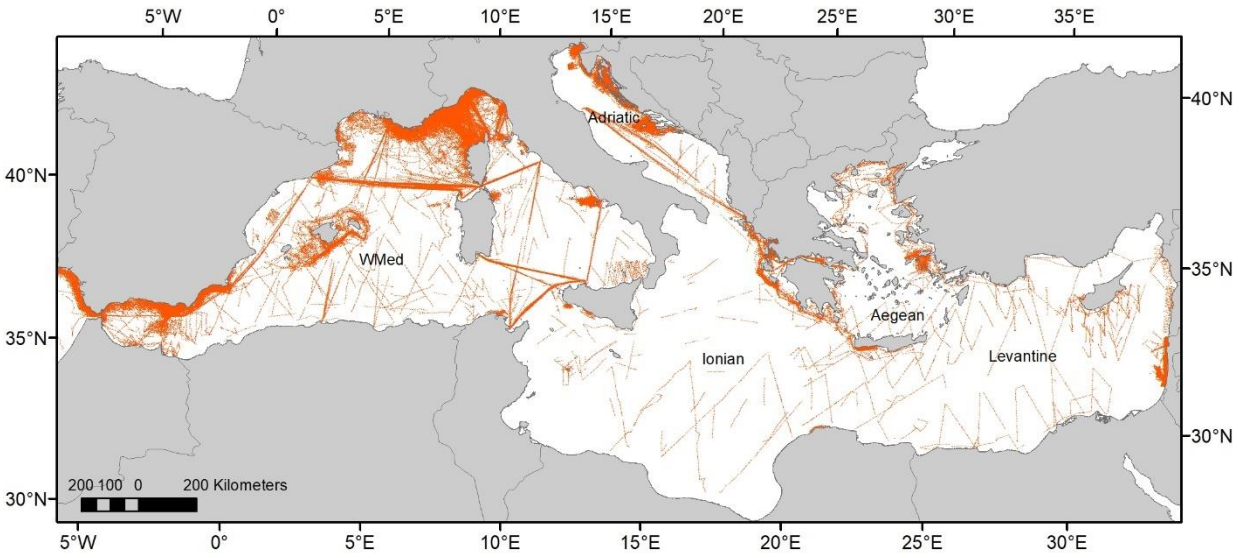

Figure 8. Shipboard survey tracks in the Mediterranean Sea.

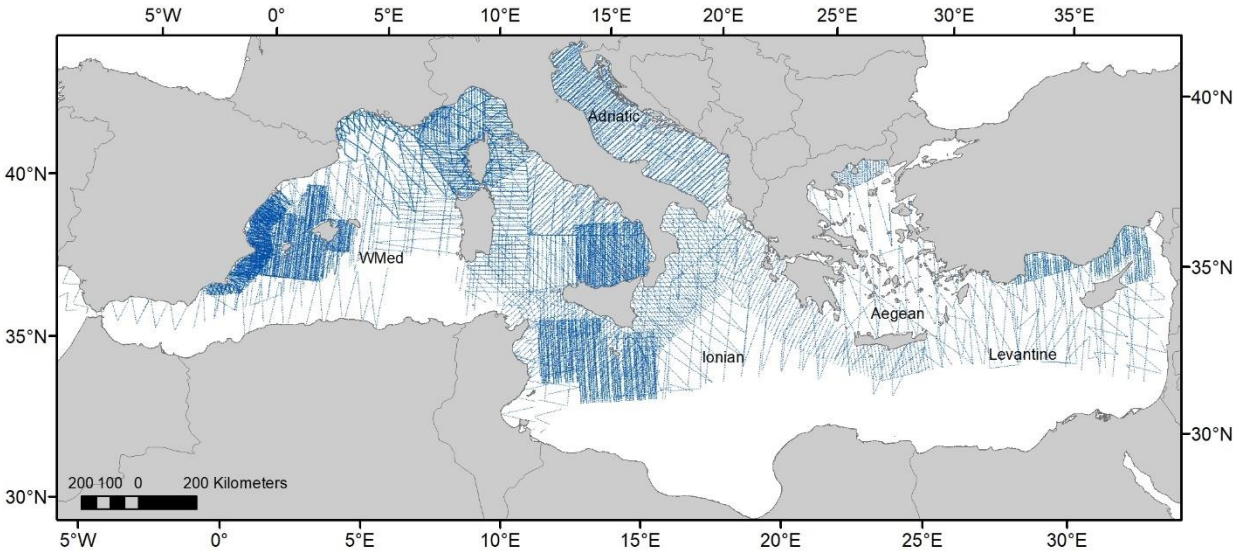

Figure 9. Aerial survey tracks in the Mediterranean Sea.

Figure 10 shows the inter-annual survey coverage in the Black Sea. There is large heterogeneity in the inter-annual survey coverage. The large survey effort in 2019 corresponds to the ACCOBAMS aerial survey.

The Mediterranean survey effort from 1991 to 2022, as shown in **Figure 11**, demonstrates significant inter-annual variability. While there is an overall upward trend in effort until around 2011, it stabilizes thereafter and declines post-2019. Notably, there are two peaks: one in 2013 and another in 2018. The 2018 peak corresponds with the ACCOBAMS aerial survey effort, which aimed to assess cetacean populations and other marine mega-fauna. Interestingly, the

reasons behind the increase in effort in 2013 for both the Mediterranean and the Black Sea remain unclear, suggesting probably coincidental factors.

Given the interest of the Navy that we focus the analysis on the most recent data, and the fact that the majority of the dynamic environmental covariates were available starting in 1999, with some starting in 1985, it was decided that, whenever possible given the available data per species, models would be restricted to the period 1999–2022. However, if the models improved substantially by adding the data from 1991 to 1998 (i.e., modeling the period 1991–2022), then this expansion was considered. For the Black Sea, the full range of years (2001–2022) was used for the analysis. The added effort from 1991 to 1998 occurred primarily in two locations: the northern Alboran Sea and the western Ligurian Sea, with a third smaller location off the coast of Greece.

For practical reasons, the year was divided into two large seasons, summer (May to October) and winter (November to April). The amount of survey effort was much larger in summer in both basins, with large inter-month heterogeneity. **Figure 12** shows the monthly survey coverage in the Black Sea, where the largest effort occurred in July (when the ACCOBAMS survey took place). **Figure 13** shows the monthly survey coverage in the Mediterranean Sea, where the largest effort occurred during the central summer months from June to August, partly attributed to the ACCOBAMS survey too.

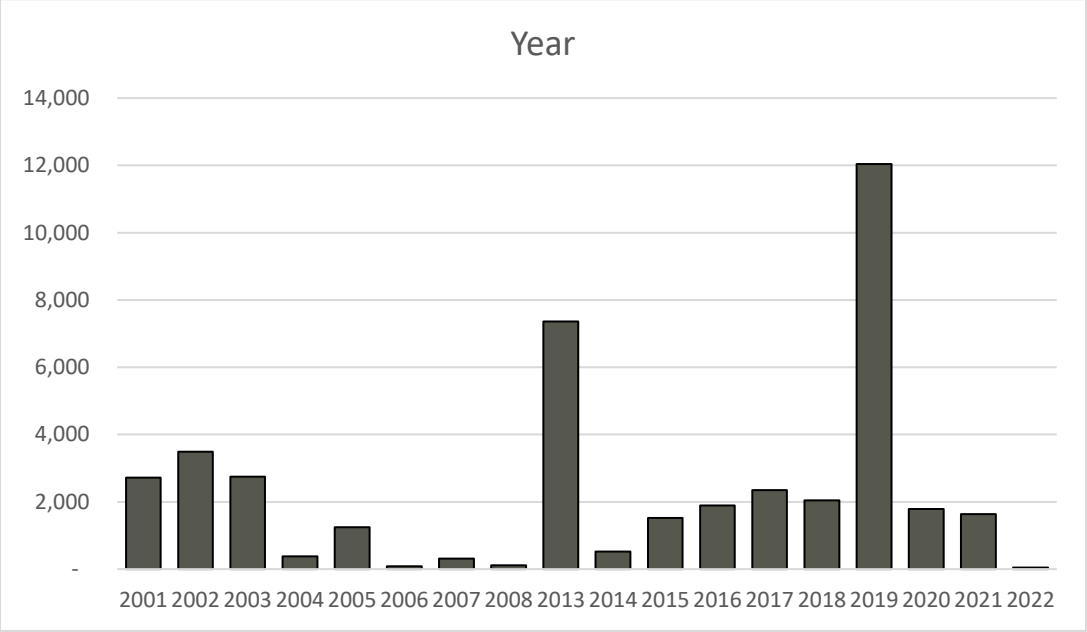

Figure 10. Total survey effort (km) per year available in the Black Sea.

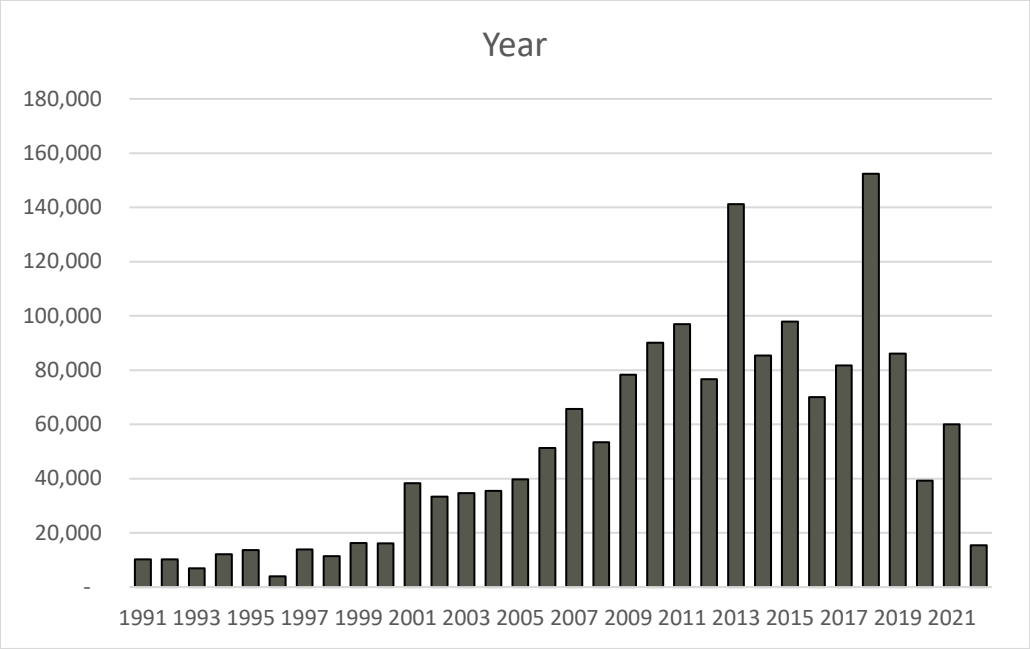

Figure 11. Total survey effort (km) per year available in the Mediterranean.

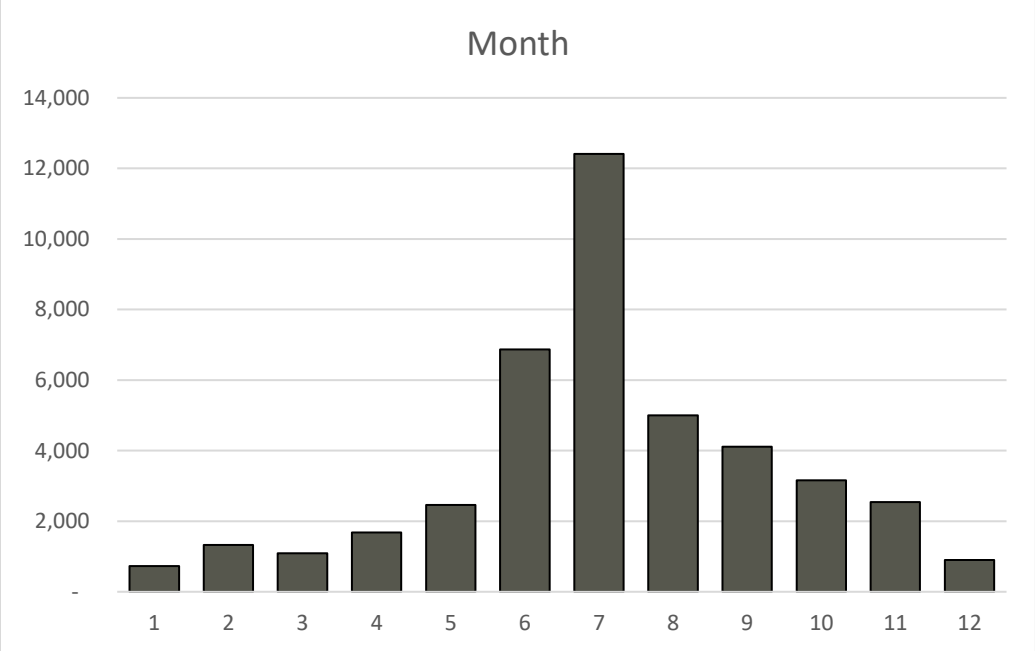

Figure 12. Total survey effort (km) per month available in the Black Sea.

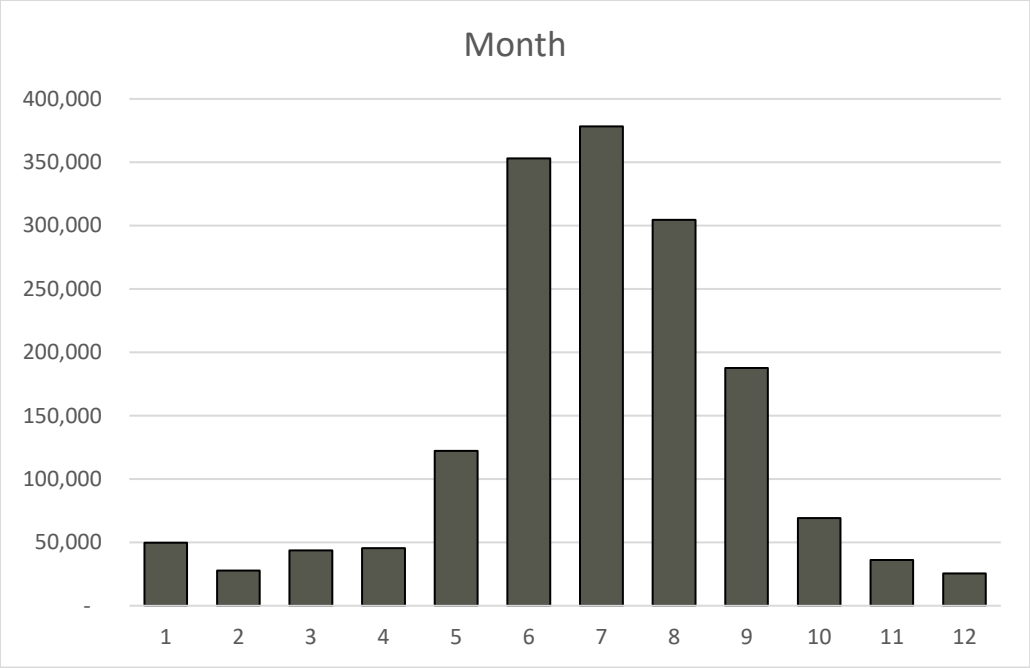

Figure 13. Total survey effort (km) per month available in the Mediterranean.

Figure 14 and **Figure 15** show the tracklines during the summer and winter months, respectively, in the Black Sea. **Figure 16** and **Figure 17** show the tracklines during the summer and winter months, respectively, in the Mediterranean Sea. In both basins the large inter-seasonal heterogeneity of effort is very clear, especially the very patchy distribution of the effort in winter, particularly in the Black Sea.

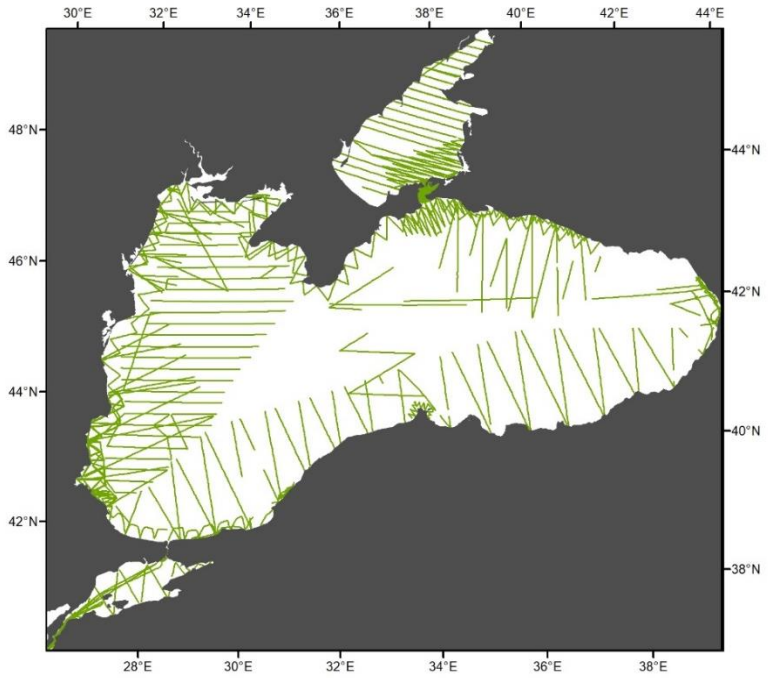

Figure 14. Tracklines during summer in the Black Sea.

Figure 15. Tracklines during winter in the Black Sea.

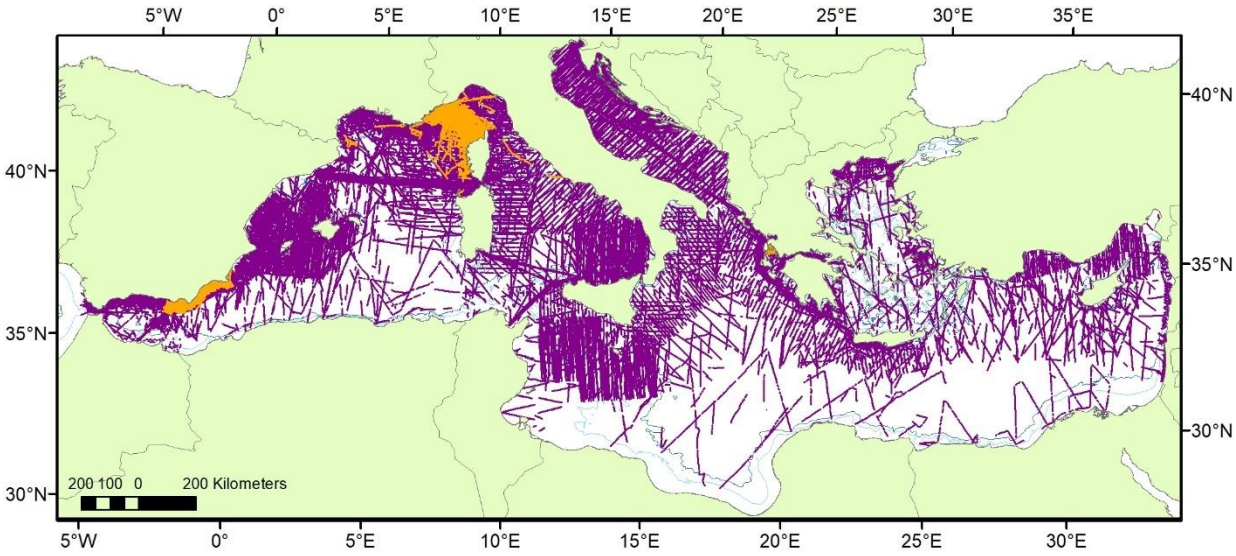

Figure 16. Tracklines during summer in the Mediterranean Sea (in purple from 1999 to 2022, in orange from 1991 to 1998).

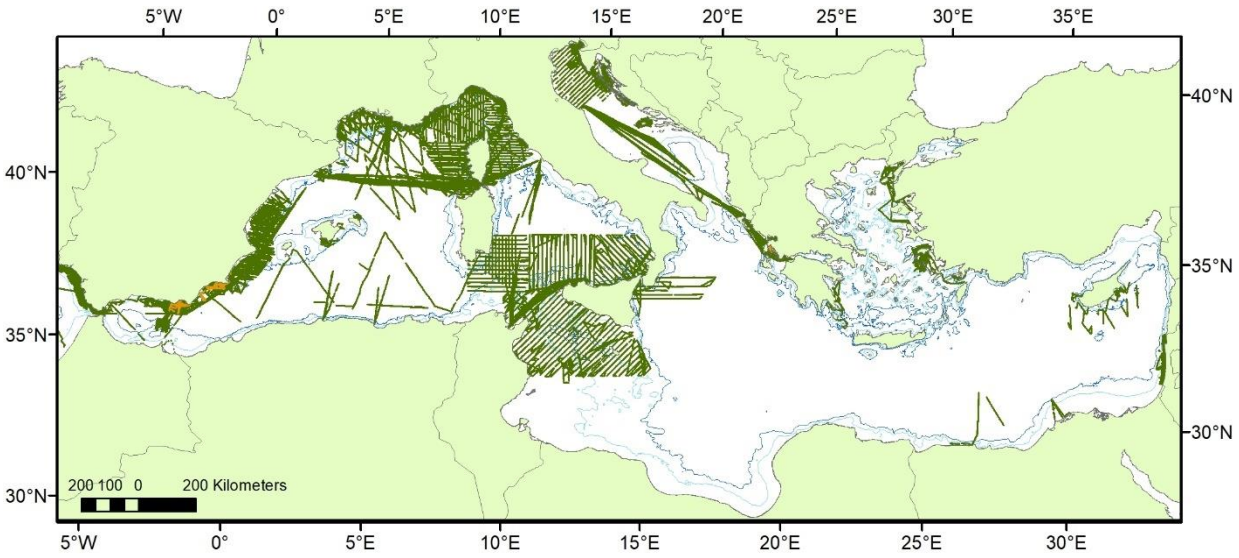

Figure 17. Tracklines during winter in the Mediterranean Sea (in green from 1999 to 2022, in orange from 1991 to 1998).

2.5.2. Overview of Sightings Data

The complete dataset included 40,987 observations of cetaceans, 83% more than in the previous analysis (Mannocci et al. 2018), for which 6,851 sightings were available. The full list of observations in the present dataset is shown in **Table 3**, separated by blocks (sub-basins).

The incorporated surveys provided sightings on effort and adequate conditions (as established for the effort) for 3 cetacean species in the Black Sea totaling 7,896 observations with definitive identification, and 14 cetacean species with definitive identification in the Mediterranean totaling 38,371 observations between 1991 and 2022 and 35,414 between 1999 and 2022. Of the 14 species identified in the Mediterranean, only 10 had enough observations to be modeled. The species with too few observations were: false killer whale (n=1), humpback whale (n=1), minke whale (n=4), and rough-toothed dolphin (n=9). There were 16 observations of harbor porpoise in the Aegean Sea, and a simple model was attempted for them.

Additionally, there were observations with ambiguous identification of species in both basins. In the Black Sea, 18 observations were classified as “Unidentified cetacean”, and 30 as “Unidentified dolphin”. These accounted for 0.6% of all observations and given the small number, they were not considered for analysis.

Only five observations of monk seals were done within the search effort available.

In the Mediterranean, 2,570 observations (6.3% of the total from 1991 to 2022) or 2,467 (6.5% of the total from 1999 to 2022) had ambiguous species identification. Of these, 2,288 (1991 to 2022) and 2,207 (1999 to 2022) were labeled as striped or common dolphin, unidentified Balaenoptera, unidentified beaked whale, unidentified dolphin, and unidentified small dolphin. Unidentified Balaenoptera was assigned to the fin whale dataset given that, with the exception

of a few very rare minke whales, it is the only baleen whale inhabiting the Mediterranean. Similarly, unidentified beaked whale was assigned to Cuvier's beaked whale, as it is the only beaked whale species inhabiting the Mediterranean with the exception of very rare Mesoplodon encounters. The other three categories went through a classification process (see **Section 2.9**, Dealing with Ambiguous Species Identification in the Mediterranean) to be assigned to either common, striped or bottlenose dolphins. The remaining records were species with very low numbers not suitable to be modeled (3 false killer whales, 1 humpback whale, 4 minke whales, 9 rough-toothed dolphins, and 19 hybrid striped-common dolphins), or too taxonomically ambiguous to be used in the density models (total of 54 observations in the Black Sea and 260 observations in the Mediterranean). The species used in the analysis, both with definitive and ambiguous identification, are shown in gray shade in **Table 3**.

Table 3. Number of observations per species in each Mediterranean block. The "Acronym" column shows the acronyms used for each species modeled in the rest of the report.

Species	Acronym	Adriatic	Aegean	Alboran	Ionian	Levantine	WMed	Gibraltar	Total	Previous
Bottlenose beaked whale				4					4	
Bottlenose dolphin	Ttr	3,277	228	525	1,590	389	3,681	446	10,136	743
Common dolphin	Dde	6	220	1,328	507	68	233	434	2,796	902
Cuviers beaked whale	Zca	4	19	121	52	41	430		667	17
False killer whale				1		1	1		3	
Fin whale	Bph	2		54	5	2	3,586	64	3,713	384
Harbor porpoise	Pph		17					6	23	10
Humpback whale							1		1	
Hybrid Striped-Common dolphin					19				19	
Killer whale	Oor							103	103	2
Long-finned pilot whale	Gme			637	8		181	453	1,279	452
Minke whale				2	1		1		4	
Monk seal			4			1			5	
Risso's dolphin	Ggr	18	23	185	41	14	509	1	791	150
Rough toothed dolphin					4	1	4		9	
Sperm whale	Pma		12	32	110	108	1,355	477	2,094	113

Species	Acronym	Adriatic	Aegean	Alboran	Ionian	Levantine	WMed	Gibraltar	Total	Previous
Striped and common dolphin					1				1	
Striped dolphin	Sco	263	170	1,861	599	159	13,235	482	16,769	3,364
Striped or common dolphin	Sco or Dde		7	26	8	4	241	3	289	126
Unidentified Balaenoptera	Bal						8		8	14
Unidentified beaked whale	Ziph		2	29	3		33		67	51
Unidentified cetacean				2	22	1	41		66	9
Unidentified dolphin	Udo	10	85	486	97	33	764	17	1,492	514
Unidentified large cetacean					1		58		59	
Unidentified large dolphin		2					4		6	
Unidentified large whale							2		2	
Unidentified medium cetacean		2	2		2		37	2	45	
Unidentified odontocete							41		41	
Unidentified small cetacean		2			3		13		18	
Unidentified small dolphin	Udo_Small	50	8		33	17	317	29	454	
Unidentified small whale					2				2	
Unidentified whale				5	5	2	9		21	
Total		**3,636**	**797**	**5,298**	**3,113**	**841**	**24,785**	**2,517**	**40,987**	**6,851**

*** Species used in the analysis: bottlenose dolphin, common dolphin, Cuvier's beaked whale, fin whale, harbor porpoise, killer whale, long-finned pilot whale, Risso's dolphin, sperm whale, striped dolphin, striped or common dolphin, unidentified Balaenoptera, unidentified beaked whale, unidentified dolphin, and unidentified small dolphin.**

Table 4 tallies the sightings of the fully identified species and the ambiguous taxa that were considered for modeling, both for the entire time span of the dataset and the more recent period. The percentage columns show how much of the data of a given taxon is retained when restricting the temporal span of the used data. Striped dolphin was by far the most frequently

sighted species, followed by common bottlenose dolphin. Sightings were generally most numerous in summer months, reflecting the large amount of effort in these months.

Habitat-based density models were developed for all the definitively identified species in **Table 4**. Maps of sighting distributions for each of the modeled species, for the two groups of years, are provided in **Appendix A**.

Table 4. Usable sightings in the data set for the two groups of years. The % columns represent the percentage of all the sightings remaining in each group of years. Only the species considered for modeling are shown in this table. These numbers include both the Mediterranean and the Black Seas.

Species	1991-2002	1999-2022	1991-2022 (%)	1999-2022 (%)
Bottlenose dolphin	10,136	9,768	100	96
Common dolphin	2,796	2,261	100	81
Cuviers beaked whale	667	650	100	97
Fin whale	3,713	3,352	100	90
Harbor porpoise	17	17	100	100
Long-finned pilot whale	1,279	1,103	100	86
Risso's dolphin	791	696	100	88
Sperm whale	2,094	2,031	100	97
Striped dolphin	16,769	15,418	100	92
Striped or common dolphin	289	289	100	100
Unidentified Balaenoptera	8	8	100	100
Unidentified beaked whale	67	61	100	91
Unidentified dolphin	1,492	1,395	100	93
Unidentified small dolphin	454	454	100	100
TOTAL	**40,572**	**35,751**	**100**	**88**

The final sightings used for each species, together with the effort tracks, are shown in **Figure 18** to **Figure 23** for the Black Sea and in **Figure 24** to **Figure 39** for the Mediterranean Sea, in both cases differentiating between summer months and winter months. The final range of years to be used for each species in the Mediterranean was decided after inspection of results for both periods we considered. Only the final range of years we selected is presented here for each species/guild.

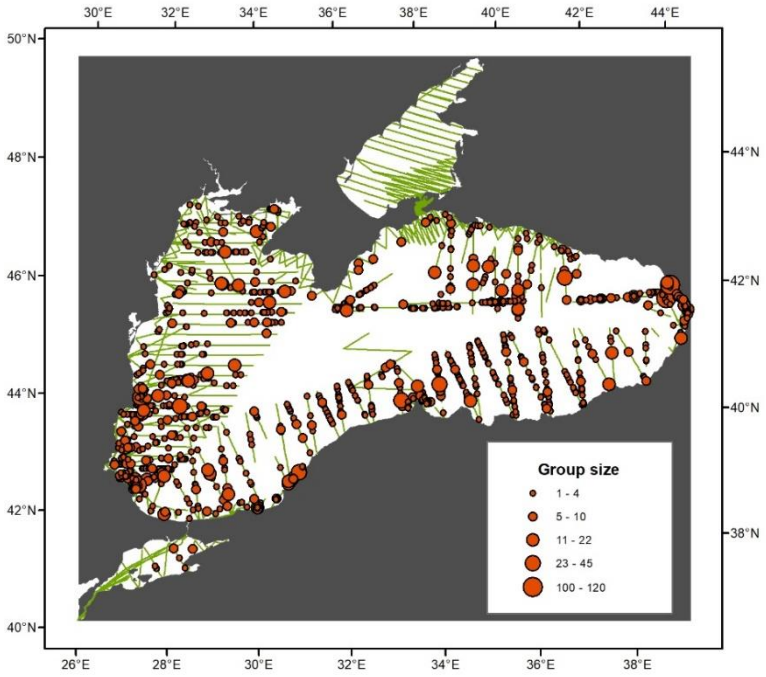

Figure 18. All usable sightings of common dolphins reported from the incorporated surveys in the Black Sea in summer.

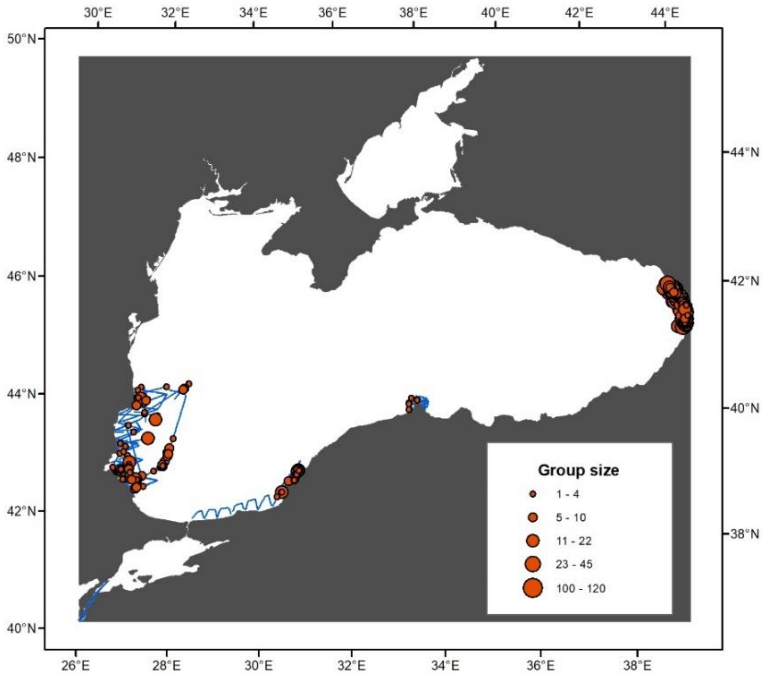

Figure 19. All usable sightings of common dolphins reported from the incorporated surveys in the Black Sea in winter.

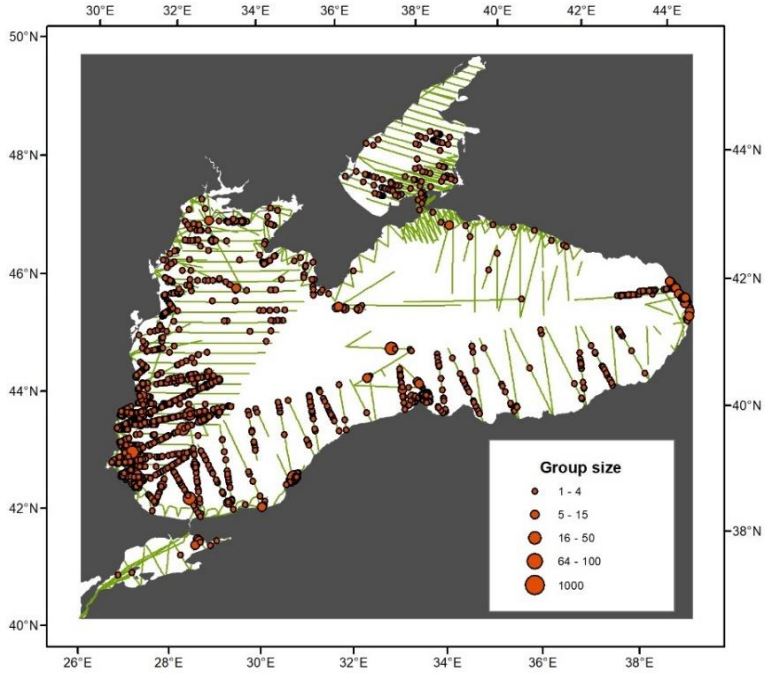

Figure 20. All usable sightings of harbor porpoise reported from the incorporated surveys in the Black Sea in summer.

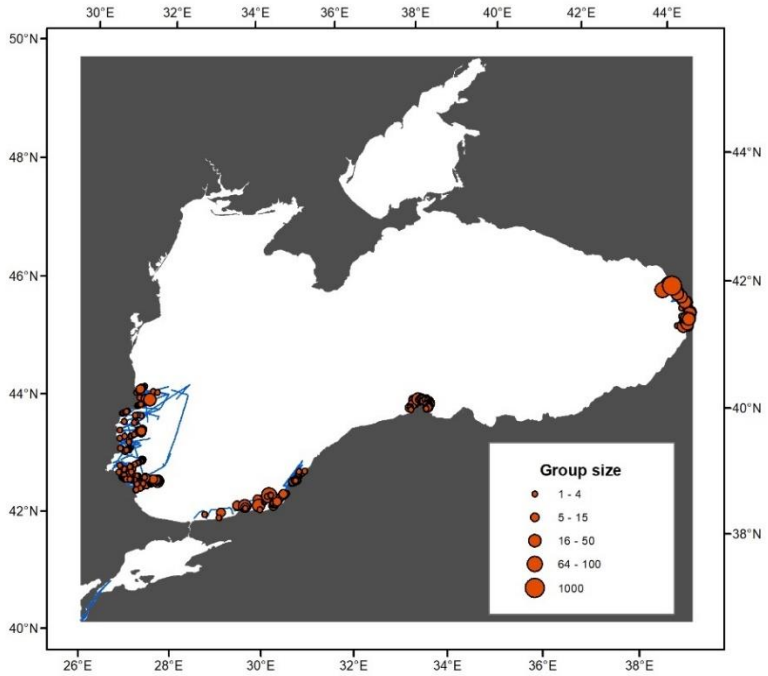

Figure 21. All usable sightings of harbor porpoise reported from the incorporated surveys in the Black Sea in winter.

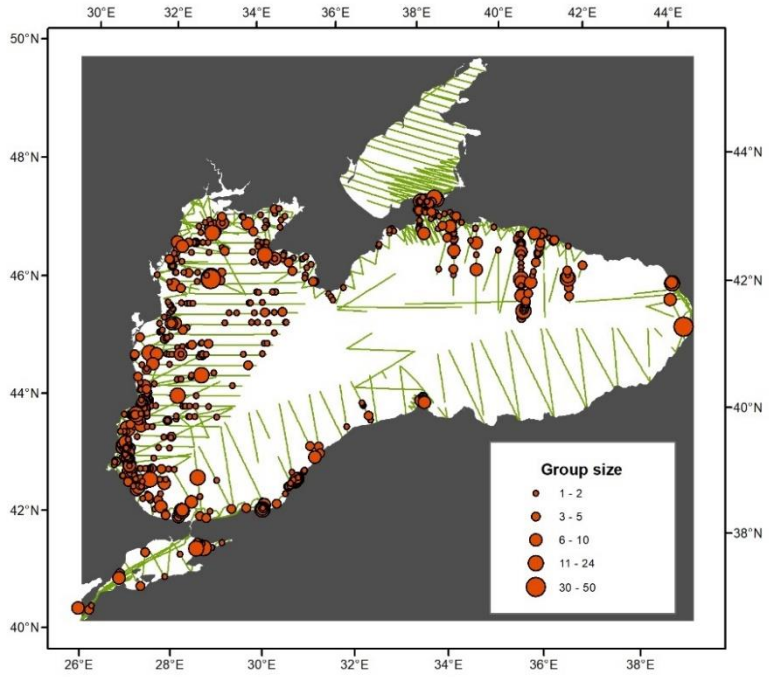

Figure 22. All usable sightings of bottlenose dolphins reported from the incorporated surveys in the Black Sea in summer.

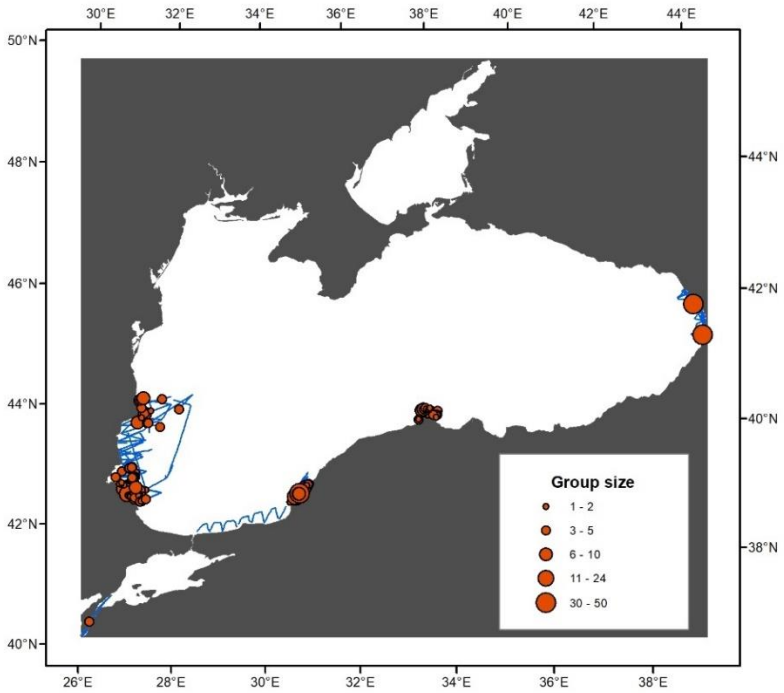

Figure 23. All usable sightings of bottlenose dolphins reported from the incorporated surveys in the Black Sea in winter.

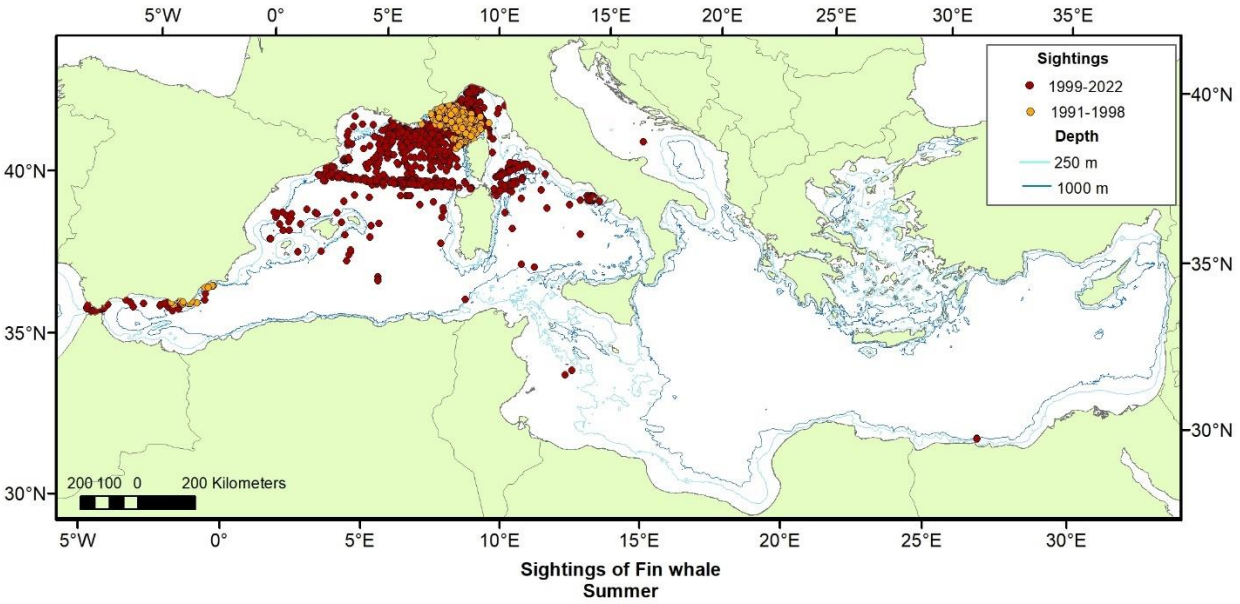

Figure 24. All usable sightings of fin whales (including Unidentified Balaenoptera) reported from the incorporated surveys in the Mediterranean Sea in summer

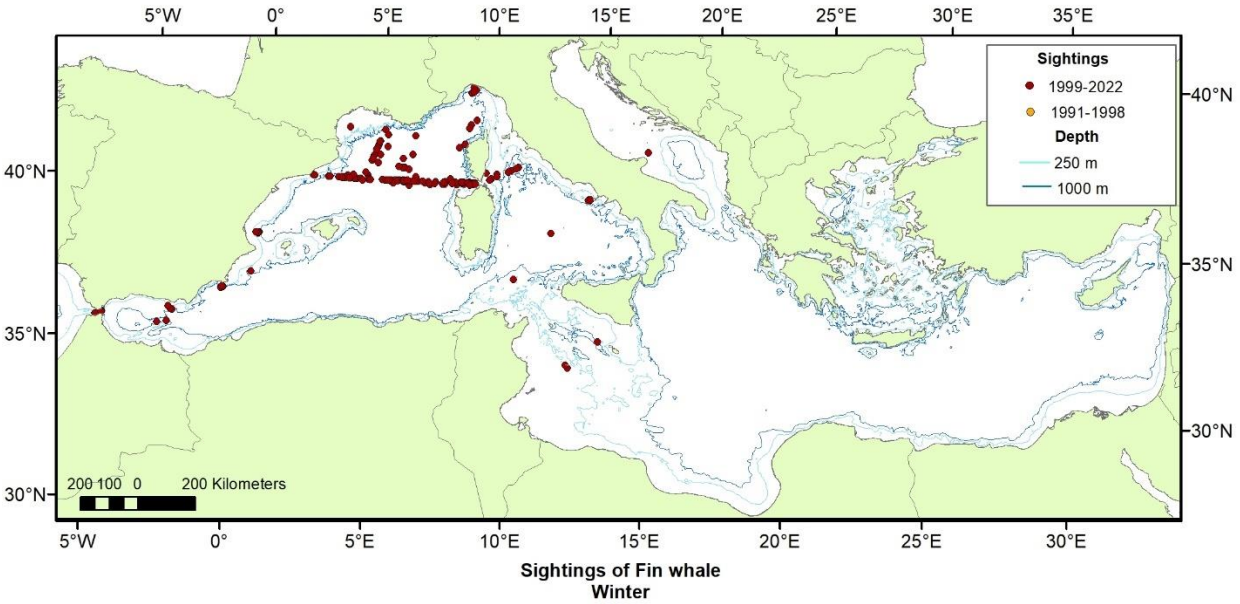

Figure 25. All usable sightings of fin whales (including Unidentified Balaenoptera) reported from the incorporated surveys in the Mediterranean Sea in winter

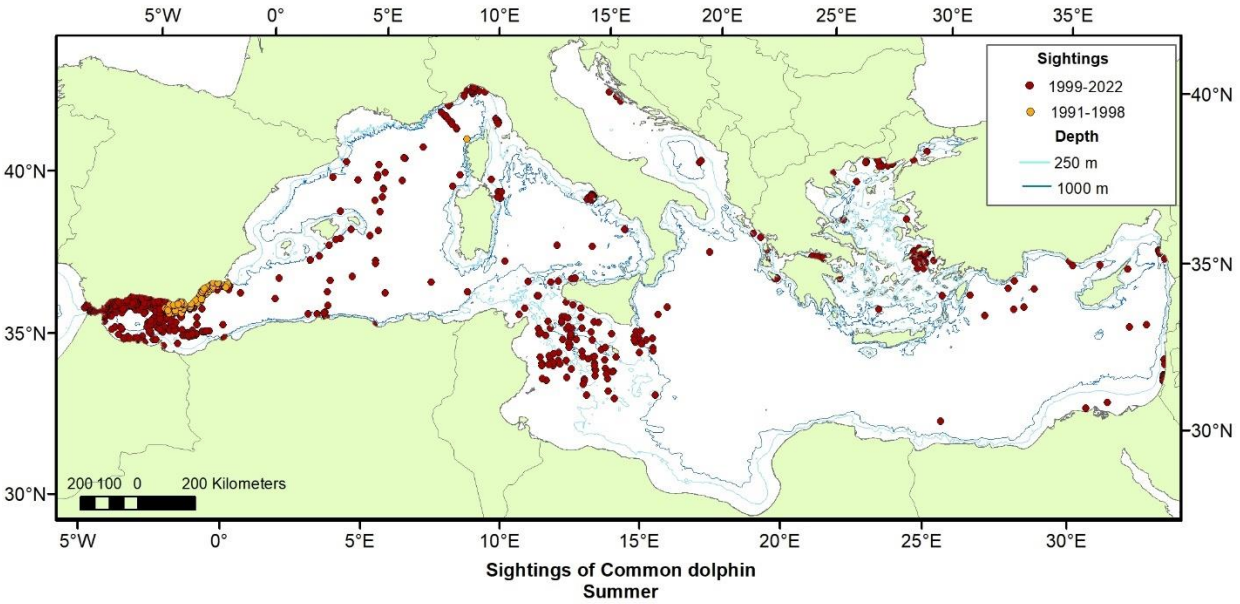

Figure 26. All usable sightings of common dolphins reported from the incorporated surveys in the Mediterranean Sea in summer.

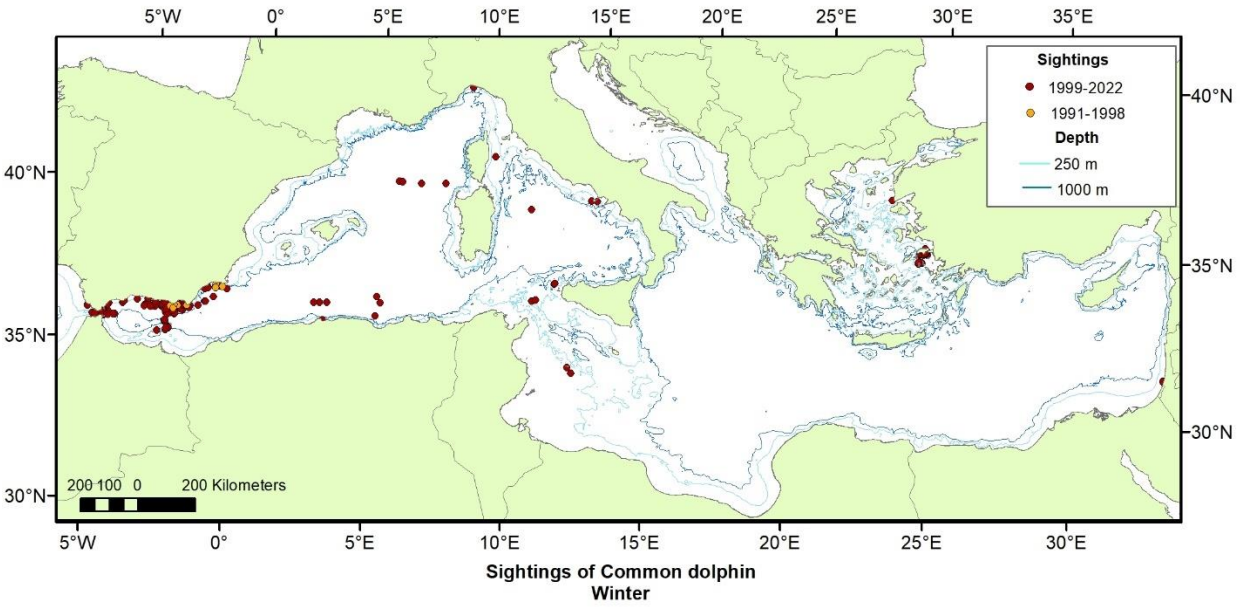

Figure 27. All usable sightings of common dolphins reported from the incorporated surveys in the Mediterranean Sea in winter.

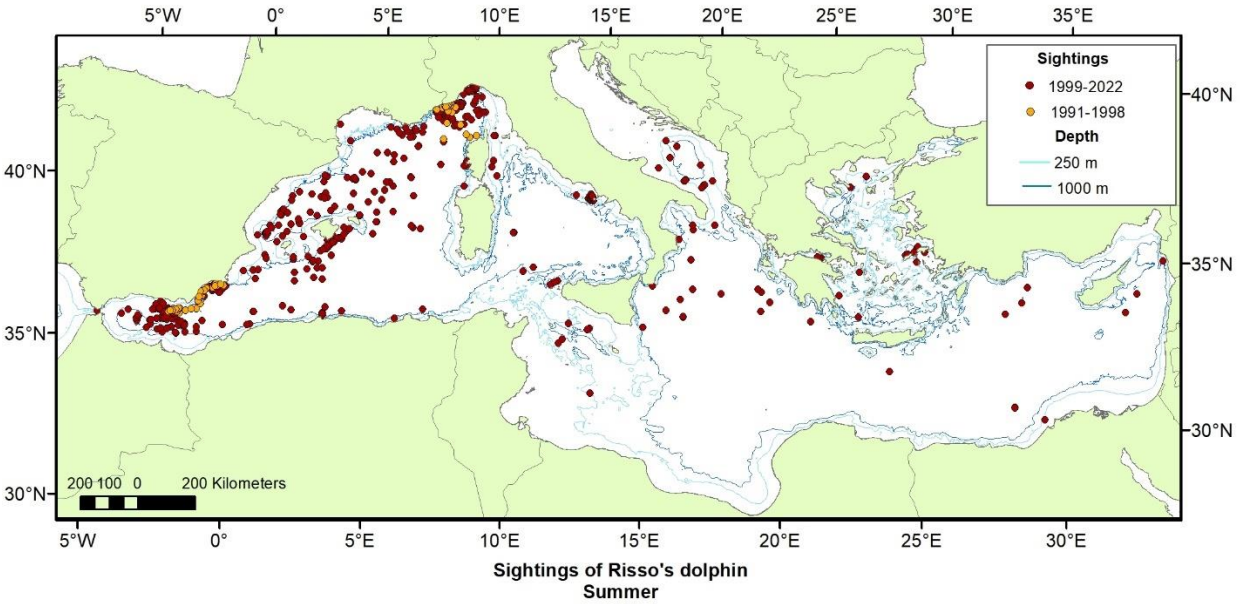

Figure 28. All usable sightings of Risso's dolphins reported from the incorporated surveys in the Mediterranean Sea in summer.

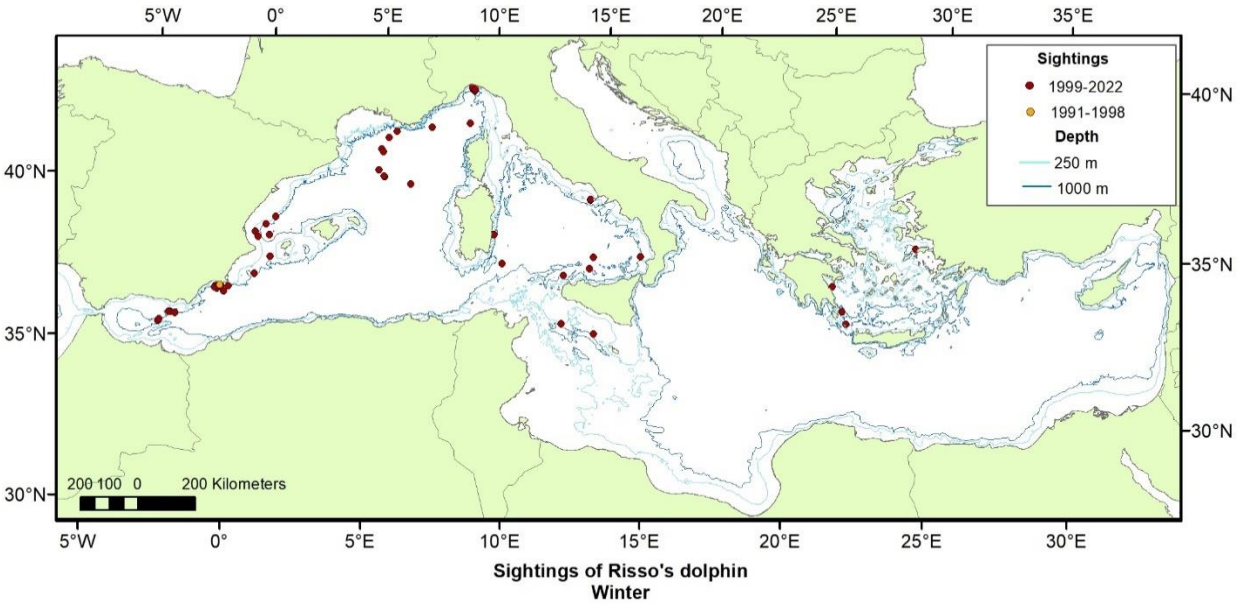

Figure 29. All usable sightings Risso's dolphins reported from the incorporated surveys in the Mediterranean Sea in winter.

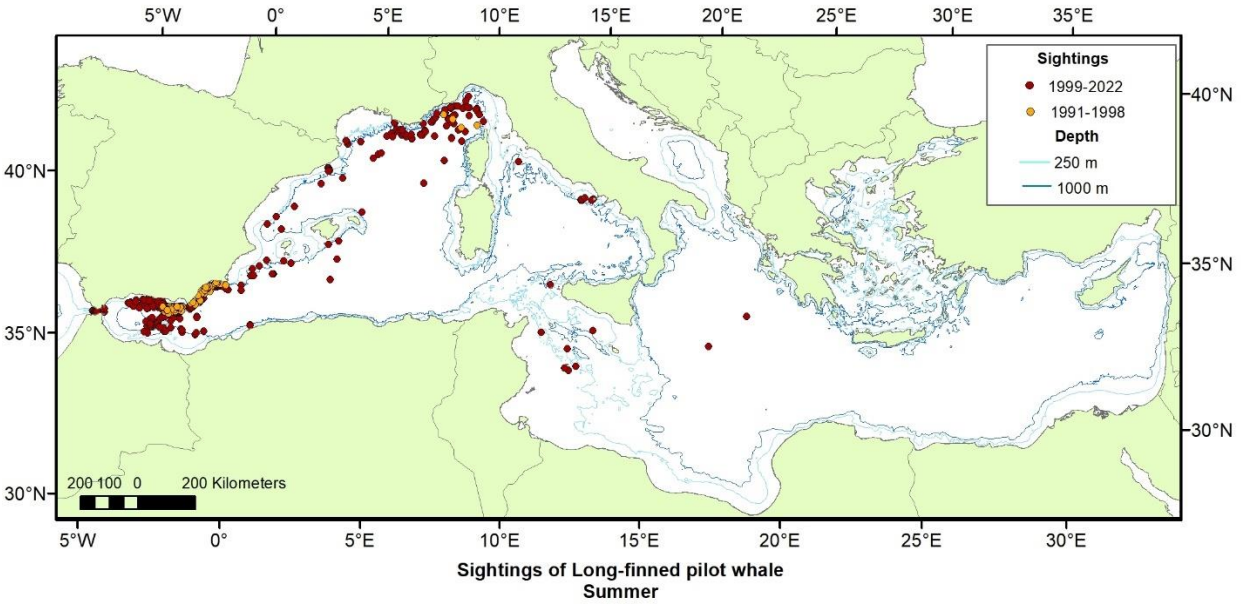

Figure 30. All usable sightings of long-finned pilot whales reported from the incorporated surveys in the Mediterranean Sea in summer.

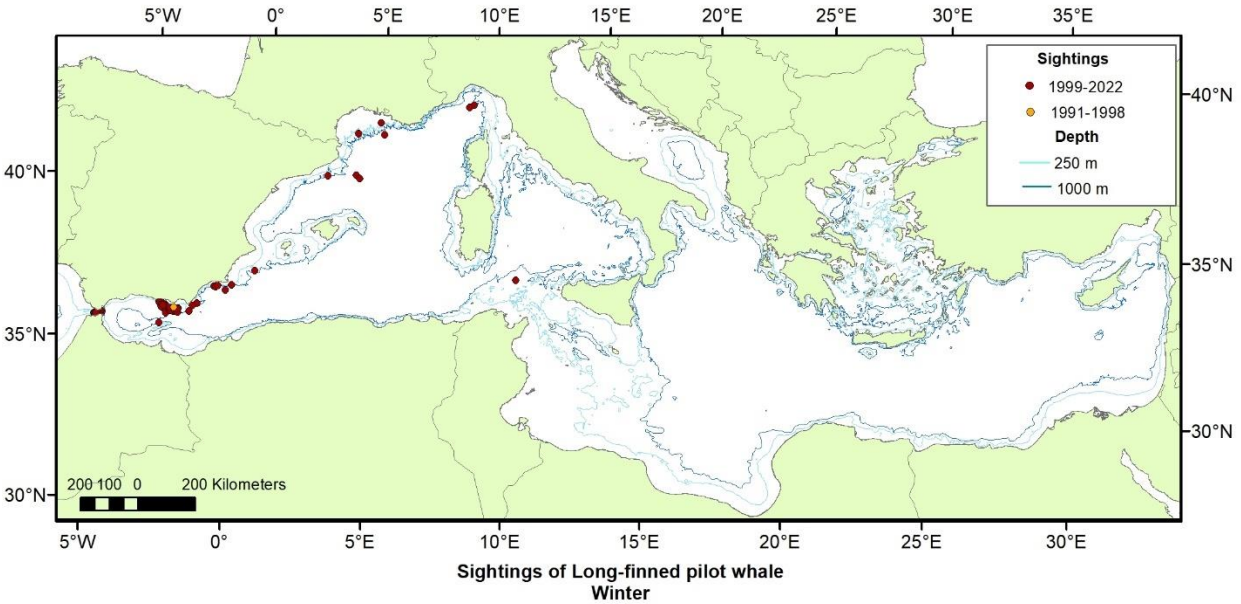

Figure 31. All usable sightings of long-finned pilot whales reported from the incorporated surveys in the Mediterranean Sea in winter.

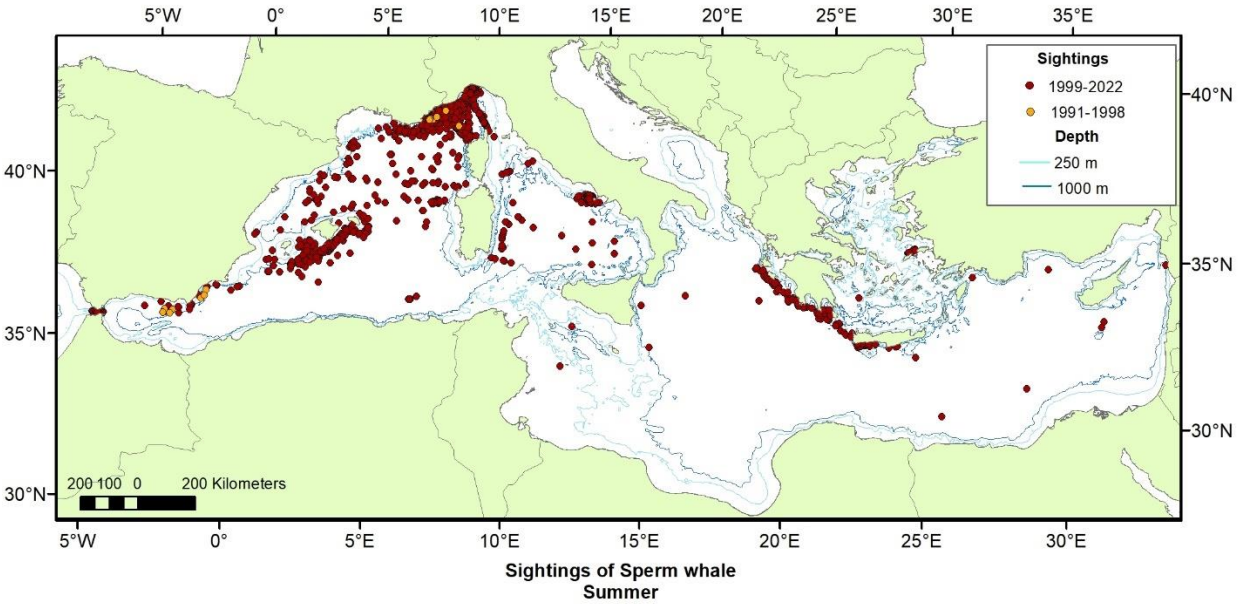

Figure 32. All usable sightings of sperm whales reported from the incorporated surveys in the Mediterranean Sea in summer.

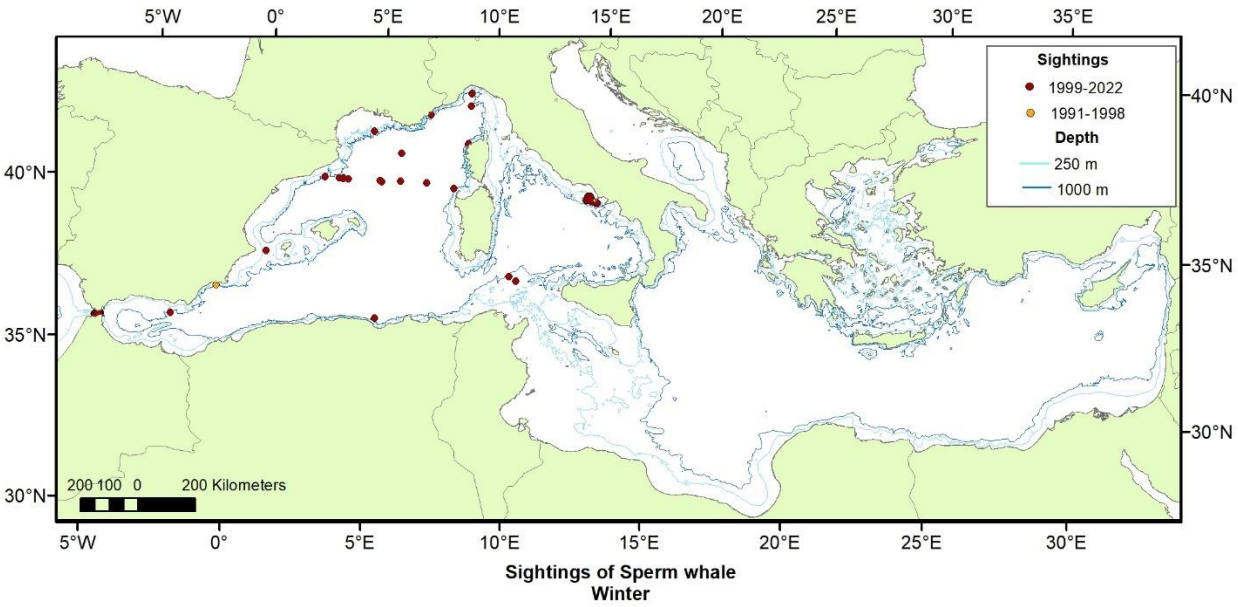

Figure 33. All usable sightings of sperm whales reported from the incorporated surveys in the Mediterranean Sea in winter.

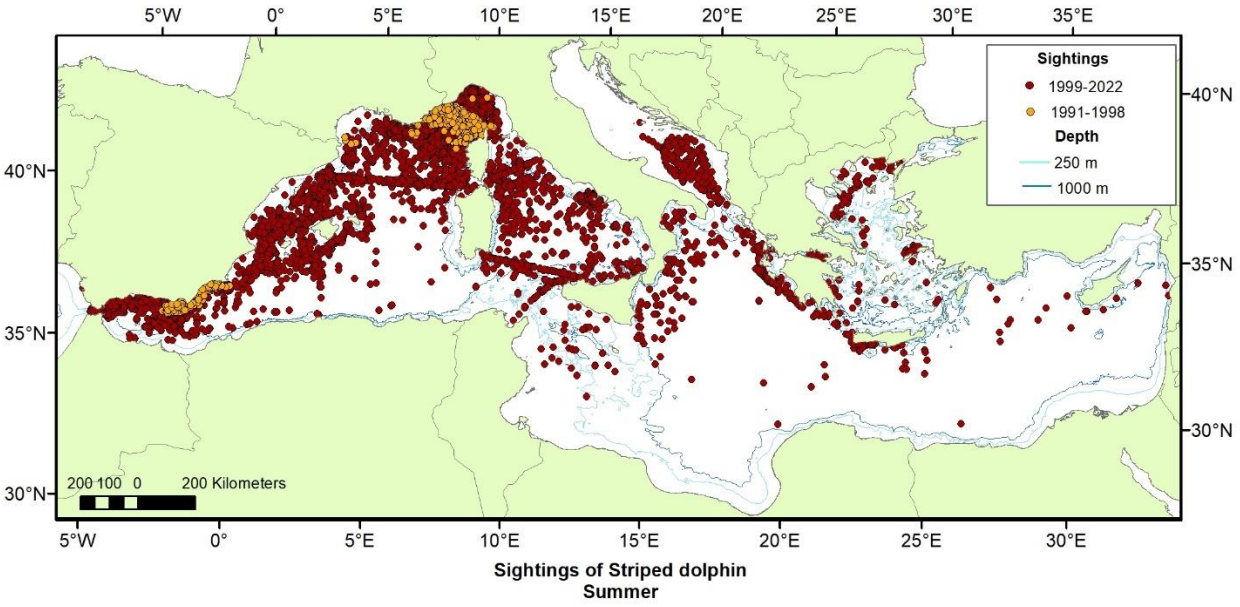

Figure 34. All usable sightings of striped dolphins reported from the incorporated surveys in the Mediterranean Sea in summer.

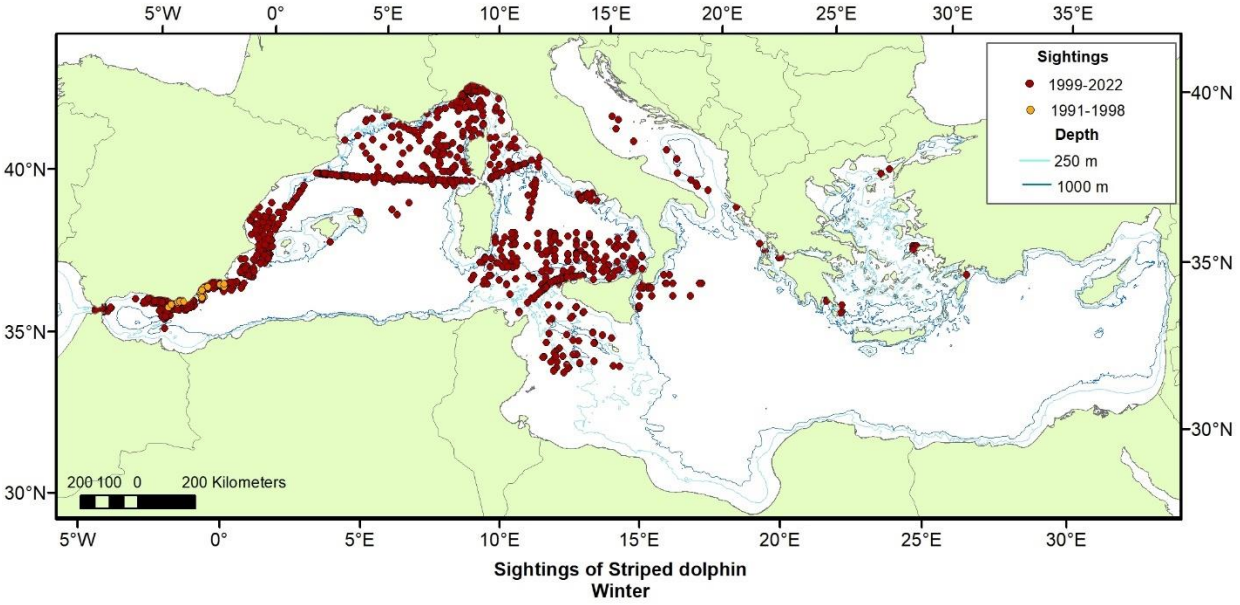

Figure 35. All usable sightings of striped dolphins reported from the incorporated surveys in the Mediterranean Sea in winter.

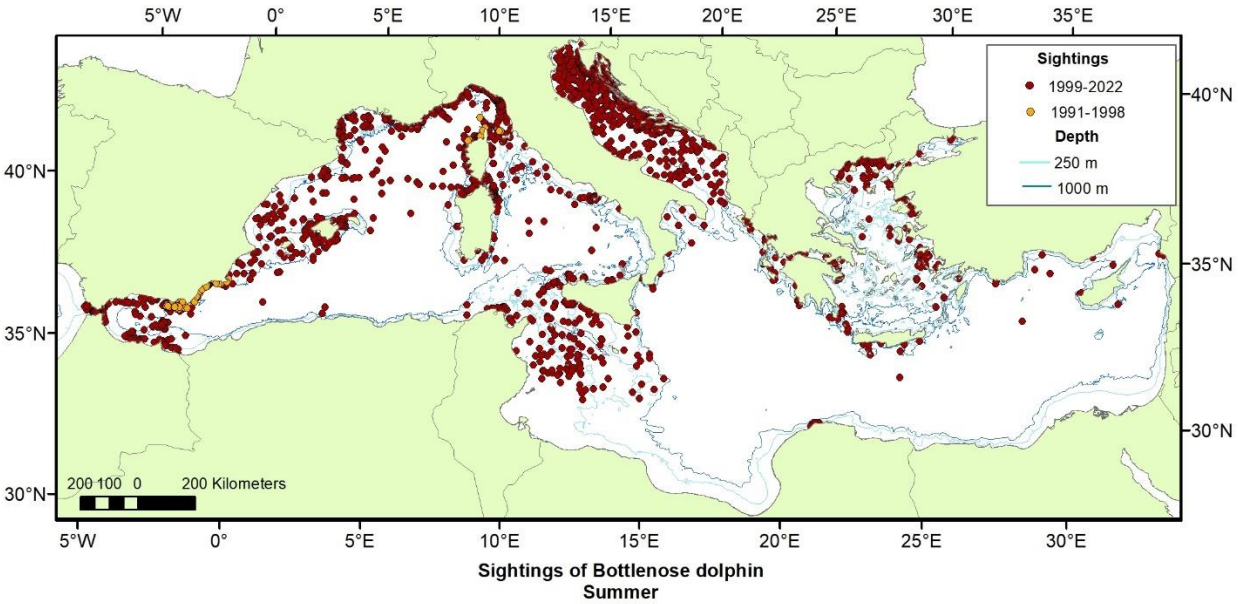

Figure 36. All usable sightings of bottlenose dolphins reported from the incorporated surveys in the Mediterranean Sea in summer.

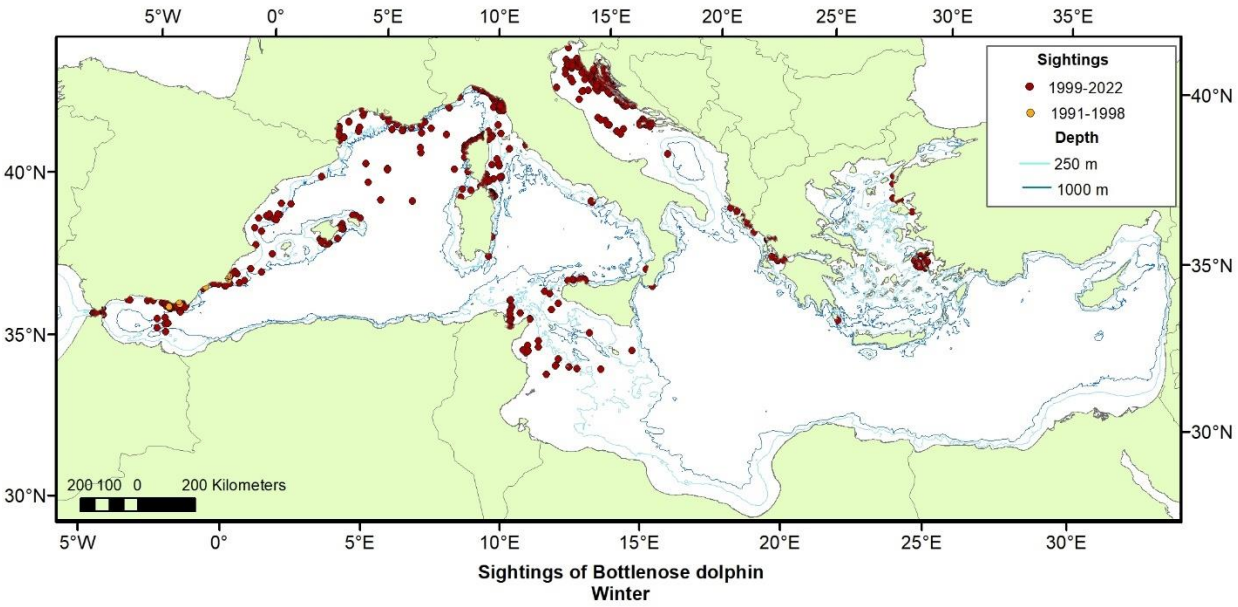

Figure 37. All usable sightings of bottlenose dolphins reported from the incorporated surveys in the Mediterranean Sea in winter.

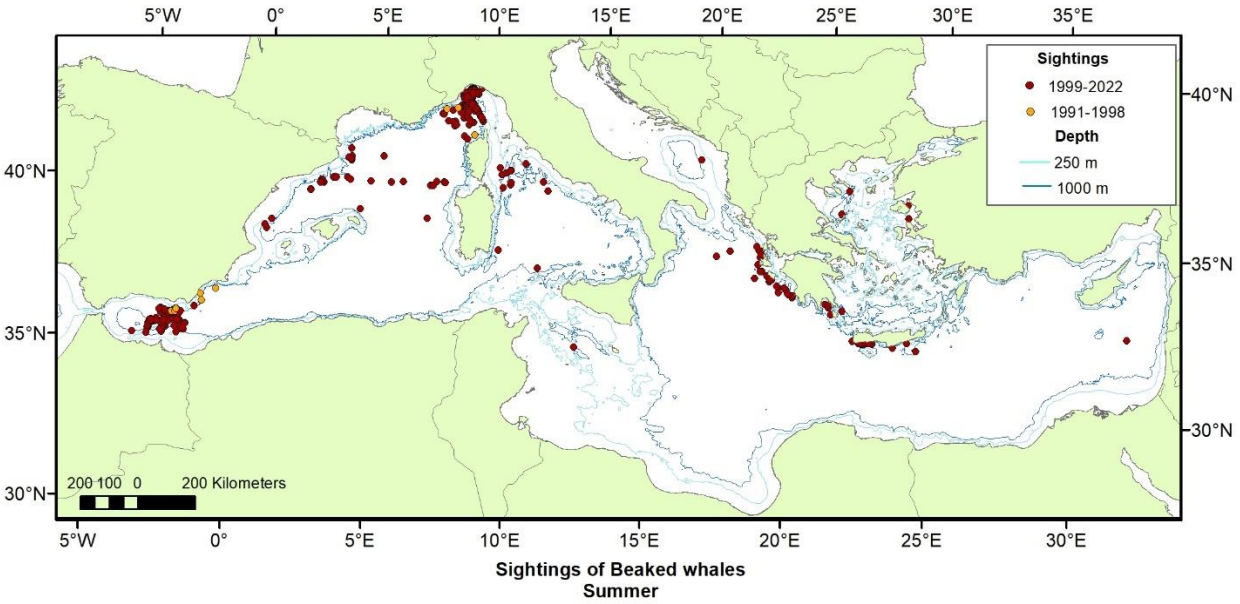

Figure 38. All usable sightings of beaked whales (including Cuvier's beaked whales and Unidentified beaked whales) reported from the incorporated surveys in the Mediterranean Sea in summer.

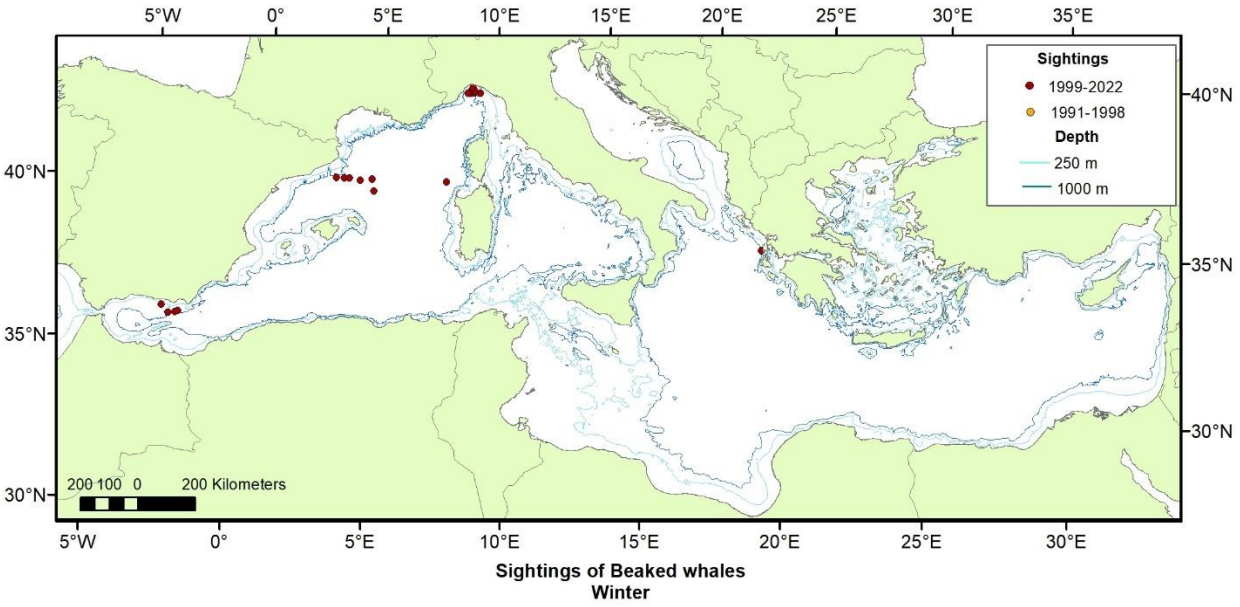

Figure 39. All usable sightings of beaked whales (including Cuvier's beaked whales and Unidentified beaked whales) reported from the incorporated surveys in the Mediterranean Sea in winter.

2.5.3. Classification of Platform Types

Given the large amount and heterogeneity of survey organizations, protocols, and platforms, and given that in most cases there were not enough sightings of each species per platform to model a detection function, it was decided to create “platform groups” by pooling together platforms with similar characteristics. The same classification was applied for the Black Sea and the Mediterranean Sea, and the detection functions per platform group were done by pooling the observations in both basins.

Table 5 shows the classification of platform groups for aerial surveys, based on the mean flight altitude and the type of window, flat or bubble, which are the two survey-specific characteristics that most frequently affect detectability of animals at sea from planes.

Table 5. Classification of platform groups for aerial surveys. Number of surveys falling into each group are shown.

Group	Altitude (m)	Window	Surveys
150-F	150	Flat	2
229-F	229	Flat	1
123-B	123	Bubble	1
150-B	150	Bubble	4
183-B	183	Bubble	14
200-B	200	Bubble	3
229-B	229	Bubble	15
Total			**40**

Table 6 shows the classification of platform groups for shipboard surveys, based on speed and platform height, which are the two survey-specific characteristics that most frequently affect detectability of animals at sea from ships. A second level of classification was done according to the existence of a second higher observation platform (at 3–5 m, 6–8 m, 10–11 m, or None).

Table 6. Classification of platform groups for shipboard surveys. Number of surveys falling into each group are shown. Speed is in km/hr and platform height is in m.

Group	Min speed	Max speed	Min height	Max height	Platform 2	No. of surveys	Total surveys
G1	7	10	1	1.5	None	7	7
G2	7	10.1	2	3.1	10_11	1	27
					6_8	1	
					None	25	
G3	7	10	4.5	6.5	None	6	6
G4	10.1	12.3	1	1.5	3_5	7	25
					6_8	4	
					None	14	
G5	9.2	12.3	2	3.6	10_11	2	34
					3_5	1	
					6_8	2	
					None	29	
G6	12.6	15	0.5	1.5	None	16	16
G7	15.7	18	0.5	1.5	3_5	1	7
					None	6	
G8	13	15	2	3.5	3_5	2	17
					None	15	
G9	15.7	20	2	3.5	3_5	2	11
					6_8	2	
					None	7	
G10	11.1	15.7	4	7	10_11	2	13
					None	11	
G11	16.7	25.9	4	7	None	9	9
G12	11	14.3	16	17	None	11	11
G13	25.9	37	12	15	None	4	4
G14	31.5	37	20	27	None	9	9
G15	46.3	46.3	29	29	None	2	2
G16	18	25	0.5	1	None	6	6
G17	22.4	22.4	22	22	None	2	2
G18	11.1	11.1	10	10	None	2	2
Total							**208**

2.6. Overall Workflow of the Analytical Process

The overall workflow is described schematically in **Figure 40**.

The main data used for the analysis were: a) covariate rasters covering the whole study area; b) effort table (composed of all the segments of tracklines prepared during the data processing phase, each with environmental and geographical covariates extracted from the covariate

rasters at matching geographic and time coordinates, as well as the sightability conditions, unique to each segment, reported by the survey teams); and c) sightings table (composed of the observations of cetaceans, with their group sizes and perpendicular distances, and the associated sightings conditions extracted from the segments they were recorded on).

The first step was to model the detection function for a given taxon for each of the platform groups defined previously. The final objective of modeling the detection function was to obtain the esw, which was estimated from the perpendicular distance data for all the detected animals. This was effectively the width at which the number of animals detected outside the strip equaled the number of animals missed inside the strip, assuming that everything was seen at a perpendicular distance of zero. Multi-Covariate Distance Sampling methods were used to allow detection probability to be modeled as a function of detectability covariates in addition to perpendicular distance from the transect line (see **Section 2.7**, Detection Modeling below). For the surveys with observations but without recorded distances, the esw estimated for segments with similar characteristics and with the same platform group was assigned according to the covariates in the detection function.

All detectability covariates were constant for each effort segment (by virtue of the tracklines being split whenever detectability covariates changed) except for “group size,” which varied by sighting. If group size was not included in the final detection function, the esw was estimated directly for each segment according to its detectability covariates. If group size was selected, a group size value first needed to be estimated for each segment before the esw could be estimated. In these cases, we used the mean group size of the taxon averaged over all sightings reported by the detection function’s platform group.

A correction factor including both availability and perception bias was then applied to the segments to obtain a corrected prediction of individuals (see **Section 2.8**, Correction Factors for Availability and Perception Biases).

Using the effort segments, candidate density surface models were then fitted using generalized additive models (GAMs), with the number of individual animals sighted during the segment as the response variable, the effective area surveyed as an offset (obtained from the detection function and corrected for availability and perception biases), and the environmental and spatial covariates (see **Section 2.10**, Spatial Modeling Process). The candidate models were evaluated, and once a final model was selected, density predictions were made over the study area and modeled time period using the environmental rasters according to the covariates selected in the models, and then summarized across all years by month into monthly climatologies of density.

The uncertainty around the estimates was obtained using an analytical method that accounted for model parameter and uncertainty and interannual variability in dynamic environmental covariates, discussed further below in **Section 2.11**, Spatial Modeling Predictions and Uncertainty. Maps of unmodeled sightings per unit effort (**Section 2.13**, Sightings per Unit Effort) were also produced and model extrapolation tests (**Section 2.12**, Characterizing Extrapolation from the Spatial Model) were also conducted.

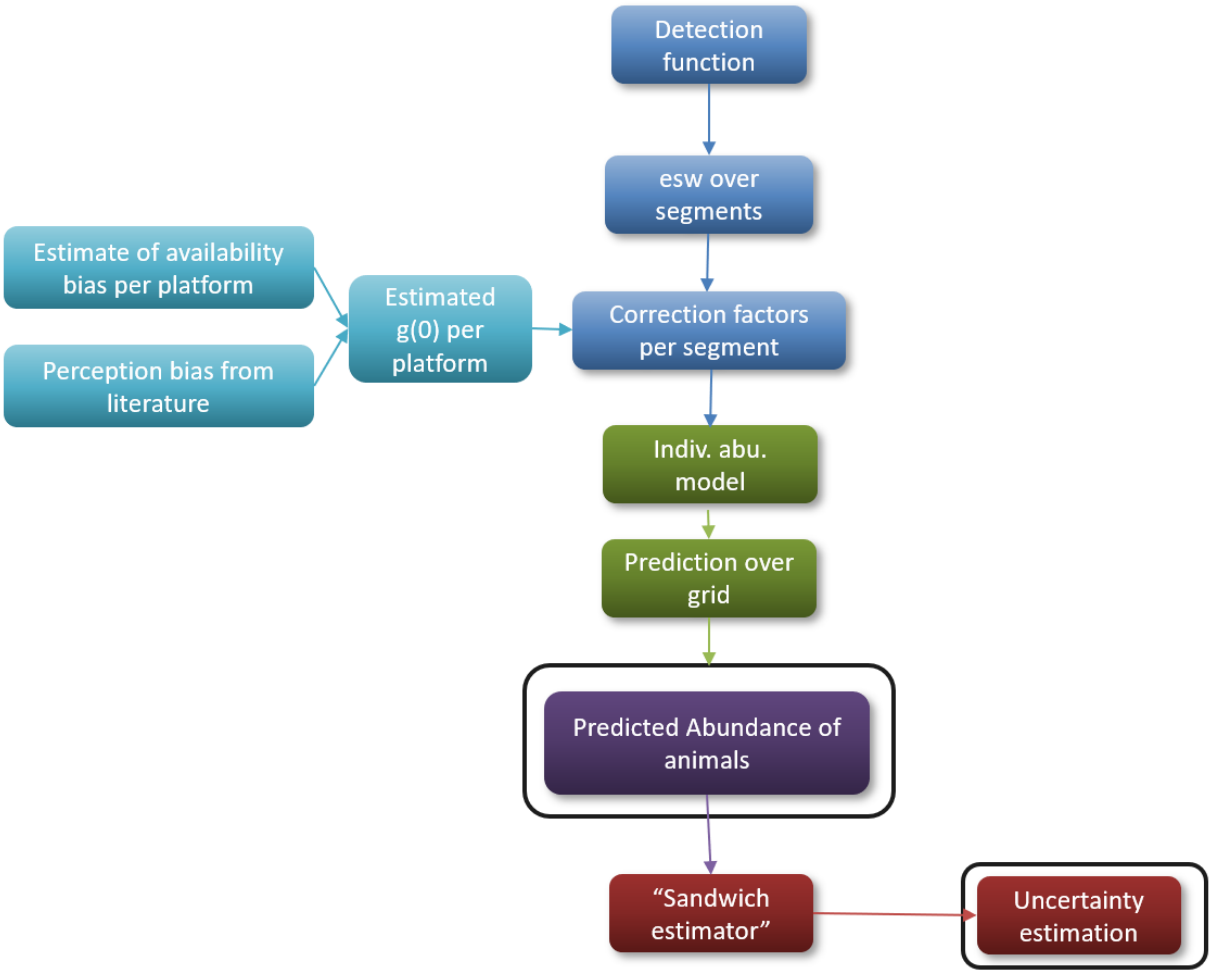

Figure 40. General workflow for the analytical process.

2.7. Detection Modeling

Detection modeling is the first stage of the two-stage density surface modeling approach (Miller et al. 2013). Detection modeling was performed using single-team "distance sampling" methodology (Buckland et al. 2001), using the data from all years, under the assumption that detection probabilities have not changed significantly over the years for each platform.

The overall workflow for the modeling of the detection functions is shown in **Figure 41**. We applied it to develop a detection function for each modeled taxon for each platform group, as follows.

1. We generated a histogram of perpendicular distance of on-effort sightings from the trackline. We inspected this for initial outliers, quality assurance and quality control.
2. We assessed the need for left truncation by visually inspecting histograms with 25 m bins.

3. We assessed the need for right truncation by fitting several null detection functions (with no covariates) with different truncation distances and exploring the resulting diagnostics.
4. We then tested each covariate, one at a time in a single-covariate detection function, to assess its effect and statistical significance.
5. We discarded problematic covariates after completion of step 4. We considered covariates problematic when any of several conditions occurred: there was no convergence; there was an extremely large coefficient of variation (CV) for the estimate, or for the coefficient of any level of a categorical covariate (>100%); there was an extremely anomalous *esw*, probability of detection, or Cramér–von Mises (CvM) goodness of fit test compared to the rest of models.
6. We then tested the non-problematic covariates in groups of two or three, in detection functions fitted with multiple-covariate distance sampling (MCDS) techniques, iterating over all possible combinations of covariates, but avoiding using related covariates in the same model (for example, Beaufort and BeaufortCode).
7. We reviewed the output from each multiple-covariate model, ranked them by Akaike Information Criterion (AIC), and selected a final model, usually that with the lowest AIC. If two or more models were within the lowest 2 points of AIC, we looked into the value of the CvM and the CV of the model to make the final decision.
8. We predicted the final model on each effort segment to obtain its esw.

All of this work was carried out using R software (R version 4.2.2, R Core Team 2022). Detection functions were fitted using the Mark-Recapture Distance Sampling (mrds) package version 2.2.3 and model selection was carried out using custom code. The selection procedure was iterated over all possible combinations of models and covariates, occasionally yielding hundreds of possible detection functions to choose from. In the remainder of this section, we give additional details of the overall procedure outlined above.

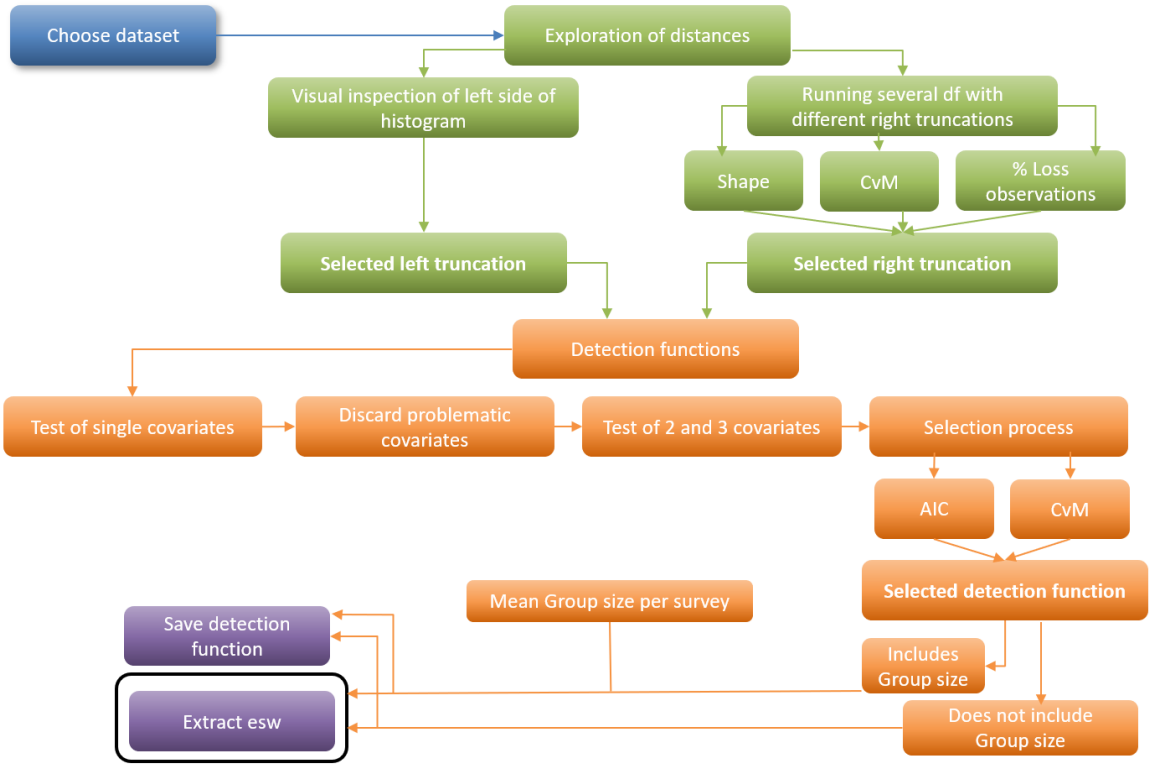

Figure 41. Workflow for the detection modeling.

2.7.1. Distance Exploration and Truncation

In distance sampling, detectability is modeled from the perpendicular distances to the sightings from the survey trackline.

It is common practice to right truncate perpendicular distance data to eliminate sightings at large distances that have little or no influence on detection probability but adversely affect overall fit of the model. Following this practice, after inspecting histograms of perpendicular distances, we tested different right truncation distances. We used a compromise between the comparison of the diagnostics of each of the different truncation distances and the percentage of data lost for each of those truncations to decide on the final right truncation distance. The main diagnostics that we used were Q-Q (quantile-quantile) plots and CvM tests (the smaller the value, the better the fit of the detection function to the data). AIC indicates the compromise between fit of the model and its complexity (number of parameters) and can only be used to compare models based on exactly the same dataset. The AIC could not be used, therefore, to compare the performance of detection functions with different truncation distances, as different truncation distances meant that the datasets used to fit the detection functions were different (more or less observations used).

Under ideal conditions, when the trackline is fully visible to observers and they dedicate sufficient effort to watching it, left truncation is not necessary. But particularly for aerial surveys, it is common practice to left truncate perpendicular distance data if histograms of perpendicular

distances show that the area close to the line transect (distance = 0) has significantly fewer observations than nearby distance bins. This often happens when the aircraft has flat windows, and the observers cannot see directly under the plane. Additionally, even when there are bubble windows, observers sometimes tend to look further away and do not concentrate on the transect line (e.g., the windows are narrow, and observers find it uncomfortable to look directly under the plane). Finally, in some cases, left truncation is applied if animal attraction to the vessel is suspected or observed (this typically does not apply to aerial surveys). In shipboard surveys, a left truncation might be necessary if there is a high spike near zero due to attractive movement of animals before detection, observer behavior (tending to look mostly very close to the ship), or other circumstances; or in the case of lower than expected proportion of observations near the trackline due to observer behavior or other causes. On aerial surveys with flat windows, a left truncation was applied to the extent of the distance missed under the plane. Both on shipboard and aerial (with bubble windows) surveys, a left truncation was applied due to abnormal proportion of observations close to the trackline. In these cases, we treated that left truncation as a strip transect, where the probability of detection was considered uniform, at the same level of the chosen left truncation, but during abundance estimation those observations were taken into account and given the probability of detection at the left truncation value, including those distances in the effective strip width. It is important to highlight, however, that treating left truncation as a strip transect in a detection function could potentially mean an overestimation of the probability of detection close to the trackline. This could potentially create a slight underestimation of the abundance estimate, if the number of observations in the strip were lower than expected. It could also mean an underestimation of the probability of detection close to the trackline that could create a potential slight overestimation of the abundance estimate, if the number of observations in the strip were higher than expected.

2.7.2. Detection Function Covariates

Table 7 shows the numeric covariates and **Table 8** shows the factor covariates tested in the fitting of the detection functions. Candidate covariates included those related to survey conditions, e.g., Beaufort sea state, cloud coverage, visibility, and swell. Also, four covariates related to the animals, i.e., species common name, confidence (Definitive-Probably and Ambiguous), group size, and logarithm of group size. Candidate covariates also included some forms of survey identification or location (Black Sea or Mediterranean Sea). Some ordinal covariates (e.g., Beaufort sea state) were tested both as continuous covariates (Beaufort) and as factors (Beaufort.fac).

The availability of survey condition covariates varied by survey, as different surveys recorded different information and in different formats. A lengthy process was followed to homogenize all the different values assigned to the covariates recorded by each survey, so at the end a single set of values was used for each covariate (**Table 7** and **Table 8**). Some covariates are variations or subclasses of others; therefore “groups” of correlated covariates were created so that only one of each “group” would be included in each combination of covariates for the detection function. For example, VisibilityCode and Visibility were interrelated, with VisibilityCode being a condensed categorical form of the numerical covariate Visibility. Similarly, Beaufort, and

BeaufortCode were grouped, as were the other groups shown in **Table 8**. Also Log.detsize was derived from detsize and therefore they were not included together in the same model.

Table 7. Numeric covariates tested in the detection functions.

Name	Value
Beaufort	0, 0.5, 1, 1.5, 2, 2.5, 3, 3.5, 4 (>4 discarded)
Swell	0, 0.2, 0.5, 1, 1.5, 2 (m)
Clouds	0, 1 , 2, 3, 4, 5, 6, 7, 8 (octaves)
Visibility	3, 5, 7, 10 (km)
Year	Year
Month	Month
detsize	Group size
Log.detsize	Logarithm of group size
PlatformHeight	Observation platform height (in m)
Speed	Mean speed of the platform (km/h)

Table 8. Factor covariates tested in the detection functions.

Name	Value
BeaufortCode	0_1, 2_3, 4_5 (only including 4 for some species)
Beaufort.fac	0, 1, 2, 3, 4 (>4 discarded)
SubjectiveCode	Excellent, Good, Moderate (Poor discarded)
GlareCode	None, Slight, Moderate, Severe
CloudsCode2	0_3, 4_5, 6_8 (Eighths of sky covered)
TurbidityCode	Clear, Moderate, Turbid
VisibilityCode	2_5, 5_10 (km of visibility)
WeatherCode	Fair, Unknown
SkyGlint	0, 1
Name	Survey name
CommonName	Species name
Confidence	Definitive-Probably, Ambiguous
Region	BlackSea, Mediterranean
PlatformHeight.fac	Observation platform height (in mts)
Group.plat	Platform group
Group.plat2	None, 3_5, 6_8, 10_11 (Second platform)

2.7.3. Detection Function Fitting

We fitted detection functions following the multiple covariate distance sampling framework (Marques and Buckland 2004).

We tested half normal and hazard rate key functions without adjustment terms.

The best functional form (half normal or hazard rate) of the detection function and the covariates retained by the best fitting models were selected based on model fitting diagnostics, which included AIC, goodness of fit tests, Q-Q plots, and inspection of plots of fitted functions.

Q-Q plots compare the distribution of two variables; if they follow the same distribution, a plot of the quantiles of the first variable against the quantiles of the second should follow a straight line. To compare the fit of a detection function model to the data, we used a Q-Q plot of the fitted cumulative distribution function (cdf) against the empirical distribution function (edf).

For goodness of fit tests, we used the CvM statistic, which focuses on the squared differences between cdf and edf. The smallest value of the CvM indicates best fit. The smaller AIC was also preferred as it means a better compromise between the fit of the model and its complexity (number of parameters).

AIC was the main diagnostic used. If there were several competing models (similar AIC within 2 points), then we looked at the CvM and Q-Q plot to assess which of them produced a better fit.

Once the final model was selected, a prediction was made of the esw for each segment according to the final model covariates values present in each segment. An offset was calculated then for each segment as 2*L*esw where L was the length of the segment.

2.8. Correction Factors for Availability and Perception Biases

The probability of detecting an animal on the trackline (i.e., at perpendicular distance of 0), or g(0), is affected by both availability bias (i.e., observers fail to detect animals because they are submerged) and perception bias (i.e., observers fail to detect animals present at the surface) (Pollock et al. 2006). Distance sampling assumes that g(0) = 1, but one or both biases are usually present, invalidating this assumption and leading to a g(0) that is less than 1. If g(0) is nonetheless assumed to be 1, density and abundance will be underestimated, as detectability will be assumed to be higher than it actually is. This problem may be corrected by estimating g(0) with various techniques, which usually require additional data to be collected during surveying (e.g., by the platform circling back to resample a sighting, or by using double-platform experiments).

The availability bias (â)—the probability that an object is available to be seen—depends mainly on two factors:

- observer field of view, which is the same for all species
- surface and dive duration, which varies by species (and within species depending on behavior)

The perception bias—the probability that the observer detects an object that is available to be seen—can be assessed with these parameters:

- multiple covariates distance sampling detection function, which gives the shape of the detection function curve and how it varies with distance and covariates.
- trackline detection probability (p0), which is the probability that an observer will detect an available object located at a distance of zero (i.e., on the trackline) or at the left-truncation distance. This probability determines the intercept of the curve of the detection function.

None of the surveys used in these models had either availability bias (â) or perception bias (p0) estimates available for their data. As the use of a correction factor is fundamental in studies like this one, where heterogeneous platforms with very different detectability and biases are modeled together, we did estimate g(0)s that corrected for availability and perception biases, as follows.

Perception bias

We assigned the values from published perception biases most similar in terms of platform characteristics (the final values are shown in **Appendix D**).

Availability bias

We followed the process described below.

First, for each species, we searched the literature and extracted mean dive duration and surfacing times (**Table 9**). Then, for each survey, we estimated *â(S,x)* by applying the Laake equation (Laake et al. 1997), which estimates availability bias from those times and the main characteristics of the platform, as follows:

$$\hat{a}(S,x) = \frac{E[s]}{E[s]+E[d]} + \frac{E[d](1-e^{-w/E[d]})}{E[s]+E[d]}$$

Where:

â(S,x) - probability that an animal at forward distance x was at the surface and within the observer's field of view
S = "event"
x = distance

s – average time at the surface and thus available to be detected

d – average time under the surface and thus unavailable to be detected

w – window of time in which an animal is within detectable range (amount of time an animal at forward distance x from the trackline remains in view of the observers, which depends on the speed of the observation vessel):
= forward distance / speed

Following Cañadas and Vazquez (2014), we estimated *w* using the mean speed of the vessel during the survey and where the distance was taken as the 90th percentile of forward distances for the survey.

This equation was designed for individual animals (S), but our sightings often consisted of groups of more than one animal, not all of which were submerged at the same time. To account for this effect, we estimated the availability of the group as follows:

$$\hat{a}_{groups} = 1 - (1 - \hat{a}_{indiv})^{groupSize}$$

where $\hat{a}_{indiv}$ was the result from the Laake equation, applicable to a single individual, and groupSize was the number of individuals in the group. This approach assumes that animals in a group surface asynchronously (which, in many cases, is not true, but more investigation, beyond the scope of our project, is needed to obtain a more accurate correction). With this correction we obtained an availability bias for all the sightings of each survey, each one according to the radial or perpendicular distance, platform speed, and group size. Next, we computed the average $\hat{a}_{groups}$ for all the sightings in each survey ($\hat{a}_{survey}$) and assigned the ($\hat{a}_{survey}$) to all the segments on effort of its corresponding survey. Then, for each segment, we multiplied the offset by the ($\hat{a}_{survey}$) to correct for survey-specific availability bias.

Table 9. Mean diving and surfacing times from literature for the modeled species.

Species	Mean surface time (mins)	Mean diving time (mins)	Region	Platform	Source	Notes
Bottlenose dolphin	3.86	1.15	Med	ship	Mannocci et al. 2016	From Forcada et al. (2004)
Bottlenose dolphin	3.86	1.15	Med	plane	Mannocci et al. 2016	From Forcada et al. (2004)
Common dolphin	2.21	1.11	Med	plane	Mannocci et al. 2016	
Common dolphin	2.21	1.11	Med	ship	Mannocci et al. 2016	taken from ship in Med
Cuvier's beaked whale	2.03	26.23	Med	plane	Cañadas et al. 2017	taken from ship in Med
Cuvier's beaked whale	2.03	26.23	Med	ship	Cañadas et al. 2017	
Fin whale	1.50	3.79	Med	ship	Jahoda et al. 2003	
Fin whale	1.50	3.79	Med	plane	Jahoda et al. 2003	taken from ship in Med
Long-finned pilot whale	4.98	3.64	Med (Alboran)	ship	Mannocci et al. 2016	From Cañadas 2011
Long-finned pilot whale	4.98	3.64	Med (Alboran)	plane	Mannocci et al. 2016	taken from ship in Med
Risso's dolphin	5.37	2.92	WNA	plane	Palka et al. 2017	
Risso's dolphin	5.37	2.92	WNA	ship	Mannocci et al. 2016	From Palka et al. (2021)
Sperm whale	9.14	44.77	Med	ship	Mannocci et al. 2016	From Drouot et al. (2004a)
Sperm whale	9.14	44.77	Med	plane	Mannocci et al. 2016	taken from ship in Med
Striped dolphin	2.21	1.11	Med	ship	Mannocci et al. 2016	From Gomez de Segura et al. (2006)
Striped dolphin	2.21	1.11	Med	plane	Mannocci et al. 2016	taken from ship in Med
Harbor porpoise	0.07	0.44	ENA	ship	Paxton et al. 2016	
Harbor porpoise	0.82	1.07	WNA	plane	Palka et al. 2017	

Key: ENA = eastern North Atlantic; WNA = western North Atlantic; Med = Mediterranean.

2.9. Dealing with Ambiguous Species Identification in the Mediterranean

As mentioned before, in the Mediterranean, 2,467 cetacean observations (6.5% of the total from 1999 to 2022) had ambiguous species identification, which is not an insignificant proportion. Not dealing with them in order to incorporate the adequate proportion to the models of the species would mean a certain amount of underestimation would persist in the resulting abundance estimates. Therefore, we developed a new approach to deal with these ambiguous classifications, namely striped or common dolphin (**Figure 42**), unidentified small dolphin (**Figure 43**) and unidentified dolphin (**Figure 44**) (see **Table 4**). The species to which we attempted to assign these ambiguously identified observations were common, striped and bottlenose dolphins, which are the three species (especially the first two) that have more probabilities to be confused at sea, rather than the rest of modeled species in the Mediterranean.

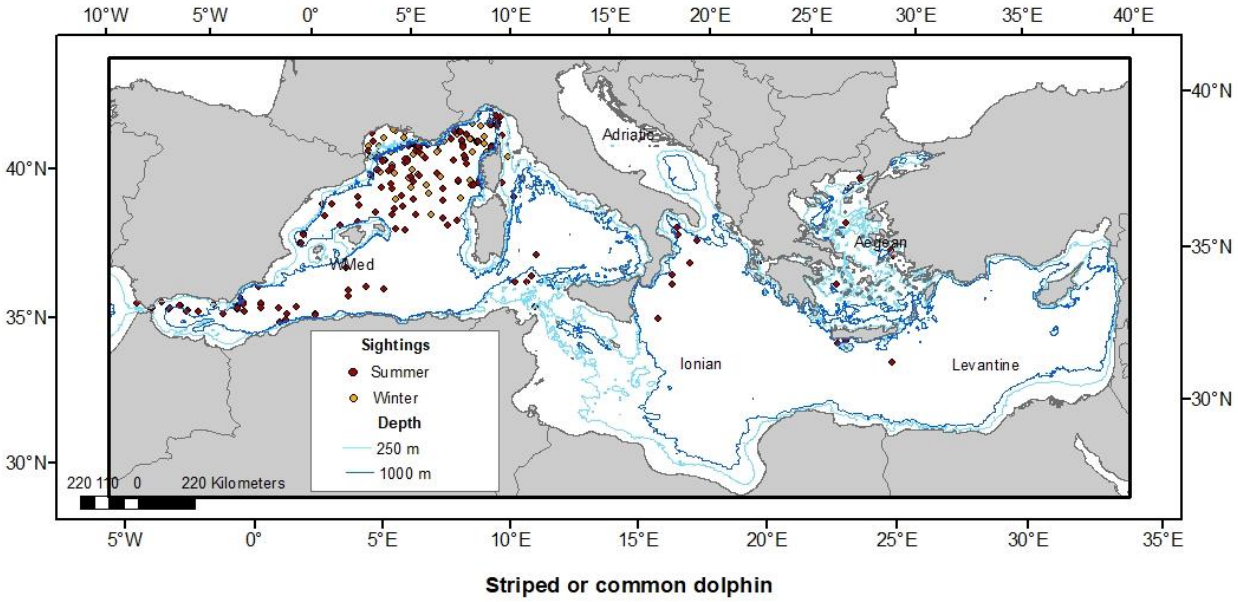

Figure 42. Observations of ambiguous species: striped or common dolphin.

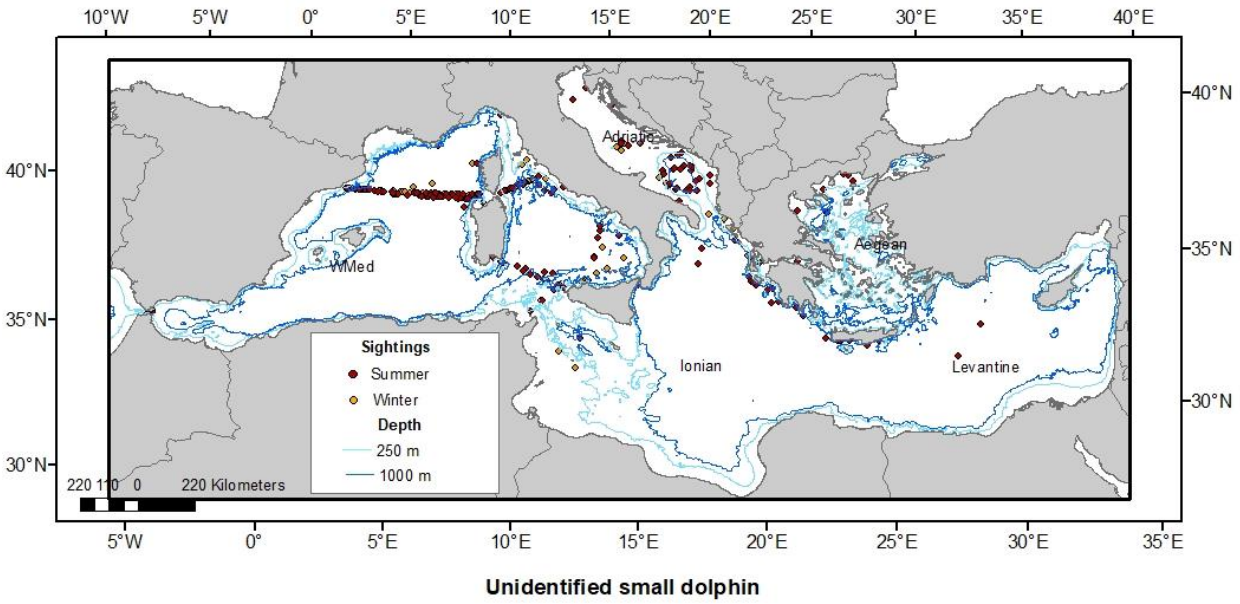

Figure 43. Observations of ambiguous species: unidentified small dolphin.

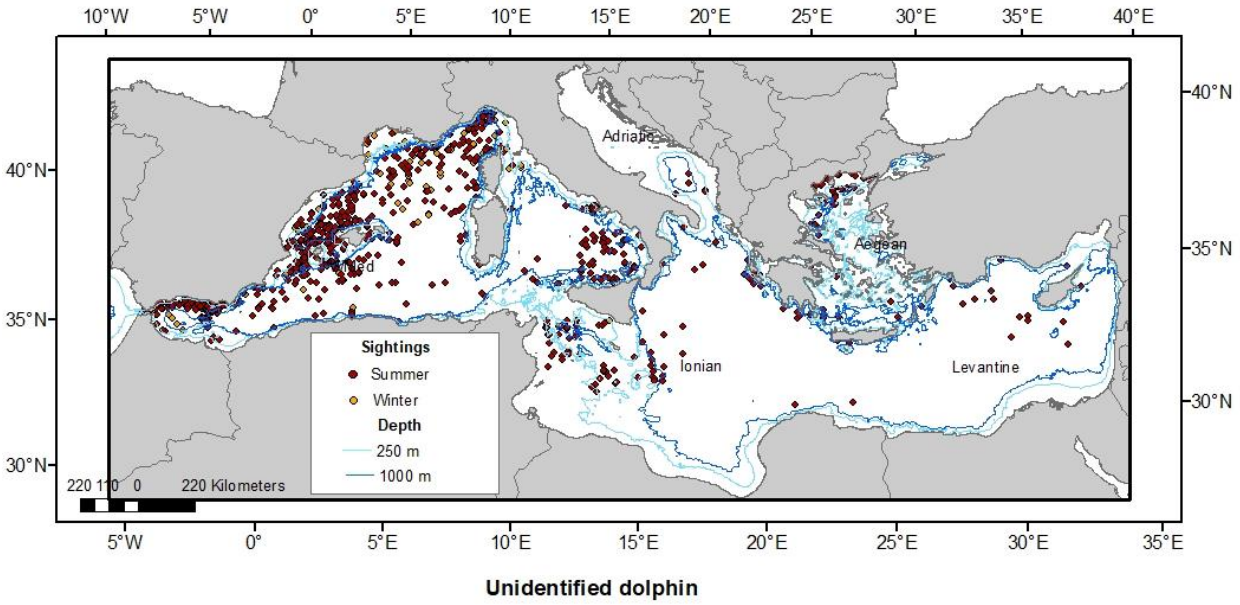

Figure 44. Observations of ambiguous species: unidentified dolphin.

The workflow of this process is shown in **Figure 45**. The data used was from the period 1999 to 2022. A file was created with all the sightings of the species with ambiguous identification. The general approach was to use three independent classification methods and look for consensus among them: a) Random forests; b) Encounter rates of individuals; and c) Spatial models of occurrence. These are described below.

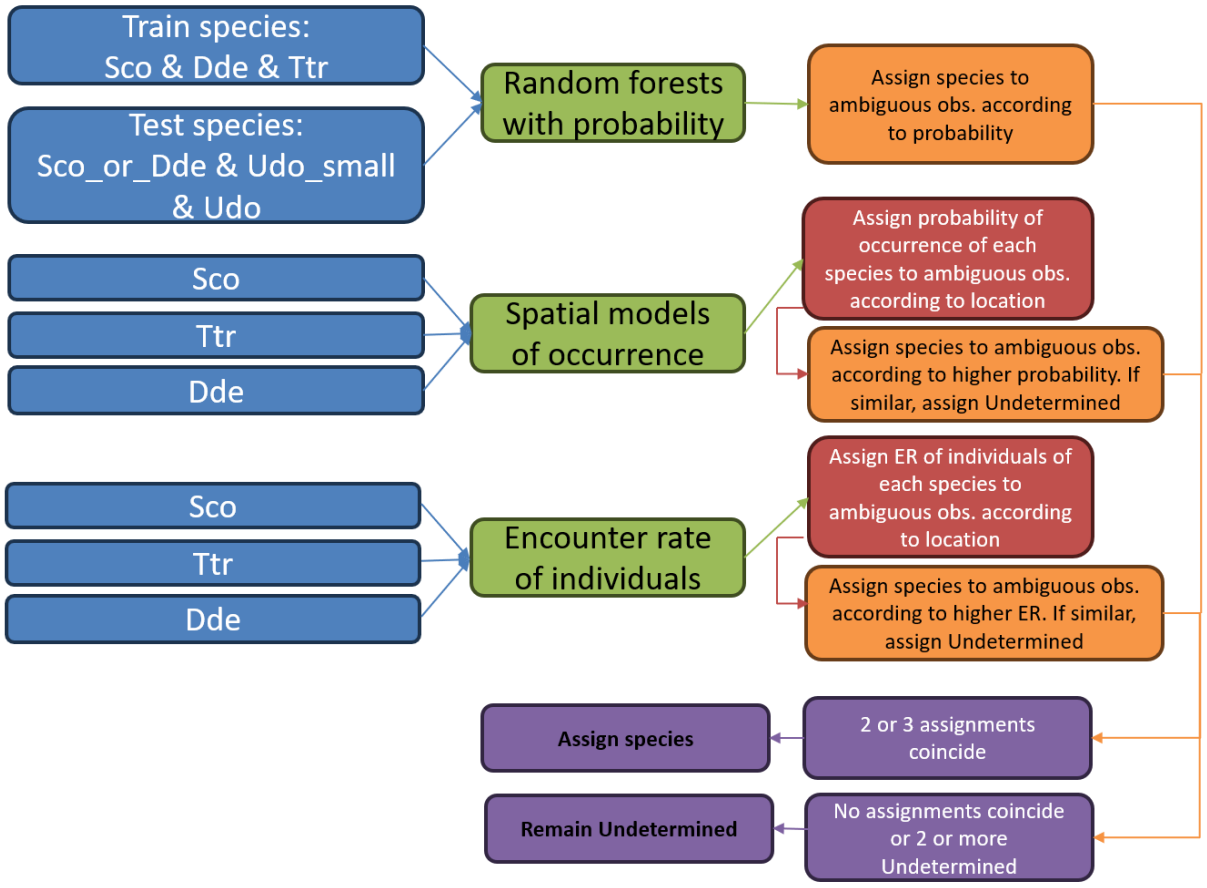

Figure 45. Workflow for the assignment of ambiguous species identifications to species (Sco = striped dolphin, Dde = common dolphin, Ttr = bottlenose dolphin, Sco_or_Dde = striped or common dolphin, Udo_small = unidentified small dolphin, Udo = unidentified dolphin).

2.9.1. Random Forests

Random forests (Breiman 2001) are an ensemble learning method used for classification, regression, and other tasks.

They create a “forest” of decision trees during training and output the mode of the classes (classification) or mean prediction (regression) of the individual trees. Each tree in the forest is built from a different bootstrap sample of the training data. This means each tree is trained on a random subset of the data. This helps in making the trees less correlated. Also, by averaging multiple deep decision trees, random forests reduce overfitting.

The main diagnostics for the random forests are:

- Sensitivity (True Positive Rate): Sensitivity measures the ability of the model to correctly identify the positive class (e.g., striped or common dolphin) among all actual positive instances.

- Specificity (True Negative Rate): Specificity measures the ability of the model to correctly identify the negative class (e.g., unidentified small dolphin) among all actual negative instances.
- Accuracy: Accuracy measures the overall correctness of the model's predictions.
- ROC (receiver operating characteristic) curve: A ROC curve is a graphical representation of a classifier's performance. It plots the True Positive Rate (or sensitivity) against the False Positive Rate (or 1-specificity) at various threshold settings.
- AUC (area under the ROC curve): The AUC is the area under the ROC curve. It provides an aggregate measure of the model's performance across all possible classification thresholds. An AUC of 0.5 suggests no discriminative power, equivalent to random guessing. An AUC closer to 1 indicates better model performance, with 1 being a perfect model.

We used the three species (common, striped, and bottlenose dolphins) as training species, and then applied the prediction to the other three classes (test species: striped or common dolphin, unidentified small dolphin, and unidentified dolphin). All diagnostics were very good for the training species, with the lowest sensitivity attributed to common dolphins (0.766). The percentage success in classifying the training species was very high for the three species, above 95% (**Table 10**, **Figure 46**, and **Table 11**). The classification of the ambiguous observations with the random forest is shown in **Table 12**. This classification was added to the file with ambiguous species sightings, so there was a field in which each sighting had the predicted identification according to the random forests.

Table 10. Diagnostics for the random forest system of classification of species.

Test	Value
Accuracy	0.971
Sensitivity (Bottlenose dolphin)	0.974
Sensitivity (Common dolphin)	0.766
Sensitivity (Striped dolphin)	0.995
Specificity (Bottlenose dolphin)	0.996
Specificity (Common dolphin)	0.998
Specificity (Striped dolphin)	0.943
AUC	0.968

Table 11. Percentage success of the random forest for the training species.

Prediction	Common dolphin	Striped dolphin	Bottlenose dolphin
Bottlenose dolphin	0.68	1.48	99.32
Common dolphin	96.31	2.67	0.43
Striped dolphin	3.01	95.85	0.25

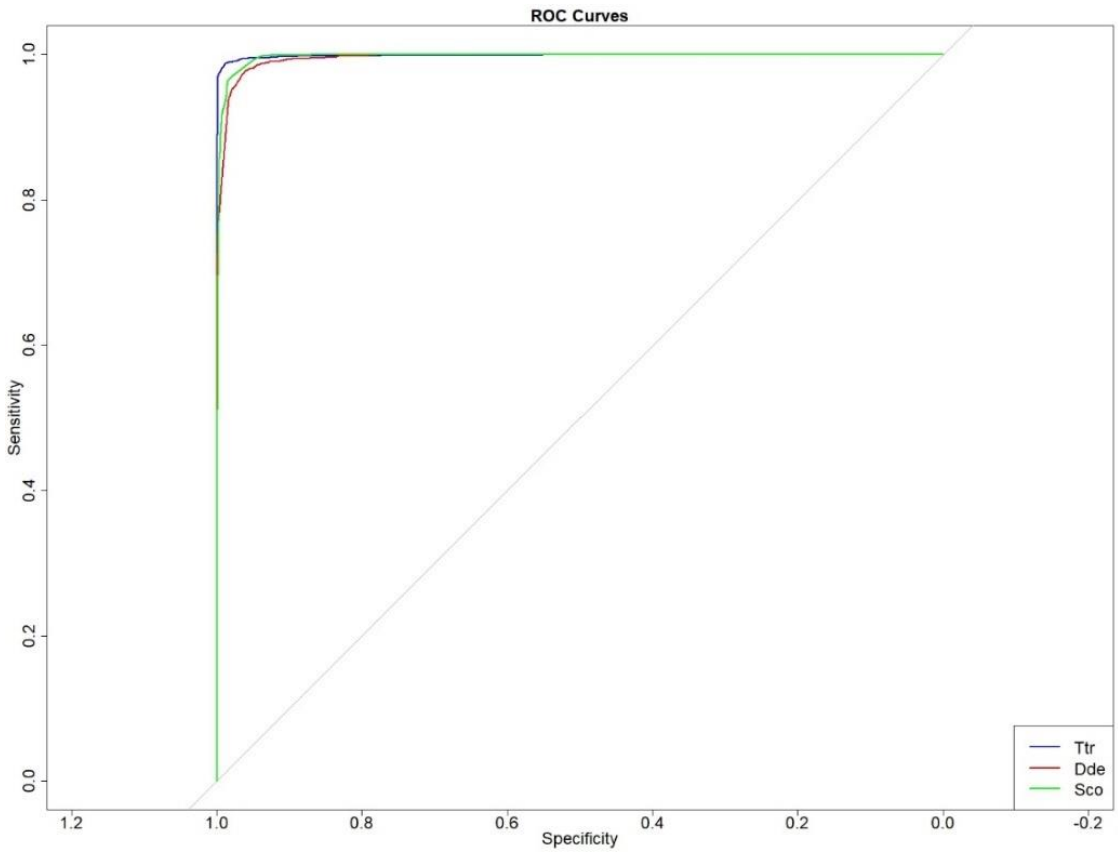

Figure 46. ROC curves for the random forest on the training species (Ttr = bottlenose dolphin, Dde = common dolphin, Sco = striped dolphin).

Table 12. Assignment of ambiguous species according to random forests.

Ambiguous species	Common dolphin	Striped dolphin	Bottlenose dolphin	Total
Striped or common dolphin	5	224	55	**284**
Unidentified dolphin	77	824	115	**1,016**
Unidentified small dolphin	15	236	27	**278**
Total	**97**	**1,284**	**197**	**1,578**

2.9.2. Encounter Rates of Individuals (ER)

Effort and sightings were aggregated in pixels of 50 x 50 km, and the encounter rate of groups and animals was calculated for each pixel. The encounter rates of animals for the three training species were extracted for the location of each sighting of ambiguous species and added as new fields to the file for the ambiguous species with the predictions from the random forest. An ER_pred (prediction from encounter rate) field was then created assigning the species with the largest encounter rate in the pixel where the sighting occurred. If the encounter rates (ERs) for the three training species were very similar, the value “Undetermined” was assigned to the ER_pred field. See the encounter rate maps under each species in **Section 3.3**, Sightings per Unit Effort.

2.9.3. Spatial Models of Occurrence

Spatial models of occurrence were created for the three training species. For these models, the segments file was modified creating a new field “occ” that was composed of either 0 (no sightings in that segment) or 1 (1 or more sightings in that segment). The offset was also transformed to be 1 for all segments. The distribution family used was binomial with link “logit.” The general shape of the equation was the same as for the density models (**Section 2.10.3**, Generalized Additive Models). The prediction was produced also in the same way as the spatial models, with the values in the range of the response variable (0–1), therefore yielding a probability of occurrence. The predicted probabilities of occurrence for the three training species were extracted for the location of each sighting of ambiguous species and added as new fields to the file for the ambiguous species. An occ_pred (prediction from occurrence models) field was then created assigning the species with the largest probability of occurrence in the pixel where the sighting occurred. If the probabilities of occurrence for the three training species were very similar, the value “Undetermined” was assigned to the occ_pred field.

Figure 47 to **Figure 52** show the predictions of occurrence of the three species, with and without sightings superimposed.

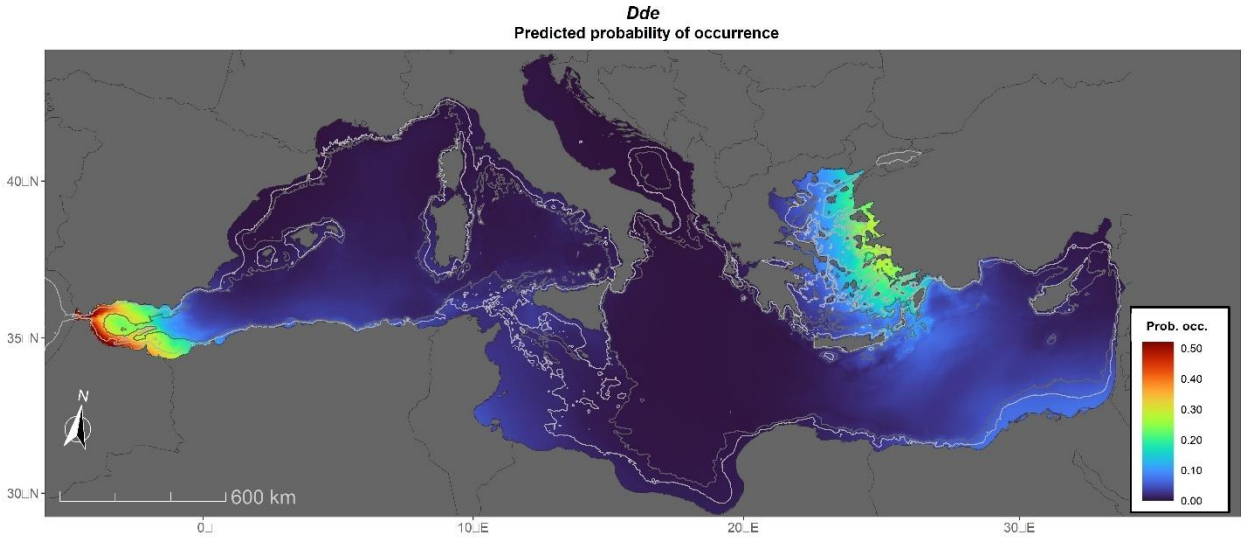

Figure 47. Prediction of occurrence of common dolphins.

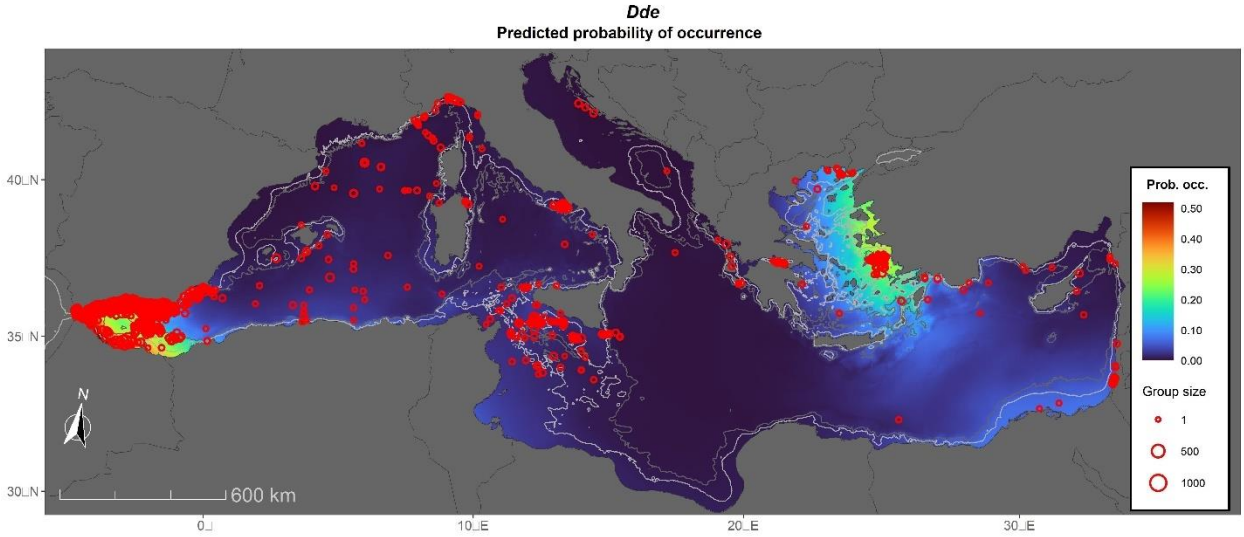

Figure 48. Prediction of occurrence of common dolphins, showing sightings.

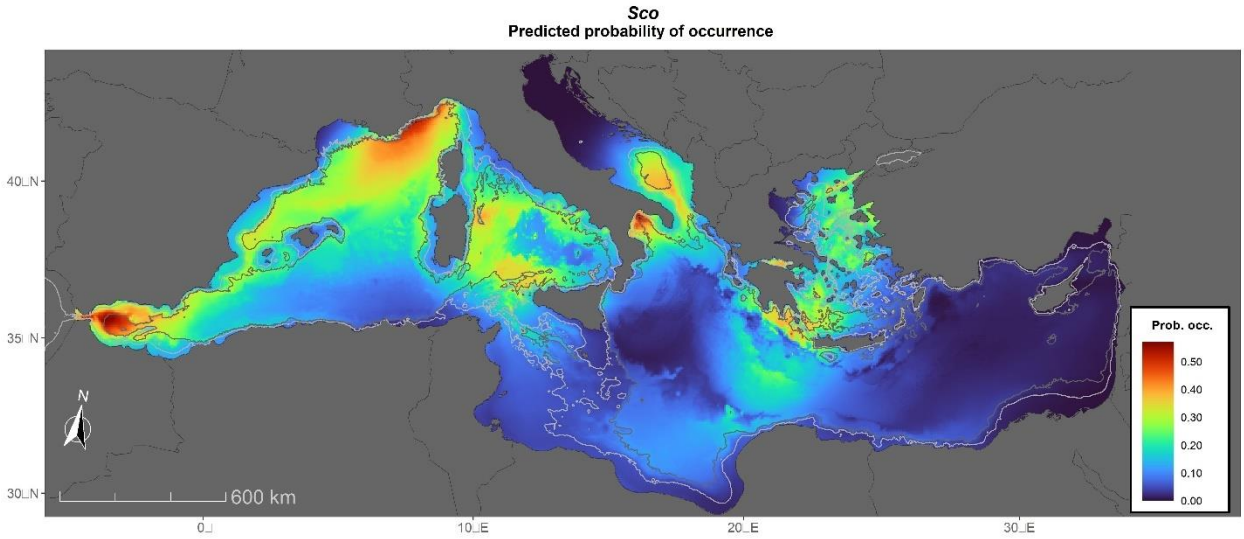

Figure 49. Prediction of occurrence of striped dolphins.

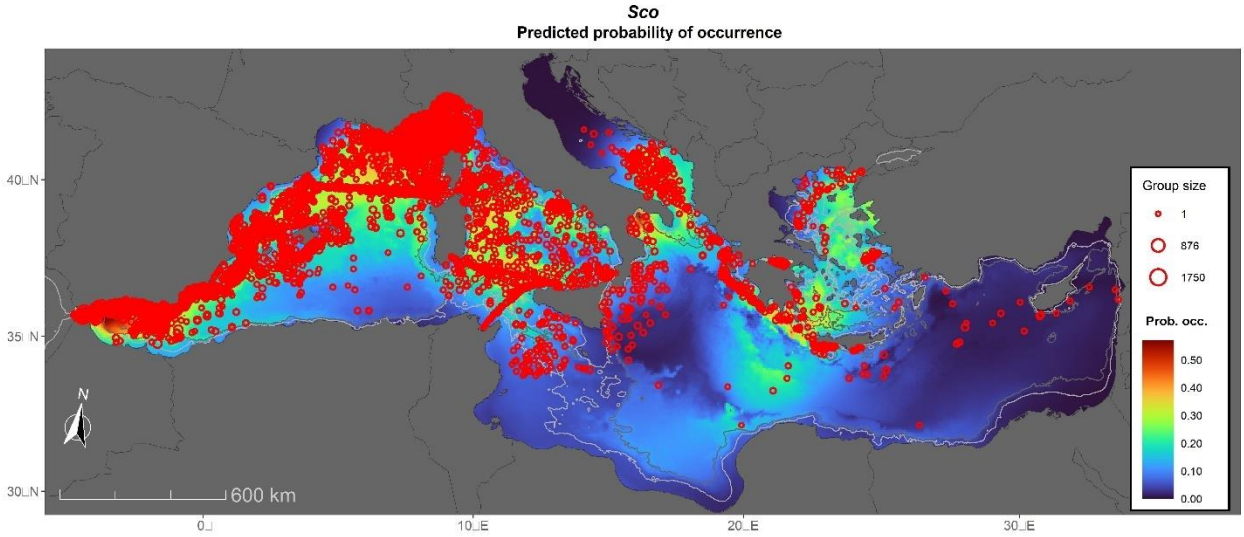

Figure 50. Prediction of occurrence of striped dolphins, showing sightings.

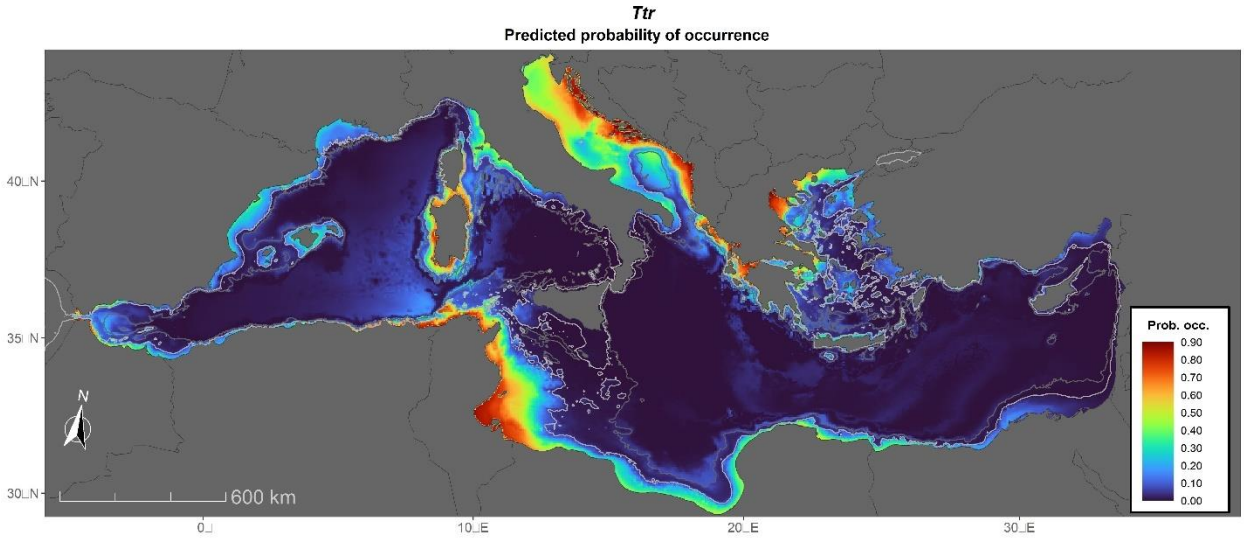

Figure 51. Prediction of occurrence of bottlenose dolphins.

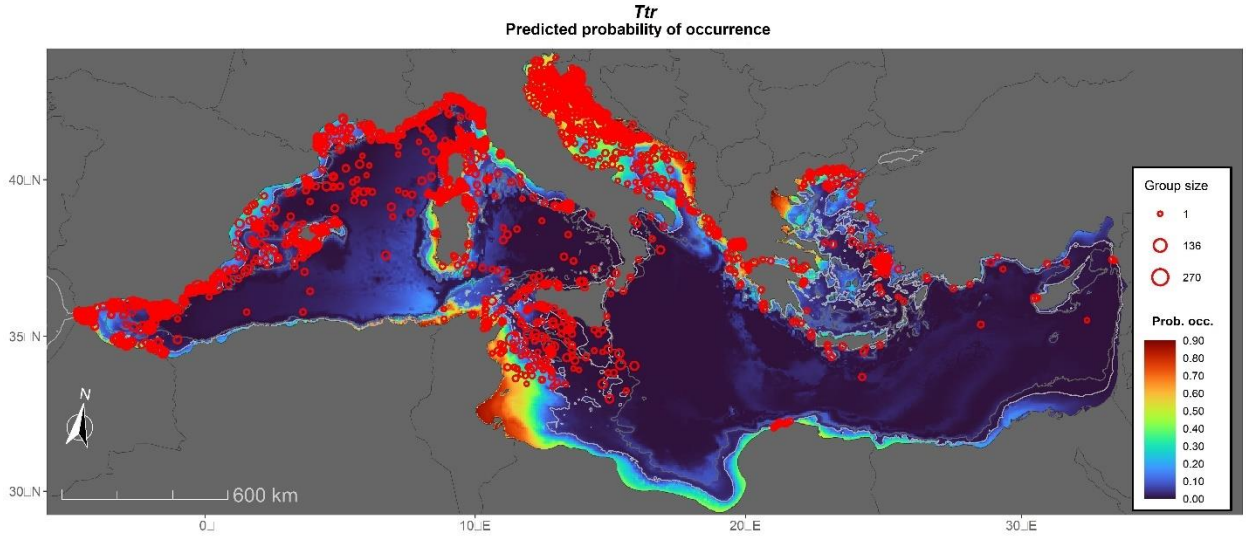

Figure 52. Prediction of occurrence of bottlenose dolphins, showing sightings.

2.9.4. Final Assignment of Species

Table 13 shows the final assignment of species (or Undetermined) to the ambiguous species after the entire workflow was completed. The sightings labeled as Undetermined were not used for any of the subsequent models, meaning that 9.4% of the ambiguous sightings were lost to analysis as they could not be assigned to any species with any level of confidence. **Figure 53** to **Figure 56** show the location of the ambiguous species assigned to common, striped or bottlenose dolphin and Undetermined, respectively. The color pattern underneath reflects the probability of occurrence for each species to which the sightings were assigned, where cooler colors indicate a low probability of occurrence and warmer colors a higher probability of occurrence.

Table 13. Final assignment of ambiguous species.

Ambiguous species	Common dolphin	Striped dolphin	Bottlenose dolphin	Undetermined	Total
Striped or common dolphin	2	250	14	18	**284**
Unidentified dolphin	34	806	65	110	**1,015**
Unidentified small dolphin	8	221	29	20	**278**
Total	**44**	**1,277**	**108**	**148**	**1,577**

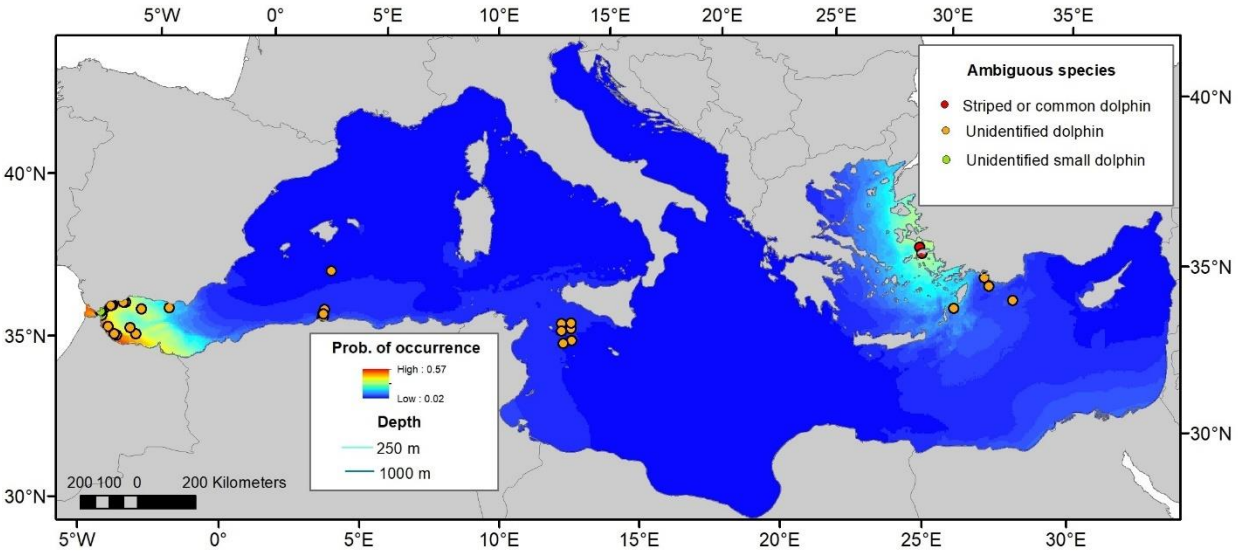

Figure 53. Location of ambiguous sightings assigned to common dolphins.Color map shows the prediction of occurrence for common dolphins.

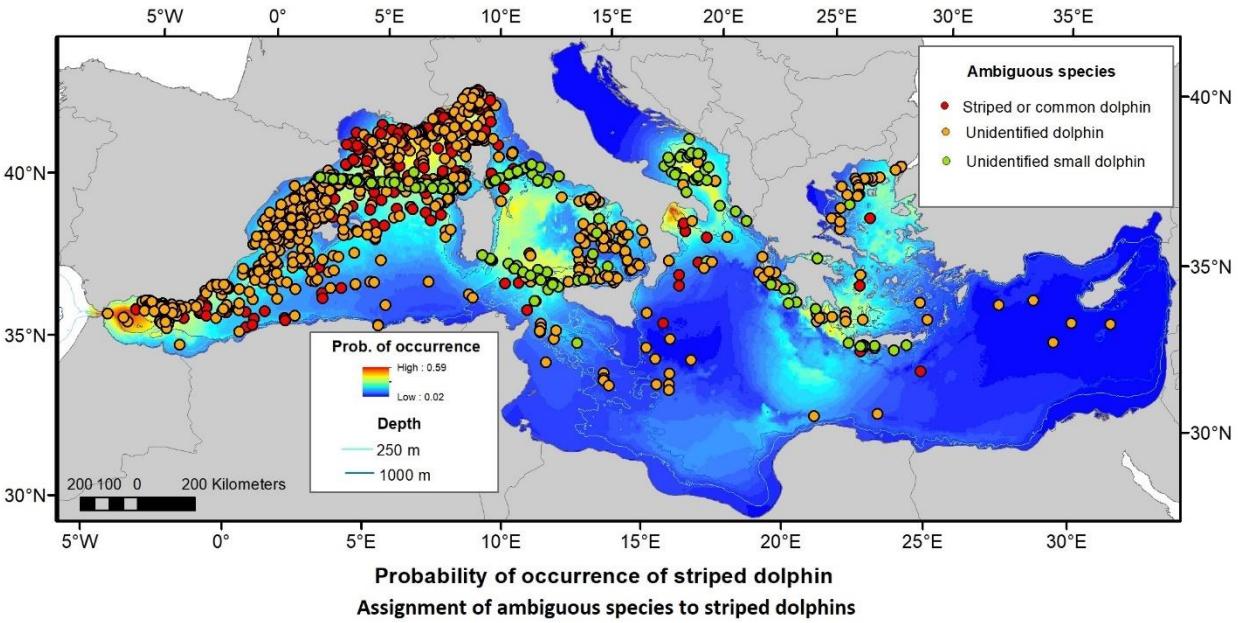

Figure 54. Location of ambiguous sightings assigned to striped dolphins.Color map shows the prediction of occurrence for striped dolphins.

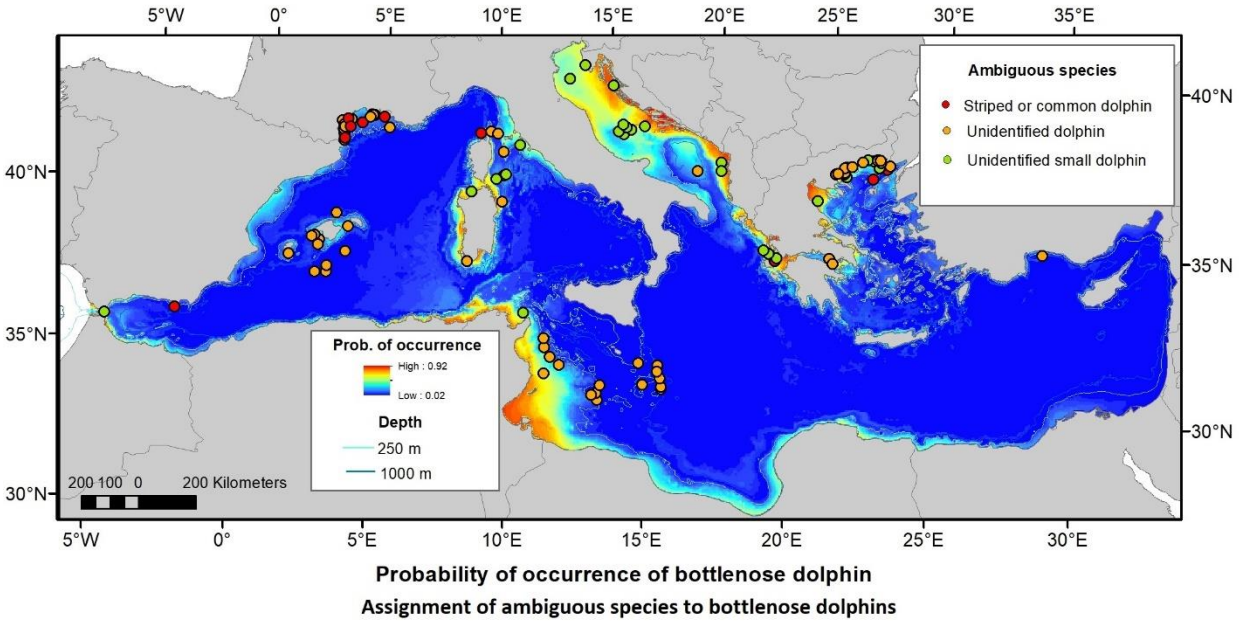

Figure 55. Location of ambiguous sightings assigned to bottlenose dolphins.Color map shows the prediction of occurrence for bottlenose dolphins.

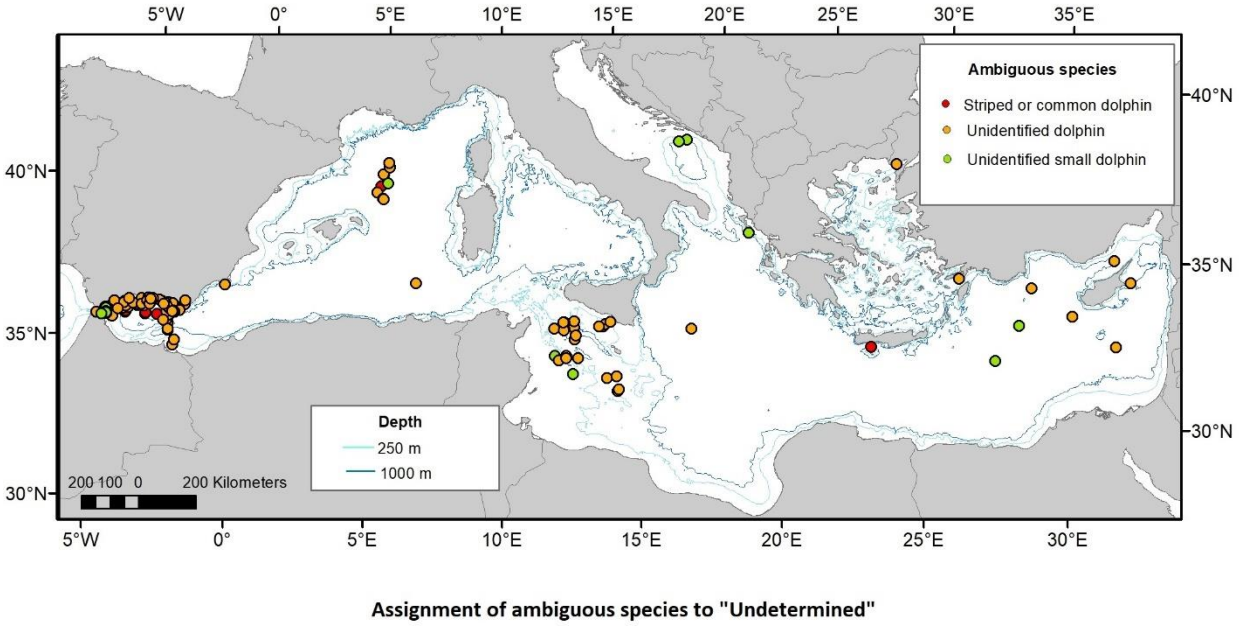

Figure 56. Location of ambiguous sightings assigned to Undetermined.

2.10. Spatial Modeling Process

Spatial modeling was the second stage of the two-stage density surface modeling approach (Miller et al. 2013).

2.10.1. Environmental Covariates

We derived covariates from remote sensing and ocean models and projected them to the 5 x 5 km grid of the study area. Physiographic or static covariates included depth, slope, and distance to shore, canyons, escarpments, and ecologically relevant isobaths (**Table 14**). Dynamic covariates included physical oceanographic and biological covariates (**Table 15**), prepared at monthly resolution. For dynamic covariates provided at higher temporal resolution, we prepared monthly rasters by aggregating time slices into monthly groups and computing per-cell means. We obtained covariate values for the survey segments by interpolating the 5 x 5 km grid at the segment centroids.

The distances to the different features in the static covariates were calculated in ArcMap 10.8.2. Dynamic covariates were downloaded from the online Copernicus Marine Service (or Copernicus Marine Environment Monitoring Service) of the Copernicus Programme of the European Union (see details in **Table 15**). Datasets were downloaded via ftp-server transfer of original files in the multidimensional NetCDF format. A custom-built model was created in ArcGis Pro 2.5 to geoprocess the original NetCDF files, iteratively extract the necessary covariates, crop the resulting data to the necessary extent, obtain monthly averages and store the output.

The resulting files were resampled to match the spatial resolution of the sampling grid and to align them with it. Before further analysis in R, the software for statistical programming, all covariates were assigned to the centroid of each grid cell.

Given the strong spatial-temporal heterogeneity of the survey effort in both the Mediterranean and the Black Seas, we used climatologies (values per pixel averaged over all the years for each month) as dynamic covariates. These climatological covariates smooth out the inter-annual variability, but also decrease the potential biases created by the heterogeneous survey effort (e.g., some areas heavily surveyed in some months/years and other areas in different time periods).

Table 14. List of candidate static environmental covariates for the density models.

Name	Description	Origin
Lat	Latitude (º)	ArcMap
Lon	Longitude (º)	
Depth	Depth of the sea floor (m)	GEBCO (https://www.gebco.net)
Dist25	Distance to the 25 m isobath	
Dist50	Distance to the 50 m isobath	
Dist100	Distance to the 100 m isobath	
Dist250	Distance to the 250 m isobath	
Dist500	Distance to the 500 m isobath	
Dist1000	Distance to the 1000 m isobath	
Dist2000	Distance to the 2000 m isobath	
Dist3000	Distance to the 3000 m isobath	
DistLand	Distance from the nearest coast	
SlopePct	Slope of the sea floor in percentage	Derived from depth from GEBCO (https://www.gebco.net)
DistToAtl	Distance to the Atlantic	Calculated with MGET (Roberts.et al. 2010)
WindFetch	Distance from all coasts (360º)	
DistAbyss	Distance from the Abyss	Derived from geomorphic features from https://pacific-data.sprep.org/dataset/global-seafloor-geomorphic-features-blue-habitats
DistSlope	Distance from the Slope	
DistShelf	Distance from the Continental Shelf	
DistCan	Distance from canyons	
DistEsc	Distance from escarpments	
DistCanEsc	Distance from canyons and escarpments	

Table 15. List of candidate dynamic environmental covariates for the density models.

Name	Unit	First year	Description	Origin
Chl	mg m-3	1998	Concentration of Chlorophyll in sea water	Mediterranean Sea Biogeochemistry Reanalysis
Phytoplankton	mmol m-3	1999	Concentration of Phytoplankton Biomass in sea water	
Primary prod	mg m-3 day-1	1999	Net primary production of biomass expressed as carbon per unit volume in sea water	
Sst sd	°C	1981	Sea surface temperature-standard deviation	Reprocessed Mediterranean dataset Sea Surface Temperature
Sst	°C	1981	Sea surface temperature-mean	
Salinity	Ppt (gr/Kg)	1987	Salinity	Mediterranean Forecasting System (Med-Physics) dataset
Ssh	m	1987	Sea surface height	
Current_E_vel	m s-1	1987	Eastward ocean current velocity	
Current_N_vel	m s-1	1987	Northward ocean current velocity	
Mix_layer-thickness	m	1987	Ocean mixed layer thickness defined by density	
Chl_front_dist	km	1998	Distance to nearest major front	European Centre for Medium-Range Weather Forecasts, Ocean Front Datasets
Chl_fron_strength	log Chl mg m-3 km-1	1998	Frontal gradient magnitude	
Sst_front_dist	km	1991	Distance to nearest major front	
Sst_front_strength	°C km-1	1991	Frontal gradient magnitude	

We tested for collinearity among covariates and established 0.7 and -0.7 as threshold values to identify correlations. **Figure 57** shows the correlations matrix. Covariates were also grouped as "families." For the static covariates we had the following families:

- Lat
- Lon
- Depth
- Depth deep: Dist500, Dist1000, Dist2000, Dist3000, DistAbyss, DistSlope
- Depth shallow: Dist25, Dist50, Dist100, Dist250, DistLand, DistShelf, WindFetch
- Slope
- Distance contours: DistCan, DistEsc, DistCanEsc

For the dynamic covariates we had the following families:

- Sst
- Sst_sd
- Sst fronts: Sst_front_dist, Sst_front_strength
- Chl: Chl,Primary_prod
- Chl fronts: Chl_front_dist , Chl_front_strength
- Salinity
- Ssh
- Mix_layer_thickness
- Current velocities: Current_E_vel, Current_N_vel

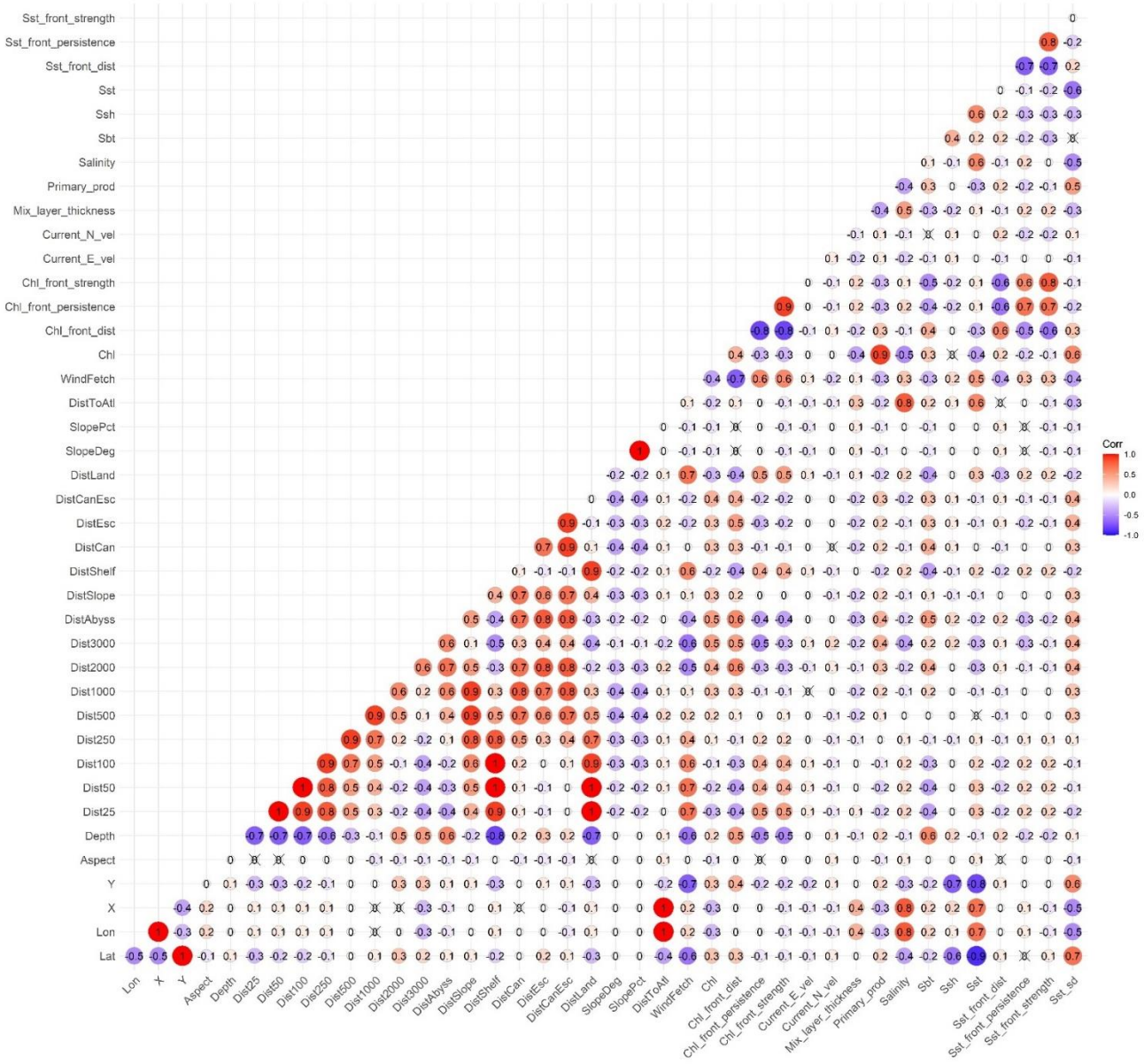

Figure 57. Collinearity matrix plot with all the covariates, static and dynamic.

During model selection, when generating candidate models, we avoided including two or more collinear covariates or covariates from the same "family" in a single model, i.e., if any two covariates (even if they were from different "families") had a collinearity value of 0.7/-0.7 or greater, they were not selected for use in the same model. As such, two different models would be fitted, one using one of the covariates of the pair and another using the other paired covariate.

2.10.2. General Procedure

We used GAMs to fit the statistical relationships that explain the observed abundance from the covariates at the segment level. The workflow was consistent across each species and

proceeded as shown in **Figure 58**. Model fitting and selection was carried out with custom R code (R version 4.2.2, R Core Team 2022). We used the following procedure:

1. We fitted a series of univariate models, one for each covariate, and predicted each over the study area raster.
2. We examined the results of step 1 and discarded covariates that either: (a) did not have any effect on the response variable (evidenced by an estimated degrees of freedom <0.1, i.e., a flat horizontal line for the smooth plot); or (b) explained less than 1% of deviance.
3. Using the remaining set of candidate covariates, we fitted models to all combinations of these covariates, excluding those combinations that would include covariates determined to be collinear or in the same family.
4. We ranked these candidate models by AIC, predicted them, and examined the results to select the final model.

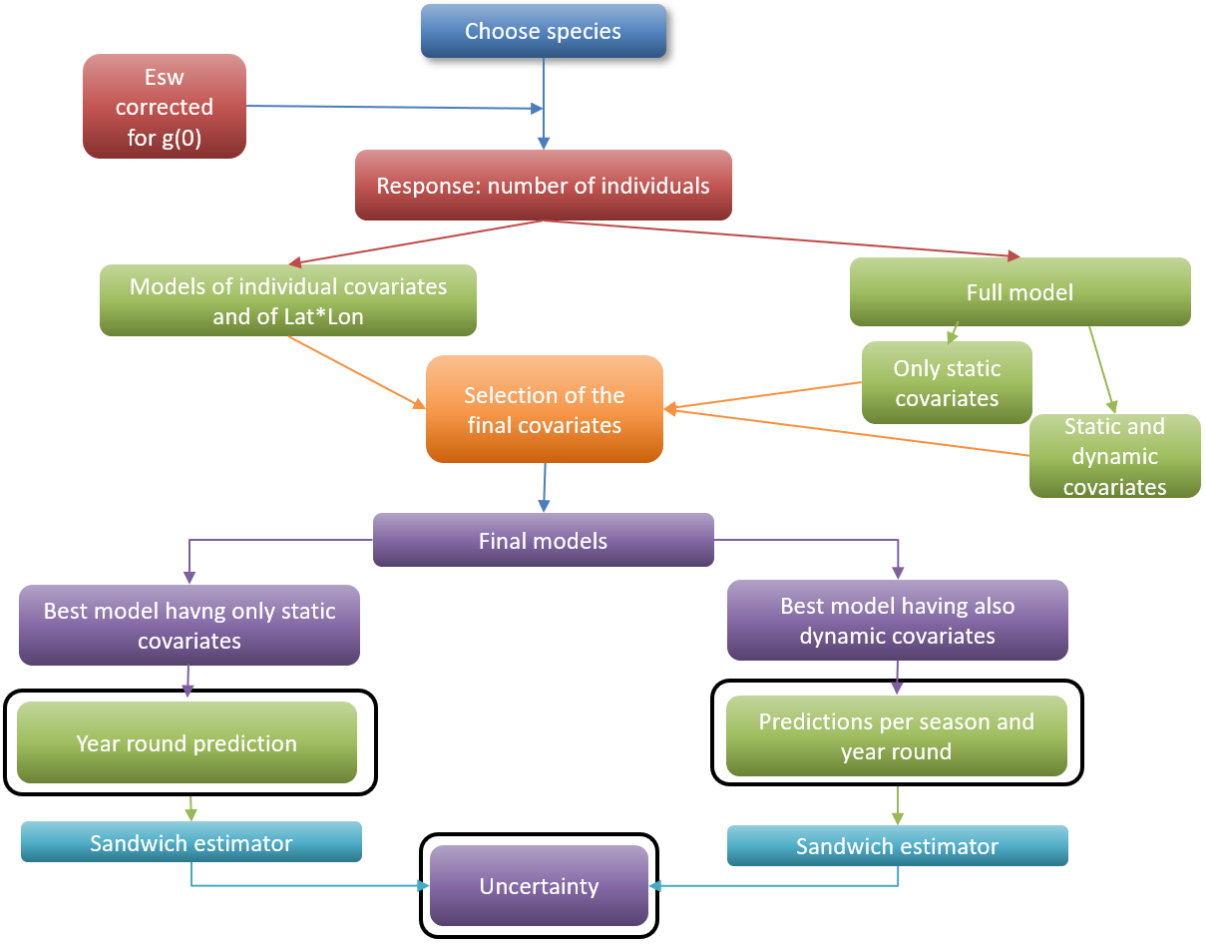

Figure 58. General workflow of the spatial modeling.

2.10.3. Generalized Additive Models

GAMs were trained on the survey effort segments. The response variable was the count of individual animals of the target species observed on each segment. The effective searched area was calculated as *esw x 2 x L*, where L was the length of the segment. The effective searched area was then provided as an offset, corrected for availability and perception bias.

All models used a logarithmic link function and a Tweedie error distribution to allow for over-dispersion. The general structure of the model was:

$$n_i = \exp\left[\ln(a_i) + \theta_0 + \sum_k f_k(z_{ik})\right]$$

where n_i is the number of animals in the i^{th} segment, the offset a_i is the corrected effective area searched for the i^{th} segment, Θ is the intercept, f_k are smoothed functions of the explanatory covariates, and z_{ik} is the value of the k^{th} explanatory covariate in the i^{th} segment.

We used the R package mgcv and fitted models of the form:

gam(*resp var ~ s(var1,k=6,bs="ts") + s(var2,k=6,bs="ts")* + …… + log(offset), family="tw", method=REML, data)

where *resp var* is the response variable to be modeled (i.e., the count of individuals), *s* indicates a thin plate smoothing spline, and *k* is the maximum allowed complexity of the basis functions in the spline (degrees of freedom = *k*-1). bs="ts" and family="tw" specified that thin-plate regression splines with shrinkage smoothers and the Tweedie distribution be used. "REML" specified that models be fitted using restricted maximum likelihood.

For all covariates other than Lon and Lat, we used thin-plate regression splines with shrinkage to allow smooth term effects to be removed from the model during fitting. We restricted the basis size to 6 for each smooth term to avoid excessive "wiggliness." We used restricted maximum likelihood (REML) as the criterion for estimating smooth parameters because it penalizes overfitting and leads to more pronounced optima (Wood 2011).

We computed and compared AIC values of all candidate models. We selected the model we judged best. Usually this was the model with the lowest AIC, but we also considered models with similar AIC (within 2 units) that had higher % deviance explained or significance of terms. We also visually inspected the prediction maps for each model and discarded those that produced unrealistic extrapolations. Model selection based on AIC effectively reduces overfitting by penalizing models with excessive complexity (Wenger and Olden 2012). We fitted all GAMs in R with the mgcv package (version 1.8.17) (Wood 2014).

Model fitting was tested for segments including years from 1991 to 2022, and 1999 to 2022 for the Mediterranean, and from 2001 to 2022 for the Black Sea, with covariates that were available for those periods.

2.10.4. Winsorizing

The problem of “edge effects” in a density surface model is a common issue, particularly when there is an extrapolation of the prediction. Extrapolation can occur when predictions are made beyond the sampled ranges of covariates, resulting in predictions for novel ranges of individual covariates or novel combinations of covariates. This often occurs when models are predicted beyond the geographic areas that were surveyed, but even when the prediction area is cropped to tightly fit surveyed areas, there can always be portions that have extreme values not sampled or poorly sampled, which, depending on the shape of the smooth function, may still create an edge effect. This problem has higher probability of occurring in very large study areas like the one considered here.

To minimize this problem, we used a method called “Winsorizing” (Dixon and Yuen 1974). Winsorizing is not equivalent to excluding data, but rather to censuring data, where the extreme values are replaced (instead of discarded) by certain percentiles or values. For model fitting, R can use the functions pmax() and pmin(), which return the “parallel maxima” or “parallel minima” of two or more input vectors. For example:

```
model<- gam(resp.var~s(pmax(pmin(X,20)),10))
```

means that the model will take whatever is larger, the value of X or 10, and whatever is smaller, the value of X or 20.

We applied this method to the covariates that tended to create these edge effect problems, using the 0.999 percentile as value for pmax, and 0.001 percentile as value for pmin.

2.11. Spatial Modeling Predictions and Uncertainty

2.11.1. Density Predictions

The final phase of the modeling process was to use the final GAMs to predict species density across both space and time. For all species, densities (individuals per 25 km²) were predicted initially at a monthly time step for all months averaged over all years, and subsequently for the two full seasons: summer (May to October) and winter (November to April). These seasonal climatologies of density are known as “densitologies.”

To create these dynamic predictions, we used the fitted relationships between species abundance and the environmental and spatial covariates to predict smooth density surfaces across the seascape. We predicted these values on a 5 x 5 km grid raster, the extent of which corresponds to the spatial extent of the whole final study area.

The problem of “edge effects” in a density surface model is a common issue, particularly when there is an extrapolation of the prediction (Miller et al. 2013). Extrapolation can occur when predictions are made beyond the sampled ranges of covariates, resulting in predictions for novel ranges of individual covariates or novel combinations of covariates (see **Section 2.12** on extrapolation tests). This problem has higher probability of occurring in very large study areas like the one considered here, so we used the “Winsorizing” method to minimize this problem (**Section 2.10.4**).

When multiple blocks were modeled separately, the final prediction rasters for all blocks were merged, and their abundances were summed.

2.11.2. Uncertainty from the Spatial Model

The topic of how to estimate density surface model uncertainty and summarize density and uncertainty is the focus of a manuscript (Miller et al. 2022) we developed with the DenMod working group (https://synergy.st-andrews.ac.uk/denmod/). The description of the application of those methods, known as "sandwich estimator," to the Mediterranean and Black Sea density models are the same as used for the Atlantic Fleet Training and Testing (AFTT) models (Roberts et al. 2023) and the 6th Fleet density models (Cañadas et al. 2021). For complete details of those methods, please see the published paper.

To visualize parameter uncertainty from the spatial stage of the model, we produced maps of the mean CV. To do this, we first generated monthly and seasonal maps of standard errors (SE) that spanned all the years, similar to how we generated mean monthly and seasonal maps of density but using an approach that: (1) accounted both for the estimated errors in GAM parameter estimates and the interannual variability in dynamic covariates, and (2) assumed that Navy activities would occur in a random year rather than across the entire modeled period (yielding a statistic that was akin to a standard deviation). Please see Roberts et al. (2021) for methodological details. We then divided these monthly and seasonal maps of SE by the monthly and seasonal maps of mean density for every grid cell to obtain monthly and seasonal maps of CV.

When multiple blocks were modeled separately, the final CV rasters for all blocks were merged. The overall CV was calculated using the following procedure:

- First, the variance for each block was determined by summing the squared SE for all individual blocks.
- Then, the total standard error for the combined blocks was computed by taking the square root of this sum of squared SE values.
- Finally, the CV for the total was calculated as the ratio of the total SE to the total predicted abundance, which was obtained by summing the predictions across all blocks.

For the calculation of the 95% CI (95% CI), we assumed that the data were log-normally distributed. In this process, the 95% CI is derived by applying a multiplicative factor (c) to the abundance, based on the CV:

$$c = \exp\left(1.96 \times \sqrt{\log\left(1 + CV^2\right)}\right)$$

The lower and upper bounds of the CI are then determined by dividing and multiplying the abundance by this factor, respectively. This approach relies on the assumption that the abundance data follows a log-normal distribution, which accounts for skewness and multiplicative variability commonly observed in ecological and abundance data.

For the NMSDD, we prepared seasonal maps of density and CV for each species. The decision to use only the seasonal maps, and not the monthly ones, was due to the high spatial-temporal heterogeneity of the survey effort across months, which yielded unrealistic high density variability among months in these two almost enclosed basins.

2.11.3. Predicted Abundances, Challenges, and Exceptions

For each species, total predicted abundances were obtained by summing predicted abundances across all cells of the study area. Subtotals were also obtained for several blocks in the Mediterranean Sea. We implemented the sandwich estimator to compute SE of the total abundance estimates for arbitrary sets of cells so that we could get an SE for each of the Navy's areas of interest and an SE for the entire study area. Raster maps were created with both the predictions and the CVs. This was done for each season separately and for both seasons pooled together.

There were some special cases where we had to adapt our results to existing abundance estimates. The most extreme cases in which areas were totally excluded from the modeling and published information was used to assign abundances were:

- Marmara Sea: There were insufficient observations in the Marmara Sea to model any of the three species. Consequently, we applied a uniform distribution based on the published abundance estimates from a line transect survey for all three species (Dede et al. 2022).
- Gulf of Ambracia (Greece): a semi-enclosed gulf with a local population of bottlenose dolphins very well studied for many years. We applied the best estimate provided in Gonzalvo et al. (2016).
- Gulf of Corinth (Greece). A semi-enclosed gulf with very well studied local populations of striped, common and bottlenose dolphins and one single individual Risso's dolphin. The estimates assigned to this gulf were extracted from the IUCN Red List assessments. For the common dolphin Gulf of Corinth subpopulation: Bearzi et al. (2020). For the striped dolphin Gulf of Corinth subpopulation: Bearzi et al. (2022). For the bottlenose dolphins and the single Risso's dolphin: Bearzi et al. (2016).

In the Strait of Gibraltar we produced models for all species (except Risso's dolphins and Cuvier's beaked whales, which have never been observed there). Our abundance estimates for three species—killer whales, pilot whales and bottlenose dolphins—were scaled to exactly match those from the long-term ongoing photo-identification work for these species in the Strait, keeping the distribution patterns from our models. The estimates for long-finned pilot whales were obtained from Ouled-Cheikh et al. (2023). The estimates for bottlenose dolphins and killer whales were personal communication from the expert in the region (de Stephanis, pers. Comm.).

Estimating abundance of sperm whales in the eastern Mediterranean posed severe challenges. After discussions with regional experts, it became clear that the visual observations occurred following initial acoustic detections. This led to a significant underestimation of the esw,

consequently inflating the abundance estimate. We corrected this by applying esw values derived from acoustic surveys in the Hellenic Trench, stratified by group sizes (Gkikopoulou 2012).

The Adriatic Sea presented unique challenges for modeling. The majority of observations came from long-term photo-identification studies along the Croatian and Slovenian Coasts on the eastern side, which lacked distance data. To address this, we initially assigned esw values from similar platforms to these surveys. Of the 2,965 total bottlenose dolphin observations in the Adriatic, only 435 (15%) included distance data—all from aerial surveys—while the remaining 2,530 (85%)—mostly from photo-identification surveys—did not. This meant that any inaccuracies in the esw assignments could significantly skew abundance estimates. Additionally, the eastern Adriatic coastline is complex, with numerous small islands. Aerial surveys often underestimate abundance in these coastal areas due to the limited time spent over narrow coastal waters. To balance these issues, we included all aerial surveys and only the most recent year of data from each photo-identification study, which reduced the photo-identification observations to 206.

For monk seals, the abundance estimates used during the process of designating Important Marine Mammal Areas (IMMAs) in the Mediterranean Sea (as detailed on the IMMA e-Atlas, https://www.marinemammalhabitat.org/imma-eatlas/) were applied as a uniform distribution, similar to our approach for the Gulfs of Ambracia and Corinth. Additionally, we incorporated the most recent range distribution area for monk seals, as defined by Karamanlidis (2023), by creating a buffer around the IMMAs. Due to the lack of precise abundance estimates for monk seals outside of these designated areas, we arbitrarily selected a value equal to 5% of the total abundance from all IMMAs and distributed it uniformly throughout the broader range distribution area beyond the IMMAs.

2.12. Characterizing Extrapolation from the Spatial Model

In addition to mapping CVs, we mapped the extent of interpolation *versus* univariate and multivariate extrapolation throughout the study area for each final species model. Extrapolation can occur when predictions are made beyond the boundaries of the study regions where the data used to fit density surface models were originally collected (e.g., Mannocci et al. 2015; Bouchet et al. 2020), resulting in model prediction for novel ranges of individual covariates (univariate or NT1 extrapolation) or novel combinations of covariates (multivariate or NT2 extrapolation) (Mesgaran et al. 2014). Following Mesgaran et al. (2014), we first calculated univariate NT1 extrapolation by calculating a univariate distance (UD_{ij}):

$$\mathrm{UD}_{ij} = \frac{\min\{\mathrm{P}_{ij} - \min(\mathrm{r}_j), \max(\mathrm{r}_j) - \mathrm{P}_{ij}, 0\}}{\max(\mathrm{r}_j) - \min(\mathrm{r}_j)}$$

where P_{ij} is the value of grid cell *i* from the projection data (P) over the covariate *j* and $\min(r_j)$ and $\max(r_j)$ are the minimum and maximum values for the same covariate, *j*, over the effort segments that serve as the reference data (r), respectively. The calculation returns negative values for points that are beyond the ranges of the reference covariates and zero values for points within the range of reference covariates.

Then, for the remaining points that were inside the range of the reference data (i.e., with NT1 = 0), we tested for novel covariate combinations (i.e., multivariate NT2 novelty) using the Mahalanobis distance metric (D^2). That is, for every point r in the reference data, we calculated:

$$D_r^2 = (r_i - \bar{r})' C^{-1} (r_i - \bar{r})$$

The maximum distance found in the reference data ($D_{r_{max}}^2$) was used to identify the edge of the data (e.g., dashed red ellipse in **Figure 59**).

We then calculated the NT2 statistic for each cell, based on its Mahalanobis distance to the edge of data (ellipse) using the following formula (Mesgaran et al. 2014):

$$NT2_i = \frac{D_{ei}^2}{D_{r_{max}}^2}$$

where D_{ei}^2 is the Mahalanobis distance of *ei* from the center of the reference data (i.e., r):

$$D_{ei}^2 = (e_i - \bar{r})' C^{-1} (e_i - \bar{r})$$

NT2 can range from zero up to unbounded positive values. NT2 values between zero and one indicate similarity (in both univariate range and multivariate combination), with values closer to zero being more similar. Values larger than one indicate novel combinations of covariates (Mesgaran et al. 2014).

Following Bouchet et al. (2020), once NT1 and NT2 statistics were calculated for each final species model and rasters were produced, we plotted overlays of the two statistics to create an ExDet raster whereby all cells are assigned values based on the NT1 and NT2 results, where univariate extrapolation is indicated by values less than one, cells in range of covariates (e.g., no extrapolation) are indicated by values between zero and one, and cells with multivariate extrapolation are indicated by values greater than one.

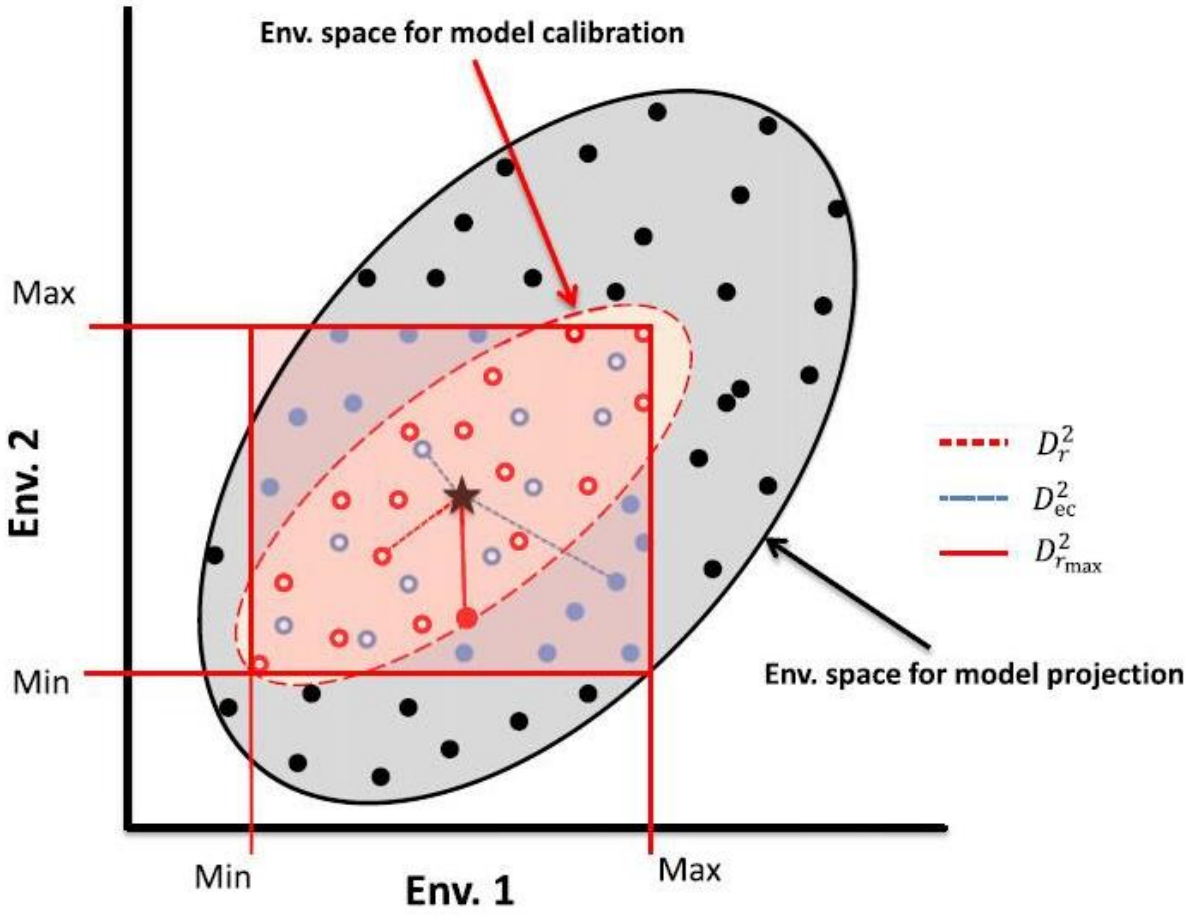

Figure 59. Schematic of ExDet extrapolation (from Mesgaran et al. 2014).

Note: "Schematic presentation of the ExDet tool for the detection and quantification of extrapolation in correlative species distribution models using two hypothetical environmental variables. Red open circles represent the distribution records that define the sampled environmental space (small pink oval) used for model calibration, and the red rectangle shows the univariate coverage of this space. Black and blue solid circles and blue open circles represent grids on which the model is going to be projected and thus define the projection environmental space (large grey oval). All grids from the projection domain that are outside the rectangle (black solid circles: Type 1 novelty; NT1) are trimmed, and the degree of their dissimilarity is calculated using the NT1 component of the tool. The remaining projection grids may represent covariate combinations not captured (blue solid circles: Type 2 novelty; NT2) or captured (blue open circles) in the sampled environments of calibration data. For each grid within the rectangle, the Mahalanobis distance (D2) is calculated with respect to the center of the environmental space of the calibration data (black solid asterisk). The maximum distance found in the calibration data (D2r max: red line with corresponding point shown as solid red circle) is then used to delineate the 'boundary' of data (dashed red ellipse). If the Mahalanobis distance of a point in the projection space (D2 ei) is larger than the D2r max, that point represents a novel environment (blue solid circle). For both analogous and novel points, a multivariate combination novelty index (NT2) is then calculated." (Mesgaran et al. 2014).

2.13. Sightings per Unit Effort

For each species, 50 x 50 and 100 x 100 km grid cells were created for the study area and the offset (L*2*esw) (km^2) and number of sightings were summed for each grid cell for the overall effort and for each month and season. The sum of sightings per grid cell and effort (km^2) per grid cell were then converted to rasters in R (R Core Team 2022). The package ggplot2 (Wickham 2016) was used to create Sightings Per Unit Effort (SPUE) maps. The maps of sightings per unit effort (also called Encounter Rate) in grid cells of 50 x 50 km resolution for the Black Sea and 100 x 100 km resolution for the Mediterranean Sea are provided in **Appendix B**.

3. Results

3.1. Detection Functions

A final working detection function model was chosen typically based on AIC score. However, for some species there were several detection function models within two AIC units of the “best” model (not shown). In these cases, we chose the model with the lowest CvM test, indicating a better fit. Though we chose one “best” model, we acknowledge several plausible models exist for several species.

In cases with simpler model forms, i.e., one covariate, we can easily interpret the influence of the covariate on the detection function. As the complexity of the model increases—when multiple covariates are used—this becomes more difficult. In each species/platform combination, we have depicted the best detection function, along with the Q-Q plot evaluating the fit. This diagnostic can be combined with the tabular values for an indication of overall fit. Plots of the detection functions and the Q-Q plots are provided in Appendix C.

Summary tables with the final model for the detection function for each species/guild and platform group are provided below.

Some species were observed from all platform groups, and some from only a few. In some cases, some platforms had enough observations for a particular species to be modeled on its own, but in others there were too few, or the performance of the detection function was much better when pooled together with other similar species, so a guild was used to derive the esw for target species.

Table 16 shows the number of observations available for the detection functions of each species from aerial surveys; **Table 17** shows the number of observations available for the detection functions of each species from shipboard surveys; and **Table 18** shows the total number of observations available for the detection functions of each species. All these detection functions include data from both the Black Sea and the Mediterranean Sea.

The acronyms used in the following tables for species/guilds are described in **Table 3**.

Table 16. Number of observations for detection functions from aerial surveys (n.dist = number of observations with distance data; n.nodist = number of observations without distance data; total number of observations; n.df = number of detection functions modeled).

Species/Guild	Platform	n.dist	n.nodist	n.total	n.df
Bottlenose dolphin	Plane	1,331	26	1,357	6
Common dolphin	Plane	1,134	11	1,145	7
Cuvier's beaked whale	Plane	20	0	20	2
Fin whale	Plane	213	3	216	3
Harbor porpoise	Plane	1,047	0	1,047	3
Long-finned pilot whale	Plane	61	4	65	2
Risso's dolphin	Plane	246	6	252	5
Sperm whale	Plane	90	1	91	1
Striped dolphin	Plane	3,249	64	3,313	5
Striped or common dolphin	Plane	592	0	592	2
Unidentified beaked whale	Plane	3	0	3	1
Unidentified dolphin	Plane	493	27	520	3
Unidentified small dolphin	Plane	72	2	74	2
All	**Plane**	**8,551**	**144**	**8,695**	**42**

Table 17. Number of observations for detection functions from shipboard surveys (n.dist = number of observations with distance data; n.nodist = number of observations without distance data; total number of observations; n.df = number of detection functions modeled).

Species/Guild	Platform	n.dist	n.nodist	n.total	n.df
Bottlenose dolphin	Ship	2,026	8,432	10,458	30
Common dolphin	Ship	3,340	551	3,891	30
Cuvier's beaked whale	Ship	387	482	869	15
Fin whale	Ship	2,268	1,392	3,660	17
Harbor porpoise	Ship	3,134	15	3,149	17
Long-finned pilot whale	Ship	986	86	1,072	20
Risso's dolphin	Ship	383	205	588	17
Sperm whale	Ship	828	1,137	1,965	15
Striped dolphin	Ship	6,401	4,960	11,361	25
Striped or common dolphin	Ship	0	0	0	0
Unidentified beaked whale	Ship	44	6	50	3
Unidentified dolphin	Ship	553	104	657	14
Unidentified small dolphin	Ship	213	9	222	6
All	**Ship**	**20,563**	**17,379**	**37,942**	**209**

Table 18. Number of total observations for detection functions from aerial and shipboard surveys (n.dist = number of observations with distance data; n.nodist = number of observations without distance data; total number of observations; n.df = number of detection functions modeled).

Species/Guild	Platform	n.dist	n.nodist	n.total	n.df
Bottlenose dolphin	All	3,357	8,458	11,815	36
Common dolphin	All	4,474	562	5,036	37
Cuvier's beaked whale	All	407	482	889	17
Fin whale	All	2,481	1,395	3,876	20
Harbor porpoise	All	4,181	15	4,196	20
Long-finned pilot whale	All	1,047	90	1,137	22
Risso's dolphin	All	629	211	840	22
Sperm whale	All	918	1,138	2,056	16
Striped dolphin	All	9,650	5,024	14,674	30
Striped or common dolphin	All	592	0	592	2
Unidentified beaked whale	All	47	6	53	4
Unidentified dolphin	All	1,046	131	1,177	17
Unidentified small dolphin	All	285	11	296	8
All	**All**	**29,114**	**17,523**	**46,637**	**251**

Note (for all tables with detection functions): Species/Guild = species or guild modeled to extract the esw for this species; Plat. group = platform group; n = number of observations of the target species in the detection function; Med = number of observations in the detection function in the Mediterranean Sea (only for species in both seas); BS = number of observations in the detection function in the Black Sea (only for species in both seas); L_tr = Left truncation applied (in km); R_tr = right truncation applied (in km); % loss obs. = percentage of the available observations lost after truncation; esw = average effective strip width (in km); CvM = Cramér–von Mises goodness of fit test value; Aver. P = average probability of detection; key = key function applied; covars = covariates in the final model.

3.1.1. Fin Whales

Fin whales were pooled together with Unidentified Balaenoptera in the groups where this ambiguous species was recorded (some aerial surveys, **Table** 19). In a single case it was necessary to pool them together with sperm whales and unidentified whales to have a large enough sample size for modeling. Detection functions for aerial surveys are shown in **Table 19** and for shipboard surveys in **Table 20**.

Table 19. Summary of the final models of the detection functions for each platform group for fin whales for aerial surveys.

Species/ Guild	Plat. group	n	L_tr	R_tr	% loss obs.	esw	CvM	Aver.p	key	covars
Bph-Bal	183-200-B	60	0	1.741	4.9	0.503	0.04	0.2890	hr	CommonName -Beaufort-log.detsize
Bph	229-B	153	0	1.622	3.2	0.726	0.049	0.4473	hr	Glare

Table 20. Summary of the final models of the detection functions for each platform group for fin whales for shipboard surveys.

Species/ Guild	Plat. group	n	L_tr	R_tr	% loss obs.	esw	CvM	Aver.p	key	covars
Bph	G1-G2-G3-G8-G10-None	91	0	1.989	8.1	0.377	0.075	0.1895	hr	null
Bph	G12-None	96	0	6.457	5.0	3.322	0.018	0.5145	hr	null
Bph	G13-None	921	0	6.078	0.3	1.915	0.097	0.3151	hr	log.detsize-PlatformHeight
Bph	G14-None-20m	228	0	9.438	0.9	4.423	0.909	0.4686	hr	null
Bph	G14-None-no20m	37	0	7.971	0.0	1.355	0.101	0.1700	hr	BeaufortCode
Bph	G15-None	309	0	1.775	2.5	0.885	0.065	0.4985	hn	CloudsCode
Bph	G2-All*	85	0	1.245	8.1	0.351	0.065	0.2820	hr	null
Bph-Pma-Uwh^	G4-3_5	22	0	3.38	4.6	0.896	0.038	0.2651	hr	BeaufortCode-CommonName
Bph-Bal	G4-6_8	28	0	1.919	0.0	0.477	0.027	0.2484	hr	null
Bph-Bal	G4-All**	57	0	2.5	3.4	0.49	0.033	0.1959	hr	BeaufortCode-Speed-PlatformHeight
Bph	G4-G6-G7-G16-All***	59	0	2.122	4.8	0.442	0.242	0.2083	hr	PlatformHeight
Bph	G5-10_11****	33	0	4.536	0.0	0.608	0.1526	0.2580	hr	null
Bph	G5-3_5	51	0	2.244	2.0	0.383	0.057	0.1705	hr	null
Bph	G5-None	125	0	2.443	4.8	1.021	0.034	0.4180	hr	Beaufort
Bph	G5-G9-G11-None*****	127	0	5.822	0.0	1.115	0.0233	0.1915	hr	BeaufortCode

*** Except G2-None; ** To extract esw only for G4-None; *** To extract esw for G6, G7 and G16; **** Also used for G10-10_11; *****To extract esw for G9 and G11. ^Uwh = Unidentified whale**

3.1.2. Sperm Whales

Sperm whales had to be pooled together for all aerial surveys to have enough of a sample size (**Table 21**). Several shipboard platform groups also had to be pooled together to increase sample size (**Table 22**).

Table 21. Summary of the final models of the detection functions for each platform group for sperm whales for aerial surveys.

Species/ Guild	Plat. group	n	L_tr	R_tr	% loss obs.	esw	CvM	Aver.p	key	covars
Pma	183-200-229-B	90	0	2.606	0	0.708	0.0465	0.2717	hr	Platform Height

Table 22. Summary of the final models of the detection functions for each platform group for sperm whales for shipboard surveys.

Species/ Guild	Plat. group	n	L_tr	R_tr	% loss obs.	esw	CvM	Aver.p	key	covars
Pma	G1-G2-G3-G10-G11-None	37	0.01	2.069	5.4	0.36	0.028	0.0718	hr	null
Pma	G12-None	74	0	7.797	2.7	5.30	0.039	0.6796	hr	null
Pma	G12-G18-None*	80	0	7.797	2.6	5.17	0.058	0.6635	hr	null
Pma	G13-None	107	0	5.946	0.0	2.03	0.034	0.3415	hr	null
Pma	G14-None	33	0	8.725	0.0	2.18	0.057	0.2497	hr	null
Pma	G15-None	42	0	1.423	4.8	0.80	0.085	0.5594	hr	null
Pma	G2-All	40	0.01	2.293	4.8	0.37	0.043	0.1605	hr	null
Bph-Pma-Uwh^	G4-3_5	12	0	3.38	4.7	0.90	0.038	0.2651	hr	BeaufortCode-CommonName
Bph-Bal-Pma	G4-6_8	9	0	2.217	0.0	0.57	0.018	0.2550	hr	null
Bph-Bal-Pma-Uwh^	G4-All**	18	0	1.331	13.6	0.45	0.018	0.3354	hr	Group.plat2-Speed
Pma	G5-10_11	22	0	4.256	0.0	2.29	0.087	0.5372	hn	null
Pma	G5-3_5	290	0.025	2.349	3.1	0.41	0.076	0.1761	hr	null
Pma	G5-None	28	0	2.092	0.0	0.47	0.150	0.2236	hr	Beaufort-PlatformHeight
Bph-Bal-Pma-Uwh^	G6-G7-G16-All	18	0	1.331	13.6	0.45	0.018	0.3354	hr	Group.plat2-Speed
Pma	G8-G9-None	18	0	1.798	0.0	0.73	0.051	0.4059	hr	null

*** To extract esw for G18; ** To extract esw for G4-None. ^Uwh = Unidentified whale**

3.1.3. Risso's Dolphins

Risso's dolphins had to be pooled together with bottlenose dolphins and in one case with long-finned pilot whales for the aerial surveys to have a large enough sample size for modeling (**Table 23**). The same situation happened with most shipboard platform groups, where Risso's dolphins had to be pooled together, usually with bottlenose dolphins although sometimes also with long-finned pilot whales, to increase sample size (**Table 24**). For two shipboard platform groups, there were no observations of this species. Two other species were used as proxy so that tracks from those platforms could be used to inform absence in the models: G1-None, where the detection function of bottlenose dolphins was used, and G16-None, where common dolphins were used because there were no observations of bottlenose dolphins either.

Table 23. Summary of the final models of the detection functions for each platform group for Risso's dolphins for aerial surveys.

Species/ Guild	Plat. group	n	L_tr	R_tr	% loss obs.	esw	CvM	Aver.p	key	covars
Ttr-Ggr	150-F	22	0.087	0.568	0.0	0.18	0.042	0.3653	hn	DisplayName-log.detsize-Month
Ttr-Ggr-Gme	150-229-F*	26	0.087	0.628	1.4	0.16	0.020	0.2901	hr	Beaufort
Ggr	183-B	88	0	0.411	3.5	0.23	0.106	0.5640	hn	BeaufortCode
Ttr-Ggr	200-B	15	0	1.299	0.0	0.45	0.056	0.3438	hr	Name-CommonName-detsize
Ggr	229-B	95	0	0.749	0.0	0.37	0.038	0.4983	hn	null

*** To extract esw for 229-F**

Table 24. Summary of the final models of the detection functions for each platform group for Risso's dolphins for shipboard surveys.

Species/ Guild	Plat. group	n	L_tr	R_tr	% loss obs.	esw	CvM	Aver.p	key	covars
Ttr	G1-None*	0	0	0.143	10.5	0.02	0.068	0.1425	hr	null
Ttr-Ggr	G11-None	10	0	1.448	0.0	0.33	0.050	0.2258	hr	null
Ggr	G12-None	43	0	4.213	4.7	1.87	0.049	0.4438	hn	PlatformHeight.fac-log.detsize
Ggr	G12-G18-None**	1	0	4.851	13.0	1.91	0.038	0.3932	hr	Speed
Ttr-Ggr	G13-None	10	0	1.734	1.6	0.21	0.064	0.1213	hr	null
Ttr-Ggr	G14-None	8	0.01	0.731	11.1	0.17	0.030	0.2355	hr	CommonName-log.detsize
Ttr-Ggr	G15-None	10	0	1.41	0.0	0.45	0.072	0.3155	hn	log.detsize
Dde	G16-None***	0	0	0.9	2.0	0.11	0.059	0.1194	hr	detsize
Ggr	G2-All	22	0	2.403	0.0	0.39	0.026	0.1637	hr	detsize-Speed
Ttr-Ggr	G3-G10-None	6	0.01	0.863	0.0	0.37	0.113	0.4308	hn	BeaufortCode-detsize
Ggr	G4-All****	77	0	0.958	5.1	0.20	0.075	0.2084	hr	detsize-PlatformHeight
Ggr	G4-None	36	0	0.958	5.5	0.22	0.071	0.2265	hr	detsize
Ggr	G5-10_11	77	0	2.034	12.2	0.71	0.053	0.3473	hr	log.detsize-PlatformHeight
Ttr-Ggr	G5-3_5	7	0	1	6.5	0.11	0.155	0.1102	hr	log.detsize
Ttr-Ggr	G5-None	19	0	0.8	20.8	0.29	0.046	0.3641	hr	log.detsize-Speed
Ttr-Ggr-Gme-Sbr-Pcr^	G6-G7-All*****	7	0	0.752	0.0	0.09	0.130	0.1132	hr	Group.plat2-detsize-PlatformHeight

Species/ Guild	Plat. group	n	L_tr	R_tr	% loss obs.	esw	CvM	Aver.p	key	covars
Ttr-Ggr-Gme-Sbr-Pcr^	G7-All	7	0	0.752	1.7	0.10	0.049	0.1364	hr	null
Ttr-Ggr	G8-None-Med	4	0.025	0.4	68.4	0.11	0.033	0.3043	hr	null
Ttr-Ggr-Gme	G9-None ******	0	0.1	1.646	0.0	0.29	0.053	0.1860	hr	null

*** Using Ttr as a proxy for this platform group; ** To extract esw for G18;**
***** Using Dde as a proxy; **** except G4-None; ***** To extract esw for G6;**
******* All Ggr with no distances; ^Sbr = rough-toothed dolphin, Pcr = false killer whale**

3.1.4. Long-finned Pilot Whales

In most cases, long-finned pilot whales had to be pooled together with other species to have a large enough sample size for modeling, usually with Risso's and bottlenose dolphins, both for aerial and shipboard surveys (**Table 25** and **Table 26**). In some platform groups (groups G16-All, G8-None and G9-None) there were no sightings of pilot whales, so the detection function for other species was used as a proxy.

Table 25. Summary of the final models of the detection functions for each platform group for long-finned pilot whales for aerial surveys.

Species/ Guild	Plat. group	n	L_tr	R_tr	% loss obs.	esw	CvM	Aver.p	key	covars
Ttr-Ggr-Gme	150-229-F	5	0.087	0.628	1.43	0.157	0.02	0.2901	hr	Beaufort
Gme	183-200-229-B	56	0	1.155	6.67	0.327	0.067	0.2828	hr	Beaufort-log.detsize-PlatformHeight

Table 26. Summary of the final models of the detection functions for each platform group for long-finned pilot whales for shipboard surveys.

Species/ Guild	Plat. group	n	L_tr	R_tr	% loss obs.	esw	CvM	Aver.p	key	covars
Ttr-Ggr-Gme	G10-All*	3	0.01	0.785	40	0.327	0.045	0.4224	hr	null
Ttr-Ggr-Gme	G10-None	3	0.01	0.863	0	0.296	0.045	0.3467	hr	null
Ttr-Ggr-Gme	G11-None	15	0	2.273	0	0.325	0.031	0.1431	hr	PlatformHeight
Gme	G12-None	36	0	3.969	8.5	0.498	0.1	0.1255	hr	Beaufort-log.detsize
Ggr-Gme-Oor	G13-None	23	0	2.125	0	0.755	0.021	0.3552	hr	null
Ggr-Gme	G14-G15-None	8	0	1.284	27.3	0.468	0.067	0.3648	hn	log.detsize-PlatformHeight

Species/ Guild	Plat. group	n	L_tr	R_tr	% loss obs.	esw	CvM	Aver.p	key	covars
Ttr-Ggr-Gme-Sbr-Pcr^	G16-All	0	0	0.752	0	0.085	0.130	0.1132	hr	Group.plat2-detsize-PlatformHeight
Ttr-Ggr-Gme	G2-10_11	21	0	1.212	4.5	0.416	0.023	0.3428	hr	null
Ttr-Ggr-Gme	G2-None	20	0	1.501	2.4	0.309	0.092	0.2058	hr	log.detsize
Gme	G2-All**	39	0	1.212	0	0.224	0.038	0.185	hr	PlatformHeight
Gme	G2-G4-G7-None***	22	0	1.638	15.4	0.24	0.046	0.1462	hr	null
Ttr-Ggr-Gme	G3-G10-None	6	0.01	0.785	33.3	0.321	0.056	0.4146	hr	null
Ttr-Ggr-Gme-Sbr-Pcr^	G4-3_5	6	0	0.415	10.7	0.036	0.019	0.0405	hr	Beaufort
Ttr-Ggr-Gme-Udo	G4-6_8	12	0	0.826	0	0.469	0.024	0.5681	hr	Speed
Gme	G5-10_11	349	0	3.281	3.3	1.127	0.043	0.3436	hr	Beaufort
Gme	G5-3_5	350	0	1.25	3.2	0.239	0.262	0.1915	hr	null
Gme	G5-None	69	0	2.499	3.0	0.661	0.029	0.2644	hr	BeaufortCode
Ttr-Ggr-Gme-Sbr-Pcr^	G6-G7-All	4	0	0.752	0	0.085	0.13	0.1132	hr	Group.plat2-detsize-PlatformHeight
Ttr-Ggr-Gme	G8-G9-None****	0	0.1	1.646	0	0.287	0.053	0.186	hr	null

*** Except G10-None; ** To extract esw for the rest of the G2; *** To extract esw for G4-None; **** No Gme with distances, G8 derived from G9; ^Sbr = rough-toothed dolphin, Pcr = false killer whale**

3.1.5. Cuvier's beaked Whales

Cuvier's beaked whales were pooled together with other species (bottlenose and Risso's dolphins and long-finned pilot whales) in one of the aerial survey platform groups (**Table 27**). In most cases, several similar platform groups had to be pooled together to have a large enough sample size for the detection function model (**Table 27** and **Table 28**). Unidentified beaked whales ("Ziph") were modeled together with Cuvier's beaked whales when they occurred in the platform groups because there were not enough sightings to model them separately.

Table 27. Summary of the final models of the detection functions for each platform group for Cuvier's beaked whales for aerial surveys.

Species/ Guild	Plat. group	n	L_tr	R_tr	% loss obs.	esw	CvM	Aver.p	key	covars
Ttr-Ggr-Gme-Zca	150-F	2	0.087	0.568	33.33	0.186	0.024	0.3859	hr	null
Zca-Ziph	183-200-229-B	21	0	0.359	5.26	0.25	0.063	0.6966	hn	BeaufortCode

Table 28. Summary of the final models of the detection functions for each platform group for Cuvier's beaked whales for shipboard surveys.

Species/ Guild	Plat. group	n	L_tr	R_tr	% loss obs.	esw	CvM	Aver.p	key	covars
Zca	G10-G11-All	22	0	2.189	8.33	0.318	0.018	0.1453	hr	BeaufortCode-log.detsize
Zca	G12-None	81	0	7.358	3.57	2.339	0.143	0.3179	hn	VisibilityCode
Ziph	G12-None	24	0	8.039	0	2.346	0.038	0.3188	hr	CommonName-PlatformHeight
Zca	G12-G18-None*	78	0	7.358	3.7	2.4	0.029	0.3262	hr	Speed
Zca	G13-None	75	0	4.188	3.85	0.899	0.028	0.2147	hr	BeaufortCode
Zca	G14-None	18	0.2	4.262	0	1.576	0.028	0.1888	hr	null
Zca	G15-None	25	0	1.275	0	0.816	0.105	0.6399	hn	null
Zca	G3-G10-G11-None	16	0	1.546	0	0.295	0.0424	0.1909	hr	Beaufort-detsize
Zca-Ziph	G1-G4-G6-G7-G16-All**	15	0.05	1.641	0	0.477	0.057	0.3	hn	Speed
Zca	G5-10_11	26	0	2.347	0	0.964	0.158	0.4105	hn	Beaufort.fac
Ziph	G5-10_11	20	0	3.227	4.76	0.986	0.082	0.3055	hn	Beaufort.fac
Zca-Ziph	G2-G5-G8-None***	20	0	0.828	0	0.602	0.039	0.7266	hn	null
Zca	G8-G9-None	17	0	1.164	0	0.653	0.047	0.5613	hn	null

*** To derive esw for G18; **Only G4 and G7 with distances; *** To derive esw for G2 and G5**

3.1.6. Bottlenose Dolphins

Bottlenose dolphins were pooled together with other species (Risso's dolphins and long-finned pilot whales) in one of the aerial survey platform groups (**Table 29**) and in some of the shipboard survey platform groups (**Table 30**).

Table 29. Summary of the final models of the detection functions for each platform group for bottlenose dolphins for aerial surveys.

Species/ Guild	Plat. group	n	L_tr	R_tr	% loss obs.	esw	CvM	Aver.p	key	covars
Ttr	150-F	36	0.087	0.568	0	0.131	0.078	0.2722	hn	log.detsize
Ttr-Ggr-Gme	150-229-F*	3	0.087	0.628	1.43	0.157	0.02	0.2901	hr	Beaufort
Ttr	123-B	123	0	0.233	0.0	0.09	0.107	0.3943	hn	null
Ttr	150-B	43	0.04	0.363	0.0	0.18	0.073	0.5646	hn	null
Ttr	183-B	474	0.04	0.503	14.8	0.17	0.047	0.3721	hr	Beaufort.fac-TurbidityCode
Ttr	200-B	405	0	2.618	2.9	0.44	0.053	0.1687	hr	Name-Beaufort-log.detsize
Ttr	229-B	247	0	0.492	4.6	0.25	0.046	0.4996	hn	BeaufortCode-SubjectiveCode-log.detsize

*** To derive esw for 229-F**

Table 30. Summary of the final models of the detection functions for each platform group for bottlenose dolphins for shipboard surveys.

Species/ Guild	Plat. group	n	L_tr	R_tr	% loss obs.	esw	CvM	Aver.p	key	covars
Ttr-Dde-Sco-Udo	G10-10_11	2	0	2.441	0	0.924	0.056	0.3785	hr	Beaufort.fac
Ttr	G10-None	22	0.01	0.704	2.17	0.493	0.06	0.7097	hn	null
Ttr	G11-None	34	0	1.448	0	0.3	0.028	0.2072	hr	null
Ttr-Ggr	G12-None	12	0	4.851	0	2.267	0.047	0.4674	hr	null
Ttr	G13-None	48	0	1.151	15.79	0.188	0.059	0.1631	hr	PlatformHeight
Ttr	G14-None	70	0.01	0.65	5.41	0.136	0.031	0.2131	hr	log.detsize
Ttr	G15-None	92	0	0.777	5.15	0.432	0.09	0.5555	hn	log.detsize
Dde	G16-None*	0	0	0.9	2.04	0.107	0.059	0.1194	hr	detsize
Dde	G17-None*	0	0.02	0.504	2.2	0.14	0.037	0.2855	hr	null
Ttr	G1-None	44	0	0.143	10.53	0.02	0.068	0.1425	hr	null
Ttr-Ggr	G2-10_11	13	0	2.323	4.76	0.492	0.022	0.2119	hr	CommonName
Ttr	G2-None**	51	0.01	2.166	1.92	0.353	0.024	0.1636	hr	Region-Beaufort
Ttr	G2-None-BDRI	52	0.01	2.166	1.89	0.399	0.026	0.185	hr	log.detsize
Ttr	G3-G10-None***	46	0.01	0.863	0	0.344	0.093	0.4035	hn	BeaufortCode-detsize
Ttr-Ggr-Gme-Sbr-Pcr^	G4-3_5	17	0.01	1.286	0	0.176	0.031	0.1382	hr	null
Ttr-Ggr-Gme-Udo	G4-6_8	4	0	0.826	0	0.469	0.024	0.5681	hr	Speed
Ttr	G4-None	184	0	0.816	11.79	0.094	0.225	0.115	hr	BeaufortCode
Ttr	G5-10_11	247	0	3.299	2.76	0.753	0.019	0.2283	hr	BeaufortCode-PlatformHeight. fac-log.detsize
Ttr	G5-3_5	339	0	1.5	3.97	0.127	0.15	0.0847	hr	Beaufort.fac-log.detsize
Ttr	G5-6_8	145	0	0.828	2.0	0.08	0.061	0.0909	hr	null
Ttr	G5-None	123	0	0.77	8.66	0.3	0.036	0.3897	hr	log.detsize-PlatformHeight
Ttr	G6-G7-G8-None	97	0	0.525	0.0	0.08	0.062	0.1586	hr	Region
Ttr	G7-All****	42	0	0.6	4.7	0.08	0.069	0.1318	hr	null
Ttr	G8-3_5-Afalina-2003	42	0	0.375		0.17		0.4490	hn	null
Ttr	G8-3_5-MC-2003	44	0	2.007		0.30		0.1470	hn	null
Ttr-Dde-Pph	G9-3_5	13	0	1.2	0.0	0.47	0.050	0.3923	hr	detsize
Ttr-Dde	G9-6_8	10	0	0.551	2.1	0.26	0.097	0.4676	hn	Year.fac-log.detsize
Ttr	G9-None	34	0	1.646	0.0	0.61	0.073	0.3730	hr	null

*** No Ttr with distances, using Dde as proxy; ** Except BDRI; ***To derive esw for G10 only; **** Except G7-None; ^Sbr = rough-toothed dolphin, Pcr = false killer whale**

3.1.7. Common Dolphins

Common dolphins were pooled together with striped dolphins in some of the aerial survey platform groups (**Table 31**) as well as some of the shipboard survey platform groups (**Table 32**). In one of the aerial survey platform groups (150-B), there were no sightings of either common or striped dolphins, so the detection function for bottlenose dolphins was used as a proxy.

Table 31. Summary of the final models of the detection functions for each platform group for common dolphins for aerial surveys.

Species/ Guild	Plat. group	n	L_tr	R_tr	% loss obs.	esw	CvM	Aver.p	key	covars
Sco-Dde	150-F	5	0.087	0.568	0	0.131	0.085	0.2732	hn	Name-detsize
Sco	229-F*	0	0.087	0.63	0.0	0.14	0.054	0.2711	hr	SubjectiveCode
Dde	123-B	244	0	0.227	0	0.118	0.063	0.5179	hn	log.detsize
Ttr	150-B*	0	0.04	0.363	0	0.182	0.073	0.5646	hn	null
Dde	183-B	778	0.05	0.564	22.6	0.188	0.053	0.3664	hr	Region-Beaufort-log.detsize
Sco-Dde	200-B	1	0	1.3	1.0	0.41	0.109	0.3119	hr	Name-detsize
Dde	229-B	106	0	1.702	0.0	0.58	0.125	0.3422	hn	SubjectiveCode-log.detsize

*** Used as proxy**

Table 32. Summary of the final models of the detection functions for each platform group for common dolphins for shipboard surveys.

Species/ Guild	Plat. group	n	L_tr	R_tr	% loss obs.	esw	CvM	Aver.p	key	covars
Ttr-Dde-Sco-Udo	G10-10_11	5	0	2.441	0	0.924	0.056	0.3785	hr	Beaufort.fac
Dde	G10-None	46	0.01	1.57	0	0.346	0.078	0.2217	hn	BeaufortCode-PlatformHeight
Dde	G11-None	38	0	0.927	0	0.317	0.1269	0.3419	hn	Beaufort.fac-detsize
Sco	G12-G18-None*	0	0	7.779	0.26	0.872	0.461	0.1121	hr	SubjectiveCode
Dde	G12-None	73	0.01	2.5	3.95	1.204	0.152	0.4835	hn	Beaufort
Dde	G13-None	32	0	2.26	0	0.072	0.053	0.0317	hr	null
Dde	G14-None	35	0.01	0.4	10.26	0.117	0.03	0.3009	hr	Speed
Sco-Dde	G15-None	8	0	0.8	2.2	0.05	0.170	0.0671	hr	Beaufort.fac
Dde	G16-None	98	0	0.9	2.04	0.107	0.059	0.1194	hr	detsize
Dde	G17-None	169	0.02	0.504	2.2	0.14	0.037	0.2855	hr	null
Dde	G1-G2-None	69	0.02	0.898	2.82	0.127	0.51	0.1445	hn	BeaufortCode-Group.plat-PlatformHeight
Sco-Dde	G2-10_11	10	0	1.819	2.53	0.18	0.022	0.0992	hr	BeaufortCode-CommonName-log.detsize
Dde	G2-6_8**	0	0	2.235	0	0.104	0.099	0.0467	hr	null

Species/ Guild	Plat. group	n	L_tr	R_tr	% loss obs.	esw	CvM	Aver.p	key	covars
Sco-Dde	G3-None	6	0.01	1.025	0	0.351	0.024	0.0287	hr	null
Sco-Dde	G4-3_5	37	0.01	1.183	0	0.249	0.059	0.2123	hr	CloudsCode2-Beaufort-log.detsize
Sco-Dde	G4-6_8	2	0.01	1.463	0	0.332	0.021	0.2455	hr	Beaufort.fac-Speed
Dde	G4-None	196	0.01	0.799	0.51	0.199	0.039	0.2524	hr	detsize-Speed
Dde	G5-10_11	728	0	2.424	5.49	0.494	0.203	0.2037	hr	Beaufort.fac-Name-log.detsize
Dde	G5-3_5	218	0	1.149	6.44	0.086	0.275	0.0752	hr	BeaufortCode-Region-log.detsize
Dde	G5-6_8	160	0	0.828	2.5	0.08	0.040	0.1016	hr	log.detsize
Dde	G5-None	245	0	0.86	5.77	0.269	0.077	0.3124	hr	BeaufortCode-log.detsize
Dde	G6-G7-None**	33	0	0.315	10.8	0.07	0.023	0.2159	hr	null
Sco-Dde	G7-3_5	19	0	1.643	19.67	0.211	0.024	0.1282	hr	null
Sco-Dde	G7-All***	21	0	1.643	4.6	0.18	0.026	0.1065	hr	Beaufort
Dde	G8-3_5-Afalina-2003	69	0	2.504		0.35		0.1390	hn	null
Dde	G8-3_5-MC-2003	9	0	1.498		0.34		0.2250	hn	null
Dde	G8-None	34	0	0.4	5.9	0.06	0.015	0.1446	hr	BeaufortCode-Speed
Ttr-Dde-Pph	G9-3_5	17	0	1.2	0.0	0.47	0.050	0.3923	hr	detsize
Dde	G9-6_8	547	0	0.5	7.3	0.25	0.118	0.5068	hn	Year.fac
Dde	G9-None	30	0	0.992	0.0	0.28	0.042	0.2824	hr	null

*** To derive esw for G18 from Sco; ** To derive esw for G6; *** To derive esw for G7-None**

3.1.8. Striped Dolphins

Striped dolphins were pooled together with common dolphins in one of the aerial survey platform groups (**Table 33**) and some of the shipboard survey platform groups (**Table 34**). They were also pooled together with common, striped and unidentified dolphins in the ship-based platform group G10-10_11 to have a large enough sample size for the model. Platform group G14 was divided between several surveys as their detection functions were quite different, and there were enough observations in each to do so.

Table 33. Summary of the final models of the detection functions for each platform group for striped dolphins for aerial surveys.

Species/ Guild	Plat. group	n	L_tr	R_tr	% loss obs.	esw	CvM	Aver.p	key	covars
Sco-Dde	150-F	216	0.087	0.568	0	0.131	0.085	0.2732	hn	Name-detsize
Sco	183-B	554	0	0.359	5.2	0.17	0.098	0.4858	hn	TurbidityCode-Glare-log.detsize
Sco	200-B	205	0	1.3	1	0.404	0.11	0.3111	hr	Name-detsize
Sco	229-B	2,190	0	0.594	2.57	0.332	0.397	0.5589	hr	Beaufort-log.detsize-Speed
Sco	229-F	84	0.087	0.63	0	0.136	0.054	0.2711	hr	SubjectiveCode

Table 34. Summary of the final models of the detection functions for each platform group for striped dolphins for shipboard surveys.

Species/ Guild	Plat. group	n	L_tr	R_tr	% loss obs.	esw	CvM	Aver.p	key	covars
Sco-Dde	G1-G2-None	385	0.01	0.796	6.78	0.121	0.122	0.1541	hr	BeaufortCode-detsize-PlatformHeight
Ttr-Dde-Sco-Udo	G10-10_11	10	0	2.441	0	0.924	0.056	0.3785	hr	Beaufort.fac
Sco	G10-None	32	0	0.933	6.25	0.161	0.098	0.1722	hn	BeaufortCode-PlatformHeight
Sco	G11-None	101	0	2.127	0	0.291	0.1737	0.1369	hr	log.detsize-Speed-PlatformHeight
Sco	G12-None	361	0	5.659	1.39	0.788	0.362	0.1393	hr	SubjectiveCode
Sco	G12-G18-None*	386	0	7.779	0.26	0.872	0.461	0.1121	hr	SubjectiveCode
Sco	G13-None	1,555	0.01	1.569	11.04	0.458	0.03	0.2937	hr	PlatformHeight.fac-Beaufort-log.detsize
Sco	G14-None-20-22m	363	0	4.195	2.2	0.91	0.070	0.2172	hr	BeaufortCode-Name-log.detsize
Sco	G14-None-24-25m	99	0	0.833	8.08	0.166	0.02	0.1989	hr	detsize-Speed
Sco	G14-None-Carbonara	87	0.02	1.593	0.0	0.30	0.035	0.1874	hr	log.detsize
Sco	G14-None-Uni_Barcelona	104	0.01	0.351	13.33	0.058	0.018	0.1712	hr	Visibility
Sco	G14-None-Uni_Palermo	144	0	0.515	5.56	0.087	0.057	0.1696	hr	log.detsize

Species/ Guild	Plat. group	n	L_tr	R_tr	% loss obs.	esw	CvM	Aver.p	key	covars
Sco	G15-None	482	0.025	0.709	4.74	0.183	0.061	0.267	hr	log.detsize
Dde	G16-None**	0	0	0.9	2.04	0.107	0.059	0.1194	hr	detsize
Sco	G2-10_11	66	0	1.994	2.94	0.169	0.033	0.0848	hr	BeaufortCode-log.detsize
Sco	G2-All***	426	0	0.672	13.62	0.08	0.1402	0.119	hr	Beaufort-detsize-Speed
Sco-Dde	G3-None	22	0.01	1.025	0	0.351	0.024	0.0287	hr	null
Sco	G4-3_5	105	0	2.352	0.96	0.062	0.077	0.0264	hr	Beaufort.fac-log.detsize
Sco	G4-6_8	65	0.01	1.277	2.86	0.364	0.039	0.2873	hr	Beaufort-Speed
Sco	G4-None	177	0.01	1.023	4.5	0.11	0.044	0.1047	hr	detsize
Sco	G5-10_11	956	0	2.707	3.94	0.543	0.48	0.2007	hr	Beaufort.fac-log.detsize-PlatformHeight
Sco	G5-3_5	265	0.01	1.061	2.7	0.16	0.083	0.1564	hr	log.detsize
Sco	G5-None	534	0	0.829	9.9	0.123	0.17	0.1489	hr	Beaufort-log.detsize-PlatformHeight
Sco	G6-G7-All	40	0	1.229	4.8	0.20	0.028	0.1584	hr	null
Sco-Dde	G7-3_5	40	0	1.643	19.7	0.21	0.024	0.1282	hr	null
Sco-Dde	G8-None	21	0.01	0.752	0.0	0.27	0.036	0.4498	hn	PlatformHeight
Sco-Dde-Hyb-Udo small^	G9-None	1	0	0.992	0.0	0.23	0.025	0.2263	hr	BeaufortCode

*** To derive esw for G18; ** Used Dde as a proxy; *** To derive esw for G2-6_8; ^ Hyb = hybrids between striped and common dolphin**

3.1.9. Harbor Porpoises

All aerial surveys included only this species (**Table 35**). Harbor porpoises were only pooled together with common and bottlenose dolphins in one of the shipboard survey platform groups (**Table 36**). Platform group G8 was divided between several surveys as their detection functions were quite different, and there were enough observations to model surveys separately in this case.

Table 35. Summary of the final models of the detection functions for each platform group for harbor porpoises for aerial surveys.

Species/ Guild	Plat. group	n	L_tr	R_tr	% loss obs.	esw	CvM	Aver.p	key	covars
Pph	123-B	142	0	0.156	2.1	0.118	0.255	0.7547	hr	null
Pph	150-B	134	0.05	0.473	9.5	0.120	0.045	0.2907	hn	Name
Pph	183-B	771	0.025	0.345	10.0	0.194	0.174	0.6076	hr	Beaufort.fac-SubjectiveCode

Table 36. Summary of the final models of the detection functions for each platform group for harbor porpoises for shipboard surveys. The values given for platform groups G8-3_5-Affalina-2003 and G8-3_5-MC-2003 were obtained from a publication as the distances were not provided for these surveys (Severtsov Institute of Ecology and Evolution, Russian Academy of Sciences [Moscow] and Bram Laboratory Cooperative Enterprise [Simferopol] 2003).

Species/ Guild	Plat. group	n	L_tr	R_tr	% loss obs.	esw	CvM	Aver.p	key	covars
Pph	G1-None	178	0	0.4	4.81	0.088	0.024	0.2209	hr	PlatformHeight. fac-log.detsize
Pph	G1-G2-None*	187	0	0.4	2.14	0.093	0.0509	0.2333	hr	PlatformHeight
Pph	G10-None	91	0	0.574	0	0.282	0.089	0.4914	hr	Beaufort-detsize
Pph	G11-None	91	0	0.574	0	0.282	0.0886	0.4914	hr	Beaufort-detsize
Pph	G16-None	132	0	0.6	2.27	0.245	0.052	0.4086	hr	log.detsize
Pph	G17-None	75	0.07	1.307	5.06	0.25	0.042	0.2024	hr	Month.fac
Pph	G4-None	584	0	0.591	7.59	0.209	0.113	0.353	hr	log.detsize
Pph	G5-6_8	254	0	0.756	1.2	0.24	0.020	0.3104	hr	null
Pph	G5-All**	280	0	0.439	9.29	0.209	0.0386	0.4755	hn	Group.plat2
Pph	G6-None	73	0	0.358	6.4	0.07	0.051	0.1913	hr	Beaufort
Pph	G8-3_5-Afalina-2003	14	0	0.25		0.25		1	hn	null
Pph	G8-3_5-MC-2003	6	0	0.501		0.268		0.5350	hn	null
Pph	G8-None-Bulgaria	72	0	4.284	0	2.749	0.2	0.6417	hr	Beaufort.fac-detsize
Pph	G8-None-Tudav	44	0	0.493	2.22	0.194	0.046	0.3933	hn	Swell
Ttr-Dde-Pph	G9-3_5	9	0	1.2	0	0.471	0.05	0.3923	hr	detsize
Pph	G9-6_8	905	0.03	0.324	13.23	0.199	0.111	0.6785	hn	log.detsize
Pph	G9-None	139	0	1.222	0	0.381	0.05	0.3116	hr	null

*** To derive esw for G2; ** To derive esw for G5 except G5-None**

3.1.10. Killer Whales

Killer whales were only observed in the Strait of Gibraltar, and therefore by very few platforms. Only one sighting was available in a group of aerial survey platforms (pooled together with pilot whales, **Table 37**). Only one platform group of shipboard surveys (G5-3_5) had enough

observations to model a detection function for this species on its own. Three other groups had one observation each, so they were pooled together with other species (Risso's dolphins, long-finned pilot whales and/or false killer whales depending on the platform group) (**Table 38**).

Table 37. Summary of the final models of the detection functions for each platform group for killer whales for aerial surveys.

Species/ Guild	Plat. group	n	L_tr	R_tr	% loss obs.	esw	CvM	Aver.p	key	covars
Gme-Oor	183-200-229-B	1	0	1.155	50	0.316	0.076	0.2737	hr	Beaufort-log.detsize-PlatformHeight

Table 38. Summary of the final models of the detection functions for each platform group for killer whales for shipboard surveys.

Species/ Guild	Plat. group	n	L_tr	R_tr	% loss obs.	esw	CvM	Aver.p	key	covars
Ggr-Gme-Oor	G13-None	1	0	2.125	0	0.755	0.021	0.3552	hr	null
Gme-Oor-Pcr^	G5-10_11	1	0	2.556	10.7	0.63	0.343	0.2471	hr	Beaufort.fac
Oor	G5-3_5	78	0	1.007	11.36	0.204	0.031	0.2023	hr	null
Gme-Oor	G5-None	1	0	2.499	2.9	0.70	0.030	0.2783	hr	BeaufortCode-log.detsize

*** To derive esw for G2; ** To derive esw for G5 except G5-None; ^Pcr = false killer whale**

3.1.11. Striped or Common Dolphins

The ambiguous "identification group striped or common dolphins" was only recorded from aerial surveys (**Table 39**).

Table 39. Summary of the final models of the detection functions for each platform group for striped or common dolphins ambiguous identification for aerial surveys.

Species/ Guild	Plat. group	n	L_tr	R_tr	% loss obs.	esw	CvM	Aver.p	key	covars
Sco_or_Dde	183-B	295	0	0.503	0	0.261	0.144	0.5194	hr	TurbidityCode-Year.fac-log.detsize
Sco_or_Dde	183-229-B*	297	0	0.503	0.0	0.26	0.062	0.5183	hr	BeaufortCode-log.detsize

*** To derive esw for 229-B**

3.1.12. Unidentified Small Dolphins

The Unidentified small dolphins group was recorded both from aerial and shipboard surveys, but only from a few platform groups (**Table 40** and **Table 41**). On shipboard surveys they were

pooled together with other species to have a large enough sample size for modeling, except for G15 where there were enough observations.

Table 40. Summary of the final models of the detection functions for each platform group for unidentified small dolphins for aerial surveys.

Species/ Guild	Plat. group	n	L_tr	R_tr	% loss obs.	esw	CvM	Aver.p	key	covars
Udo small	183-200-B	46	0	2.607	2.27	0.571	0.046	0.219	hn	PlatformHeight.fac-Beaufort-log.detsize
Udo small	229-B	26	0	0.513	0.0	0.33	0.043	0.6441	hn	null

Table 41. Summary of the final models of the detection functions for each platform group for unidentified small dolphins for shipboard surveys.

Species/ Guild	Plat. group	n	L_tr	R_tr	% loss obs.	esw	CvM	Aver.p	key	covars
Sco-Dde-Hyb-Udo small^	G10-None	16	0.01	1.025	4	0.324	0.1994	0.0429	hn	BeaufortCode-log.detsize
Udo-Udo small	G13-None	23	0	2.58	0.0	1.10	0.046	0.4269	hr	null
Udo-Udo small	G14-None	34	0.02	1.131	0	0.2	0.141	0.1803	hr	Beaufort-log.detsize
Udo small	G15-None	139	0.01	0.877	9.2	0.25	0.029	0.2846	hr	Beaufort-detsize
Sco-Dde-Udo small	G8-None	1	0.01	0.867	50.0	0.30	0.267	0.4712	hn	log.detsize
Sco-Dde-Hyb-Udo small^	G9-None*	0	0	0.992	0.0	0.23	0.025	0.2263	hr	BeaufortCode

*** No Udo_small with distances; ^Hyb = hybrids between striped and common dolphin**

3.1.13. Unidentified Dolphins

The Unidentified dolphins group was recorded both from aerial and shipboard surveys, but only from a few platform groups (**Table 42** and **Table 43**). On one platform group in aerial surveys (the combination of 150-229-F), they had to be pooled together with several species to have a large enough sample size for the model. On shipboard surveys they were also pooled together with other species in several platform groups to have a large enough sample size for modeling.

Table 42. Summary of the final models of the detection functions for each platform group for unidentified dolphins for aerial surveys.

Species/ Guild	Plat. group	n	L_tr	R_tr	% loss obs.	esw	CvM	Aver.p	key	covars
Ttr-Ggr-Gme-Zca-Udo-Udolar^	150-229-F	15	0.087	0.566	9.41	0.21	0.047	0.4384	hn	null
Udo	183-B	171	0	0.503	2.4	0.33	0.041	0.6542	hr	Glare-detsize
Udo	229-B	307	0	1.708	5.5	0.658	0.133	0.385	hr	CloudsCode2-log.detsize

^Udolar = unidentified large dolphin

Table 43. Summary of the final models of the detection functions for each platform group for unidentified dolphins for shipboard surveys.

Species/ Guild	Plat. group	n	L_tr	R_tr	% loss obs.	esw	CvM	Aver.p	key	covars
Ttr-Ggr-Gme-Udo	G10-None	3	0.01	0.863	0	0.394	0.122	0.4614	hn	BeaufortCode-detsize
Udo	G11-None	26	0	1.514	0.0	0.73	0.040	0.4819	hn	BeaufortCode
Udo	G12-None	95	0	5.182	1.06	2.016	0.076	0.389	hr	null
Udo-Udo small	G13-None	1	0	2.58	0.0	1.10	0.046	0.4269	hr	null
Udo-Udo small	G14-None*	0	0.02	1.131	0.0	0.20	0.141	0.1804	hr	Beaufort-log.detsize
Sco-Dde-Udo	G2-10_11	11	0	1.979	2.2	0.22	0.041	0.0965	hr	BeaufortCode-CommonName-log.detsize
Sco-Dde-Udo	G2-None	4	0	0.755	9.9	0.07	0.183	0.0982	hr	BeaufortCode-log.detsize
Sco-Dde-Udo	G3-None	17	0.01	1.017	0.0	0.37	0.021	0.3671	hr	null
Udo	G4-3_5	103	0.01	1.384	11.7	0.13	0.109	0.0945	hr	detsize
Ttr-Ggr-Gme-Udo	G4-6_8	6	0	0.826	0.0	0.47	0.024	0.5681	hr	Speed
Udo	G4-None	38	0	1.688	0.0	0.30	0.037	0.1798	hr	detsize
Udo	G5-10_11	188	0	3.578	2.7	1.20	0.042	0.3362	hr	log.detsize
Udo	G7-3_5	57	0	2	7.6	0.32	0.055	0.1608	hr	Beaufort
Ttr-Ggr-Pcr-Udo^	G8-None	4	0	1.882	1.6	0.07	0.065	0.0358	hr	Confidence-Region

*** No Udo with distances; ^Pcr = false killer whale**

3.2. Correction Factors for Availability and Perception Biases

Final correction factors (g(0)) including both â and p0 were obtained for each survey estimating â from diving/surfacing times and speed and distances of the survey (see **Section 2.8**, Correction Factors for Availability and Perception Biases). The mean values per platform group, and within them for different sightability conditions and platform groups, are shown in **Appendix D**, as showing the estimated g(0) for each survey results is impractical for inclusion in the main report.

3.3. Sightings per Unit Effort

Appendix B contains the maps of sightings per unit effort (i.e., encounter rate) in grid cells of 50 x 50 km (2,500 km²) for the Black Sea and in grid cells of 100 x 100km (10,000 km²) for the Mediterranean Sea.

3.4. Spatial Models

Table 44 to **Table 46** show the selected final GAM models for each species in the Black Sea. **Table 47** to **Table 56** show the selected final GAM models for each species in the Mediterranean. For the GAM models, the effort and the observations were filtered for the same thresholds used to filter the data for the detection functions (e.g., maximum sea state allowed). The observations beyond the truncation distances for each detection function were also discarded for the spatial models. In this way, the data used for the GAM models were the same as used for the detection functions. The number of observations and individuals shown in the tables are those after applying these filters. The bottlenose, common and striped dolphin models for the Mediterranean include the ambiguous species identification assigned to those species.

Appendix E provides detailed GAM summaries and GAM smooth plots for each species. Long-finned pilot whale models included data from 1991 to 2022. The rest of the species/guilds used data from 1999 to 2022.

Table 44. Selected final models for bottlenose dolphins in the Black Sea (Num.obs = number of observations; Num.ind = number of individuals; Dev.expl. = deviance explained).

Species	Season	Block	Num.obs	Num.ind	Covariates	Dev.expl.
Ttr	AllYear	BSonly	969	3,014	Depth + Salinity + Sst + Lon,Lat	15.94 %
Ttr	Summer	Azov	42	145	Depth + Lon,Lat	53.55 %

Table 45. Selected final models for common dolphins in the Black Sea (Num.obs = number of observations; Num.ind = number of individuals; Dev.expl. = deviance explained).

Species	Season	Block	Num.obs	Num.ind	Covariates	Dev.expl.
Dde	AllYear	BSonly	2,320	8,425	Ssh + Sst + Sst_sd + Lon,Lat	15.69 %

Table 46. Selected final models for harbor porpoises in the Black Sea (Num.obs = number of observations; Num.ind = number of individuals; Dev.expl. = deviance explained).

Species	Season	Block	Num.obs	Num.ind	Covariates	Dev.expl.
Pph	Summer	BSonly	2,074	3,542	Chl + Ssh + Sst + Sst_sd + Lon,Lat	23.01 %
Pph	Winter	BSonly	1,405	6,739	Depth + Sst_sd	20.22 %
Pph	Summer	Azov	112	168	LonLat20	43.68 %

Table 47. Selected final models for fin whales in the Mediterranean Sea (Num.obs = number of observations; Num.ind = number of individuals; Dev.expl. = deviance explained).

Species	Season	Block	Num.obs	Num.ind	Covariates	Dev.expl.
Bph-Bal	Full	Gib_dist	56	82	LonLat20	2.5 %
Bph-Bal	Full	noGibraltar	2,804	4,137	DistToAtl + Ssh + Depth + WindFetch + Lon,Lat	22.12 %

Table 48. Selected final models for sperm whales in the Mediterranean Sea (Num.obs = number of observations; Num.ind = number of individuals; Dev.expl. = deviance explained).

Species	Season	Block	Num.obs	Num.ind	Covariates	Dev.expl.
Pma	Sum	EMed	156	812	Depth + Salinity + SlopePct + Lon,Lat	15.23 %
Pma	Full	Gibraltar	362	442	Depth + Lon	19.48 %
Pma	Full	WMed	1,698	2,616	Depth + DistToAtl + SlopePct + Lon,Lat	23.95 %

Table 49. Selected final models for Risso's dolphins in the Mediterranean Sea (Num.obs = number of observations; Num.ind = number of individuals; Dev.expl. = deviance explained).

Species	Season	Block	Num.obs	Num.ind	Covariates	Dev.expl.
Ggr	Full	All	586	4,770	DistAbyss + DistToAtl + Chl_front_dist + Depth	13.18 %

Table 50. Selected final models for long-finned pilot whales in the Mediterranean Sea (Num.obs = number of observations; Num.ind = number of individuals; Dev.expl. = deviance explained).

Species	Season	Block	Num.obs	Num.ind	Covariates	Dev.expl.
Gme	Full	Wmed-Ion-noAlboran	170	1,868	Ssh + Depth	8.8 %
Gme	Full	Alboran	488	13,841	Depth + Sst + Lon,Lat	21.96 %
Gme	Full	Gibraltar	366	13,024	Depth + DistSlope + SlopePct + Lon,Lat	20.73 %

Table 51. Selected final models for Cuvier's beaked whales in the Mediterranean Sea (Num.obs = number of observations; Num.ind = number of individuals; Dev.expl. = deviance explained).

Species	Season	Block	Num.obs	Num.ind	Covariates	Dev.expl.
Zca-Ziph	Full	WMed	473	1,095	Salinity + DistCan + SlopePct + Lon,Lat	34.11 %
Zca-Ziph	Full	EMed	70	152	DistSlope + Depth + SlopePct + Lon,Lat	34.09 %

Table 52. Selected final models for bottlenose dolphins in the Mediterranean Sea (Num.obs = number of observations; Num.ind = number of individuals; Dev.expl. = deviance explained).

Species	Season	Block	Num.obs	Num.ind	Covariates	Dev.expl.
Ttr	Full	Adriatic	672	3,266	DistEsc + DistSlope + Depth + Salinity + Ssh	21.37 %
Ttr	Full	Aegean	214	937	Depth + Salinity + Sst_front_dist + Lon,Lat	16.32 %
Ttr	Full	Gibraltar	324	11,552	LonLat15	19.97 %
Ttr	Full	Alboran	300	5,856	Depth + Sst + Sst_front_strength	14.91 %
Ttr	Full	Levantine	360	1,747	Depth + Salinity + Chl	35.43 %
Ttr	Full	Ionian	269	1,791	Salinity + Depth	16.1 %
Ttr	Full	WMed_noAlboran	3,430	24,637	Depth + DistToAtl	41.85 %

Table 53. Selected final models for common dolphins in the Mediterranean Sea (Num.obs = number of observations; Num.ind = number of individuals; Dev.expl. = deviance explained).

Species	Season	Block	Num.obs	Num.ind	Covariates	Dev.expl.
Dde	Full	Gibraltar	266	12,202	DistEsc + DistLand + SlopePct + Lon,Lat	20.75 %
Dde	Sum	Alboran	667	41,998	LonLat20	20.32 %
Dde	Sum	noAlboran	524	9,007	DistToAtl + Depth + Sst_front_dist + Lon,Lat	28.66 %
Dde	Win	noAlboran	90	1,709	DistShelf + Primary_prod + Lon,Lat	69.09 %

Table 54. Selected final models for striped dolphins in the Mediterranean Sea (Num.obs = number of observations; Num.ind = number of individuals; Dev.expl. = deviance explained).

Species	Season	Block	Num.obs	Num.ind	Covariates	Dev.expl.
Sco	Full	Gibraltar	291	25,481	DistLand + DistSlope + SlopePct	7.91 %
Sco	Sum	noGibraltar	12,394	277,610	DistToAtl + Mix_layer_thickness + Ssh + Sst + Depth + Lon,Lat	17.33 %
Sco	Win	noGibraltar	1,807	26,275	DistToAtl + Depth + Sst	20.2 %

Table 55. Selected final models for harbor porpoises in the Mediterranean Sea (Num.obs = number of observations; Num.ind = number of individuals; Dev.expl. = deviance explained).

Species	Season	Block	Num.obs	Num.ind	Covariates	Dev.expl.
Pph	Sum	Aegean	16	29	DistToAtl	72.3 %

Table 56. Selected final models for killer whales in the Mediterranean Sea. (Num.obs = number of observations; Num.ind = number of individuals; Dev.expl. = deviance explained).

Species	Season	Block	Num.obs	Num.ind	Covariates	Dev.expl.
Oor	Full	Gibraltar	86	740	Depth + DistToAtl + Primary_prod	30.99 %

3.5. Predicted Densities and Uncertainty for the Black Sea

3.5.1. Bottlenose Dolphins

The final model for bottlenose dolphins in the Black Sea had four covariates (see **Appendix E**): depth, salinity, sea surface temperature and the interaction between latitude and longitude (LonLat) showing two distinct preferred areas, at the northeast and the southwest sections of the basin. Those likely correspond to the two peaks in salinity and sea surface temperature (see **Appendix E**).

In summer (**Figure 60** left), predicted density is higher along the coast in the two areas mentioned, with a smaller peak of density in the northeast of the basin and a much wider and longer coastal stretch along the shallow waters of the western half of the Black Sea, which agrees well with the distribution of the sightings (see **Appendix F**). There is a noticeable absence of bottlenose dolphins along the coast of Eastern Turkey, on the southeastern section of the basin. In winter (**Figure 60** right), the distribution is very similar to that of summer within the stretch of waters for which predictions were made for this season. A mean abundance of 76,712 bottlenose dolphins with a CV of 18.2% was predicted in summer for the Black Sea (**Table 57**). In winter, the estimate of abundance was 14,462 animals with a CV of 27.5% along the winter coast area in the south, with a density higher than the overall density in summer for the whole basin. Appendix F displays the densitologies, also with sightings and tracks overlayed, and uncertainties.

The final model for bottlenose dolphins in the Azov Sea had two covariates (see **Appendix E**): depth, and LonLat with higher density in the south of this small basin (in the Kerch Strait) where all the bottlenose dolphin records in our datasets occurred. There is some predicted density in the southern coasts of the Azov Sea, outside the Kerch Strait, but we consider this to be a potential extrapolation of the model (**Figure 61**). No data were available for winter. A mean abundance of 217 bottlenose dolphins with a CV of 32% was predicted in summer for the Azov Sea, mostly in the Kerch Strait (**Table 57**).

Table 57. Abundance and uncertainty for bottlenose dolphins in the Black Sea.

Season	Block	Abundance	Density	CV	L95ci_ abundance	U95ci_ abundance
Summer	Black Sea	76,133	0.1991	0.1817	60,403	116,221
Winter	Win_coast_area	15,311	0.2914	0.5371	7,080	38,187
Summer	Azov	217	0.0057	0.3204	437	1,300

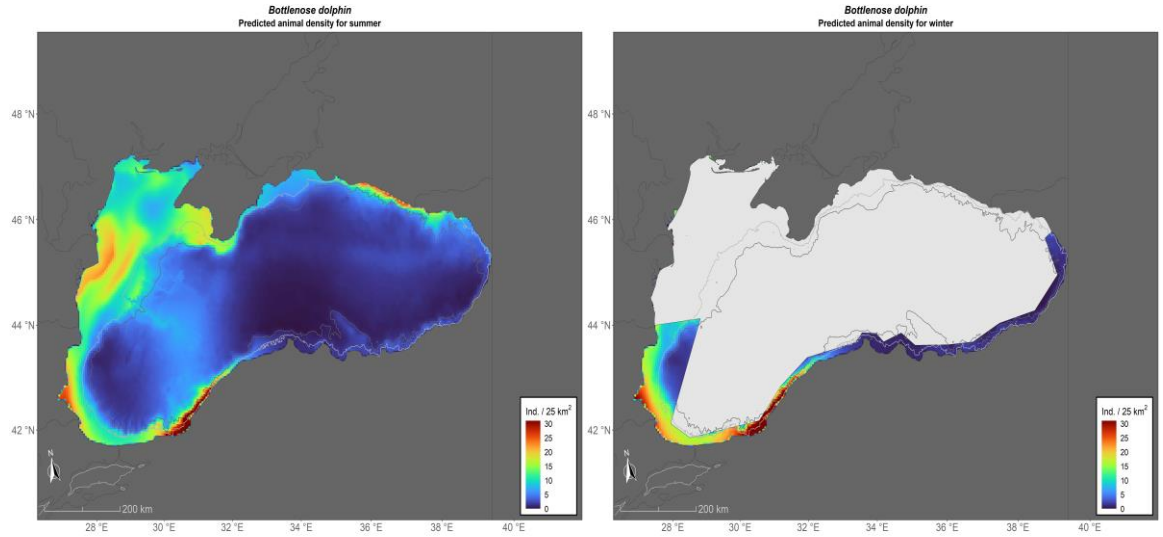

Figure 60. Map of predicted densities in summer (left) and winter (right) for bottlenose dolphins.

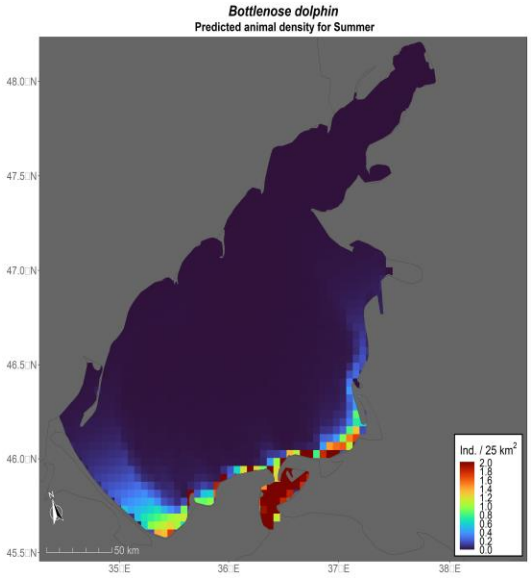

Figure 61. Map of predicted densities in summer for bottlenose dolphins in the Azov Sea.

3.5.2. Common Dolphins

The final model for common dolphins in the Black Sea had four covariates: sea surface height, sea surface temperature, standard deviation of sea surface temperature, and the interaction between latitude and longitude (LonLat) showing two distinct preferred areas, at the east and the southwest sections of the basin. Those probably correspond to the two peaks observed in sea surface temperature (see **Appendix E**).

In summer (**Figure 62** left), predicted density is higher close to the coast in the two areas mentioned. There is also prediction of intermediate density around the central coast of Turkey and the southwestern waters off the Crimea peninsula. In winter (**Figure 62** right), the distribution is very similar to that of summer within the stretch of waters for which predictions were made for this season, but with higher density in the east along the coast of Georgia. A mean abundance of 276,344 common dolphins with a CV of 24% was predicted in summer for the Black Sea (**Table 58**). In winter, the estimate of abundance was 37,121 animals with a CV of 7.6% along the winter coast area in the south, with a similar density compared to the overall density in summer for the whole basin. Appendix F displays the densitologies, also with sightings and tracks overlayed, and uncertainties.

There were no records of common dolphins in the Azov Sea.

Table 58. Abundance and uncertainty for common dolphins in the Black Sea.

Season	Block	Abundance	Density	CV	L95ci_ abundance	U95ci_ abundance
Summer	Black Sea	276,015	0.6858	0.2400	189,296	439,901
Winter	Win_coast_area	34,250	0.6745	0.2554	21,942	53,518

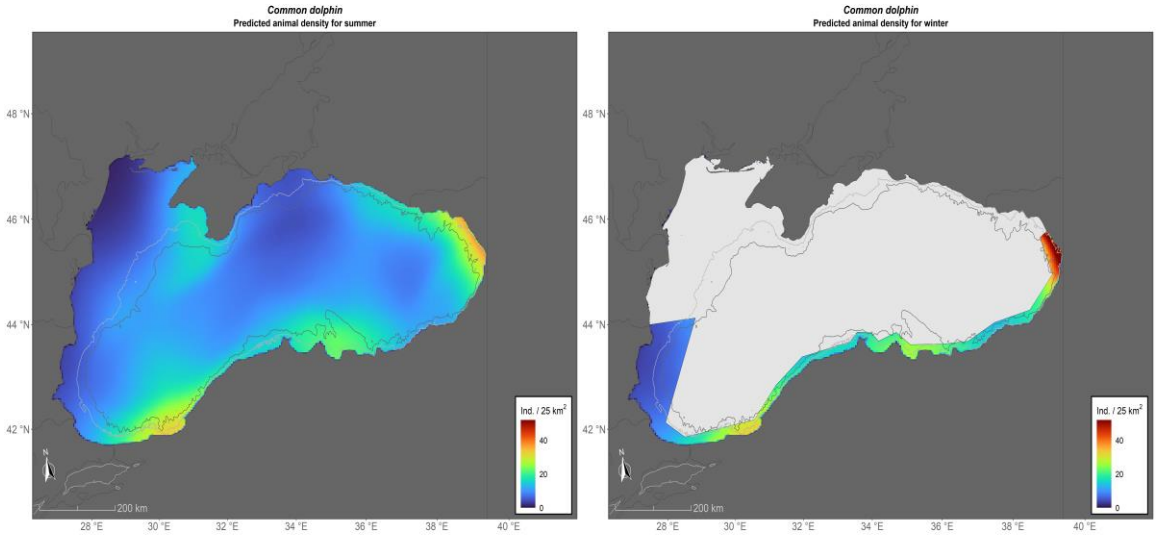

Figure 62. Map of predicted densities in summer (left) and winter (right) for common dolphins.

3.5.3. Harbor porpoises

The final model for harbor porpoises in the Black Sea had five covariates: chlorophyll, sea surface height, sea surface temperature, standard deviation of sea surface temperature, and the interaction between latitude and longitude (LonLat) showing two distinct preferred areas, at the southeast (Georgia waters) and the southwest sections of the basin. Those likely correspond to the two peaks observed in sea surface temperature (see **Appendix E**). In summer (**Figure 63** left), predicted density is higher along the coast in the two areas mentioned, with another smaller peak of density along the central coast of Turkey, which agrees well with the distribution of the sightings (see **Appendix F**).

There is a noticeable very low density of harbor porpoises throughout most of the eastern half of the basin, except the waters off Georgia and easternmost waters off Turkey. In winter (**Figure 63** right), the distribution is very similar to that of summer within the stretch of waters for which predictions were made for this season. A mean abundance of 392,406 harbor porpoises with a CV of 34.7% was predicted in summer for the Black Sea (**Table 59**). In winter, the estimate of abundance was 82,045 animals with a CV of 35% along the winter coast area in the south, with a density higher than the overall density of summer for the whole basin. **Appendix F** displays the densitologies, also with sightings and tracks overlayed, and uncertainties.

The final model for harbor porpoises in the Azov Sea had only one covariate (see **Appendix E**), the interaction LonLat. Highest density was predicted in two areas of the central basin of the Azov Sea (**Figure 64**). No data were available for winter.

Table 59. Abundance and uncertainty for harbor porpoises in the Black Sea.

Season	Block	Abundance	Density	CV	L95ci_ abundance	U95ci_ abundance
Summer	Black Sea	391,894	0.9802	0.3466	230,152	738,976
Winter	Win_coast_area	82,007	1.5607	0.3490	48,335	156,282
Summer	Azov	16,742	0.4421	0.1385	13,551	22,532

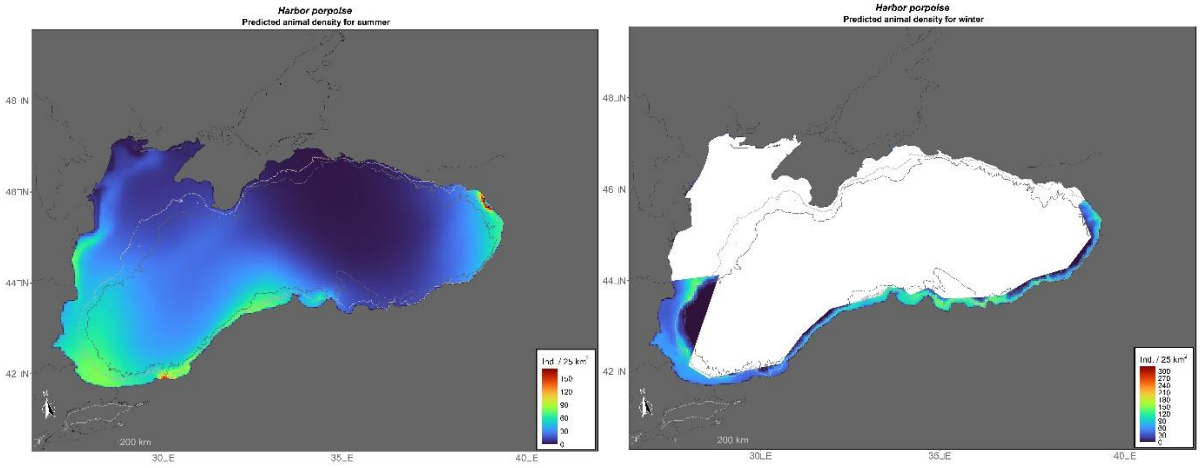

Figure 63. Map of predicted densities in summer (left) and winter (right) for harbor porpoises.

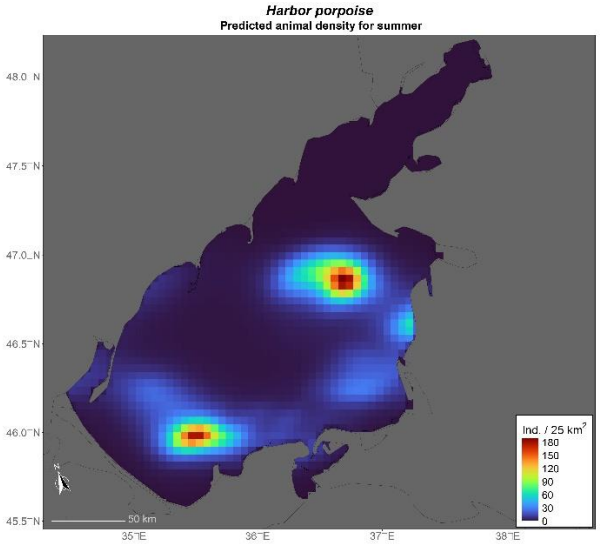

Figure 64. Map of predicted densities in summer for harbor porpoises in the Azov Sea.

3.6. Predicted Densities and Uncertainty for the Mediterranean Sea

3.6.1. Fin Whales

Fin whales were modeled together with “Unidentified Balaenoptera”, assuming that all these were actually fin whales, given that there are no observations of other Balaenopteridae in the Mediterranean except for a very small number of minke whales (four in the datasets available), which are easily differentiated due to the large difference in body size and blow. There were two models for fin whales: the Strait of Gibraltar and the rest of the Mediterranean except the Aegean and Levantine Seas where we did not have observations of this species. For the Strait of Gibraltar the best model was the interaction LonLat but with very little deviance explained (2.5%). For the rest of the Mediterranean, the best model had five covariates: the interaction LonLat, distance from the Atlantic, sea surface height, depth, and wind fetch (distance from all land). See **Appendix E** for details of the models.

Both in summer and winter (**Figure 65** and **Figure 66**), predicted density was the highest in the Liguro-Provençal area, which agrees well with the distribution of the sightings (see **Appendix F**). A mean abundance of 1,968 fin whales with a CV of 15.9% was predicted in summer, and 2,318 whales with a CV of 16% was predicted in winter (**Table 60**). CVs were highest in the Adriatic and Ionian Seas, and the southeastern portion of the Tyrrhenian Sea where very few fin whales were recorded.

Table 60. Abundance and uncertainty for fin whales in the Mediterranean Sea.

Season	Block	Abundance	Density	CV	L95ci_ abundance	U95ci_ abundance
Summer	Ionian	85	0.0001	0.8673	25	289
Summer	Adriatic	9	0.0001	0.7631	3	27
Summer	WMed_noAlboran	1,783	0.0023	0.1688	1,313	2,421
Summer	Alboran	77	0.0011	0.2114	53	112
Summer	Gibraltar	14	0.0068	0.2072	10	20
Summer	**Total**	**1,968**	**0.0008**	**0.1590**	**1,474**	**2,628**
Winter	Ionian	73	0.0001	0.8715	21	249
Winter	Adriatic	9	0.0001	0.8216	3	29
Winter	WMed_noAlboran	2,152	0.0028	0.1695	1,583	2,925
Winter	Alboran	71	0.0010	0.1854	51	99
Winter	Gibraltar	13	0.0064	0.2072	9	19
Winter	**Total**	**2,318**	**0.0009**	**0.1601**	**1,733**	**3,101**

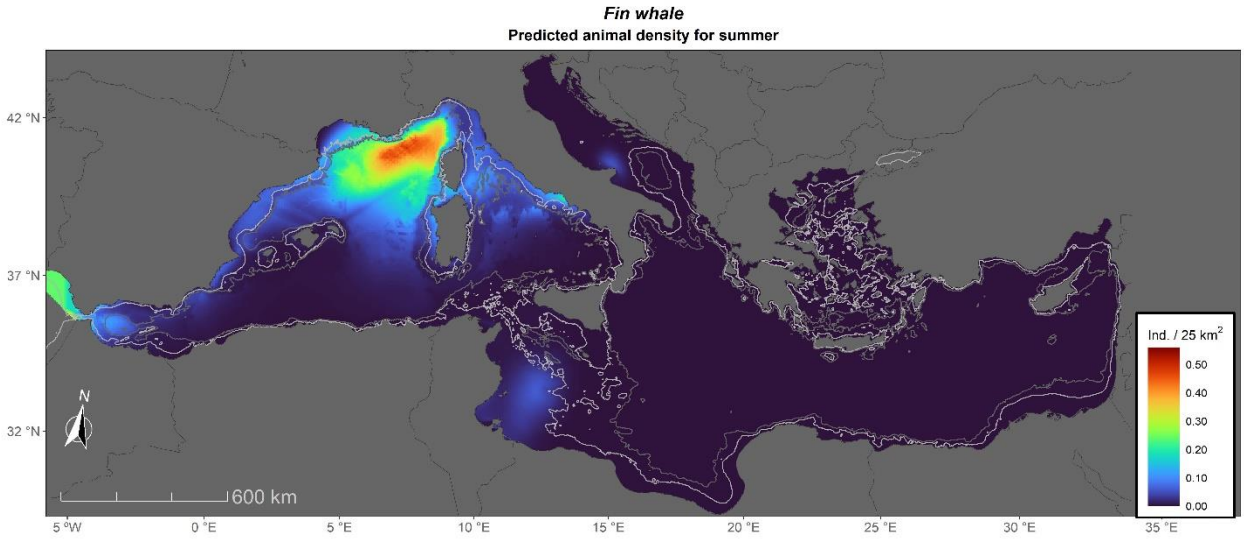

Figure 65. Map of predicted densities in summer for fin whales.

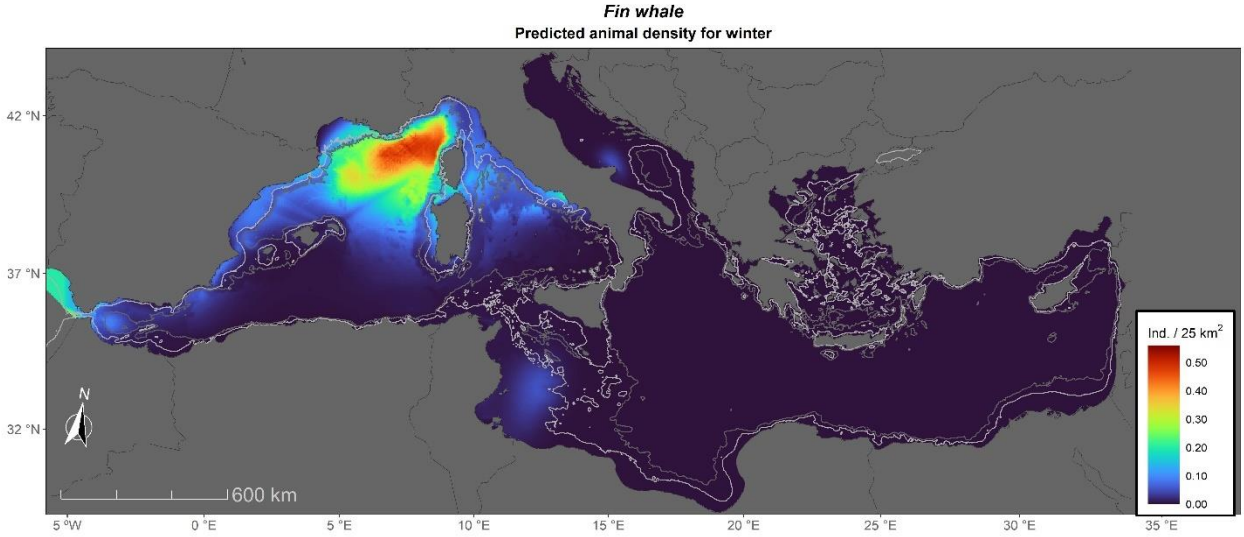

Figure 66. Map of predicted densities in winter for fin whales.

3.6.2. Sperm Whales

There were four models for sperm whales: Strait of Gibraltar (year round), western Mediterranean (summer and winter independently), and eastern Mediterranean (summer, no data available for winter). For the Strait of Gibraltar the best model had two static covariates: depth and longitude. For the western Mediterranean in summer, the best model had five covariates: the interaction LonLat, depth, distance from the Atlantic, slope of the sea floor, and sea surface temperature front strength. For the western Mediterranean in winter, the best model had three covariates: the interaction LonLat, primary productivity and wind fetch (distance from all land). The model for the eastern Mediterranean in summer had four covariates: the interaction LonLat, depth, salinity, and slope of the sea floor. See **Appendix E** for details of the

models. The eastern Mediterranean (EMed) summer model prediction was assigned also as EMed winter prediction after consulting with the expert in the area.

In the Strait of Gibraltar most of the density was concentrated in the center of the channel, matching very well the distribution of the sightings (**Figure 67**). For the rest of the Mediterranean, the models for summer predicted the highest densities around the Balearic Islands and the central-eastern portion of the Tyrrhenian Sea (**Figure 68**), but generally much higher abundance was predicted in the western Mediterranean than the eastern. In winter the general pattern of lower densities in the eastern than in the western Mediterranean is maintained, but higher density is predicted in the Tyrrhenian Sea than the Balearic Islands (**Figure 69**). A mean abundance of 4,392 sperm whales with a CV of 9.8% was predicted in summer, and 3,104 whales with a CV of 29% was predicted in winter (**Table 61**).

Table 61. Abundance and uncertainty for sperm whales in the Mediterranean Sea.

Season	Block	Abundance	Density	CV	L95ci_ abundance	U95ci_ abundance
Summer	Aegean	67	0.0004	0.1785	49	92
Summer	Levantine	323	0.0006	0.3317	184	566
Summer	Ionian	111	0.0001	0.2739	69	178
Summer	WMed	3,837	0.0045	0.1074	3,142	4,686
Summer	Gibraltar	70	0.0342	0.1000	58	84
Summer	**Total**	**4,392**	**0.0018**	**0.0981**	**3,656**	**5,276**
Winter	Aegean	67	0.0004	0.1785	49	92
Winter	Levantine	323	0.0006	0.3317	184	566
Winter	Ionian	111	0.0001	0.2739	69	178
Winter	WMed	2,538	0.0030	0.3474	1,415	4,553
Winter	Gibraltar	82	0.0401	0.1000	68	99
Winter	**Total**	**3,104**	**0.0012**	**0.2897**	**1,885**	**5,111**

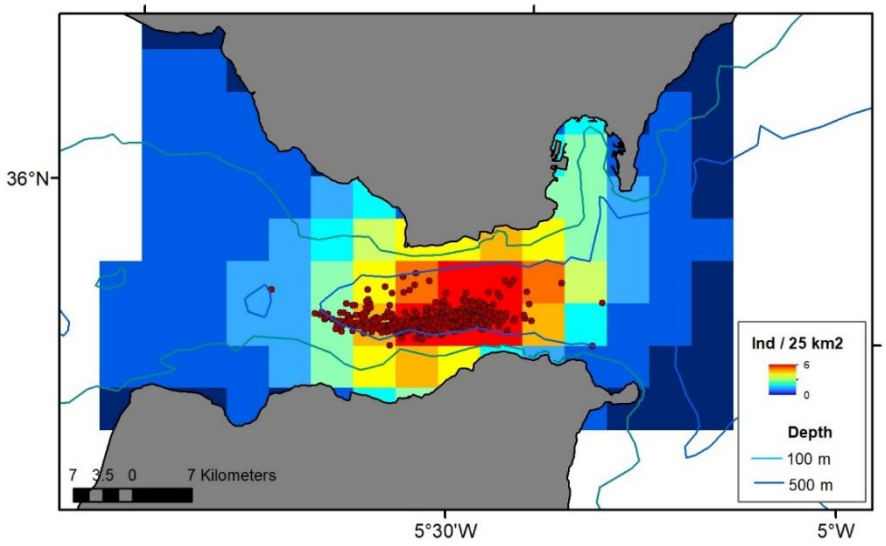

Figure 67. Map of year-round predicted densities in the Strait of Gibraltar for sperm whales.

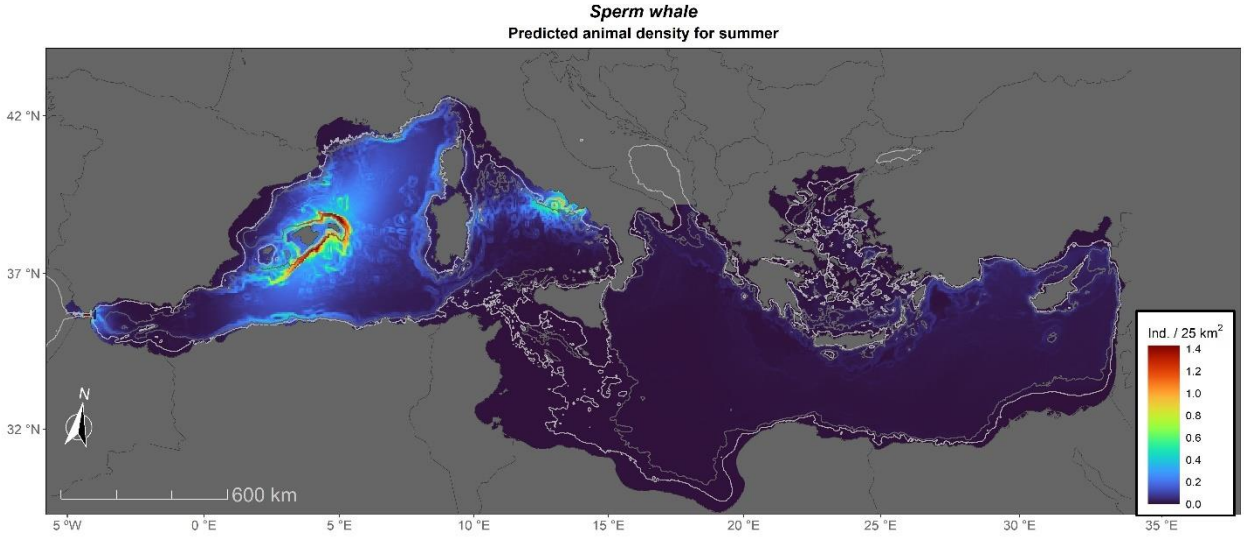

Figure 68. Map of predicted densities in summer for sperm whales.

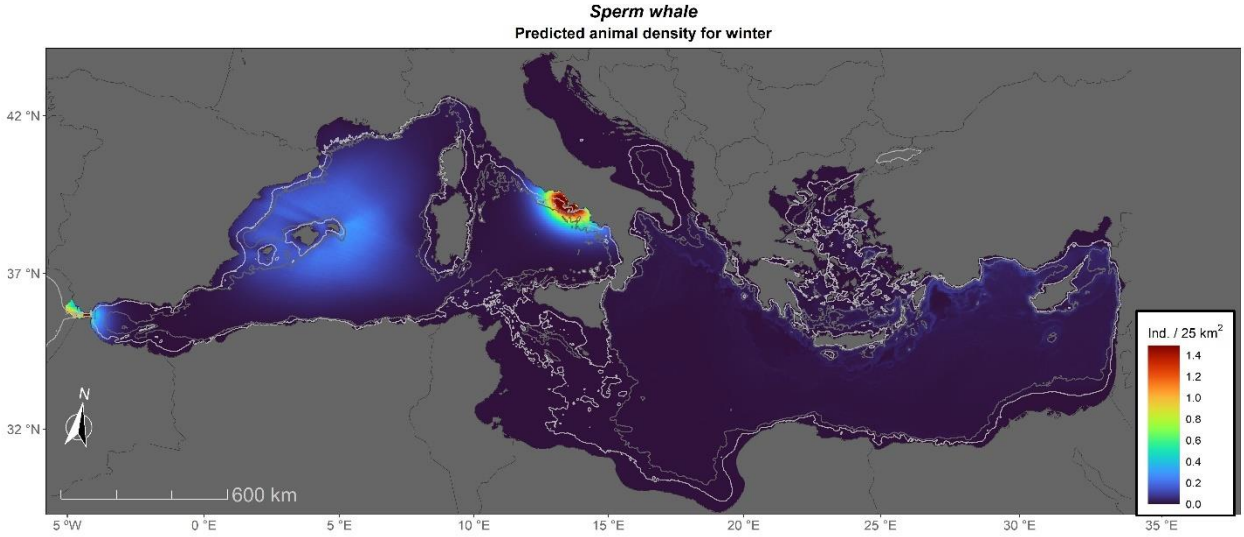

Figure 69. Map of predicted densities in winter for sperm whales.

3.6.3. Risso's Dolphins

There was a single model for Risso's dolphins, year-round, excluding the Strait of Gibraltar where density was assumed 0 as no sightings have ever been reported there. The best model had four covariates: distance from the abyss, distance from the Atlantic, distance to chlorophyll front, and depth. Risso's dolphins were predicted throughout the whole Mediterranean Sea, but the highest density was predicted in the western Mediterranean for both seasons, especially around the Balearic Islands, off the coast of Algeria, and in the Alboran Sea. See **Appendix E** for details of the models.

The model predicted a wide distribution of Risso's dolphins, but with higher densities in the western Mediterranean, similarly for summer and for winter (**Figure 70** and **Figure 71**). A mean abundance of 14,630 Risso's dolphins with a CV of 8.9% was predicted in summer, and 15,864 Risso's dolphins with a CV of 9.5% was predicted in winter (**Table 62**).

Table 62. Abundance and uncertainty for Risso's dolphins in the Mediterranean Sea.

Season	Block	Abundance	Density	CV	L95ci_ abundance	U95ci_ abundance
Summer	Aegean	1,185	0.0063	0.1049	975	1,441
Summer	Levantine	1,762	0.0031	0.1659	1,304	2,380
Summer	Ionian	2,366	0.0031	0.1624	1,762	3,178
Summer	Adriatic	488	0.0037	0.1943	345	691
Summer	WMed_noAlboran	7,807	0.0101	0.1469	5,968	10,213
Summer	Alboran	1,022	0.0149	0.2621	648	1,613
Summer	**Total**	**14,630**	**0.0058**	**0.0893**	**12,372**	**17,300**
Winter	Aegean	1,464	0.0077	0.1110	1,191	1,799
Winter	Levantine	1,772	0.0031	0.1975	1,245	2,523
Winter	Ionian	2,358	0.0031	0.1807	1,703	3,265
Winter	Adriatic	402	0.0030	0.2253	270	599
Winter	WMed_noAlboran	8,533	0.0110	0.1491	6,498	11,205
Winter	Alboran	1,335	0.0194	0.2719	833	2,139
Winter	**Total**	**15,864**	**0.0063**	**0.0954**	**13,269**	**18,966**

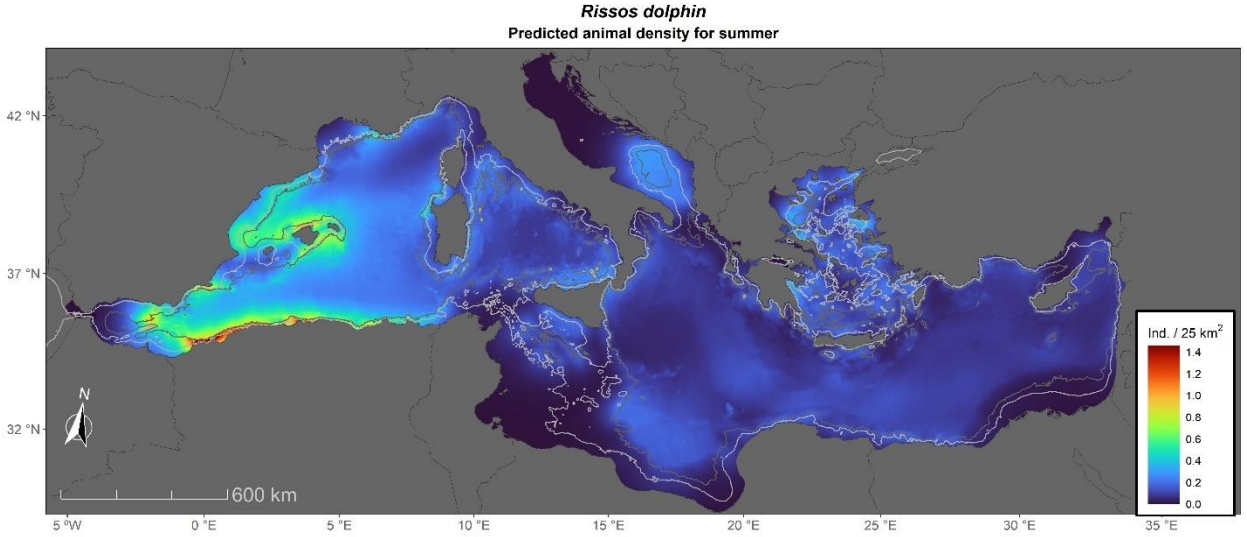

Figure 70. Map of predicted densities in summer for Risso's dolphins.

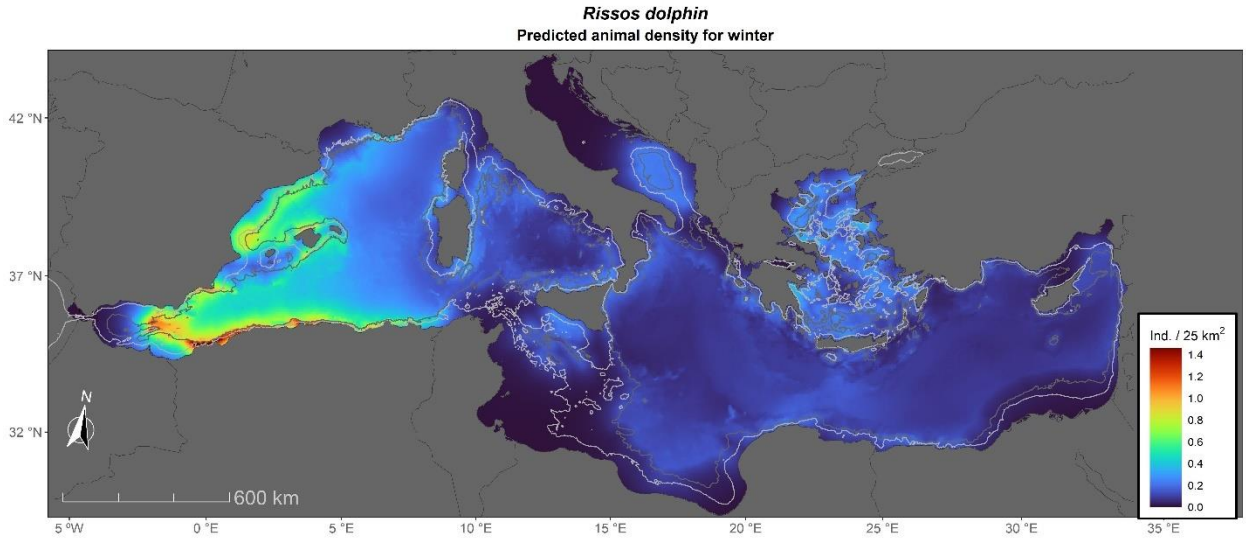

Figure 71. Map of predicted densities in winter for Risso's dolphins.

3.6.4. Long-finned Pilot Whales

Long-finned pilot whales were modeled year-round for three blocks: Strait of Gibraltar, Alboran Sea, and the western Mediterranean (except Alboran Sea) with Ionian Sea. The Adriatic, Aegean and Levantine Seas were assumed to have a density of 0 given the absence of observations in those blocks. For the Strait of Gibraltar the best model had four static covariates: the interaction LonLat, depth, distance from the continental slope, and slope of the sea floor. For the western Mediterranean plus Ionian Sea, the best model had two covariates: sea surface height and depth. For the Alboran Sea, the best model had three covariates: the interaction LonLat, depth, and sea surface temperature. See **Appendix E** for details of the models.

In the Strait of Gibraltar most of the density was concentrated in the center of the channel, matching very well with the distribution of the sightings (**Figure 72**). For the rest of the Mediterranean, the models predicted the highest densities in the Alboran Sea, both in summer and winter (**Figure 73** and **Figure 74**). A mean abundance of 8,429 long-finned pilot whales with a CV of 13.3% was predicted in summer, and 7,189 whales with a CV of 14.2% was predicted in winter (**Table 63**). In the Strait of Gibraltar, the abundance predicted by the model was scaled down to match the more accurate abundance estimate from many years of photo-identification in the area (285 individuals, Ouled-Cheikh et al. 2023).

Table 63. Abundance and uncertainty for long-finned pilot whales in the Mediterranean Sea.

Season	Block	Abundance	Density	CV	L95ci_ abundance	U95ci_ abundance
Summer	Gibraltar	285	0.1392	0.1329	659	1,075
Summer	Ionian	2,047	0.0027	0.3464	37	120
Summer	WMed_noAlboran	2,130	0.0027	0.3219	2,014	6,015
Summer	Alboran	3,967	0.0577	0.2474	2,572	6,118
Summer	**Total**	**8,429**	**0.0052**	**0.1358**	**6,511**	**10,726**
Winter	Gibraltar	285	0.1392	0.1329	659	1,075
Winter	Ionian	2,120	0.0028	0.3056	44	125
Winter	WMed_noAlboran	2,539	0.0033	0.2523	2,500	6,038
Winter	Alboran	2,245	0.0327	0.2302	1,496	3,370
Winter	**Total**	**7,189**	**0.0045**	**0.1415**	**5,436**	**9,133**

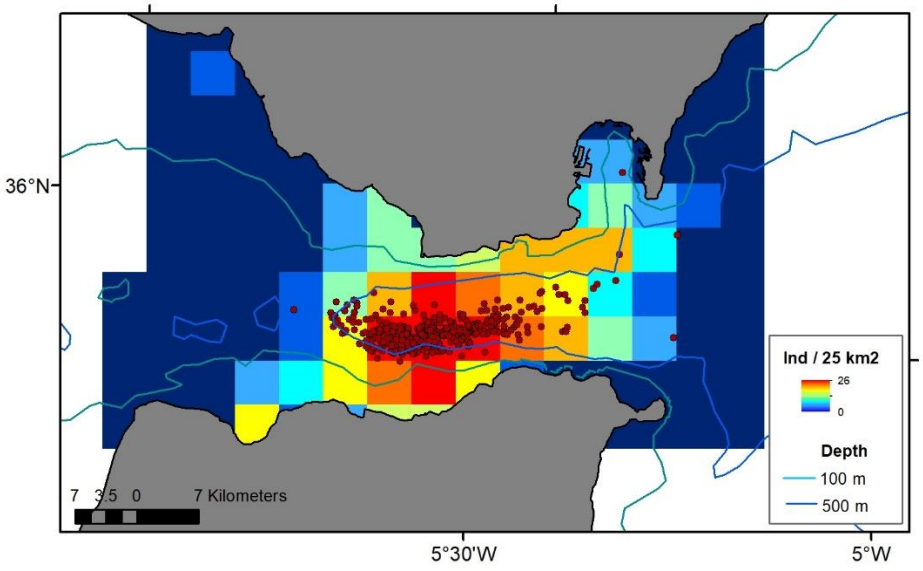

Figure 72. Map of predicted densities, all year round, in the Strait of Gibraltar for long-finned pilot whales.

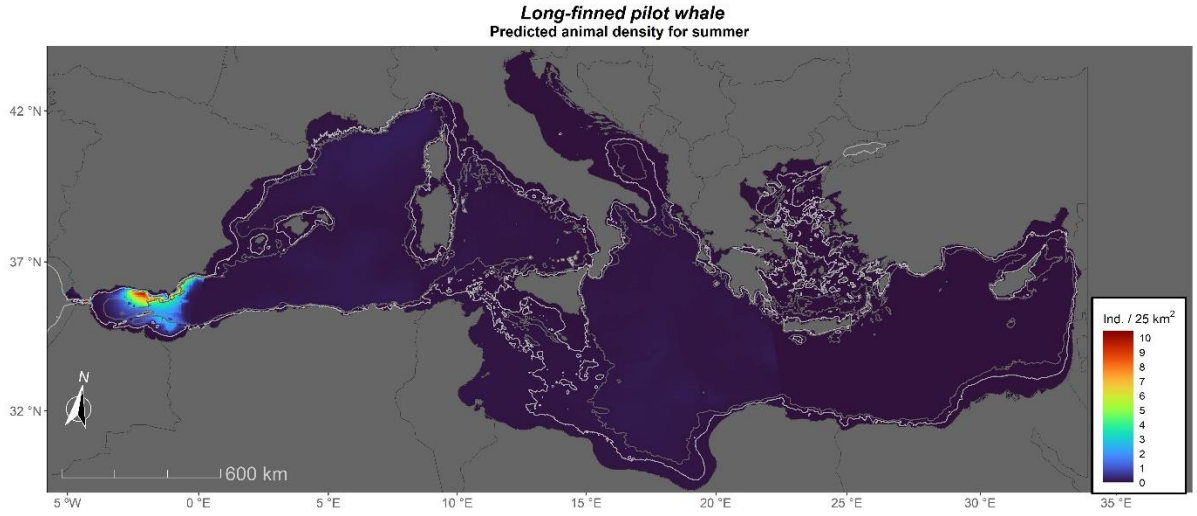

Figure 73. Map of predicted densities in summer for long-finned pilot whales.

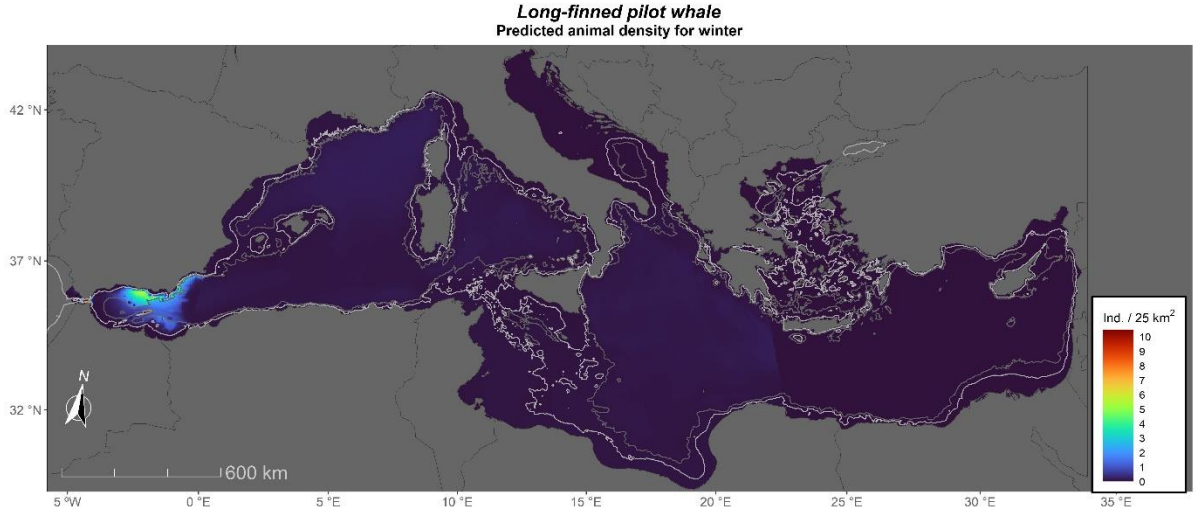

Figure 74. Map of predicted densities in winter for long-finned pilot whales.

3.6.5. Cuvier's Beaked Whales

Cuvier's beaked whales were modeled together with "Unidentified beaked whales," assuming that most, if not all, of these were Cuvier's beaked whales given that this is the only regular beaked whale inhabiting the Mediterranean Sea. Cuvier's beaked whales were modeled year-round, for two blocks: western and eastern Mediterranean.

The western and eastern Mediterranean were modeled separately as the model for the whole area did not produce reasonable results. For the western Mediterranean, the best model had four covariates: the interaction LonLat, salinity, distance from canyons, and slope of the sea floor. For the eastern Mediterranean, the best model had also four covariates: the interaction LonLat, depth, distance from the continental slope, and slope of the sea floor. See **Appendix E**

for details of the models. In the Strait of Gibraltar density was assumed 0 as no sightings have ever been reported there. Both in summer and winter, the models predicted the highest densities in the Alboran Sea, the Ligurian Sea, and the Hellenic Trench, with an additional hotspot along the southern slope of the eastern Mediterranean (**Figure 75** and **Figure 76**), aligning very well with the observations, especially in summer (see **Appendix A**). A mean abundance of 4,275 Cuvier's beaked whales with a CV of 13.4% was predicted in summer, and 4,208 whales with a CV of 13.7% was predicted in winter (**Table 64**).

Table 64. Abundance and uncertainty for Cuvier's beaked whales in the Mediterranean Sea.

Season	Block	Abundance	Density	CV	L95ci_ abundance	U95ci_ abundance
Summer	Aegean	550	0.0029	0.3270	160	484
Summer	Levantine	1,051	0.0018	0.2764	580	1,510
Summer	Ionian	1,503	0.0020	0.2596	756	1,868
Summer	Adriatic	71	0.0005	0.6874	51	393
Summer	WMed_noAlboran	651	0.0008	0.1565	491	868
Summer	Alboran	449	0.0063	0.3970	234	868
Summer	**Total**	**4,275**	**0.0017**	**0.1338**	**2,851**	**4,665**
Winter	Aegean	550	0.0029	0.3270	160	484
Winter	Levantine	1,051	0.0018	0.2764	580	1,510
Winter	Ionian	1,503	0.0020	0.2596	756	1,868
Winter	Adriatic	71	0.0005	0.6874	51	393
Winter	WMed_noAlboran	722	0.0009	0.1763	527	995
Winter	Alboran	311	0.0044	0.7137	109	897
Winter	**Total**	**4,208**	**0.0017**	**0.1366**	**2,785**	**4,600**

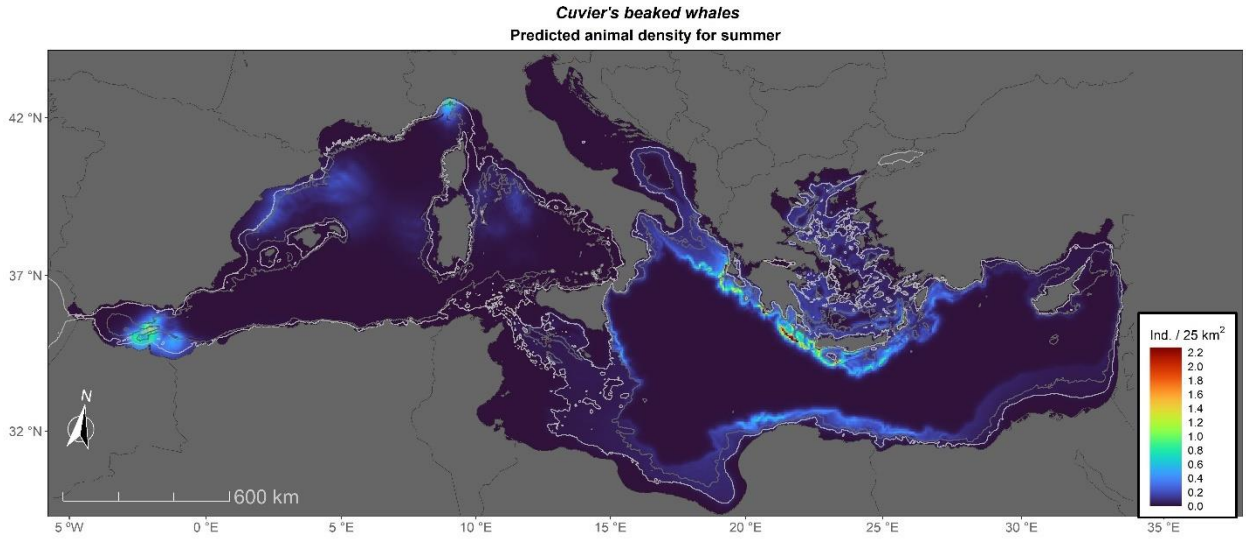

Figure 75. Map of predicted densities in summer for Cuvier's beaked whales.

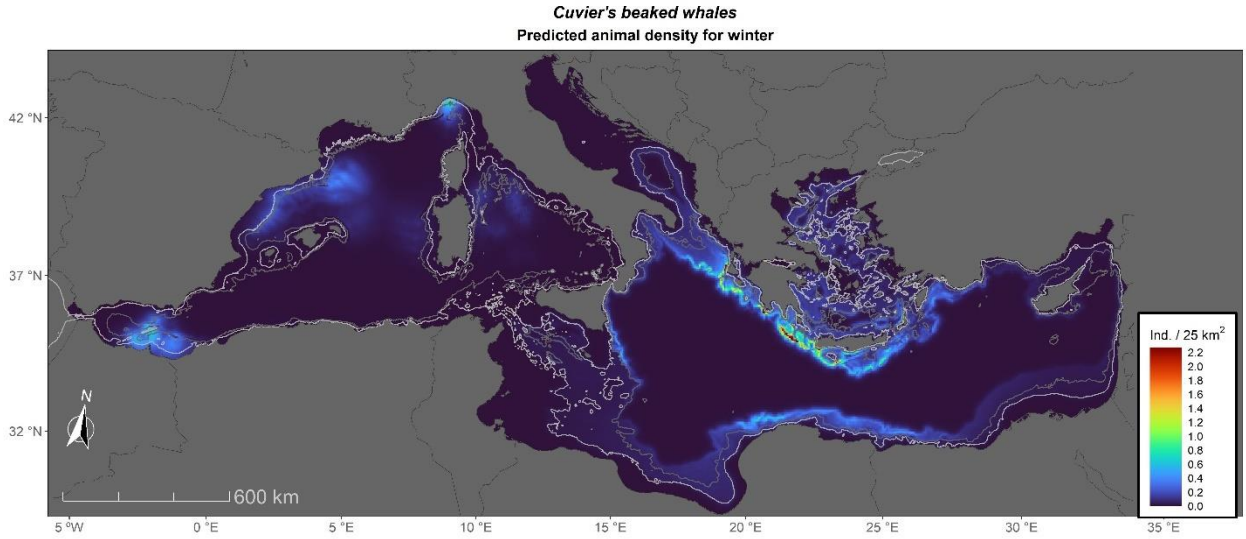

Figure 76. Map of predicted densities in winter for Cuvier's beaked whales.

3.6.6. Bottlenose Dolphins

Bottlenose dolphins were modeled year-round, for each block separately: Strait of Gibraltar, Alboran Sea, western Mediterranean (except Alboran Sea), Ionian Sea, Adriatic Sea, Aegean Sea, and Levantine Sea. For the Strait of Gibraltar the best model had just the interaction LonLat. For the Alboran Sea, the best model had three covariates: depth, sea surface temperature, and sea surface temperature front strength. For the western Mediterranean, the best model had only two covariates: depth and longitude. For the Ionian Sea, the best model had two covariates: salinity and depth. For the Adriatic Sea, there were five covariates in the best model: distance from escarpments, distance from the continental slope, depth, salinity, and sea surface height. For the Aegean Sea, there were four covariates in the best model: depth, salinity, distance from sea surface fronts, and the interaction LonLat. For the Levantine Sea, the best model had three covariates: depth, salinity, and chlorophyll. See **Appendix E** for details of the models.

In the Strait of Gibraltar most of the density was concentrated in the center of the channel, matching well with the distribution of the sightings (**Figure 77**). For the rest of the Mediterranean, the models predicted the highest densities along most coastal areas, but especially in the eastern part of the Adriatic Sea, Gulf of Lyon, Alboran Sea, eastern part of the Ligurian Sea, around the Corsica and Sardinia islands, the northern Tunisian waters, and the southeasternmost area of the Levantine Sea, both in summer and winter (**Figure 78** and **Figure 79**), aligning very well with where the majority of observations were recorded, especially in summer. A mean abundance of 85,674 bottlenose dolphins with a CV of 6.6% was predicted in summer, and 94,748 whales with a CV of 9.4% was predicted in winter (**Table 65**). In the Strait of Gibraltar, the abundance predicted by the model was scaled down to match the more accurate abundance estimate from many years of photo-identification in the area (162 animals, de Stephanis, pers. comm.).

Table 65. Abundance and uncertainty for bottlenose dolphins in the Mediterranean Sea.

Season	Block	Abundance	Density	CV	L95ci_ abundance	U95ci_ abundance
Summer	Gibraltar	162	0.0791	0.1095	736	1,106
Summer	Aegean	6,098	0.0322	0.2525	3,922	9,481
Summer	Levantine	14,349	0.0251	0.1835	10,314	19,963
Summer	Ionian	17,326	0.0226	0.1217	13,834	21,700
Summer	Adriatic	16,165	0.1215	0.2361	10,670	24,491
Summer	WMed_noAlboran	26,300	0.0339	0.0311	26,363	29,726
Summer	Alboran	5,274	0.0768	0.2245	3,546	7,844
Summer	**Total**	**85,674**	**0.0342**	**0.0657**	**77,777**	**99,811**
Winter	Gibraltar	162	0.0791	0.1095	736	1,106
Winter	Aegean	4,458	0.0236	0.2197	3,021	6,580
Winter	Levantine	27,088	0.0474	0.2385	17,812	41,196
Winter	Ionian	18,054	0.0236	0.1096	14,725	22,136
Winter	Adriatic	14,459	0.1086	0.3902	7,581	27,578
Winter	WMed_noAlboran	26,300	0.0339	0.0311	26,363	29,726
Winter	Alboran	4,227	0.0615	0.1945	2,984	5,988
Winter	**Total**	**94,748**	**0.0378**	**0.0938**	**81,521**	**115,852**

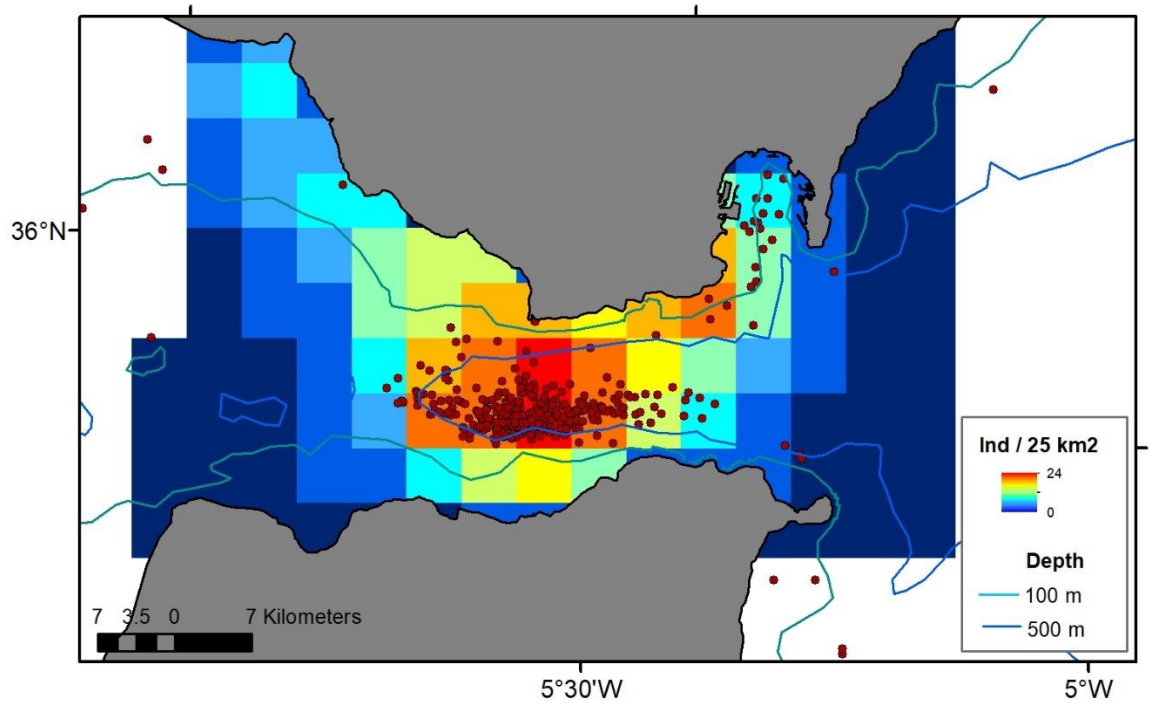

Figure 77. Map of year-round predicted densities in the Strait of Gibraltar for bottlenose dolphins.

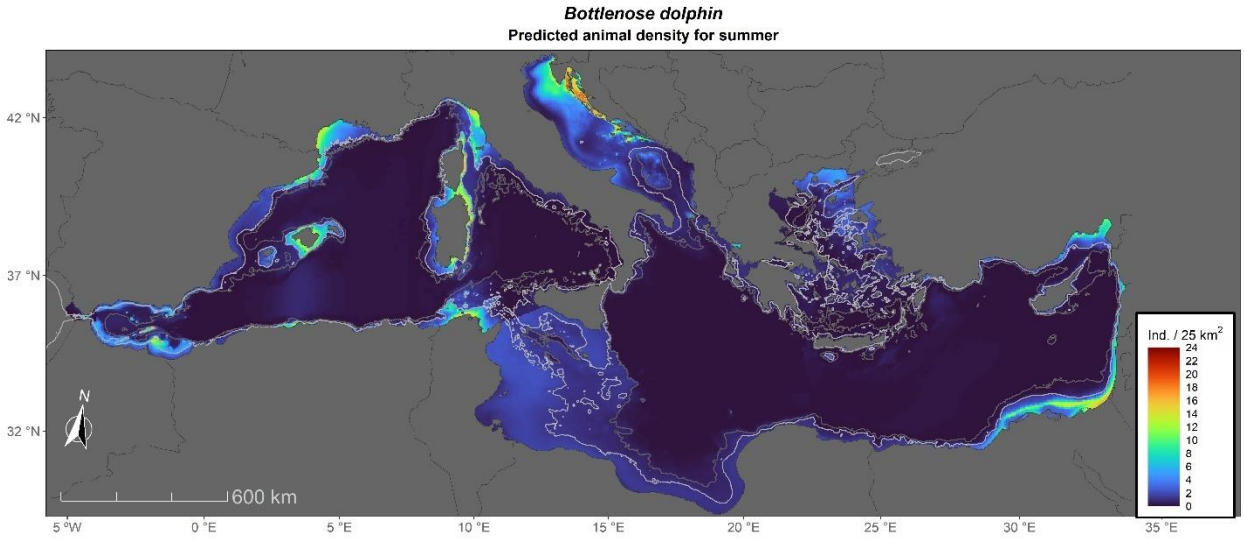

Figure 78. Map of predicted densities in summer for bottlenose dolphins.

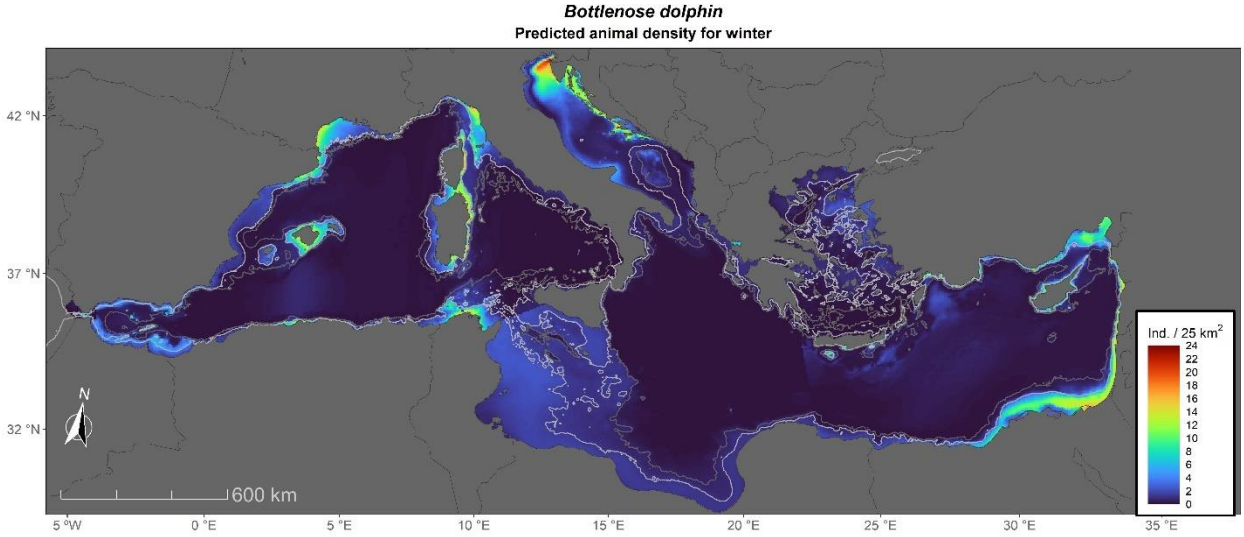

Figure 79. Map of predicted densities in winter for bottlenose dolphins.

3.6.7. Common Dolphins

Common dolphins were modeled year-round for Gibraltar, and with summer and winter seasons separately for two blocks: Alboran Sea and the rest of the Mediterranean (except Alboran Sea). For the Strait of Gibraltar the best model had four static covariates: the interaction LonLat, distance from land, distance from escarpments, and slope of the sea floor. For the Alboran Sea in summer, the best model consisted only of the interaction LonLat, while in winter it had four covariates: the interaction LonLat, depth, distance from the continental slope, and distance from the sea surface temperature fronts. For the rest of the Mediterranean in summer, the best model had four covariates: the interaction LonLat, depth, distance from the Atlantic, and distance from sea surface temperature fronts; in winter, the best model had three covariates: the interaction

LonLat, distance from the continental shelf, and primary productivity. See **Appendix E** for details of the models.

In the Strait of Gibraltar most of the density was concentrated in the eastern half of the channel, and particularly in the Bay of Algeciras and around the Gibraltar Point (**Figure 80**). For the rest of the Mediterranean, the models predicted the highest densities in the Alboran Sea, both in summer and winter (**Figure 81** and **Figure 82**). However, in summer they were more concentrated on the coastal areas of the Alboran Sea, while in winter the density spread out more into the deeper waters and along the Algerian Coast. A mean abundance of 81,506 common dolphins with a CV of 8.5% was predicted in summer, and 83,400 dolphins with a CV of 37.2% was predicted in winter (**Table 66**).

Table 66. Abundance and uncertainty for common dolphins in the Mediterranean Sea.

Season	Block	Abundance	Density	CV	L95ci_ abundance	U95ci_ abundance
Summer	Aegean	15,468	0.0818	0.2200	10,475	22,840
Summer	Levantine	7,738	0.0135	0.3369	4,380	13,670
Summer	Ionian	6,641	0.0087	0.2062	4,599	9,590
Summer	Adriatic	336	0.0025	0.5166	149	760
Summer	WMed_noAlboran	12,649	0.0163	0.2440	8,245	19,405
Summer	Alboran	35,604	0.5182	0.1232	28,353	44,709
Summer	Gibraltar	5,153	2.5173	0.1526	3,901	6,807
Summer	**Total**	**81,506**	**0.0325**	**0.0848**	**69,487**	**95,604**
Winter	Aegean	4,951	0.0262	0.7492	1,655	14,814
Winter	Levantine	5,214	0.0091	0.7438	1,753	15,506
Winter	Ionian	2,985	0.0039	0.9123	838	10,636
Winter	Adriatic	58	0.0004	1.4768	10	343
Winter	WMed_noAlboran	37,317	0.0481	0.5785	15,253	91,299
Winter	Alboran	28,943	0.4212	0.3372	16,376	51,155
Winter	Gibraltar	5,136	2.5090	0.1526	3,888	6,784
Winter	**Total**	**83,400**	**0.0333**	**0.3352**	**47,326**	**146,973**

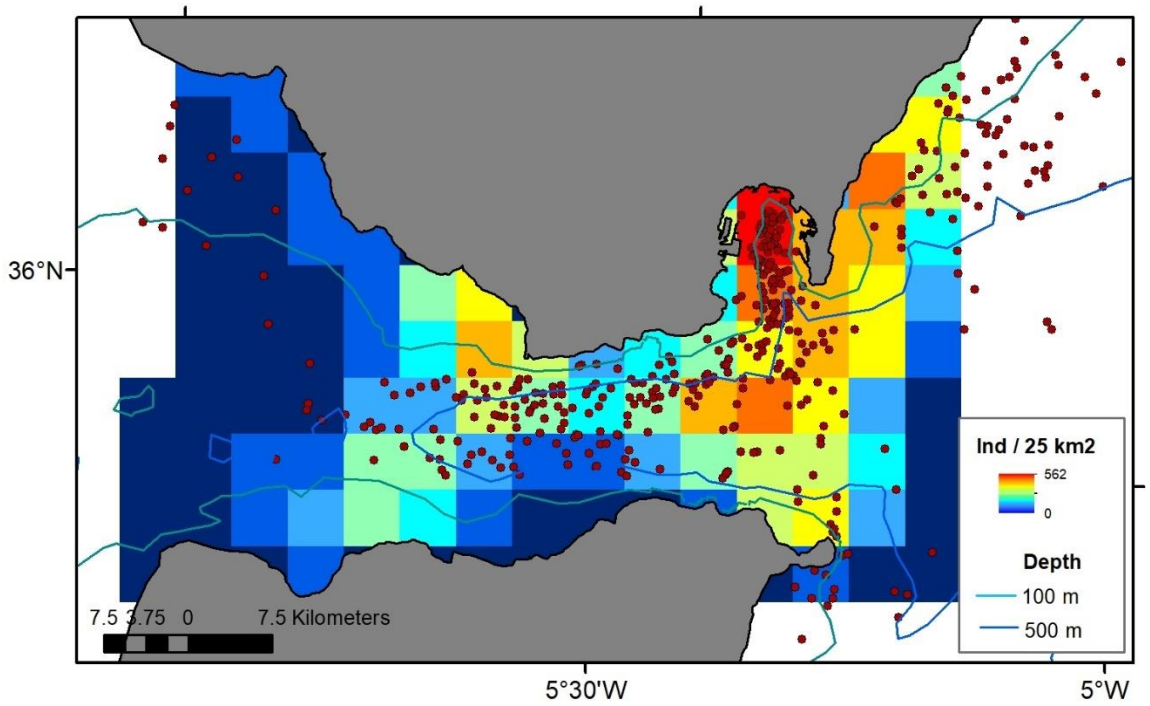

Figure 80. Map of year-round predicted densities in the Strait of Gibraltar for common dolphins.

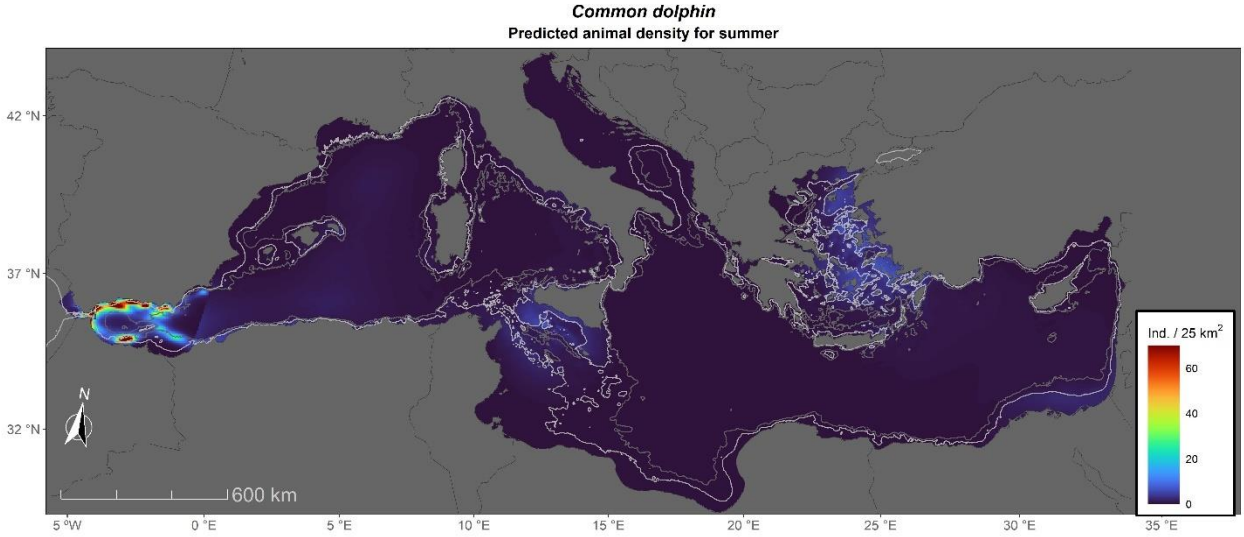

Figure 81. Map of predicted densities in summer for common dolphins.

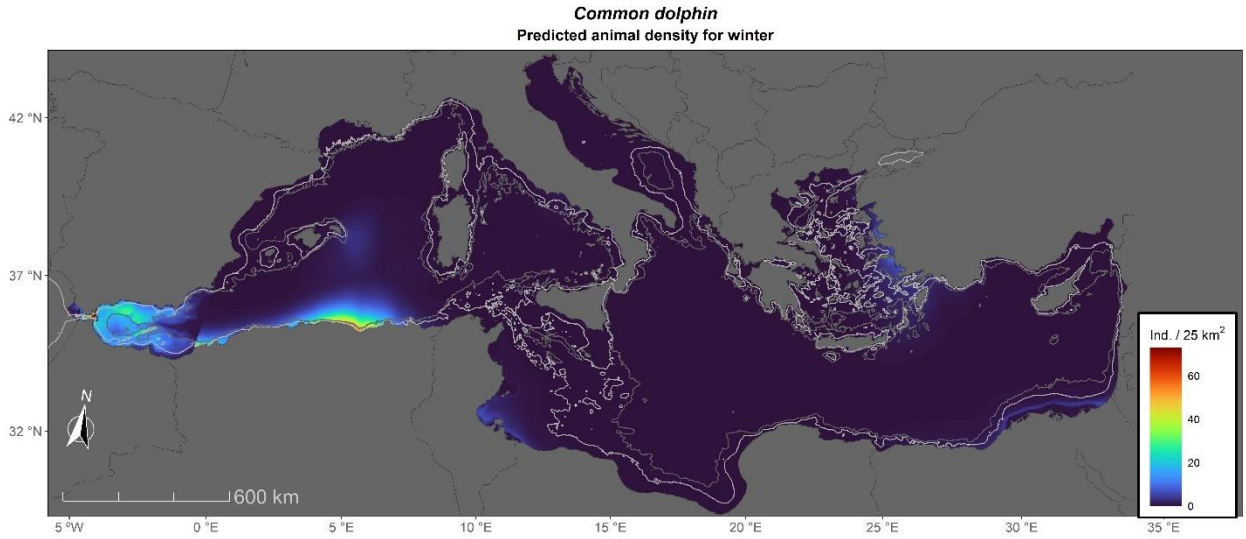

Figure 82. Map of predicted densities in winter for common dolphins.

3.6.8. Striped Dolphins

Striped dolphins were modeled year-round for Gibraltar, and with summer and winter seasons separately for the rest of the Mediterranean Sea. For the Strait of Gibraltar the best model had three static covariates: distance from land, distance from the continental slope, and slope of the sea floor. For the rest of the Mediterranean in summer, the best model had six covariates: the interaction LonLat, depth, distance from the Atlantic, mixed layer thickness, sea surface height, and sea surface temperature; in winter, the best model had three covariates: distance from the Atlantic, depth, and sea surface temperature. See **Appendix E** for details of the models.

In the Strait of Gibraltar most of the density was concentrated in the center and the eastern part of the channel, and particularly at the entrance of the Bay of Algeciras and around the Gibraltar Point (**Figure 83**). For the rest of the Mediterranean, the models predicted the highest densities in the Alboran Sea, both in summer and winter (**Table 67**, **Figure 84**, and **Figure 85**). The density was higher in summer than in the winter in the Alboran Sea, the Liguro-Provençal area, the Tyrrhenian Sea, and the Aegean Sea. However, in winter the density seemed to be more spread out over the whole western Mediterranean. In both seasons density decreased towards the eastern basin and the patterns of density aligned very well with the observations recorded. A mean abundance of 484,615 striped dolphins with a CV of 8.7% was predicted in summer, and 496,266 dolphins with a CV of 11.5% was predicted in winter (**Table 67**).

Table 67. Abundance and uncertainty for striped dolphins in the Mediterranean Sea.

Season	Block	Abundance	Density	CV	L95ci_ abundance	U95ci_ abundance
Summer	Aegean	45,964	0.2430	0.2102	31,624	66,806
Summer	Levantine	19,628	0.0343	0.2480	12,714	30,301
Summer	Ionian	48,936	0.0639	0.2396	32,122	74,552
Summer	Adriatic	10,427	0.0783	0.1866	7,456	14,581
Summer	WMed_noAlboran	267,224	0.3442	0.1430	205,639	347,253
Summer	Alboran	90,400	1.3157	0.0938	75,832	107,767
Summer	Gibraltar	4,653	2.2731	0.1052	3,825	5,661
Summer	**Total**	**484,615**	**0.1933**	**0.0872**	**411,368**	**570,904**
Winter	Aegean	8,298	0.0439	0.1992	5,812	11,847
Winter	Levantine	10,953	0.0192	0.2633	6,928	17,318
Winter	Ionian	173,886	0.2270	0.2048	120,690	250,529
Winter	Adriatic	8,004	0.0601	0.2303	5,332	12,015
Winter	WMed_noAlboran	215,998	0.2782	0.1904	153,494	303,954
Winter	Alboran	75,888	1.1045	0.2974	45,556	126,415
Winter	Gibraltar	4,646	2.2697	0.1052	3,819	5,652
Winter	**Total**	**496,266**	**0.1980**	**0.1148**	**401,059**	**614,074**

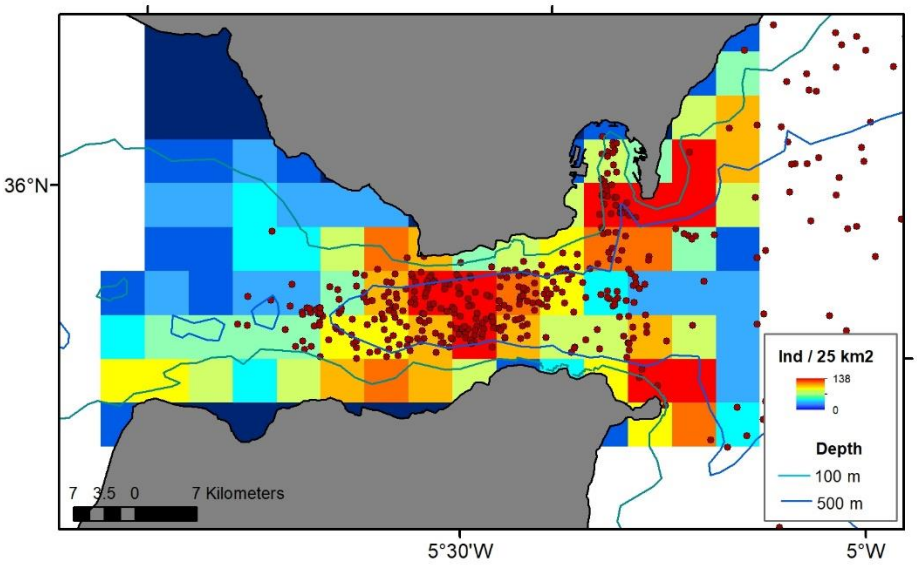

Figure 83. Map of year-round predicted densities in the Strait of Gibraltar for striped dolphins.

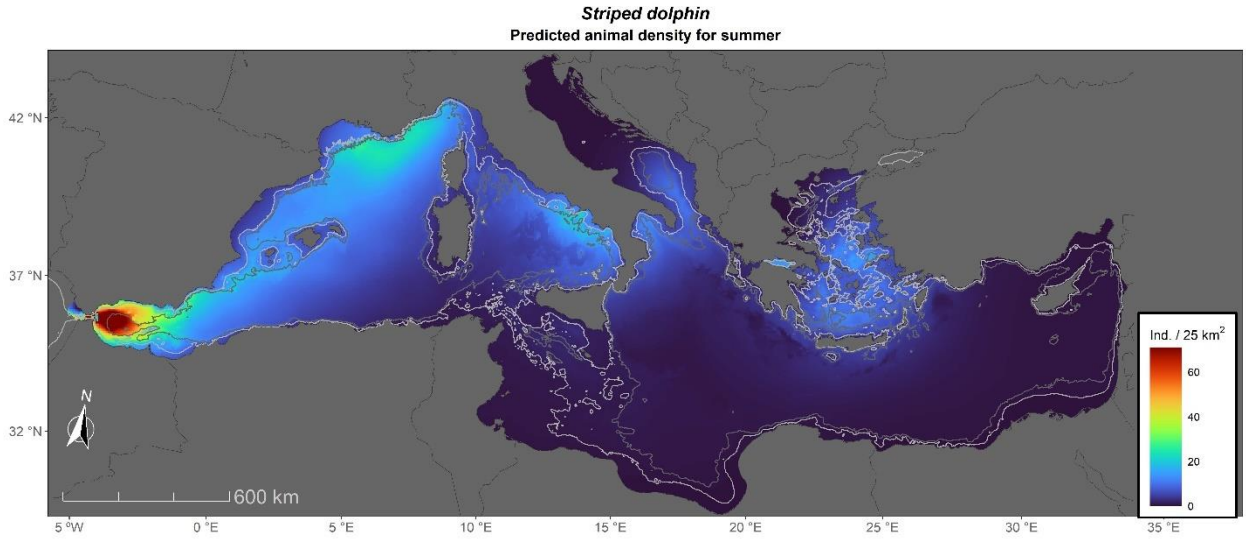

Figure 84. Map of predicted densities in summer for striped dolphins.

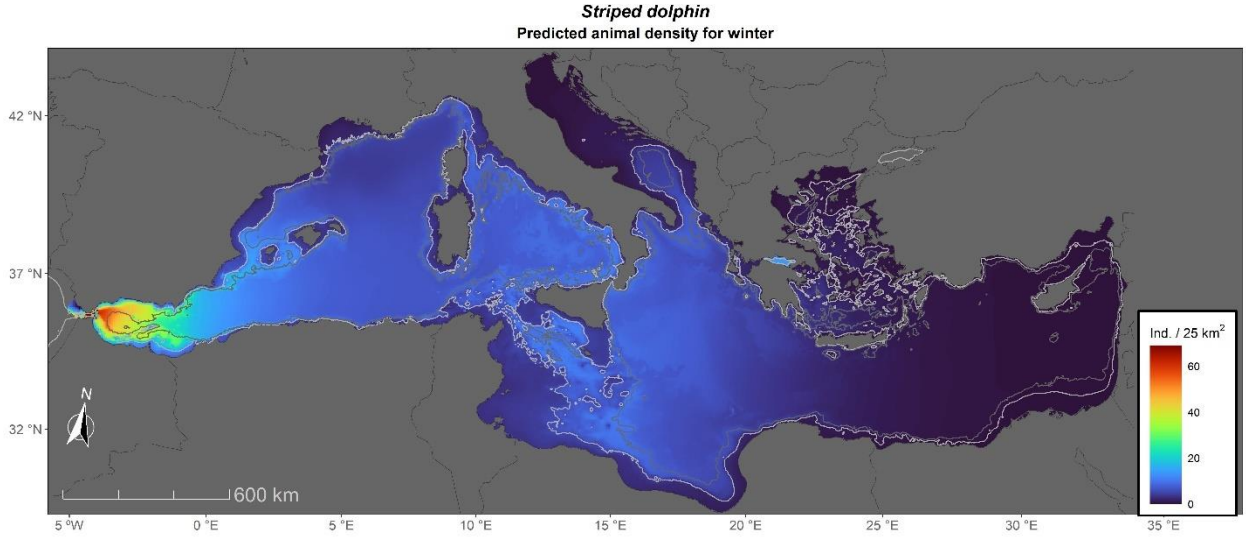

Figure 85. Map of predicted densities in winter for striped dolphins.

3.6.9. Harbor Porpoises

There were only observations of harbor porpoise in the northeastern end of the Aegean Sea in summer in the datasets, associated with effort, so a simple univariate model was developed given that there were only 16 observations available. The best covariate was distance from the Atlantic, which explained 72% of the deviance, reflecting the area where the observations were made (**Figure 86** and see **Appendix E**). The abundance predicted by the model was scaled down to match the abundance estimate of 118 animals from an acoustic survey in the area (Cucknell et al. 2016). Additionally, a very small population of around 30 harbor porpoises has been detected in the northwestern Alboran Sea in summer (no winter data available). Those

were added to the 118 animals for the Aegean Sea, to complete a Mediterranean abundance estimate (**Table 68**).

Table 68. Abundance and uncertainty for harbor porpoises in the Mediterranean Sea.

Season	Block	Abundance	Density	CV	L95ci_ abundance	U95ci_ abundance
Summer	Aegean	148	0.0006	0.3933	62	226

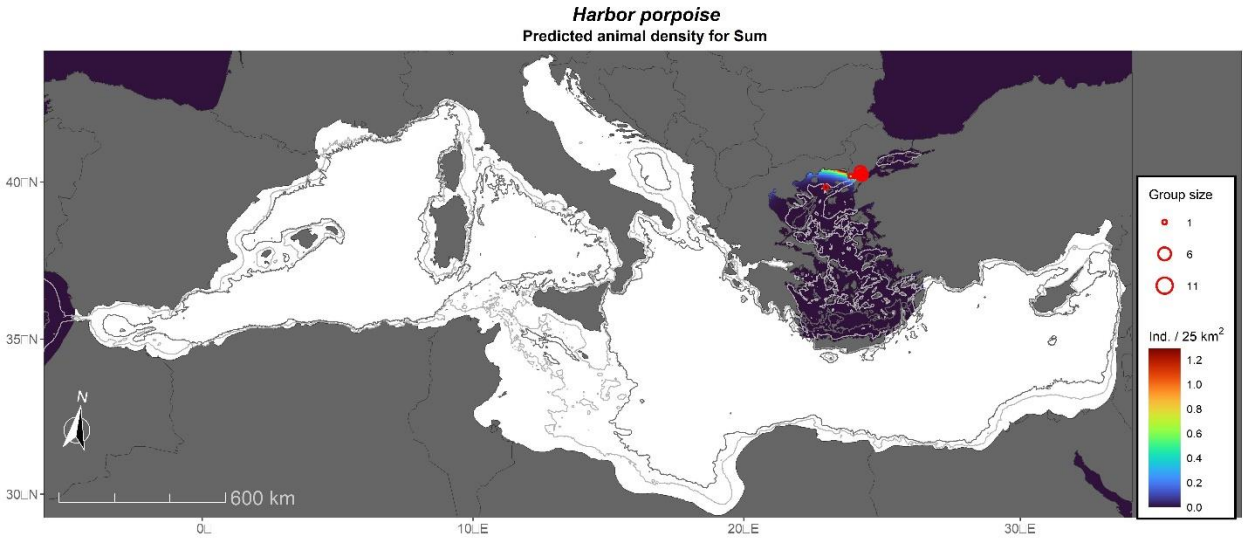

Figure 86. Map of predicted densities in summer for harbor porpoises in the Aegean Sea.

3.6.10. Killer Whales

Killer whales were only modeled in the Strait of Gibraltar, the only place where they were observed in the dataset. A year-round model was constructed that allowed for seasonal variation by the inclusion of a dynamic covariate. Three seasons were defined for this species to match the three seasons of differing abundance observed by the local researchers: spring (April to June), summer (July and August), and winter (September to March). The best model included three covariates: depth, distance from the Atlantic (which would be the westernmost edge of the area), and primary productivity (see **Appendix E**). Models predicted higher density closer to the continental shelf and edge of the Atlantic as well as in waters with higher productivity (which could be a proxy for prey). The abundance predicted by the model for each season was scaled down to match the accurate census available from many years of photo-identification in the area (de Stephanis, pers. comm.). The uncertainty shown here (**Table 69** and **Appendix F**) reflects the spatial variability, as the abundance estimate is considered exact. Killer whales are mainly restricted to the western half of the strait, particularly in the center and the northwesternmost part (**Figure 87** to **Figure 89**). The highest abundance occurs in spring, with 45 animals, followed by summer with 20 animals and the lowest in winter with 10 animals (**Table 69**).

Table 69. Abundance and uncertainty for killer whales in the Mediterranean Sea.

Season	Block	Abundance	Density	CV	L95ci_ abundance	U95ci_ abundance
Summer	Gibraltar	20	0.0098	0.2128	14	29
Winter	Gibraltar	10	0.0049	0.2128	7	15
Spring	Gibraltar	45	0.0220	0.2088	31	65

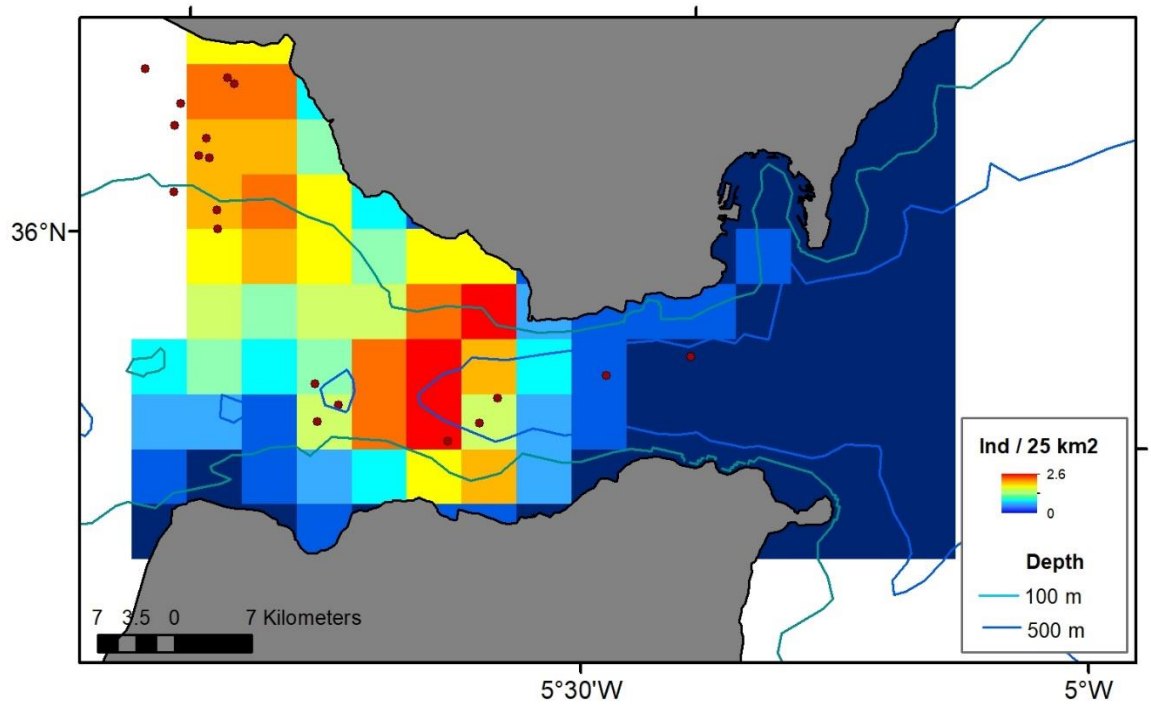

Figure 87. Map of predicted densities in Spring for killer whales in the Strait of Gibraltar.

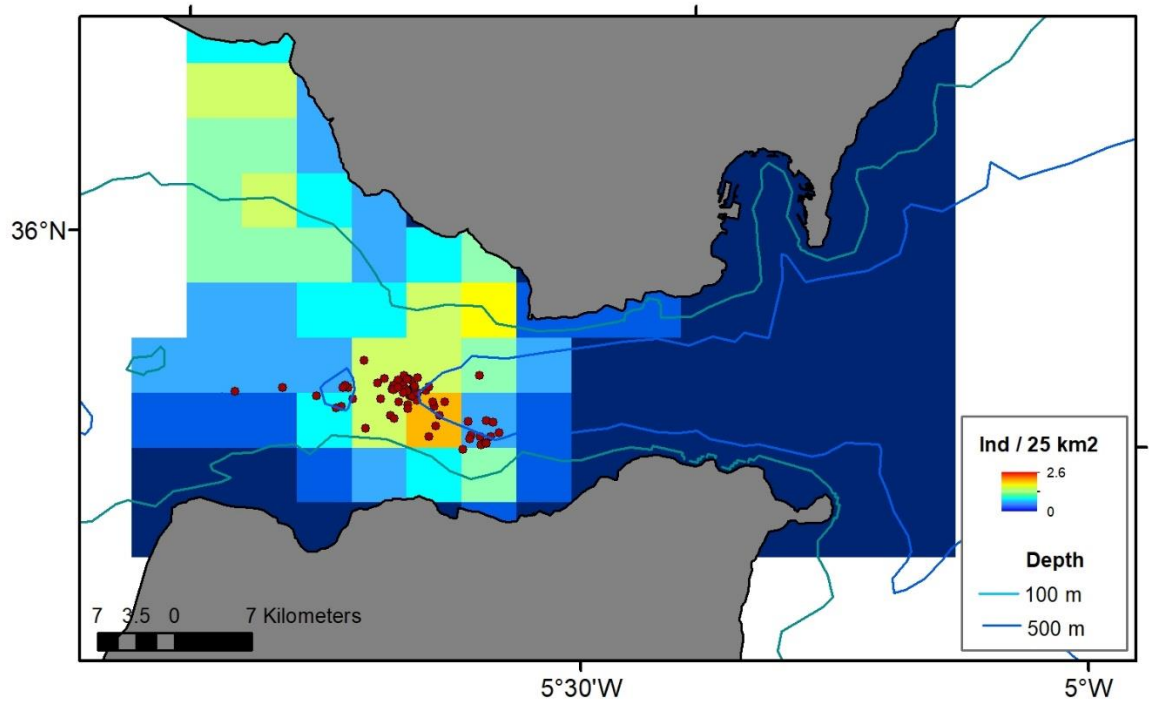

Figure 88. Map of predicted densities in summer for killer whales in the Strait of Gibraltar.

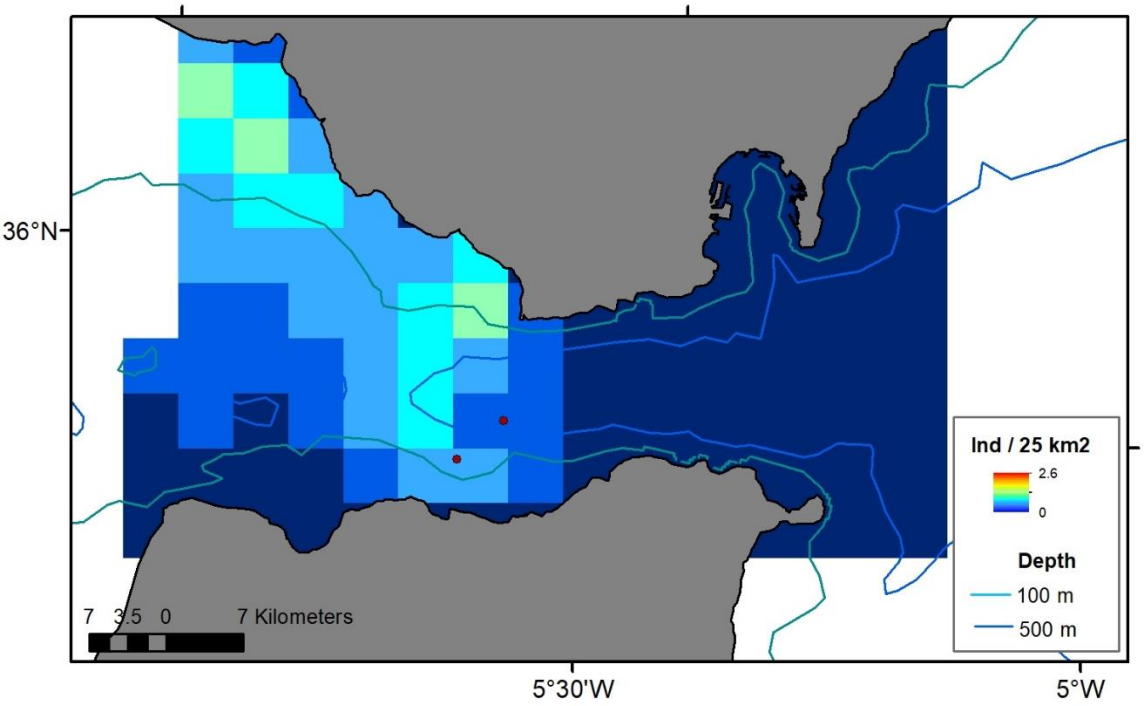

Figure 89. Map of predicted densities in winter for killer whales in the Strait of Gibraltar.

3.6.11. Monk Seals

Appendix G presents a review of the state of the science on Mediterranean monk seal (*Monachus monachus*): abundance, distribution, and research in support of the development of density estimates for the Mediterranean and Black Seas.

The IMMAs used for our analysis were the following (all together in **Figure 90**):

- Central Aegean IMMA: The main criterion upon which the IMMA was identified was based on the knowledge that the area contains pupping nuclei of monk seals, and caves discovered to be used for resting and pupping.Minimum number estimated for the species in the area is 151 animals, including pups (**Figure 91**).
- Northern Sporades IMMA: The main criterion upon which the IMMA was identified was based on the knowledge that the area contains important breeding nuclei of monk seals, including 13 breeding shelters and 35 resting shelters. The seal population in the Northern Sporades is estimated at 52 adult individuals (**Figure 92**).
- Chios and Turkish Coast IMMA: The main criterion upon which the IMMA was identified was based on the knowledge that the area contains important breeding nuclei of monk seals. Eleven caves were potential seal habitats,in which nine seals have been observed. The minimum population size estimate for Greece is 179 adult individuals (**Figure 93**).
- Ionian Archipelago IMMA: The Ionian Archipelago is an area where breeding of the local population of Mediterranean monk seal is well observed and documented. According to recent reports the Ionian islands have at least 194 resting and 2 breeding shelters recorded for the species. Recent population is estimated around 37 to 60 individuals in the area (**Figure 94**).
- Cilician Basin IMMA: The area contains important caves that the monk seals use for their resting and breeding. Currently the number is estimated at about 350–450 in the eastern Mediterranean. There have been 30 seals identified in the area (**Figure 95**)**.**
- Akamas and Chrysochou IMMA: The Akamas Peninsula of Cyprus is an area along the rocky shoreline with caves where Mediterranean monk seals rest. These caves are also used to rear and nurse pups in safety. It is confirmed that within this area, there are 4-5 individuals (**Figure 96**).
- Akrotiri IMMA: This area has several caves where Mediterranean monk seals rest and pup. The discovery of a pup in 2011 in one of these caves has confirmed the area as an important habitat for the Endangered Mediterranean monk seal (**Figure 97**).
- Northern Coast of Cyprus IMMA: The sea caves present in this area offer resting and pup nursing areas for the monk seal. There are only a handful of such caves on the island that were located in the monk seal surveys carried out and this area contains some of them. A juvenile female (<1 years old) was observed during the survey. Eight caves were identified as suitable for pupping and pup nursing. The population inhabiting

the area was estimated to be around 40 individuals of the species and the population is now at a critical stage in the northern coastal area of Cyprus (**Figure 98**).

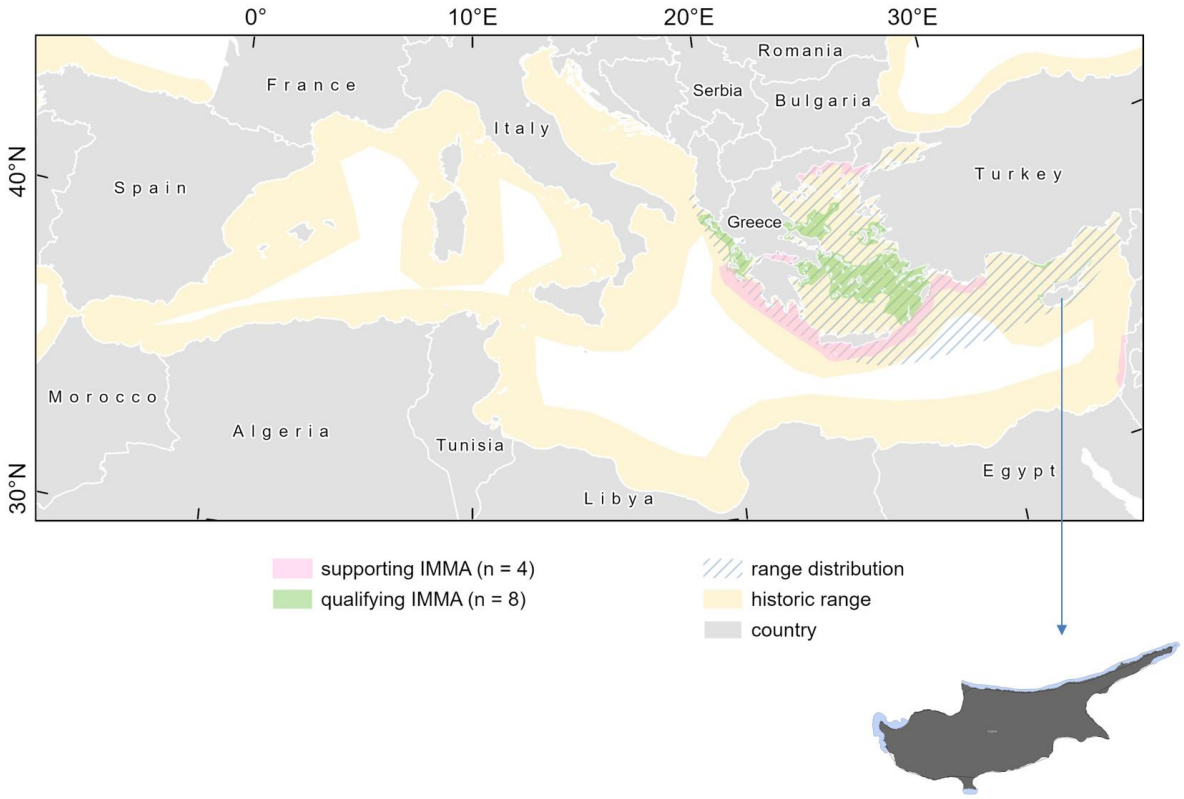

Figure 90. Historic Mediterranean monk seal distribution (Salmona et al. 2022) and current distribution (Karamanlidis et al. 2019, 2023).

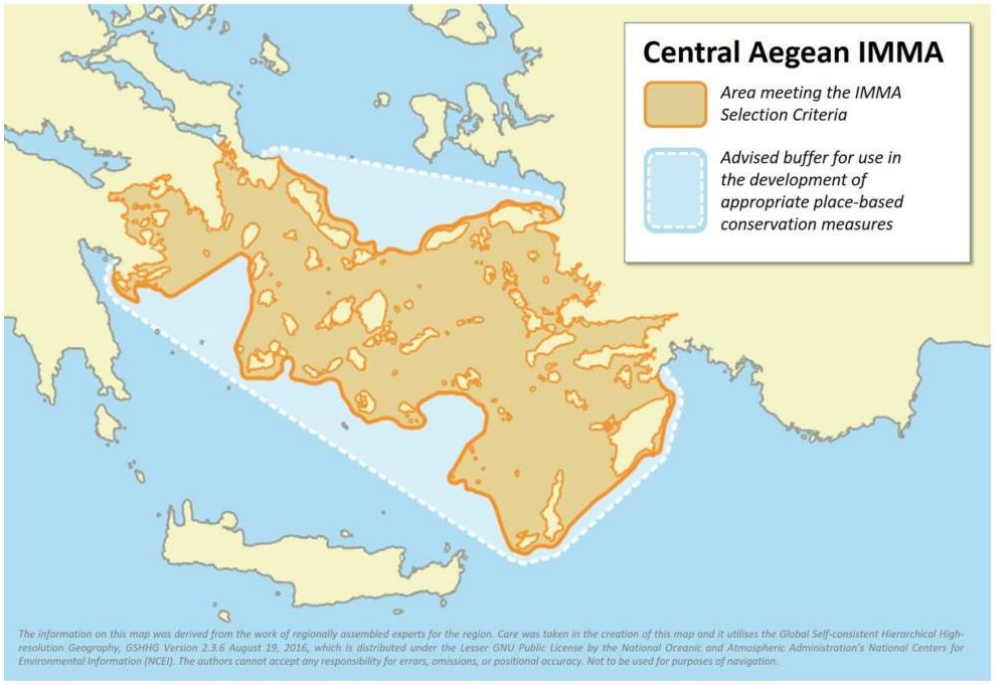

Figure 91. Central Aegean IMMA (extracted from IUCN MMPATF 2024).

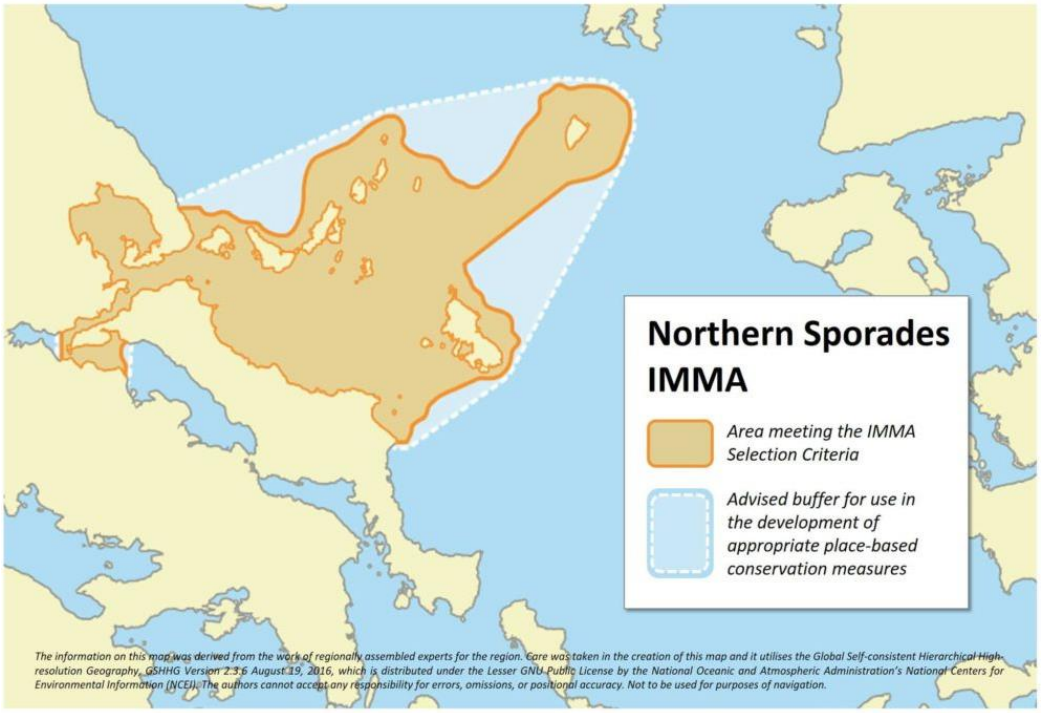

Figure 92. Northern Sporades IMMA (extracted from IUCN MMPATF 2024).

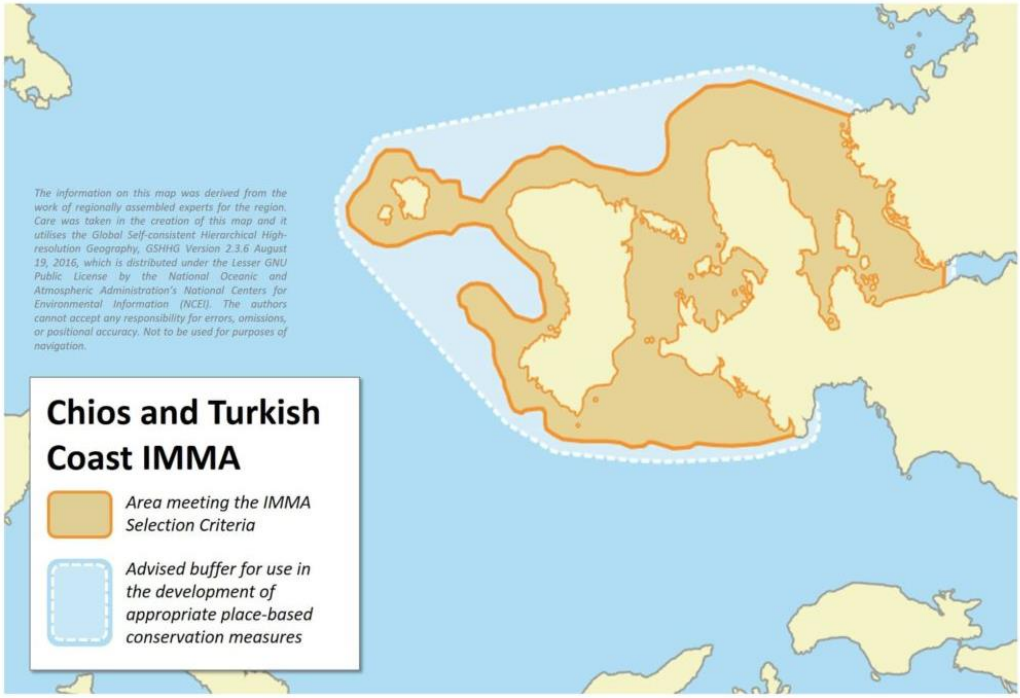

Figure 93. Chios and Turkish Coast IMMA (extracted from IUCN MMPATF 2024).

Figure 94. Ionian Archipelago IMMA (extracted from IUCN MMPATF 2024).

Figure 95. Cilician Basin IMMA (extracted from IUCN MMPATF 2024).

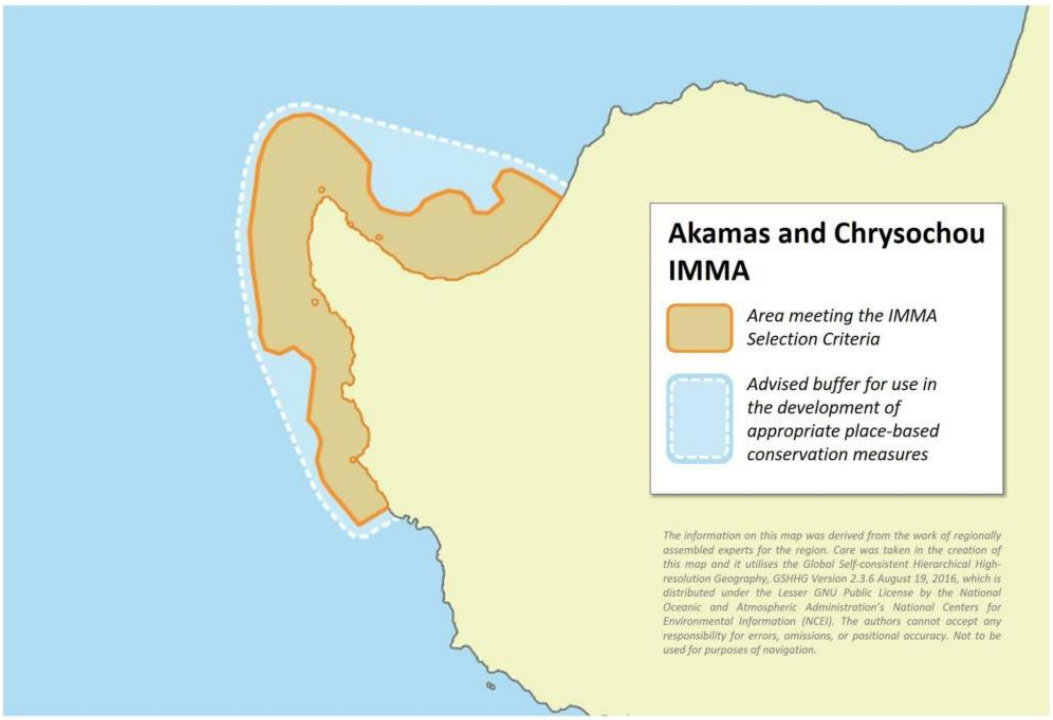

Figure 96. Akamas and Chrysochou IMMA (extracted from IUCN MMPATF 2024).

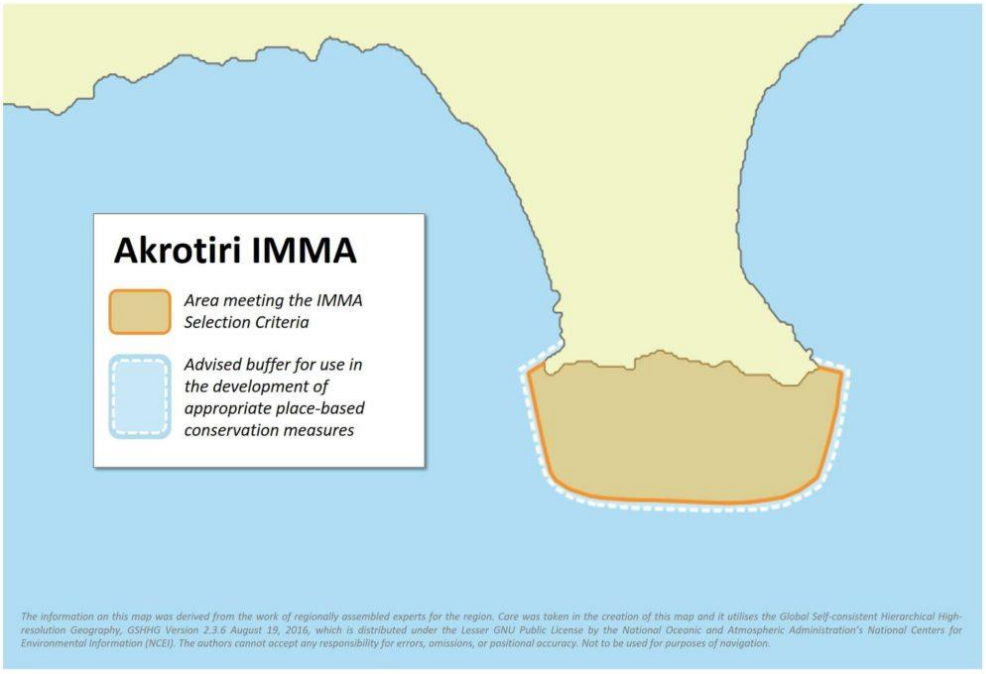

Figure 97. Akrotiri IMMA (extracted from IUCN MMPATF 2024).

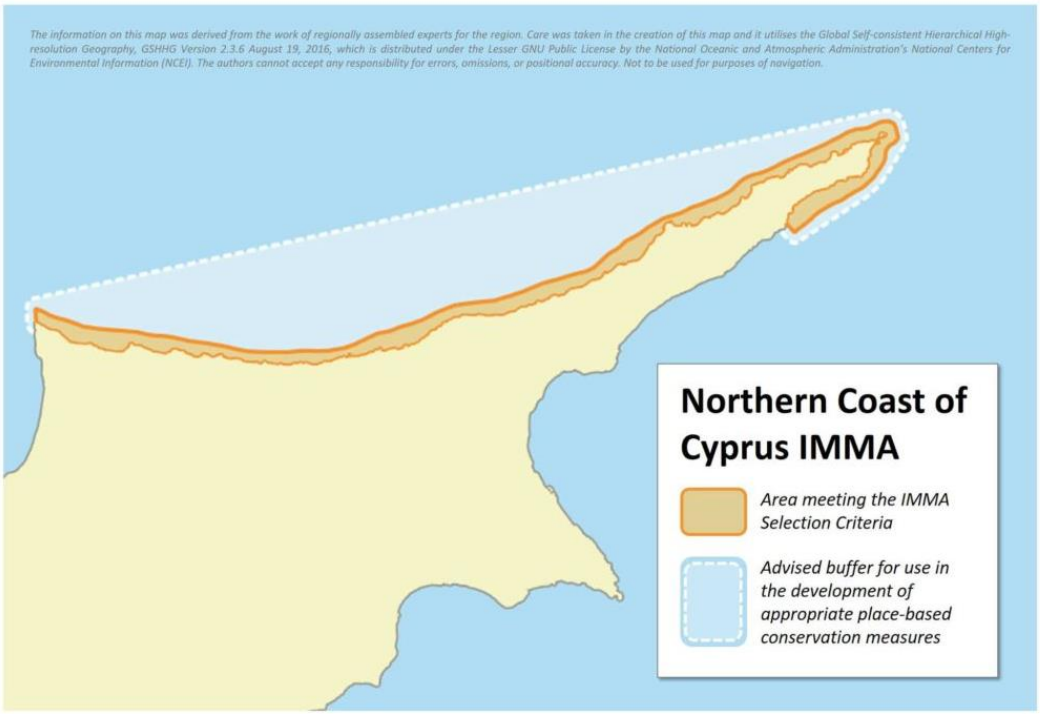

Figure 98. Northern Coast of Cyprus IMMA (extracted from IUCN MMPATF 2024).

The total abundance of monk seals across all IMMAs amounts to 518 individuals. Applying 5% of this total gives 26 animals, which were then uniformly distributed across the remaining pixels

in the broader range distribution area. This results in an overall estimated abundance of 544 monk seals. **Figure 99** illustrates the density map for monk seals, incorporating data from both the IMMAs and the extended range distribution.

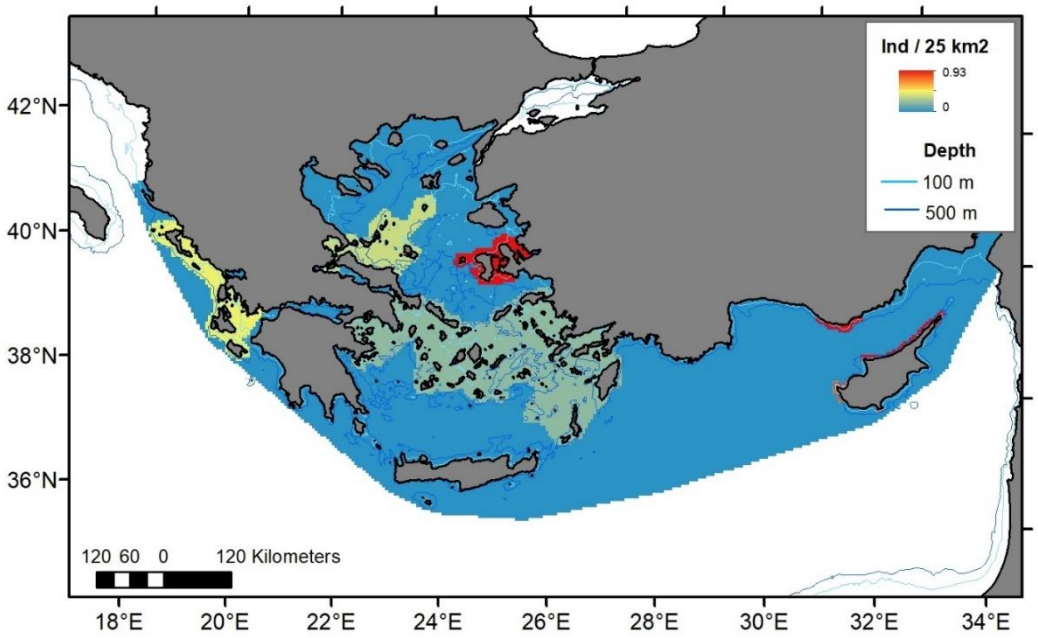

Figure 99. Density map for monk seals, after merging all IMMAs and distribution range.

3.7. Mean Predicted Abundances

Mean predicted abundances in the entire study area and associated CVs are presented in **Table 70** for the Black Sea region and **Table 71** for the Mediterranean for each species, stratified by season.

Table 70. Mean predicted abundance in the entire study area, along with associated CV for each species for the Black, Azov and Marmara Seas. Predicted abundances are the seasonal means for all species. Density is in individuals per km². *Marmara Sea estimates are from published abundances (no models were run).

Species	Season	Total predicted abundance (individuals)	Density	CV
Black Sea				
Bottlenose dolphin	Summer	76,133	0.1991	0.1817
	Winter	15,311	0.2914	0.5371
Common dolphin	Summer	276,015	0.6858	0.24
	Winter	34,250	0.6745	0.2554
Harbor porpoise	Summer	391,894	0.9802	0.3466
	Winter	82,007	1.5607	0.349
Azov Sea				

Species	Season	Total predicted abundance (individuals)	Density	CV
Bottlenose dolphin	Summer	217	0.0057	0.3204
Harbor porpoise	Summer	16,742	0.4421	0.1385
Marmara*				
Bottlenose dolphin	Summer	1978	0.1689	0.49
Common dolphin	Summer	702	0.0599	0.55
Harbor porpoise	Summer	1940	0.1657	0.58

Table 71. Mean predicted abundance in the entire study area, along with associated CV for each species for the Mediterranean Sea. Predicted abundances are the seasonal means for all species. Density is in individuals per km².

Species	Season	Total predicted abundance (individuals)	Density	CV
Bottlenose dolphin	Summer	85,674	0.0342	0.0657
	Winter	94,748	0.0378	0.0938
Common dolphin	Summer	81,506	0.0325	0.0848
	Winter	83,400	0.0333	0.3352
Cuvier's beaked whale	Summer	4,275	0.0017	0.1338
	Winter	4,208	0.0017	0.1366
Fin whale	Summer	1,968	0.0008	0.1590
	Winter	2,318	0.0009	0.1601
Harbor porpoise	Summer	148	0.0006	0.3933
	Winter	-	-	-
Killer whale	Spring	45	0.022	0.2088
	Summer	20	0.0098	0.2128
	Winter	10	0.0049	0.2128
Long-finned pilot whale	Summer	8,429	0.0052	0.1358
	Winter	7,189	0.0045	0.1415
Risso's dolphin	Summer	14,630	0.0058	0.0893
	Winter	15,864	0.0063	0.0954
Sperm whale	Summer	4,392	0.0018	0.0981
	Winter	3,104	0.0012	0.2897
Striped dolphin	Summer	484,615	0.1933	0.0872
	Winter	496,266	0.1980	0.1148

3.8. Extrapolation

Appendix H shows the extrapolation maps across all time slices and model covariates for each species/guild modeled (most were year-round models). The first map shows the NT1 Statistic (any single covariate is out of range); the second map shows the NT2 Statistic (any single combination of covariates is out of range); the third map shows the ExDet Statistic (either a single or a combination of 2 or more covariates are out of range).

In the Black and Azov Seas, there was very little univariate extrapolation, occurring only in very coastal pixels in a few areas. There were also some small areas along the northwestern coast of the Black Sea that showed small multivariate extrapolation for common and bottlenose dolphins. This was also shown in the northeastern tip of the Azov Sea for the two species modeled there (bottlenose dolphins and harbor porpoises). For harbor porpoises there was, however, large multivariate extrapolation in the center of the basin in the winter model, but this is outside of the winter coastal area on which we focused during these analyses. It shows, however, how dangerous it would be to extrapolate models to large, unsurveyed areas. Extrapolating without adequate survey data can lead to misleadingly high or low density estimates due to the lack of data to accurately capture species-habitat relationships in those regions. Such extrapolations may falsely reflect animal distribution patterns, potentially resulting in misinformed management decisions based on these unreliable predictions.

This case underscores the importance of focusing models within surveyed or well-understood areas to ensure that predictions are grounded in actual data. In the absence of localized information, extrapolations may fail to account for environmental, ecological, or behavioral variations that are critical to accurate density modeling. Therefore, caution should be exercised when applying models to extensive, unobserved areas to avoid the risk of significant errors in population assessments and habitat use predictions for harbor porpoises or other species.

In the Mediterranean Sea there were varying results for the different species. In general, there was often a univariate extrapolation in the easternmost edge and/or the southernmost edge of the Levantine Sea, due to longitude and latitude, respectively, and given the very little survey effort available for those areas. Apart from that, there were only very small spots or univariate extrapolation in some areas due to different covariates. Generally, there was very little or no multivariate extrapolations.

4. Discussion

We developed habitat-based density models for 3 species in the Black Sea and 2 species in the Azov Sea, and for 10 cetacean species in the Mediterranean Sea, totaling 15 species, incorporating surveys since 2001 in the Black Sea and the Azov Sea, and since 1991 or 1999 (depending on the species) in the Mediterranean. We used a variety of static, physical, and biological covariates. We then predicted these models across the entire study areas, offering the first basin-wide density predictions for most of these species in the Black Sea and an important update in the Mediterranean Sea.

4.1. Species-specific Considerations in the Black Sea

4.1.1. Bottlenose Dolphins

Bottlenose dolphins in the Black Sea were modeled year-round, with predictions generated for both summer and winter (focusing on the defined winter coastal area). The model indicated the highest abundances over the continental shelf in the western half of the Black Sea, with much lower densities in the eastern half (**Figure 60**). This pattern held true for both seasons. The maximum density, in both summer and winter, was predicted in the coastal waters off northwestern Turkey, east of the Bosphorus Strait. This general pattern of higher densities in the western part compared to the eastern part of the basin mirrors findings from the CENOBS (CEtacean & NOise Black Sea) survey conducted in the Black Sea during summer 2019 (Paiu et al. 2024**, Figure 100**). However, the hotspot east of the Bosphorus Strait identified in our analysis was not detected in the CENOBS survey, likely because shipboard surveys included in our study, but not in CENOBS, were responsible for highlighting this area.

The relatively high density predicted in the northwestern part of the basin during summer aligns with previous studies, which suggested a strong prevalence of bottlenose dolphins over harbor porpoises in waters southwest of Crimea (Birkun 2002a), a pattern that is also reflected in our analysis (see also harbor porpoises in **Section 4.1.3**).

When extracting the summer abundance estimate for the area surveyed during the CENOBS survey, our models predicted 44,028 animals, which is higher than the CENOBS estimate of 30,093 animals (corrected for availability and perception bias) (**Figure 100**, Paiu et al. 2024). This difference is likely due to the highly coastal nature of bottlenose dolphin groups, which are more difficult to detect in aerial surveys that spend minimal time over coastal areas. In contrast, our analysis benefited from several shipboard surveys conducted close to shore, which allowed for the detection of many of these coastal dolphins.

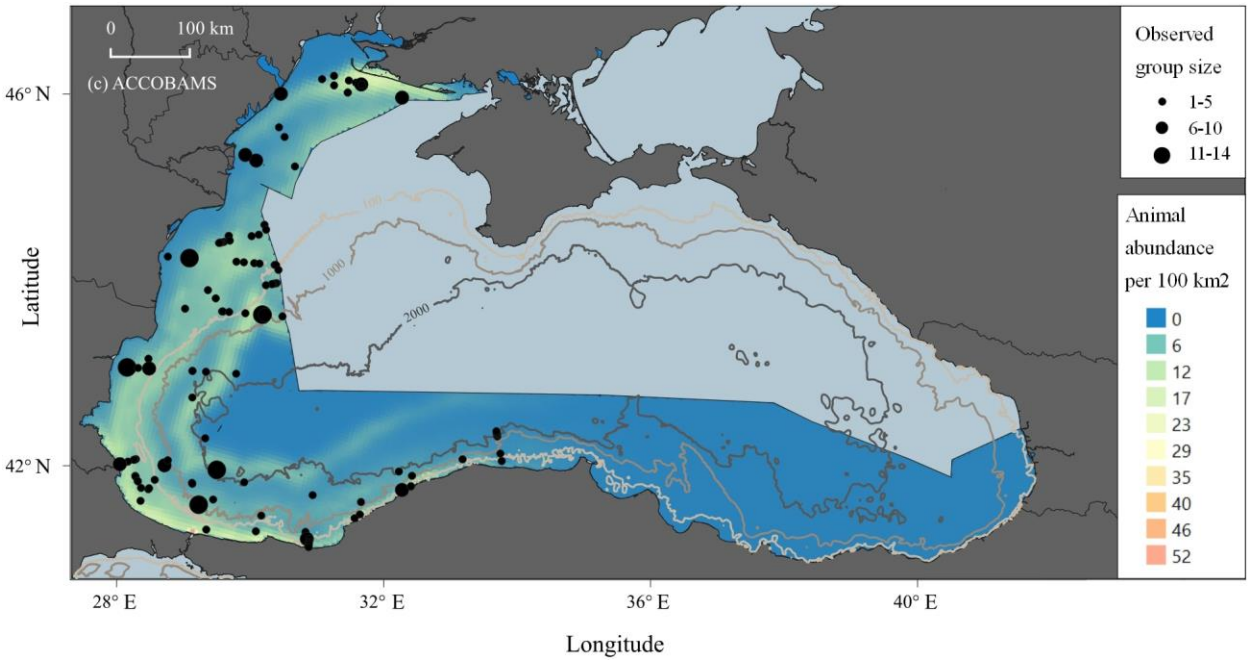

Figure 100. Prediction of estimated density of bottlenose dolphins in the Black Sea during the CENOBS survey.Figure extracted from Paiu et al. 2024.

Although no previous abundance estimates exist for winter in the Black Sea, it is reasonable to expect that overall abundance between summer and winter should be quite similar, given the almost fully enclosed nature of the sea. The extracted estimated abundance for summer for the southern coastal area defined for winter was 13,603 dolphins, very similar to the abundance estimated for the same area in winter (14,462 dolphins, **Table 57**).

In the Azov Sea, bottlenose dolphins were recorded only in the Kerch Strait in the available datasets. However, Birkun (2002a) also noted the presence of this species in the adjacent southern part of the Azov Sea, a finding consistent with our model predictions (**Figure 61**). Birkun et al. (2004) estimated an uncorrected count of 127 dolphins in the Kerch Strait, which, after applying corrections, amounted to 184 animals. This figure is comparable to our estimate of 217 dolphins, which includes a small portion of the Azov Sea near the strait. In a more recent study, Krivokhizhin (2021) found that the local population of bottlenose dolphin in the Kerch Strait has increased almost nine times, from 76 (95% CI 30 - 192; CV 47.6%) in 2001 to 676 individuals (95% CI 305 - 1499; CV 41.2%) in 2019.

Dede et al. (2022) estimated 1,978 bottlenose dolphins in the Marmara Sea, with a CV of 49%. After applying the appropriate correction factor (0.69) for the species and the survey platform used, the corrected abundance estimate is 2,867 animals. This estimate is included in the NMSDD and classified as an “External study.”

4.1.2. Common Dolphins

Common dolphins in the Black Sea were modeled year-round, with predictions generated separately for summer and winter (focusing on the defined winter coastal area). The model predicted the highest abundances along the easternmost coast of the basin (off Georgia) and

the southern coast along Turkey, particularly in the western section, during both summer and winter (**Figure 62**). However, the highest densities were predicted in winter for the waters off Georgia, which also had the highest encounter rates during this season (see **Appendix F**).

In summer, a secondary area of relatively high density was predicted southwest of the Crimean Peninsula, as well as in the northeastern Black Sea off the coast of Russia. In contrast, the northwestern part of the Black Sea, the deep waters of the basin, and the area south of the Kerch Strait showed lower densities during the summer. The distribution patterns along the western and southern parts of the basin were similar to those observed during the CENOBS survey (Paiu et al. 2024, **Figure 101**).

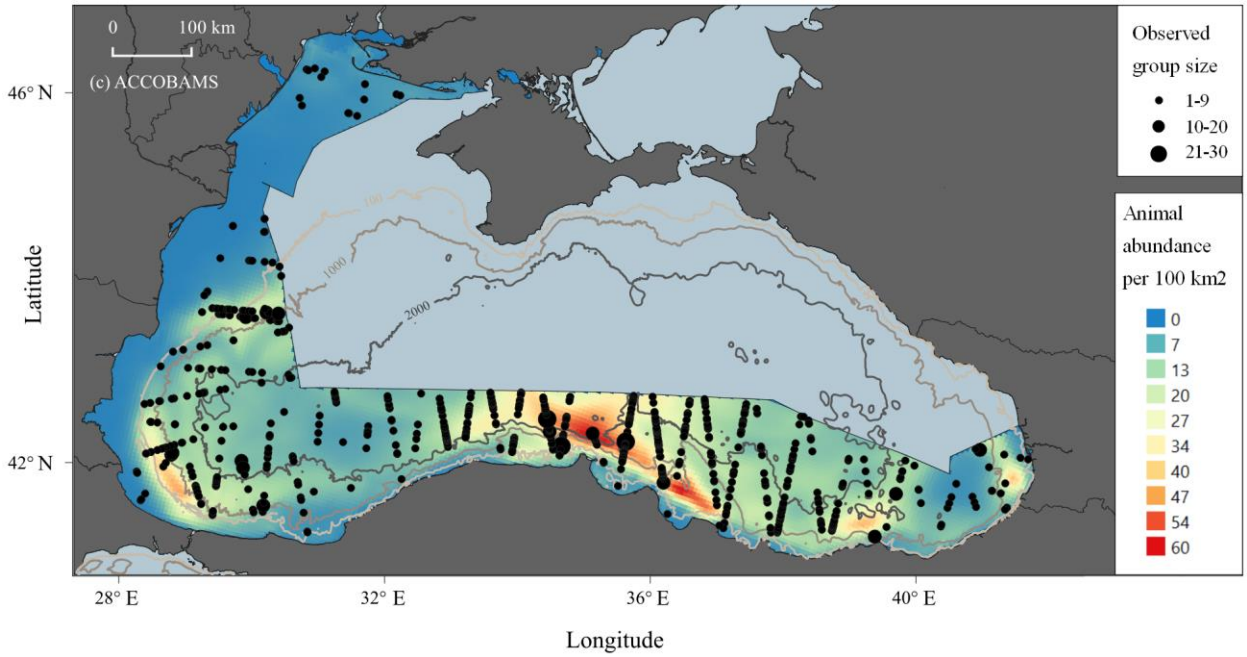

Figure 101. Prediction of estimated density of common dolphins in the Black Sea during the CENOBS survey.Figure extracted from Paiu et al. 2024.

When extracting the summer abundance estimate for the area surveyed during the CENOBS survey, we arrive at 142,747 animals, which is very close to the CENOBS estimate of 149,356 animals (corrected for availability and perception bias) (Paiu et al. 2024). Although no previous estimates exist for winter in the Black Sea, it is generally assumed—similar to bottlenose dolphins—that the overall abundance in summer and winter should be quite similar. The extracted estimated abundance for summer for the southern coastal area defined for winter was 39,824 dolphins, very similar to the abundance estimated for the same area in winter (37,121 dolphins, **Table 58**).

There were no records of common dolphins in the Azov Sea or in the Kerch Strait, which connects it to the Black Sea. This absence is consistent with Birkun (2002a), who also reported no presence of this species in the Azov Sea or Kerch Strait.

Dede et al. (2022) estimated 702 common dolphins in the Marmara Sea, with a CV of 55%. After applying the correction factor for this species and the survey platform (0.97), the corrected abundance estimate is 724 animals. This estimate is reflected in the NMSDD and classified as an “External study.”

4.1.3. Harbor Porpoises

Harbor porpoises in the Black Sea were modeled separately for summer and winter, as these seasonal models performed better than the year-round model. In the year-round model, density off Bulgarian waters dropped to very low levels in winter, while density in the waters off Georgia surged significantly in summer. These patterns did not align with the overall distribution of sightings and were therefore discarded. In summer, the model predicted the highest abundances in the southwestern part of the Black Sea and the waters off Georgia, in the easternmost part of the basin. Much lower densities were predicted in the northern half of the Black Sea, particularly in the northeastern section (**Figure 63**). In winter, the highest densities were predicted in the coastal areas throughout the entire winter range analyzed. The general pattern of higher densities in the southwestern versus southeastern parts of the basin mirrored the findings of the CENOBS survey (Paiu et al. 2024, **Figure 102**). However, the CENOBS survey did not detect the hotspot off Georgia, likely because our analysis included some shipboard surveys in that area which were not part of the CENOBS dataset.

The near absence of harbor porpoises in the northwestern part of the basin was consistent with previous studies suggesting a strong prevalence of bottlenose dolphins over harbor porpoises in the waters southwest of Crimea (Birkun 2002a), a pattern that is also reflected in our analysis (see bottlenose dolphins in **Section 4.1.1**).

When extracting the summer abundance estimate for the area surveyed during the CENOBS survey, we estimated 293,964 animals, which is very close to the CENOBS estimate of 297,803 animals (corrected for availability and perception bias) (Paiu et al. 2024).

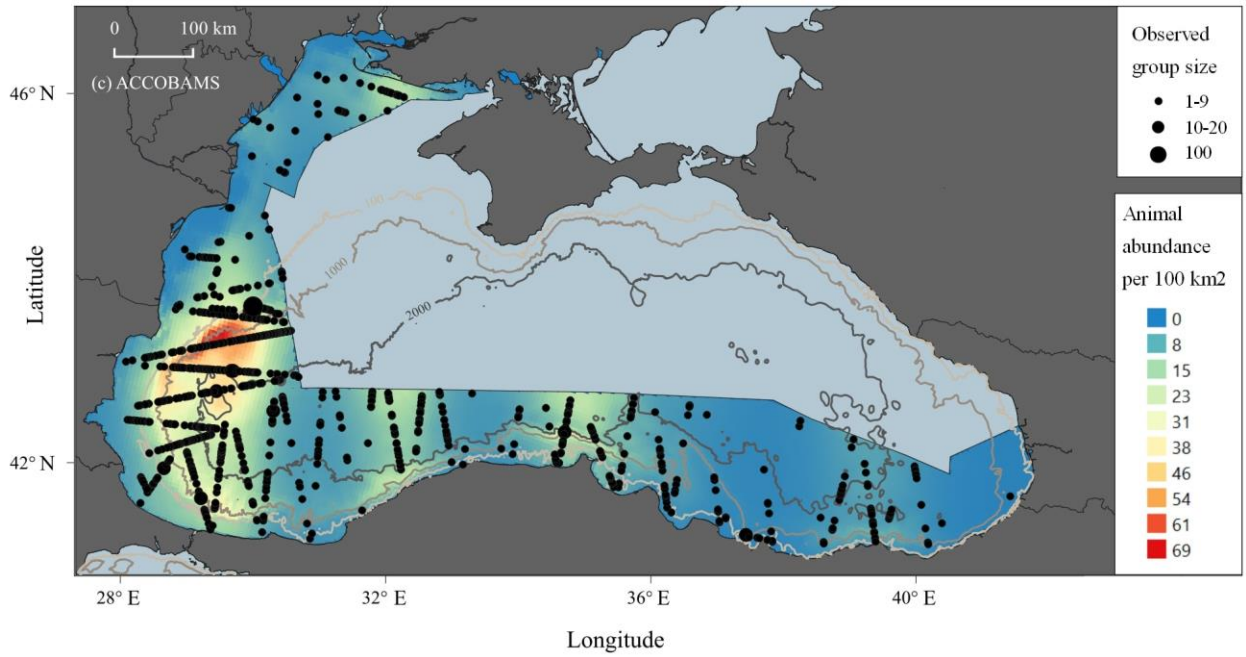

Figure 102. Prediction of estimated density of harbor porpoises in the Black Sea during the CENOBS survey.Figure extracted from Paiu et al. 2024.

There are no previous estimates for winter in the Black Sea, but as with the other two species, it is assumed that overall abundance in summer and winter should be similar. The extracted estimated abundance for summer for the southern coastal area defined for winter was 105,779 porpoises, higher than the abundance estimated for the same area in winter (82,045 porpoises, **Table 59**). However, this difference is not statistically significant due to the high uncertainty of the prediction for that area in both seasons (CV = 35% in winter, and CV = 37% in summer), with largely overlapping 95% CIs.

Harbor porpoises are the only cetacean species regularly present in the Azov Sea (**Figure 64**). Vishnyakova (2017) suggested that the harbor porpoises in the Azov Sea and the Black Sea proper might represent two distinct populations, based primarily on differences in body size and morphology, such as skull size and proportions. However, Birkun (2002a) noted that porpoises migrate through the Kerch Strait, leaving the Azov Sea before winter and returning in the spring. Birkun et al. (2002a) estimated an uncorrected population of 2,922 porpoises in the Azov Sea, which, after applying a correction factor (0.52 for this species and similar platform), resulted in an estimate of 8,349 animals for this sub-basin. This is about half of our estimate of 16,742 animals. We could not identify the cause of this discrepancy due to a lack of access to the older data.

Dede et al. (2022) estimated 1,940 harbor porpoises in the Marmara Sea, with a CV of 58%. After applying the appropriate correction factor for the species and platform (0.35), the corrected abundance estimate was 5,543 animals. This estimate is reflected in the NMSDD and classified as an “External study.”

4.2. General Considerations for the Black Sea

For the Black Sea models, two seasons were used, mirroring the approach for the Mediterranean: summer (May to October) and winter (November to April). However, due to insufficient data, it was not possible to model winter separately for bottlenose and common dolphins, so these species were modeled year-round for the whole basin and predictions were derived for summer and winter separately. The predictions for all three species were cropped to confine them to the narrow southern coastal areas where data were available, to avoid over-extrapolation.

Regional experts have suggested that for future modeling efforts, a different approach to seasonality may be needed, potentially using four seasons instead of two. They also noted that the true summer in the Black Sea likely ends in late August or early September. This mismatch in the seasonality used for the current analyses may be confounding the inter-seasonal variability of covariates and the species' habitat preferences, complicating the models and making interpretation more challenging. Therefore, for future modeling in this region, detailed consultation with regional experts is recommended to determine the best way to stratify the seasons.

Regional experts have also suggested that population changes in the Black Sea cetaceans have occurred due to climate change, as evidenced by recent stranding patterns. Additionally, it is believed that there was a significant decline in the abundance of the three species throughout the 20th century, largely driven by direct catch, bycatch, overfishing, and other anthropogenic impacts (Paiu et al. 2024). For instance, Arseniev et al. (1973), Zemsky and Yablokov (1974), and Zemsky (1975) estimated that there were between 1.5 and 2 million common dolphins alone during that period. Between 1931 and 1983, the direct catch of cetaceans in the Black Sea may have exceeded 5 million animals (Zemsky 1996; Birkun 2002a), severely depleting populations. This was compounded by significant bycatch, particularly from bottom-set gillnets (Pavlov et al. 1996; Birkun et al. 2014), which continues to some extent today.

Given these changes, regional experts have recommended that the time span of future modeling efforts in the region should be carefully determined, considering all available information on population dynamics. The inclusion of data from 21 years (2001 to 2022) in these analyses may be mixing different population statuses, including periods of both higher and lower densities, which could complicate the interpretation of results and potentially introduce bias.

There was a general consensus among regional experts that the abundance estimates for the three species might be overestimated after accounting for availability and perception biases. Several potential causes for these overestimations were suggested:

- **Inclusion of a broad time span**: The estimates did not fully account for inter-annual variability, potentially leading to biased results.
- **Use of surface/diving patterns and perception bias data from outside the Black Sea**: Data used to estimate availability and perception biases were largely derived from the northeast (NE) and northwest (NW) Atlantic, rather than from the Black Sea or even the Mediterranean. Given the distinct environmental conditions in the Black Sea,

diving/surfacing patterns and perception biases may differ significantly, potentially skewing the estimates.

- **Rounding issues in shipboard surveys**: Many surveys experienced problems with rounding bearings and radial distances, particularly rounding small angles to zero. This practice can lead to an underestimation of the esw, resulting in an overestimation of abundance.
- **Responsive movement of common dolphins**: Common dolphins appear to exhibit a general attraction response, which can result in shorter recorded distances than would be expected in the absence of this behavior. This also leads to an underestimation of esw and an overestimation of abundance.

To improve future estimates, regional experts have agreed to develop a standardized data collection protocol. This will include gathering Black Sea-specific data on diving/surfacing patterns and perception biases, more precise recording of bearings with reduced rounding of radial distances, and data collection to assess responsive movement. These improvements will enhance data quality for future modeling efforts in the region.

4.3. Species-specific Considerations in the Mediterranean Sea

4.3.1. Fin Whales

Fin whales in the Mediterranean Sea are recognized as a distinct subpopulation, genetically differentiated from those in the northeast Atlantic (Berubé et al. 1998). They are listed as Endangered by the IUCN Red List with a population decline (Panigada et al. 2021).

The species' density distribution in the Mediterranean is primarily concentrated in the Corso-Liguro-Provençal basin (**Figure 65** and **Figure 66**), a pattern consistent with previous studies (e.g., Forcada et al. 1995; Notarbartolo di Sciara et al. 2003, 2016; Panigada et al. 2017; Cañadas et al. 2023). Their strong affinity for pelagic habitats, with groups frequently observed at depths exceeding 2,000 m, aligns with earlier findings (e.g., Cotté et al. 2009; Panigada et al. 2017b; Gnone et al. 2023). Our modeling results generally agreed with those of Druon et al. (2012) for the western Mediterranean, who modeled potential fin whale feeding habitat from presence-only data and four environmental covariates (depth, chlorophyll concentration, chlorophyll fronts, and sea surface temperature). Although fin whales have occasionally been sighted in the eastern Mediterranean, such occurrences are rare (Stephens et al. 2021), a trend echoed in the studies of Mannocci et al. (2018) and Cañadas et al. (2023). The enclosed gulfs of Ambracia and Corinth were excluded from the predictions and assigned 0 density.

Our results indicate a higher abundance of fin whales in winter compared to summer (**Table 60**). Long-distance latitudinal movements within the Mediterranean have been well-documented (Panigada et al. 2017), with Gauffier et al. (2018) suggesting that some whales migrate through the Strait of Gibraltar following a distinct seasonal pattern. During late spring and summer (May–October), these whales move primarily westward towards the Atlantic, while between November and April, they migrate eastward into the Mediterranean. This pattern, supported by long-term research in the Alboran Sea (Cañadas, personal observations), corresponds with the

lower densities observed in summer relative to winter. It has been proposed that two distinct populations of fin whales exist: one that resides year-round in the Mediterranean, and another that visits the western Mediterranean seasonally from the North Atlantic. Individuals from this latter population are thought to cross the Strait of Gibraltar in winter and remain in the Mediterranean until summer (Notarbartolo di Sciara et al. 2016).

The ACCOBAMS survey initiative (ASI) conducted in the summer of 2018 estimated a design-based corrected abundance of 3,282 whales (CV=31%), using a correction factor of 0.538 (Panigada et al. 2021). A model-based estimate from the same survey yielded 2,892 whales (CV=28%) (ACCOBAMS 2021). Both estimates were higher than our summer estimate of 1,968 individuals (CV=16%), though all fall within overlapping 95% CI. A key difference to consider is that the ACCOBAMS survey reflects data from a single month, whereas our analysis covers six months across 24 years, a region characterized by significant intra-seasonal and inter-annual variability in oceanographic conditions (Nacef et al. 2016; Notarbartolo di Sciara et al. 2016; Meli et al. 2023; Painter and Tsimplis 2003).

The previous round of models in the Mediterranean (Mannocci et al. 2018) predicted a corrected summer abundance of 14,153 individuals and a corrected winter abundance of 8,073 in the entire Mediterranean Sea. Those estimates were much higher than the new ones, although the overall distribution pattern with the highest densities on the Liguro-Provençal area is very similar. The fact that the new estimates align much better with previous estimates—as shown above—suggests that the previous ones were somehow overestimated.

Between 2002 and 2019, 18 satellite tags were deployed on fin whales in the Strait of Gibraltar (**Figure 103**, unpublished data, de Stephanis, pers. comm.). These tracking data clearly demonstrate migratory movements between the northwestern Mediterranean and the northeast Atlantic through the Strait of Gibraltar.

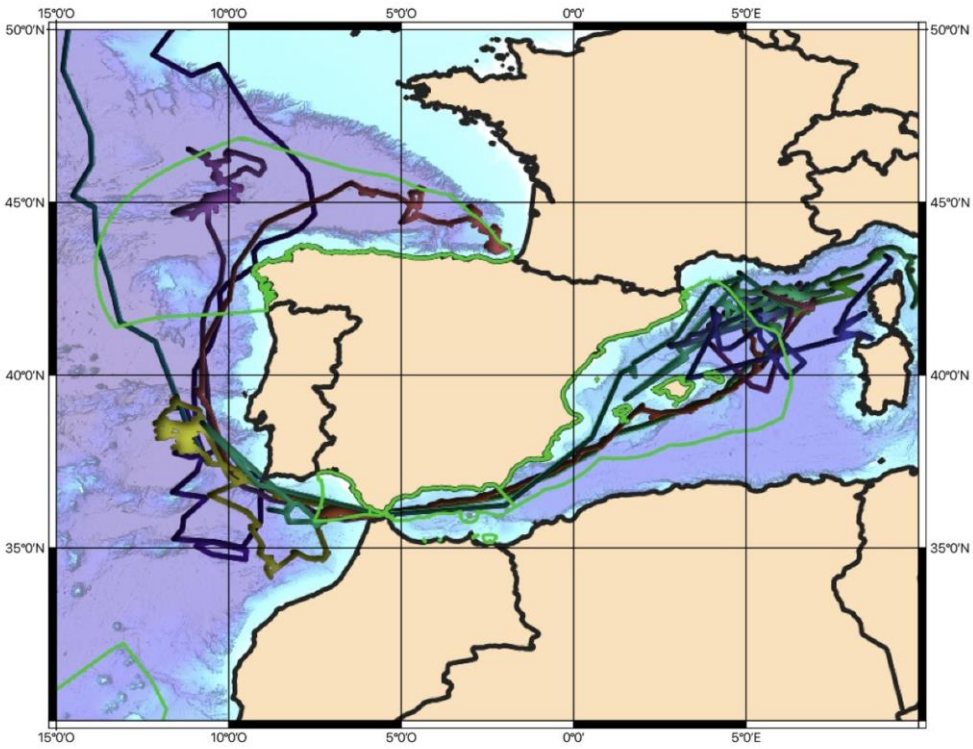

Figure 103. Satellite tags deployed on fin whales in the Strait of Gibraltar between 2002 and 2019(unpublished, de Stephanis pers. comm.).

4.3.2. Sperm Whales

A recent abundance estimate of sperm whales in the Strait of Gibraltar, based on photo-identification work conducted between 1999 and 2023, identifies 89 individuals in the catalogue (de Stephanis 2023). Many of these whales are observed repeatedly each year, indicating strong site fidelity to the area. However, some individuals have also been re-sighted in other regions of the western Mediterranean, and others have only been seen once over the years. All sperm whales observed in the Strait of Gibraltar have been recorded feeding. The regional expert, de Stephanis, concurs with our mean abundance estimate of 58 sperm whales (**Table** 61). Additionally, the predicted spatial distribution of these whales, concentrated in the deep waters of the central Strait, closely aligns with previous findings (de Stephanis et al. 2008).

In the western Mediterranean, the primary concentration area for sperm whales during the summer is around the Balearic Islands, particularly in the waters to the southeast and northeast (**Figure 68**). This aligns closely with previous studies conducted in the region (Pirotta et al. 2011; Rendell et al. 2014). Notably, this is the only area in the Mediterranean where social groups of females with calves are regularly observed (Drouot et al. 2004b; Drouot-Dulau and Gannier 2007; Pirotta, Brotons, et al. 2020; Pirotta, Vighi, et al. 2020), apart from a small region around Ischia Island off Naples in the eastern Tyrrhenian Sea (Pace et al. 2014), where our models also indicate a high concentration.

Sperm whales are also found in the Liguro-Provençal area, primarily comprising adult males or bachelor groups. However, this area was not highlighted in our models, likely due to the significant survey effort and the low visual detectability of sperm whales. Photo-identification work has shown that the sperm whales in the Liguro-Provençal area move between these waters and the Balearic Islands, where they join social groups, possibly traversing the entire western Mediterranean in their movements (Drouot-Dulau and Gannier 2007; Carpinelli et al. 2014; Rendell et al. 2014). These studies suggest that the western Mediterranean hosts a single sperm whale population, which is why eastern and western Mediterranean areas were modeled separately.

Although some limited inter-basin movement between the eastern and western Mediterranean has been observed (Frantzis et al. 2011), the populations are not completely isolated. Our model predicted higher sperm whale densities in waters with depths between 1,000 and 3,000 m and relatively steep slopes, consistent with previous findings (e.g., Praca and Gannier 2008).

Our abundance estimate for the western Mediterranean (4,404 individuals, **Table** 61) appears somewhat high compared to previous partial estimates for specific areas within this sub-basin. For example, Rendell et al. (2014) estimated approximately 400 individuals from photo-identification data in the Balearic and Liguro-Provençal areas combined, though this came with a wide 95% CI (around 200–1,000 individuals). They suggested that this estimate may be an underestimate due to heterogeneity in the mark-recapture models and the likelihood that the entire population was not fully sampled. At a later stage, Brotons (2015) provided an estimate of abundance just for the Balearic Islands of 442 (95% CI=235–1602). Additionally, Lewis et al. (2018) provided an acoustic abundance estimate for the southern portion of the western Mediterranean, estimating 602 animals (95% CI = 342–1,058). However, neither of these estimates included the eastern portion of the western Mediterranean (such as the Tyrrhenian and eastern Ligurian Seas).

In contrast, the ACCOBAMS survey covered the entire western Mediterranean using shipboard acoustic methods. This study yielded a corrected abundance estimate—accounting for acoustic availability bias—of 2,752 sperm whales (95% CI = 2,034–3,888) after excluding blocks from the eastern Mediterranean (Boisseau et al. 2024). Despite the differences in point estimates, our estimate overlaps with this study's 95% CI. It's important to note that the ACCOBAMS analysis was based on data from one summer (2018), while our analysis spans 25 years, encompassing potential inter-seasonal and inter-annual variability in both oceanographic conditions and sperm whale density.

Estimating abundance in the eastern Mediterranean posed more challenges (see **Section 2.11.3**, Predicted Abundances, Challenges, and Exceptions). It was clear that our initial overestimate in this sub-basin resulted from the visual observations following initial acoustic detections. This method led to a significant underestimation of the esw, consequently inflating the abundance estimate. The correction of the esw values derived from acoustic surveys (Gkikopoulou 2012) resulted in a more plausible estimate of 500 animals for the eastern Mediterranean.

Previous estimates for the eastern Mediterranean have not covered the entire sub-basin. Lewis et al. (2018) estimated 139 animals across areas including the southern Adriatic, northern and southern Aegean, southern Ionian, and northern Levantine Seas, excluding the northern Ionian Sea where we predicted high density. Boisseau et al. (2024) focused only on the Hellenic Trench and some waters north of Libya within the eastern Mediterranean, yielding an estimate of 83 animals for these limited areas. A photo-identification study in the Hellenic Trench reported 164 distinct individuals between 1998 and 2009 (Frantzis et al. 2014). Since none of these studies encompassed the entire eastern Mediterranean sub-basin, it remains uncertain whether our estimate is an overestimate or a more accurate reflection of the true population size across the region.

In winter, the abundance estimate for the western Mediterranean is lower, at 2,611 individuals (**Table** 61), but this is based on much scarcer data. The model still highlights the northwestern region, including the Balearic Islands, with a particular focus on the Tyrrhenian Sea around Ischia Island as a key area. However, due to the limited data, especially around the Balearic Islands during these months (**Figure 69** and see **Appendix F**), it is difficult to draw definitive conclusions about the inter-seasonal differences in these estimates.

The previous round of models in the Mediterranean (Mannocci et al. 2018) predicted a corrected abundance of 12,704 individuals in the entire Mediterranean Sea. That estimate was much higher than the new ones. Mannocci et al. (2018) recognized that it appeared high compared to existing abundance estimates. The fact that the new estimates align much better with previous estimates—as shown above—suggests that the previous ones were somehow overestimated. In particular, for the previous round there were no sightings available in the whole eastern Mediterranean, and therefore that area was completely extrapolated, which might have contributed to the overestimation.

There were no available visual observations for winter in the eastern Mediterranean, only opportunistic sightings (unrelated to survey effort) and acoustic detections. Based on input from regional experts, it was suggested that the sperm whale density in winter is likely similar to that in summer. Therefore, we applied our summer predictions to the winter period.

In both seasons, the Adriatic Sea was assumed 0 density as there were no records in that area.

4.3.3. Risso’s Dolphins

Risso’s dolphins were modeled for the entire Mediterranean Sea, year-round, excluding the Strait of Gibraltar where a density of 0 was assumed, as the species has not been recorded there for decades. Although this species is distributed throughout the Mediterranean, higher densities were predicted in the western basin, as reflected by our model. The spatial density patterns and abundance estimates for both summer and winter were nearly identical (see **Figure 70** for summer, **Figure 71** for winter, and **Table 62**). Key areas identified by the model include the Alboran Sea, the Algerian Coast, and the eastern waters off Spain. These distribution patterns align closely with those obtained from the ACCOBAMS survey (Cañadas et al. 2023) and previous studies (Gómez de Segura et al. 2008; Laran et al. 2017).

Risso's dolphins are one of the least-studied cetacean species in the Mediterranean, with only a few dedicated studies available (e.g., Azzellino et al. 2016; Borrell et al. 2021; Cipriano et al. 2022; Luna et al. 2022; Minoia et al. 2023). The species shows strong habitat preferences, often occurring in small groups and favoring slope areas, particularly in the northwestern basin (Bearzi et al. 2011). They are also frequently reported in the Alboran Sea, the Gulf of Vera, and the Provençal basin, where they are known to inhabit deep offshore waters (Cañadas et al. 2002, 2005; Laran et al. 2017), particularly in the eastern half of the Alboran Sea (Cañadas et al. 2005). Mannocci et al. (2018b) found higher densities over the continental shelf across the Mediterranean, with the majority of sightings in the western Mediterranean and fewer in the central Mediterranean and southern Adriatic.

An aerial survey over the Adriatic Sea in summer 2010 estimated an uncorrected abundance of 510 Risso's dolphins (CV = 78%; Fortuna et al. 2011). After correcting for g(0) for aerial surveys (0.84), the estimate increased to 607 animals. This closely aligns with our model's prediction for the Adriatic Sea, which estimated 448 individuals.

Our model's abundance estimate of 13,383 individuals extracted for the ACCOBAMS survey area is lower than the estimate derived from the ACCOBAMS survey, which reported 27,511 dolphins after correcting for detection probability using planes (Panigada et al. 2024). In contrast, Mannocci et al. (2018) estimated 43,889 Risso's dolphins, which was significantly higher than our estimate.

As mentioned in **Section 2.11.3**, the Gulf of Corinth was excluded from the models. Only a single Risso's dolphin has been accounted for in the gulf, repeatedly over the years, so a total abundance estimate of one animal was used (Bearzi et al. 2016).

4.3.4. Long-finned Pilot Whales

Our model predicted that the distribution of long-finned pilot whales is primarily restricted to the westernmost part of the Mediterranean Sea, consistent with previous findings. Long-finned pilot whales are almost exclusively found in the western basin (Cañadas and Sagarminaga 2000; Notarbartolo di Sciara 2016; Verborgh et al. 2016; Mannocci et al. 2018). The highest densities are thought to occur in the Strait of Gibraltar, Alboran Sea, and Gulf of Vera (Cañadas et al. 2005). The species is also present in the Balearic Sea, Provençal Basin, Ligurian Sea, and eastern Tyrrhenian Sea, though in smaller numbers (**Figure 73** and **Figure 74**).

In the Strait of Gibraltar, a long-term photo-identification study of this species has been ongoing for decades. This period includes a significant epizootic event during the winter of 2006–2007 that affected pilot whales (Verborgh et al. 2019). Verborgh et al. (2019) found that the population growth rate was positive before 2006, but turned negative during the epizootic until 2009. It rebounded positively in 2010, followed by another negative trend in 2011, coinciding with a new spike in strandings linked to a possible morbillivirus outbreak, likely transmitted from striped dolphins (Fernández et al. 2008). Due to these epizootics, the population size in the Strait of Gibraltar declined between 2006 and 2011 (Verborgh et al. 2019). Our analysis, which includes data from 1999 to 2022, reflects this inter-annual variability due to mortality events.

Within the Strait of Gibraltar, our model predicted the highest densities in the deep central waters of the strait (**Figure 72**), closely aligning with findings from local researchers (de Stephanis et al. 2008; de Stephanis 2023). For scaling the abundance estimates from our models, we used the most recent published estimate of 285 individuals (Ouled-Cheikh et al. 2023).

The Alboran Sea has the highest density of pilot whales in the entire Mediterranean, second only to the Strait of Gibraltar. This region was also impacted by the epizootic between 2006 and 2011, though to a lesser extent (Cañadas 2014). Our model includes the Gulf of Vera, located just north of the Alboran Sea along the Spanish Coast. It predicts 3,967 pilot whales in summer and 2,245 in winter for this area (**Table 63**), resulting in an average yearly estimate of 3,106 individuals (CV = 37.5%) from 1991 to 2022. Earlier estimates in the northern Alboran Sea indicate a pre-epizootic population of 2,088 individuals (CV = 13.7%) between 1992 and 2005, which decreased to 1,878 individuals (CV = 8.4%) during the epizootic years of 2006 to 2011 (Cañadas 2014). A photo-identification study in the Alboran Sea also estimated an abundance of 1,569 individuals (Verborgh et al. 2016).

Satellite tracking of pilot whales between 2010 and 2011 identified two distinct groups that do not intermix: one occupying the Strait of Gibraltar and the westernmost Alboran Sea, and another utilizing the central and eastern parts of the Alboran Sea, as well as the Gulf of Vera (Verborgh et al. 2016; **Figure 104** left). This separation was further supported by a social network analysis from photo-identification data (Verborgh et al. 2016; **Figure 104** right).

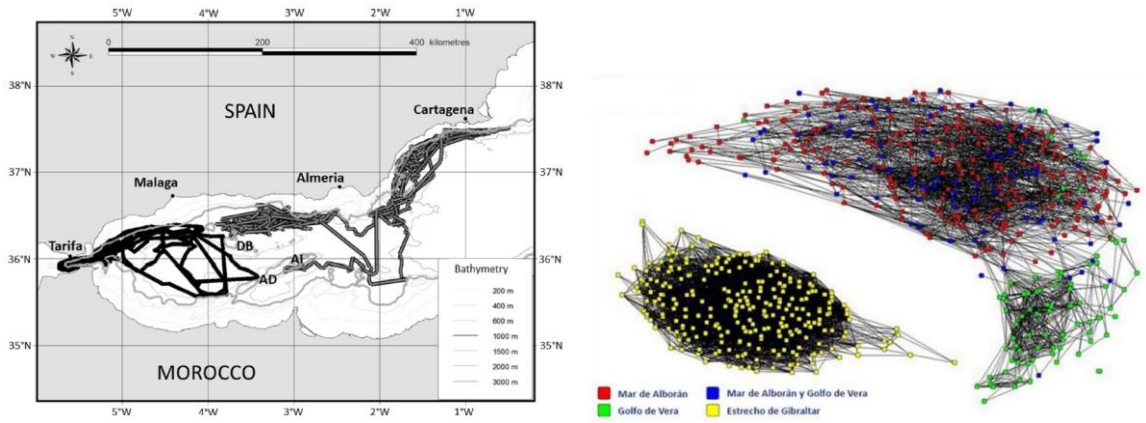

Figure 104. Social units of long-finned pilot whales in the Strait of Gibraltar and Alboran Sea.

Left: Satellite tags deployed on pilot whales (black: deployed in the Strait of Gibraltar, grey: deployed in the Alboran Sea and Gulf of Vera) (extracted from Verborgh et al. 2016). Right: Social network according to photo-identification (yellow = Strait of Gibraltar; red, green, and blue: Alboran Sea and Gulf of Vera) (extracted from Verborgh et al. 2016).

For the rest of the Mediterranean Sea, information on pilot whale distribution and abundance is limited. Although pilot whales are generally believed to be confined to the western Mediterranean (Notarbartolo di Sciara 2016), there have been occasional strandings in the northern Ionian Sea (Podestà and Bortolotto 2001) and sporadic sightings (Pirounakis 1999). Therefore, we included the Ionian Sea in our model, as its presence should not be assumed zero in this area.

Our model predicts very low densities throughout this region (**Table 63**), making distribution patterns almost undetectable in the overall maps (**Figure 73** and **Figure 74**). **Figure 105** presents a focused map of density to illustrate the predicted distribution in this area. For visualization, the density scale was adjusted from 0–11 individuals per km² (**Figure 73** and **Figure 74**) to 0-0.3 individuals per km² (**Figure 105**). Within this area, the Liguro-Provençal region showed the highest density, aligning with most recorded sightings (see **Appendix F**).

This general distribution pattern is consistent with findings from Gnone et al. (2023) and Verborgh et al. (2016), who observed similar patterns across the broader area.

Mannocci et al. (2018) estimated 81,830 pilot whales in the whole Mediterranean Sea (corrected), which was clearly an overestimation when compared to all other available estimates and the new ones.

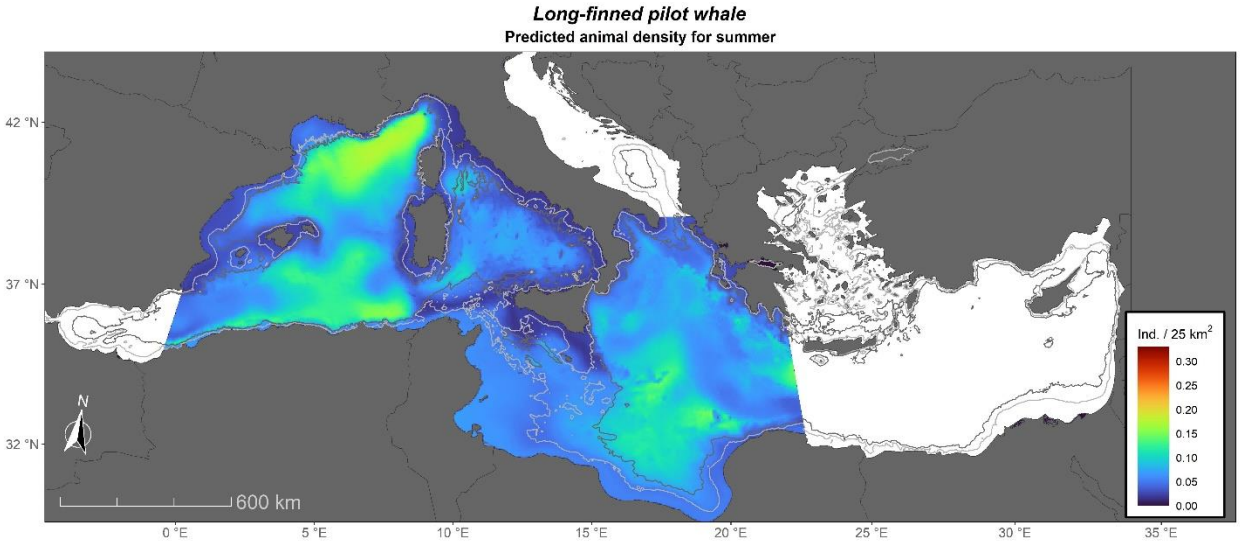

Figure 105. Map of predicted density in the western Mediterranean (without the Alboran Sea) and the Ionian Sea (rescaled to visualize the pattern).

4.3.5. Cuvier's Beaked Whales

Our predicted density maps align with existing knowledge on the basin-wide distribution of Cuvier's beaked whale, confirming that the species is found in relatively small, low-density patches. Mannocci et al. (2018) predicted higher densities in areas between 1,000 and 2,000 m depth across the basin using only static covariates, such as depth and slope, despite most observations occurring in the Alboran Sea. Similarly, Cañadas et al. (2017) observed the highest densities in the Alboran Sea, Ligurian Sea, and Ionian Sea (particularly the Hellenic Trench), with additional patches in the Tyrrhenian Sea and northeastern waters off Spain (**Figure 75** and **Figure 76**). Occurrences of this species have also been recorded in the southern Adriatic Sea (Holcer et al. 2007), an area where our model also predicted some density.

Aside from the Mediterranean-wide modeling of Cuvier's beaked whales by Cañadas et al. (2018), which yielded a corrected abundance estimate of 5,799 individuals (CV = 24%)—similar to our results (**Table 64**)—there are few abundance estimates available for the Mediterranean. In the Gulf of Genoa (eastern Ligurian Sea), mark-recapture analyses from 2002 to 2008 yielded estimates between 95 (CV = 9%) and 98 (CV = 10%) individuals, using open population models (Podestà et al. 2016; Rosso et al. 2009). When we extracted the predicted abundance for the Pelagos Sanctuary, which includes the Gulf of Genoa, our estimate was 115 animals, indicating a similar order of magnitude.

As a deep-diving and elusive species, Cuvier's beaked whale benefits from shipboard surveys equipped with acoustic arrays, which provide crucial insights into its distribution. During the ACCOBAMS survey, 31 detections of beaked whale clicks were recorded, with 21 classified as "definite" ziphiid clicks (ACCOBAMS 2021). These detections were made in the Alboran Sea, northeastern waters off Spain, the Hellenic Trench, and notably, the deep waters off Libya (**Figure 106**). Our model also predicted high densities in the waters off eastern Libya (**Figure 75** and **Figure 76**), where visual sightings were absent (see **Appendix F**) but acoustic detections from the ACCOBAMS survey confirmed their presence (**Figure 106**). All these findings reinforce existing evidence that the eastern Mediterranean is a significant habitat for Cuvier's beaked whales (Baş et al. 2003; Frantzis et al. 2003; Podestà et al. 2016; Cañadas et al. 2018).

Mannocci et al. (2018) provided a corrected estimate of 19,587 Cuvier's beaked whales in the whole Mediterranean Sea, which was clearly an overestimation when compared to all other available estimates and the new ones.

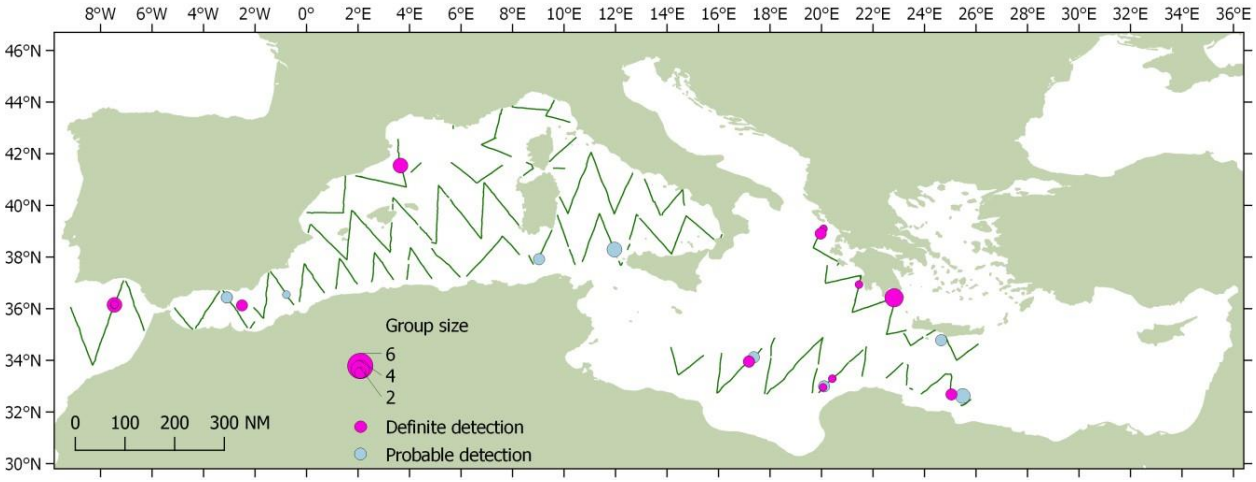

Figure 106. Acoustic detections of Cuvier's beaked whales during the ACCOBAMS survey in 2018 (extracted from ACCOBAMS 2021).

4.3.6. Bottlenose Dolphins

Bottlenose dolphins are the most common cetacean found along the Mediterranean continental shelf, ranging from Gibraltar to the Levantine Sea (Notarbartolo di Sciara 2016; Gnone et al. 2023). However, their distribution is relatively patchy (Cañadas et al. 2023; Gnone et al. 2023). Existing research indicates a preference for coastal and shelf areas (Bearzi et al. 2009;

Mannocci et al. 2018a; Notarbartolo di Sciara 2016), though bottlenose dolphins also occur in oceanic waters, particularly at lower densities, with this trend being more notable in winter (Laran et al. 2017; Gnone et al. 2023).

Although bottlenose dolphins in the Mediterranean are considered a single subpopulation, they exhibit significant genetic structure and display distinct genetic, social, and cultural differentiation across their range, often forming populations of only a few hundred individuals. Notably, significant genetic differences have been identified between populations in the eastern and western Mediterranean (Natoli et al. 2005). Further subdivision within both the eastern and western basins has also been observed, though with lower levels of differentiation (Natoli et al. 2021).

While there are numerous localized coastal studies focused on photo-identification, large-scale abundance estimates for this species are limited, with only one covering the entire Mediterranean (ACCOBAMS 2021). The distribution predicted by the ACCOBAMS aerial survey mirrors our model, showing the highest densities in the Alboran Sea, Gulf of Lyon, Balearic Islands, eastern Ligurian Sea, northern Tyrrhenian Sea, the waters between Tunisia and Sicily, and the Aegean Sea (**Figure 78** and **Figure 79**). Our model also predicts high densities along the eastern coast of Egypt, though this area was not covered by the ACCOBAMS survey.

The ACCOBAMS survey provided a model-based, uncorrected abundance estimate of 50,729 dolphins (CV = 15%; Cañadas et al. 2023), which, after accounting for availability and perception bias (g(0) = 0.85), increased to 59,681. The design-based uncorrected estimate was 59,838 (CV = 17%; Panigada et al. 2024), adjusted to 70,398 after corrections. Our corrected model prediction for the ACCOBAMS survey area was slightly higher, at 73,631 individuals (CV = 9%) (**Table 65**).

In the Strait of Gibraltar, a long-term photo-identification study on bottlenose dolphins has been ongoing for more than two decades. Our model predicted the highest densities in the central Strait and near the Spanish Coast, which aligns well with observed data (**Figure 77**) and previous findings (de Stephanis et al. 2008; de Stephanis 2023). The abundance estimates in the strait show relatively high inter-annual variability (Tenan et al. 2020). For scaling our model, we used the 2023 photo-identification estimate of 162 animals (de Stephanis pers. comm.).

In the Alboran Sea, a long-term study in the northeastern sector also revealed considerable variability in abundance over different periods. This variability was attributed, based on photo-identification, to the intermittent presence of immigrant groups that stayed for one or two years before moving on (Cañadas and Hammond 2006; Cañadas 2014). Over five consecutive periods from 1995 to 2010, the abundance estimates in that study fluctuated significantly, varying between 111, 537, 279, 550, and 300 animals. When correcting for the g(0) estimated to this platform (0.913), those abundances increased slightly to 122, 588, 306, 602 and 329, respectively (mean of 389). Our model, representing a 25-year average, predicted an abundance of 432 animals for that specific study area, in the same general range as the published ones once corrected. The total abundance estimates for summer and winter in the Alboran Sea were a bit different (**Table 65**; 5,271 dolphins in summer and 4,227 dolphins in winter), but this difference is not significant as their 95% CIs widely overlap. The design-based

abundance estimate from the shipboard part of the ACCOBAMS survey was 5,232 dolphins in the Alboran Sea (ACCOBAMS 2021), extremely similar to our summer abundance estimate. The highest abundance estimates were predicted for the shelf waters along both Spanish and north-African Coasts, as well as around the island of Alboran in the center of this block (**Figure 78** and **Figure 79**).

In the western Mediterranean (excluding the Alboran Sea), all covariates were static, resulting in the same abundance estimate for both summer and winter. Comparing our results with other published estimates is challenging, as some studies focus on small, very coastal areas—mainly through photo-identification—while others vary widely in shape and spatial extent. However, the basin-wide ACCOBAMS survey estimated an uncorrected abundance of 23,706 bottlenose dolphins in the western Mediterranean (excluding the Strait of Gibraltar) (ACCOBAMS 2021). After applying a correction factor for airplane-based surveys (0.85), this number increases to 27,889, which closely matches our estimate of 30,270 dolphins (**Table 65**). Our model predicted the highest densities around the Balearic Islands, the Gulf of Lyon, the eastern part of the Ligurian Sea and Corsica, around Sardinia, and the coasts of Tunisia, which closely matches the observations (see **Appendix F**).

The Ionian Sea had similar abundance estimates for both summer and winter (**Table 65**). The ACCOBAMS survey did not encompass the entire Ionian Sea, as it lacked permission to survey Libyan waters. Within the surveyed area, it estimated 9,979 bottlenose dolphins, corresponding to a density of 0.019 animals per km². Our model predicted 17,326 bottlenose dolphins for summer—comparable to winter—yielding a density of 0.022 animals per km². These values were thus quite similar. Interestingly, no observations of bottlenose dolphins were recorded in the deep waters of the Ionian Sea (see **Appendix F**), unlike in the western Mediterranean and the Alboran Sea, where bottlenose dolphins were frequently encountered in deeper areas. Most observations and the highest predicted abundance were in the waters off Tunisia (**Figure 78** and **Figure 79**), where the continental shelf is particularly broad. Naceur et al. (2004) also identified this area as important for bottlenose dolphins.

As mentioned in **Section 2.11.3**, the Gulfs of Ambracia and Corinth were excluded from the models. However, published abundance estimates and coefficients of variation were assigned to these areas using a uniform distribution. For the Gulf of Ambracia, the latest estimate of 134 individuals was used (Gonzalvo et al. 2016). For the Gulf of Corinth, the final abundance estimate of 39 animals (CV = 0.14) from Bearzi et al. (2016) was used.

After adjusting the esw for surveys in the Adriatic Sea, as outlined in **Section 2.11.3**, our abundance estimates remained higher than previous estimates based solely on aerial surveys. Fortuna et al. (2018) reported an uncorrected estimate of 5,700 bottlenose dolphins, which, when corrected using a g(0) of 0.86 for aerial surveys, yields an adjusted abundance of 6,628 animals. This estimate highlighted the highest densities in the northern Adriatic, with the lowest in the central region. Our model predicts a similar distribution pattern (**Figure 78** and **Figure 79**) but estimates 16,165 dolphins in summer and 14,459 in winter, averaging 15,312—more than double the published figures. Further research is needed to investigate the unique circumstances of the Adriatic Sea that may influence these estimates.

In the Aegean Sea, our model predicts the highest abundance on the eastern side of the area (**Figure 78** and Figure 79). The presence of bottlenose dolphins in the Aegean Sea is well documented (Foskolos et al. 2020; Frantzis et al. 2003). Giannoulaki et al. (2016) modeled the habitat of bottlenose dolphins in the Aegean Sea showing a preference for most of the eastern side areas, and a portion of the western area between the Cyclades and the Saronikos Gulf, where our models also showed densities similar to the eastern portion, matching very well our own predictions. A systematic survey in the northern Aegean yielded an uncorrected estimate of 462 bottlenose dolphins (Tsagarakis et al. 2021; Pierantonio et al. 2018). When adjusted with a correction factor of 0.86 for aerial surveys, this figure rises to 537 animals (CV = 38.5%). The ACCOBAMS survey estimated an uncorrected abundance of 7,072 and 9,017 bottlenose dolphins using model-based and design-based methods, respectively. After correcting for detection probability (g(0)), these figures increased to 8,223 and 10,485 dolphins. Our model's corrected abundance estimate for summer was 6,098 animals (**Table 65**), which is lower than the ACCOBAMS estimates. However, the 95% CI for both analyses overlap significantly, indicating that these differences were not statistically significant.

Our results for the Levantine Sea were very different than those from the ACCOBAMS survey. In the latter, all the waters off Libya, Egypt and Syria Economic Exclusive Zones and the southwestern waters off Cyprus remained unsurveyed by the planes due to lack of permits, which represent a very large portion of the Levantine Sea. In the remaining surveyed portion, only six observations of bottlenose dolphins were made, which contributed to an extremely large CV. Comparison with this survey, therefore, did not seem useful. Our models predict a rather large number in the Levantine Sea with a very important inter-seasonal difference: 14,349 bottlenose dolphins in summer and 27,088 in winter (**Table 65**), although their 95% CI overlap to some extent. There were many observations from a long-term study in the waters off Israel, where the model predicted high density. But more interestingly is the high density predicted for eastern Egypt, where with very little effort, several observations were made. Its presence has also been recorded as abundant off the coasts of Gaza (Abd Rabou et al. 2023) and Israel (Galili et al. 2023). A dedicated survey in a small stretch of coast off Libya yielded many observations (Ben Amer, pers. comm.). Observations were made also in the coastal waters of Lebanon, Syria, and Egypt during the shipboard part of the ACCOBAMS survey (ACCOBAMS 2021). All this information indicates that the southern and eastern coastal waters of the Levantine Sea, very scarcely surveyed (and in most parts nothing at all), might be an important habitat for bottlenose dolphins. Additionally, Baş et al. (2016) highlight the importance of the Antalya Bay, in the middle of the Turkish Coast, for bottlenose dolphins. All the Turkish coastal waters were also highlighted with moderate density by our model, and higher in winter than in summer, although the very coastal nature of these predictions makes it almost undetectable in the full map (**Figure 78** and **Figure 79**).

Mannocci et al. (2018) provided a corrected estimate of 165,320 individuals for the entire Mediterranean Sea for the previous round of modeling. This is around double of our estimate with the new models, which in turn seem to align better with previous partial estimates.

4.3.7. Common Dolphins

Like long-finned pilot whales, common dolphins mainly inhabit the Alboran Sea. Natoli et al. (2008) identified small but significant genetic differentiation between eastern and western Mediterranean populations, with Alboran Sea dolphins showing closer genetic ties to the northeast Atlantic populations. For this reason, common dolphins were also modeled separately across three blocks: the Strait of Gibraltar, the Alboran Sea, and the rest of the Mediterranean. Our common dolphin models include those ambiguous identification sightings assigned to this species (see **Section 2.9**).

Common dolphins are the most abundant cetaceans in the Bay of Algeciras, on the eastern side of the Strait of Gibraltar, where our model predicted high densities (**Figure 80**). They are also present throughout the strait. Our model's abundance estimate of 3,446 dolphins (**Table 66**) closely aligns with de Stephanis (2023), which reported 3,334 dolphins in the summer. For winter, that report estimated an abundance of 1,040 dolphins. Since our model used only static covariates, it did not produce separate seasonal estimates.

Within the Alboran Sea, our model predicted the highest densities in summer along the Spanish Coast in the north, near the entrance to the Strait of Gibraltar, and off the central coast of Morocco, all aligning well with observed data (**Figure 81** and **Appendix F**). In winter, the model indicated lower densities (**Table 66**) more evenly spread across the western Alboran Sea (**Figure 82**). This distribution is consistent with over 20 years of survey observations, which indicate that common dolphins tend to move farther offshore during winter, resulting in lower coastal densities (Cañadas and Hammond 2008).

When we derived a prediction from our model to the study area in Cañadas and Hammond (2008), we estimated 19,439 dolphins, which closely matches their corrected estimate of 20,028 animals. This agreement suggests that our overall abundance estimate for the Alboran Sea is accurate. The ACCOBAMS survey, which included only the northern half of the Alboran Sea, recorded just 11 sightings of common dolphins, resulting in an abundance estimate of 25,855 animals (Panigada et al. 2024). However, due to the high coefficient of variation (CV = 69%), drawing any firm conclusions from this estimate is challenging.

For the remainder of the Mediterranean, only eight observations were made during the ACCOBAMS survey, resulting in coefficients of variation near 100%, so meaningful comparisons could not be made. Our summer model predicted the highest densities along the eastern Aegean Sea, south of Sicily, and, to a lesser extent, in the southeastern Levantine Sea. **Figure 107** displays a partial map of predicted summer abundances for the Mediterranean (excluding the Alboran Sea), with adjusted color scaling to highlight areas of higher density predictions (density scale ranges from 0 to 8 individuals per 25 km², compared to 0 to over 120 individuals per 25 km² in **Figure 81**).

Common dolphin presence has been documented in the northern, eastern, and southwestern Aegean Sea, though they are notably absent from the Cretan Sea (Giannoulaki et al. 2016; Frantzis et al. 2003; Foskolos et al. 2020), which is consistent with our model (**Figure 107**). They are also known along the Ionian Coast of Greece, with a patchy distribution in coastal

areas among the islands (Bearzi et al. 2003; Frantzis et al. 2003). South of Sicily and around the Maltese islands, long-term studies have identified this area as a stronghold for common dolphins, with an overall density of 0.14 animals/km² (CV = 29.5%), almost 10 times our predicted density for the entire Mediterranean (excluding the Alboran Sea) as shown in **Table 66** ("noAlboran"). This area was also highlighted by our models (**Figure 107**).

In the Levantine Sea, although uncommon, common dolphins have been recorded on the Gaza Coast, primarily through strandings (Abd Rabou et al. 2023) and are considered residents in the coastal waters of Israel (Galili et al. 2023). While they were not observed off Lebanon during the ACCOBAMS survey's shipboard component, sightings occurred off the coasts of Syria and Egypt (ACCOBAMS 2021), which support our model's predictions for the southeastern Levantine Sea (**Figure 107**).

Our model also predicted relatively high densities along the Algerian Coast in both summer (**Figure 107**) and winter (**Figure 82**). This is supported by observations of common dolphins in that region across seasons, albeit with minimal effort (see **Appendix F**), and by previous studies (Boisseau et al. 2010). Notably, similar to bottlenose dolphins, common dolphins were not observed in the deep waters of the Ionian or most of the Levantine Sea (see **Appendix F**), unlike in the western Mediterranean and Alboran Sea, where they are occasionally found in deeper areas.

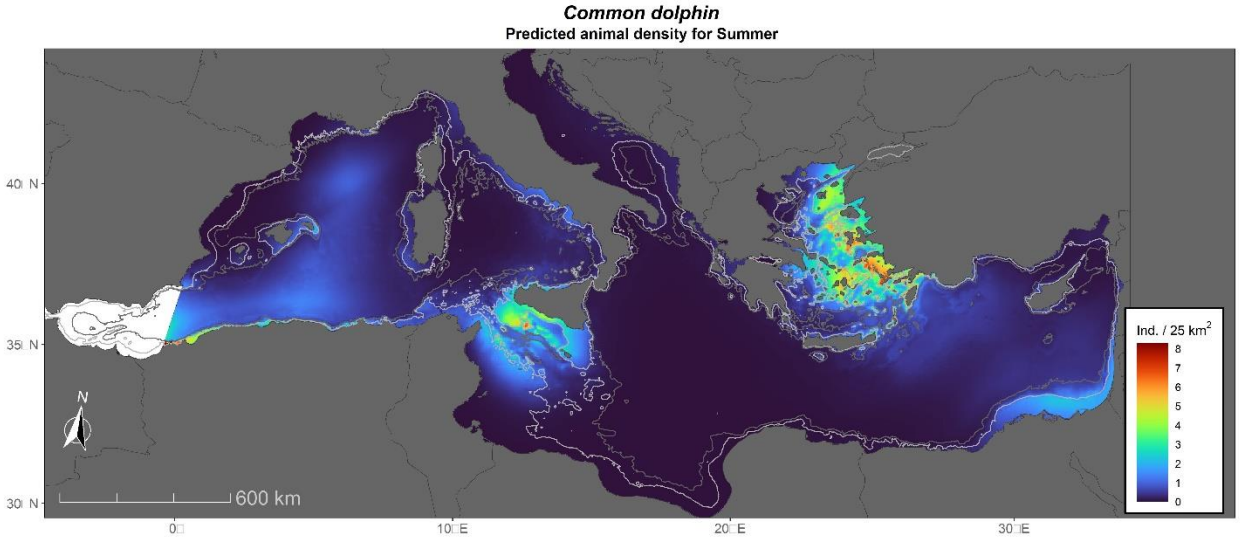

Figure 107. Highlight of the predicted summer abundance of common dolphins in the Mediterranean without the Alboran Sea.

Common dolphins were rarely observed in the Adriatic Sea despite substantial survey effort (see **Appendix F**), leading to low-density predictions for this region. However, literature suggests they are regular visitors to the Adriatic (Bearzi et al. 2024; Genov et al. 2021).

As mentioned in **Section 2.11.3**, the Gulfs of Ambracia and Corinth were excluded from the models. For the Gulf of Ambracia, density was assumed 0, as bottlenose dolphin is the only cetacean present there (Gonzalvo et al. 2016). For the Gulf of Corinth, the published abundance

estimate and coefficient of variation (22 animals, CV=0.32) were assigned to this area using a uniform distribution (Bearzi et al. 2020).

Mannocci et al. (2018) provided a corrected estimate of 164,512 individuals for the entire Mediterranean Sea for the previous round of modeling. This is around double of our estimate with the new models, which in turn seem to align better with previous partial estimates.

4.3.8. Striped Dolphins

The striped dolphin is the most abundant and widespread cetacean in the Mediterranean Sea, primarily inhabiting deep waters, with higher densities in the western basin compared to the eastern (Notarbartolo di Sciara 2016). Our models were consistent with this knowledge, showing greater densities in the western Mediterranean in both summer (**Figure 84**) and winter (**Figure 85**), with especially high density in the western half of the Alboran Sea.

Our model predictions for striped dolphins were similar for both summer and winter (**Table 67**), The summer abundance estimate for the ACCOBAMS survey area is 468,964 dolphins, closely aligning with the ACCOBAMS summer survey's corrected estimates: 532,249 dolphins (CV = 13%) using the design-based approach (Panigada et al. 2024), and 587,439 dolphins (CV = 14.5%) using the model-based approach, both with overlapping 95% CI with our models predictions (Cañadas et al. 2023).

As with other species, striped dolphins were modeled separately for the Strait of Gibraltar. Our model predicted the highest densities in the center of the strait and near the Bays of Algeciras and Ceuta, at the northeastern and southeastern edges, respectively (**Figure 83**). Striped dolphins were also present throughout the strait. Our model's abundance estimate of 3,863 dolphins (**Table 67**) aligns well with de Stephanis (2023), who reported 3,216 dolphins in summer and 630 in winter. Since our model used only static covariates, it did not generate separate seasonal estimates.

In the Alboran Sea, long-term studies have reported similar encounter rates for striped and common dolphins, though striped dolphins tend to have higher densities in deeper waters compared to common dolphins (Cañadas et al. 2005). An unpublished study provided a high uncorrected abundance estimate for the northern Alboran Sea and Gulf of Vera: 21,267 animals, which, when corrected for platform-based detection bias (g(0) = 0.97), increased to 21,925 animals (Cañadas, personal observation). When extracting the predicted abundance for this area from our models, we estimated 19,328 striped dolphins in summer and 15,834 in winter, aligning closely with previous findings. An earlier survey by Forcada and Hammond (1998) estimated 17,728 striped dolphins across the entire Alboran Sea. Although this estimate suggests a lower overall density, the 95% CI (9,507–33,059) overlaps with our results (**Table 67**), indicating that the differences were not statistically significant.

Forcada and Hammond (1998) provided abundance estimates for several areas of the western Mediterranean, excluding the Tyrrhenian Sea. Summing these partial estimates, their uncorrected total abundance estimate for this region was 217,842 dolphins, which, when corrected with a platform-specific factor of 0.86, became 253,305 dolphins, with coefficients of variation between 24% and 38%. Our model predicts an abundance of 354,894 striped dolphins

for the entire western Mediterranean, including the Tyrrhenian Sea. When we exclude most of the Tyrrhenian Sea from our calculations, we estimate around 300,000 animals. The ACCOBAMS aerial survey estimated an uncorrected abundance of 362,227 striped dolphins (CV = 16%), which increased to 458,515 dolphins after correction (Panigada et al. 2024). Although these estimates vary, they were all of the same order of magnitude, indicating general alignment despite some differences.

In the Pelagos Sanctuary (Ligurian Sea), Panigada et al. (2011) predicted a corrected summer abundance estimate of 38,488 striped dolphins. This closely matches our model's predicted abundance for the Pelagos Sanctuary area, which estimates 37,722 dolphins.

In the northwest Mediterranean, Panigada et al. (2017) and Laran et al. (2017) reported lower densities of striped dolphins in winter compared to summer. Conversely, in the Balearic Sea, Gómez de Segura et al. (2006) found no significant seasonal changes in densities. These patterns were also evident in our model predictions, with summer (**Figure 84**) and winter (**Figure 85**) showing similar trends.

In the eastern Mediterranean, our models predict relatively high densities in the southern Adriatic, the Aegean Sea, and parts of the Ionian Sea. Previous studies have shown that striped dolphins are abundant in the deep waters of the southern Adriatic (Azzolin et al. 2020; Bearzi et al. 2024). An aerial survey in 2010 estimated an uncorrected abundance of 15,343 striped dolphins (CV = 28%; Fortunat et al. 2011; Lauriano 2022), which, when corrected with a g(0)=0.79, increased to 19,421. The ACCOBAMS survey provided an uncorrected model-based abundance estimate of 13,138 dolphins (CV = 30.7%) for the southern Adriatic, which, with a g(0) correction of 0.79 for aerial surveys, corresponds to 16,630 dolphins (ACCOBAMS 2021). These estimates were higher than our model's prediction for the Adriatic Sea, which estimates 11,346 dolphins.

Our model shows an apparent shift in distribution between summer (**Figure 84**) and winter (**Figure 85**). It predicts much higher densities in the Aegean Sea during summer and higher densities in the Ionian Sea during winter. However, given the limited data available for the winter months, it is uncertain whether this shift reflects an actual seasonal movement or is simply due to the high variability in data availability across seasons and regions. Previous data on striped dolphins in the Aegean Sea is sparse; they are typically observed in offshore areas and are absent from enclosed regions (Foskolos et al. 2020; Frantzis et al. 2003). This pattern is consistent with our summer model's predictions (**Figure 84**).

For both summer and winter, our model estimates the lowest densities in the southern and easternmost parts of the eastern Mediterranean (**Figure 84** and **Figure 85**), consistent with findings by Boisseau et al. (2010). However, the ACCOBAMS shipboard survey in 2018 (ACCOBAMS 2021) recorded some observations of striped dolphins in the waters off Syria and Egypt—though less frequently than common dolphins—but none in Lebanon. Additional sightings were reported in the deep waters off Libya and along the Hellenic Trench.

As mentioned in **Section 2.11.3**, the Gulfs of Ambracia and Corinth were excluded from the models. For the Gulf of Ambracia, density was assumed 0, as bottlenose dolphin is the only

cetacean present there (Gonzalvo et al. 2016). For the Gulf of Corinth, the published abundance estimate and coefficient of variation (1,331 animals, CV = 0.14; Bearzi et al. 2022) were assigned to this area using a uniform distribution.

Mannocci et al. (2018) provided a corrected estimate of close to 2 million individuals for the entire Mediterranean Sea for the previous round of modeling. This is around four times higher than our estimate with the new models and the ACCOBAMS survey.

4.3.9. Harbor Porpoises

This was a new species modeled for the Mediterranean compared to the first round of modeling (Mannocci et al. 2018). Until recently, harbor porpoises were believed to inhabit only the northern Aegean Sea (Fontaine 2016; Foskolos et al. 2020), a presence confirmed by visual and acoustic surveys in 2013 (Cucknell et al. 2016). However, strandings have also been reported further south along both coasts of the Aegean Sea (Cucknell et al. 2016), suggesting the possibility of a small, undetected population in these areas. Genetic and morphological evidence indicates that Mediterranean harbor porpoises belong to the Black Sea subspecies *Phocoena phocoena relicta* (Viaud-Martinez et al. 2007).

Our abundance estimate for harbor porpoises in the Aegean Sea is 1,416 individuals (**Table 68**), though this is likely an overestimate. This simple model was based on limited observations (16 sightings), and the covariate used—distance from the Atlantic—likely introduced an edge effect that inflated densities toward the eastern end of the Gulf of Saros. Local experts also consider this estimate to be high.

Recent information has emerged regarding a small population of harbor porpoises between Fuengirola and Benalmádena in the northwestern Alboran Sea (**Figure 108**; paper in preparation; Salazar and de Stephanis, pers. comm.). These sightings, recorded opportunistically over the past decade during spring and summer (with no surveys in fall or winter), suggest a population of around 30 animals. Consequently, this area has been added to the NMSDD as a uniform distribution of 30 individuals. This represents the only known harbor porpoise population in the Mediterranean Sea outside of the Aegean Sea.

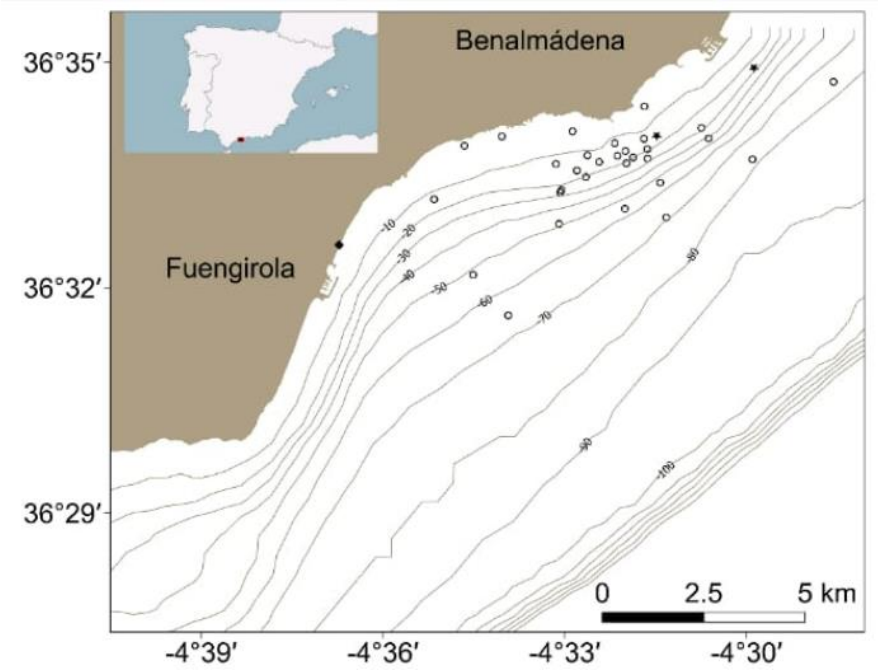

Figure 108. Sightings of harbor porpoise in the northwestern part of the Alboran Sea(unpublished, Salazar and de Stephanis, pers. comm.).

4.3.10. Killer Whales

This was a new species modeled for the Mediterranean compared to the first round of modeling (Mannocci et al. 2018). The density patterns predicted by our model, after scaling to the census data (see **Section 3.6.10**) align well with those published previously (Esteban et al. 2014; Esteban et al. 2016) for spring and summer, with a lower density and more restricted to the center of the channel in summer and extending more to the northwest during spring. No maps were available in those publications for winter.

4.3.11. Monk Seals

The density pattern provided here (**Figure 99**) was not derived from a model but rather extracted from existing data (IUCN MMPATF 2024). As such, there is no numerical uncertainty associated with this estimate (544 individuals). All the observations in recent decades occurred in the highlighted area of **Figure 99** in the northeastern section of the eastern Mediterranean, including the Hellenic Trench, the Aegean Sea, and the northern part of the Levantine Sea. However, substantial real uncertainty exists regarding the abundance and distribution of monk seals due to the fragmented and complex nature of the available data, which includes sightings of animals at sea, on beaches, and in caves. At present, quantifying this uncertainty is not feasible.

4.4. General Considerations for the Mediterranean Sea

For the Mediterranean Sea models, as in the Black Sea, two seasons were defined: summer (May to October) and winter (November to April). Survey effort showed significant heterogeneity across both seasons, especially during winter (**Figure 13**) and this heterogeneity was also

pronounced within each season across different areas of the basin. Furthermore, incorporating data from multiple years revealed substantial differences in survey effort, both in quantity and spatial coverage (**Figure 11**). To address this issue and reduce the high interannual variability, monthly climatologies of the covariates were used - meaning that monthly means were calculated across all years. This approach provided a more stable dataset for modeling. Appendix I includes plots of both static covariates and the climatologies of dynamic covariates, illustrating the significant spatial and monthly variability of the dynamic covariates. Such variability presented challenges for modeling, particularly given the use of only two seasons, each spanning six months. Despite these adjustments, considerable intraseasonal variability remained within each season, particularly for important covariates like the sea surface temperature, both for the Black Sea and the Mediterranean.

Another challenge encountered during the modeling process for the Mediterranean was the significant number of datasets lacking bearings and distances required for incorporation into the detection functions—comprising 39% of the total observations. For these datasets, esw values from similar platforms were assigned as the best estimates, though this may have introduced unquantifiable biases. The species with the highest proportions of observations lacking distance data were bottlenose dolphins, sperm whales, and Cuvier's beaked whales, with 71%, 51%, and 43%, respectively (**Table 72**). **Figure 109** illustrates all observations with distance data, while **Figure 110** shows those without. Removing datasets with no distance information would have excluded entire regions, such as Israel (the largest dataset in the Levantine Sea), and significantly reduced the number of observations in areas like the Aegean Sea, the Hellenic Trench, the eastern coast of the Adriatic Sea, the Balearic Islands, and various coastal regions. This could, in turn, have led to other spatial biases. Addressing these gaps is an important consideration for future studies.

Table 72. Proportion of observations with and without distances to be included in the detection functions in the Mediterranean.

Species	No dist.	Dist	Total	% No dist	% Dist
Bottlenose dolphin	5,624	2,314	7,938	70.8	29.2
Common dolphin	712	1,845	2,557	27.8	72.2
Cuviers beaked whale	277	372	649	42.7	57.3
False killer whale	1	2	3	33.3	66.7
Fin whale	972	2,524	3,496	27.8	72.2
Harbour porpoise		23	23	0.0	100.0
Killer whale	6	89	95	6.3	93.7
Long-finned pilot whale	90	1,141	1,231	7.3	92.7
Risso's dolphin	158	487	645	24.5	75.5
Sperm whale	832	800	1,632	51.0	49.0
Striped dolphin	4,979	10,111	15,090	33.0	67.0
Striped or common dolphin		289	289	0.0	100.0
Unidentified Balaenoptera		8	8	0.0	100.0
Unidentified beaked whale	6	35	41	14.6	85.4
Unidentified dolphin	143	1,196	1,339	10.7	89.3
Total	**13,800**	**21,236**	**35,036**	**39.4**	**60.6**

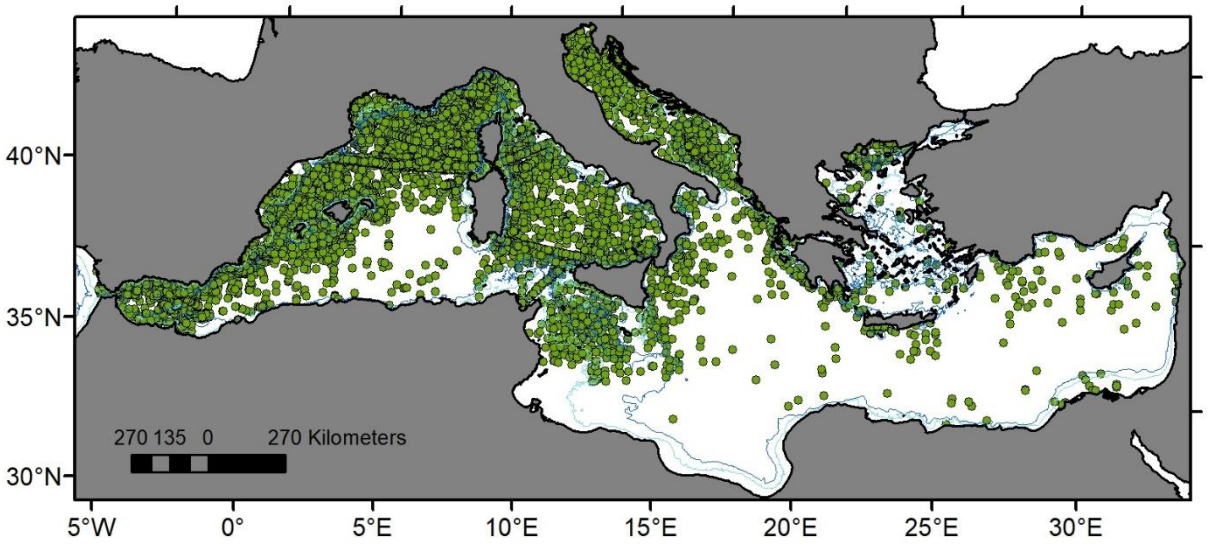

Figure 109. Observations with distances, all species together, in the Mediterranean.

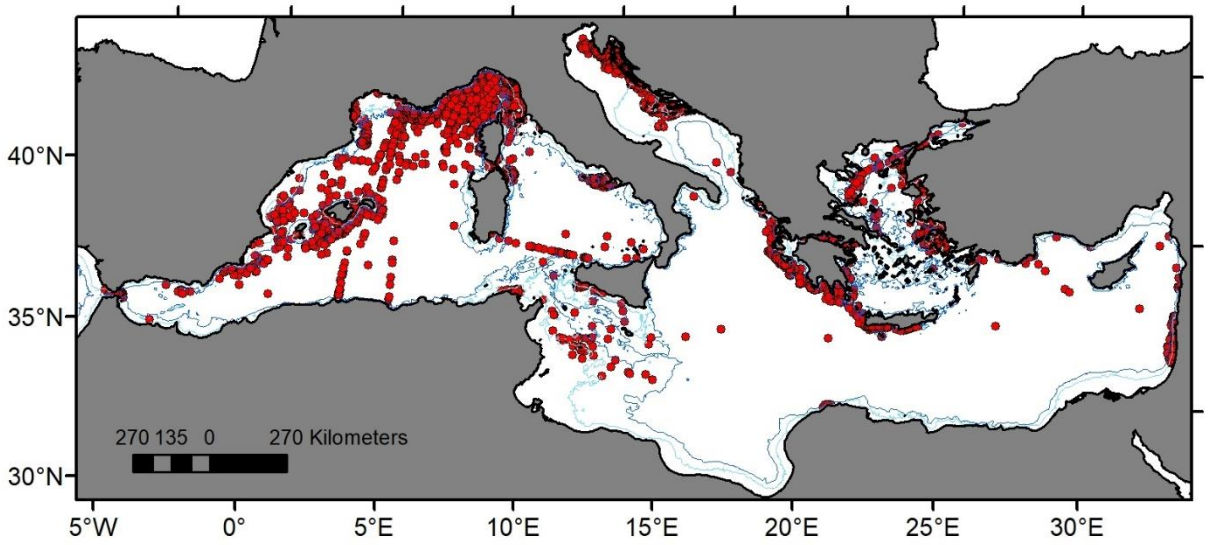

Figure 110. Observations without distances, all species together, in the Mediterranean.

An important issue that emerged was the low detectability of deep-diving species, particularly sperm whales and Cuvier's beaked whales. For sperm whales, in particular, a significant number of visual detections were made following initial acoustic detections, which introduced biases into the estimation of the esw for these visual observations. This issue was especially pronounced in the Hellenic Trench. To address this, the esw from acoustic detections were used in these analyses as a partial solution. However, this approach underscores the need for a thorough investigation to ensure that the right distance measurements are applied in future studies.

4.5. Future Work

Although the habitat-based density models we have developed constitute an important advance, these models could be improved in the future. Potential improvements include the following:

1. Acquire more data of modeled species starting from 2022 and update existing models.
2. Explore the possibility of further spliting the study areas (both the Black Sea and the Mediterranean) into different regions, according to the characteristics of the species, to be modeled independently or hierarchically, e.g., with factor-smoother relationships that incorporate the region as a factor (Pedersen et al. 2019; Mannocci et al. 2020).
3. Whenever enough data is available, further stratify the data for the detection functions. If possible, go down to the level of individual surveys when that is feasible.
4. Explore how to better deal with the observations without distance data to reduce potential biases.
5. Given sufficient data and information from collaborators, stratify sperm whales into lone adult males and social groups, given their very different detectability and habitat use.
6. Consider incorporating acoustic survey data for Cuvier's beaked whales and sperm whales to improve models.
7. Thoroughly review the issue of ambiguous sightings, potentially by stratifying observations by region as well.
8. Try to incorporate rough-toothed dolphins if more sightings become available.
9. Review abundance trends for some species and interannual variations, given the large span of the data available.

5. References

Abd Rabou, A. F. N., K. E. Elkahlout, K. J. Elnabris, A. J. Attallah, J. Y. Salah, M. A. Aboutair, ... and H. A. Madkour. 2023. An inventory of some relatively large marine mammals, reptiles, and fishes sighted, caught, by-caught, or stranded in the Mediterranean Coast of the Gaza Strip-Palestine. Open Journal of Ecology 13(2): 119-153.

Abel, O. 1905. Ein Stammtype der Delphiniden aus dem Miocän der Halbinsel Taman // Jahrbuch K. K. Geolog. Reichs-Anst. Wien, 1905. 55. S. 375–392

ACCOBAMS. 2021. Estimates of abundance and distribution of cetaceans, marine mega-fauna and marine litter in the Mediterranean Sea from 2018-2019 surveys. By S. Panigada, O. Boisseau, A. Canadas, C. Lambert, S. Laran, R. McLanaghan, A. Moscrop. Ed. ACCOBAMS - ACCOBAMS Survey Initiative Project, Monaco, 177 pp.

Arseniev, V. A., V. A. Zemsky, and I. S. Studenetskaya. 1973. Marine Mammals. Moscow: Pishchevaya Promyshlennost.

Azzellino, A., S. Airoldi, S. Gaspari, C. Lanfredi, A. Moulins, M. Podestà, et al. 2016. Risso's Dolphin, *Grampus griseus*, in the Western Ligurian Sea. In Advances in Marine Biology (Elsevier) 205–232. doi: 10.1016/bs.amb.2016.08.003.

Azzolin, M., A. Arcangeli, G. Cipriano, R. Crosti, R. Maglietta, G. Pietroluongo, ... and R. Carlucci. 2020. Spatial distribution modelling of striped dolphin (*Stenella coeruleoalba*) at different geographical scales within the EU Adriatic and Ionian Sea Region, central-eastern Mediterranean Sea. Aquatic Conservation: Marine and Freshwater Ecosystems 30(6): 1194-1207.

Barabasch, I.I. 1935. *Delphinus delphis ponticus* subsp. n. Bull[in Russian]. Moskovskogo Obshchestva Ispytateley Prirody (Biological Division), 44, 246–249.

Barabash-Nikiforov II. 1940. Cetacean fauna of the Black Sea, its composition and origin. Izd-vo Voronezh. Gos. Un-ta, Voronezh (in Russian).

Baş A. A., J. C. Lagoa, E. Atchoi. 2003. New records of Cuvier's beaked whales (*Ziphius cavirostris*) from the Turkish Levantine Sea. Turkish Journal of Zoology: 7.

Baş, A. A., M. A. Erdoğan, N. R. C. Morris, K. Yeoman, O. Humphrey, E. Gaggioli, and C. Roland. 2016. Seasonal encounter rates and residency patterns of an unstudied population of bottlenose dolphin (*Tursiops truncatus*) in the northwestern Levantine Sea, Turkey. Hyla: Heretological Bulletin 2016(1): 1-13.

Bearzi, G., Fortuna, C. M., and Reeves, R. R. 2009. Ecology and conservation of common bottlenose dolphins Tursiops truncatus in the Mediterranean Sea. Mammal Review 39, 92–123. doi: https://doi.org/10.1111/j.1365-2907.2008.00133.x.

Bearzi, G., S. Bonizzoni, and N. L. Santostasi. 2020. *Delphinus delphis* (Gulf of Corinth subpopulation) (errata version published in 2021). The IUCN Red List of Threatened Species 2020: e.T156206333A194321818. https://dx.doi.org/10.2305/IUCN.UK.2020-2.RLTS.T156206333A194321818.en.

Bearzi, G., S. Bonizzoni, and N. L. Santostasi. 2022. *Stenella coeruleoalba* (Gulf of Corinth subpopulation). The IUCN red list of threatened species 2022: e.T210188066A210188619. https://dx.doi.org/10.2305/IUCN.UK.2022-1.RLTS.T210188066A210188619.en.

Bearzi, G., S. Bonizzoni, T. Genov, and G. Notarbartolo di Sciara. 2024. Whales and dolphins of the Adriatic Sea: present knowledge, threats and conservation. Acta Adriatica 65(1).

Bearzi, G., S. Bonizzoni, N. L. Santostasi, N. B. Furey, L. Eddy, V. D. Valavanis, and O. Gimenez. 2016. Dolphins in a scaled-down Mediterranean: the Gulf of Corinth's odontocetes. In Advances in Marine Biology (Vol. 75) 297-331. Academic Press.

Bearzi, G., R.R. Reeves, G. Notarbartolo Di Sciara, E. Politi, A. Cañadas, A. Frantzis, and B. Mussi. 2003. Ecology, status and conservation of short-beaked common dolphins Delphinus delphis in the Mediterranean Sea. Mammal Review 33(3–4):224–252.

Bearzi, G., R. Reeves, E. Remonato, N. Pierantonio, and S. Airoldi. 2011. Risso's dolphin *Grampus griseus* in the Mediterranean Sea. Mammalian Biology - Zeitschrift für Säugetierkunde 76: 385–400. doi: 10.1016/j.mambio.2010.06.003.

Berubé, M., A. Aguilar, D. Dendato, F. Larsen, G. Notarbartolo Di Sciara, R. Sears, J. Singurjonsson, J. Urban-R., and P. J. Palsboll. 1998. Population genetic structure of North Atlantic, Mediterranean Sea and Sea of Cortez fin whales, *Balaenoptera physalus* (Linnaeus, 1758): analysis of mitochondrial and nuclear loci. Molecular Ecology 7: 585-599.

Bethoux, J.P., B. Gentili, P. Morin, E. Nicolas, C. Pierre, and D. Ruiz-Pino. 1999. The Mediterranean Sea: a miniature ocean for climatic and environmental studies and a key for the climatic functioning of the North Atlantic. Progress in Oceanography 44(1–3): 131–146.

Bethoux, J. P., and B. Gentili. 1999. Functioning of the Mediterranean Sea: past and present changes related to freshwater input and climate changes. Journal of Marine Systems 20(1): 33–47.

Birkun, A., Jr., D. Glazov, S. Krivokhizhin, and L. Mukhametov, L. 2002. Distribution and abundance of cetaceans in the Sea of Azov and Kerch Strait: Results of aerial survey (July 2001). P.73 In: Abstr. 16th Annual Conf. of the European Cetacean Society (Liege, 7-11 April 2002), 86 pp.

Birkun A., Jr. 2002a. The state of cetacean populations (A. Birkun). Commission on the Protection of the Black Sea Against Pollution, 335.

Birkun, A. Jr. 2002b. “Direct killing and live capture,” in Cetaceans of the Mediterranean and Black Seas: state of knowledge and conservation strategies. A report to the ACCOBAMS Secretariat. Ed. G. Notarbartolo di Sciara. Monaco: IUCN.

Birkun, A. A., Jr., S. V. Krivokhizhin, D. M. Glazov, O.V. Shpak, A. V. Zanin, and L. M. Mukhametov. 2004. Abundance estimates of cetaceans in coastal waters of the northern Black Sea: Results of boat surveys in August-October 2003. In: Marine Mammals of the Elolarctic: Collection of Scientific Papers after the 3rd Internat. Conf., pp.64-68, Koktebel, Ukraine, 11-17 October 2004, Moscow, 609 pp.

Birkun Jr, A., Northridge, S.P., Willsteed, E.A., James, F.A., Kilgour, C., Lander, M. and Fitzgerald, G.D., 2014. Studies for Carrying Out the Common Fisheries Policy: Adverse Fisheries Impacts on Cetacean Populations in the Black Sea. Final report to the European Commission, Brussels, 347p. This report and the views contained within are the views of the authors and should not be assumed to reflect the views of the European Commission.

Boisseau, O., J. Reid, C. Ryan, A. Moscrop, R. McLanaghan, and S. Panigada. 2024. Acoustic estimates of sperm whale abundance in the Mediterranean Sea as part of the ACCOBAMS Survey Initiative. Frontiers in Marine Science 11: 1164026. doi: 10.3389/fmars.2024.1164026

Boisseau, O., C. Lacey, T. Lewis, A. Moscrop, M. Danbolt, and R. McLanaghan. 2010. Encounter rates of cetaceans in the Mediterranean Sea and contiguous Atlantic area. Journal of the Marine Biological Association of the United Kingdom 90(8): 1589-1599. https://doi.org/10.1017/S0025315410000342

Bologa, A. Ş. 2015. Unicitatea Mării Negre. In: Revista Ştiinţă şi tehnică. Available online at: https://stiintasitehnica.com/%EF%BB%BF%EF%BB%BFunicitatea-%E2%80%A8marii-negre/ .

Borrell, A., M. Gazo, A. Aguilar, J. A. Raga, E. Degollada, P. Gozalbes, et al. 2021. Niche partitioning amongst northwestern Mediterranean cetaceans using stable isotopes. Progress in Oceanography 193: 102559. doi: 10.1016/j.pocean.2021.102559.

Bosc, E., A. Bricaud, and D. Antoine. 2004. Seasonal and interannual variability in algal biomass and primary production in the Mediterranean Sea, as derived from 4 years of SeaWiFS observations. Global Biogeochemical Cycles 18(1): GB1005.

Bouchet, P.J., D. L. Miller, J. J. Roberts, L. Mannocci, C. M. Harris, and L. Thomas. 2020. Dsmextra: Extrapolation assessment tools for density surface models. Methods in Ecology and Evolution 11(11): 1464-1469.

Breiman, L. 2001. Random forests. Machine Learning 45: 5-32.

Brotons, J. M. 2015. Catxalots a Balears: Una cultura amenaçada. In Llibre verd de protecció d'espècies a les Balears. Societat d'Història Natural de Balears, 151-162.

Buckland, S.T., D. R. Anderson, K. P. Burnham, J. L. Laake, D. L. Borchers, and L. Thomas. 2001. Introduction to distance sampling: estimating abundance of biological populations. Oxford University Press, New York.

Cañadas, A. 2011. Beaked whales and pilot whales in the Alboran Sea (SW Mediterranean): research towards improved science-based mitigation strategies for risks from man-made sound. DTIC Document. Final report for ONR. Grant Number: N000141010709.

Cañadas, A. 2014. Understanding the patterns and causes of variability in distribution, habitat use, abundance, survival and reproductive rates of three species of cetacean in the Alborán Sea, western Mediterranean. Final report for ONR. Grant Number: N000141110196.

Cañadas, A., N. Aguilar De Soto, M. Aissi, A. Arcangeli, M. Azzolin, A. B-Nagy, et al. 2018. The challenge of habitat modelling for threatened low density species using heterogeneous data: The case of Cuvier's beaked whales in the Mediterranean. Ecological Indicators 85: 128–136. doi: 10.1016/j.ecolind.2017.10.021.

Cañadas, A., and P. S. Hammond. 2006. Model-based abundance estimates for bottlenose dolphins off southern Spain: implications for conservation and management. Journal of Cetacean Research and Management 8(1): 13–27.

Cañadas, A., and P. S. Hammond. 2008. Abundance and habitat preferences of the short-beaked common dolphin *Delphinus delphis* in the southwestern Mediterranean: implications for conservation. Endangered Species Research 4: 309–331.

Cañadas, A., N. Pierantonio, H. Araújo, L. David, N. Di Meglio, G. Dorémus, J. Gonzalvo, D. Holcer, S. Laran, G. Lauriano, M. Perri, V. Ridoux, J. A. Vázquez, and S. Panigada. 2023. Distribution patterns of marine megafauna density in the Mediterranean Sea assessed through the ACCOBAMS Survey Initiative (ASI). Frontiers in Marine Science 10: 1270917. doi: 10.3389/fmars.2023.1270917

Cañadas, A., J. Roberts, T. Yack, and P. N. Halpin. 2021. Development of exploratory marine species density models in the NAVEUR/6CF study area. Final Report. Report prepared for Naval Facilities Engineering Command, Atlantic under Contract No. N62470-15-D-8006, Task Order 18F4048, by the Duke University Marine Geospatial Ecology Lab, Durham, North Carolina.

Canadas, A., and R. Sagarminaga. 2000. The Northeastern Alboran Sea, an important breeding and feeding ground for the long-finned pilot whale (*Globicephala melas*) in the Mediterranean Sea. Marine Mammal Science 16: 513–529. doi: 10.1111/j.1748-7692.2000.tb00948.x.

Cañadas, A., R. Sagarminaga, R. De Stephanis, E. Urquiola, and P. S. Hammond. 2005. Habitat preference modelling as a conservation tool: proposals for marine protected areas for cetaceans in southern Spanish waters. Aquatic Conservation: Marine and Freshwater Ecosystems 15: 495–521. doi: https://doi.org/10.1002/aqc.689.

Cañadas, A., R. Sagarminaga, and S. García-Tiscar. 2002. Cetacean distribution related with depth and slope in the Mediterranean waters off southern Spain. Deep Sea Research Part I: Oceanographic Research Papers 49: 2053–2073. doi: 10.1016/S0967-0637(02)00123-1.

Cañadas, A, and J.A. Vázquez. 2014. Conserving Cuvier's beaked whales in the Alboran Sea (SW Mediterranean): identification of high density areas to be avoided by intense man-made sound. Biological Conservation 178:155–162.

Carpinelli, E., P. Gauffier, P. Verborgh, S. Airoldi, L. David, N. Di-Méglio, and R. De Stephanis. 2014. Assessing sperm whale (*Physeter macrocephalus*) movements within the western Mediterranean Sea through photo-identification. Aquatic Conservation: Marine and Freshwater Ecosystems 24(S1): 23-30.

Cipriano, G., R. Carlucci, S. Bellomo, F. C. Santacesaria, C. Fanizza, P. Ricci, et al. 2022. Behavioral pattern of Risso's dolphin (*Grampus griseus*) in the Gulf of Taranto (Northern Ionian Sea, Central-Eastern Mediterranean Sea). JMSE 10: 175. doi: 10.3390/jmse10020175.

Cotté, C., C. Guinet, I. Taupier-Letage, B. Mate, and E. Petiau. 2009. Scale-dependent habitat use by a large free-ranging predator, the Mediterranean fin whale. Deep Sea Research Part I: Oceanographic Research Papers 56: 801–811. doi: 10.1016/j.dsr.2008.12.008.

Cucknell, A. C., A. Frantzis, O. Boisseau, M. Romagosa, C. Ryan, A. M. Tonay, and A. Moscrop. 2016. Harbour porpoises in the Aegean Sea, Eastern Mediterranean: the species' presence is confirmed. Marine Biodiversity Records 9: 1-13.

D'Ortenzio, F., and M. Ribera d'Alcalà. 2009. On the trophic regimes of the Mediterranean Sea: a satellite analysis. Biogeosciences 6(2): 139–148.

Daskalov, G. M. 2003. Long-term changes in fish abundance and environmental indices in the Black Sea. Marine Ecology Progress Series 255: 259–270. doi: 10.3354/meps255259

Dede, A., Ôzsandikçi, U., Tonay, A.M., Aytemiz Danyer, I., Danyer, E., Amaha Ôzturk, A. 2022. Abundance estimation of cetaceans in the Sea of Marmara using line-transect. *In*: Ôzturk, B., Ergûl, H.A., Yalçiner, A.C., Ôzturk, H., Salihoglu, B. (Eds). 2022. Marmara Denizi 2022 Sempozyumu Bildiriler Kitabi. Tûrk Deniz Arastirmalari Vafki (TÛDAV), Yayin no:63, Istambul, Tûrkiye.

de Stephanis, R. 2023. Informe de resultados de las campañas de seguimiento de cetáceos y tortugas en el área marina del Estrecho occidental. LIFE IP INTEMARES. Gestión integrada, innovadora participativa de la Red Natura 2000 en el medio marino español

de Stephanis, R., T. Cornulier, P. Verborgh, J. S. Sierra, N. P. Gimeno, and C. Guinet. 2008. summer spatial distribution of cetaceans in the Strait of Gibraltar in relation to the oceanographic context. Marine Ecology Progress Series 353: 275-288.

Department of Navy. 2012. Commander Task Force 20, 4th, and 6th Fleet Navy Marine Species Density Database. (Technical Report). Naval Facilities Engineering Command Atlantic, Norfolk, Virginia.

Dixon, W. J., and K. K. Yuen. 1974. Trimming and winsorization: A review. Statistische Hefte 15(2): 157-170.

Drouot, V., A. Gannier, and J. C. Goold. 2004a. Diving and feeding behaviour of sperm whales (*Physeter macrocephalus*) in the northwestern Mediterranean Sea. Aquatic Mammals 30(3): 419–426.

Drouot, V., A. Gannier, and J. C. Goold. 2004b. Summer social distribution of sperm whales (*Physeter macrocephalus*) in the Mediterranean Sea. Journal of the Marine Biological Association of the United Kingdom 84(3): 675-680.

Drouot-Dulau, V., and A. Gannier. 2007. Movements of sperm whale in the western Mediterranean Sea: preliminary photo-identification results. Journal of the Marine Biological Association of the United Kingdom 87: 195–200. doi: 10.1017/S0025315407054860

Druon, J-N, S. Panigada, L. David, A. Gannier, P. Mayol, A. Arcangeli, A. Cañadas, S. Laran, N. Di Méglio, and P. Gauffier. 2012. Potential feeding habitat of fin whales in the western Mediterranean Sea: an environmental niche model. Marine Ecology Progress Series 464: 289–306.

Esteban, R., P. Verborgh, P. Gauffier, D. Alarcón, J. M. Salazar-Sierra, J. Giménez, and R. De Stephanis. 2016. Conservation status of killer whales, *Orcinus orca*, in the Strait of Gibraltar. Advances in Marine Biology 75: 141-172.

Esteban, R., P. Verborgh, P. Gauffier, J. Giménez, I. Afán, A. Cañadas, and R. de Stephanis. 2014. Identifying key habitat and seasonal patterns of a critically endangered population of killer whales. Journal of the Marine Biological Association of the United Kingdom 94(6): 1317-1325.

Fernández, A., Esperón, F., Herraéz, P., de Los Monteros, A.E., Clavel, C., Bernabé, A., Sánchez-Vizcaino, J.M., Verborgh, P., DeStephanis, R., Toledano, F. and Bayón, A., 2008. Morbillivirus and pilot whale deaths, Mediterranean Sea. Emerging Infectious Diseases, 14(5), p.792.

Fiori, C., L. Giancardo, M. Aïssi, J. Alessi, and P. Vassallo. 2014. Geostatistical modelling of spatial distribution of sperm whales in the Pelagos Sanctuary based on sparse count data and heterogeneous observations. Aquatic Conservation: Marine and Freshwater Ecosystems 24(3–4): 41–49.

Fontaine, M. C. 2016. Harbour porpoises, *Phocoena phocoena*, in the Mediterranean Sea and adjacent regions: biogeographic relicts of the last glacial period. Advances in Marine Biology 75: 333-358.

Forcada, J., M. Gazo, A. Aguilar, J. Gonzalvo, and M. Fernández-Contreras. 2004. Bottlenose dolphin abundance in the NW Mediterranean: addressing heterogeneity in distribution. Marine Ecology Progress Series 275: 275–287.

Forcada, J., and P. Hammond. 1998. Geographical variation in abundance of striped and common dolphins of the western Mediterranean. Journal of Sea Research 39(3–4):313–325.

Forcada, J., G. Notarbartolo di Sciara, and F. Fabbri. 1995. Abundance of fin whales (Balenoptera physalus) and striped dolphins (*Stenella coeruleoalba*) summering in the Corso-Ligurian Basin. Mammalia 59. doi: 10.1515/mamm.1995.59.1.127.

Fortuna, C. M., A. Cañadas, D. Holcer, B. Brecciaroli, G. P. Donovan, B. Lazar, G. Mo, L. Tunesi, and P. C. Mackelworth. 2018. The coherence of the European Union Marine Natura 2000 Network for wide-ranging charismatic species: a Mediterranean case study. Frontiers in Marine Science 5: 356. doi: 10.3389/fmars.2018.00356

Fortuna, C.M., D. Holcer, E. Filidei Jr, G.P. Donovan, and L. Tunesi. 2011. The first cetacean aerial survey in the Adriatic sea: summer 2010. 7th Meeting of the ACCOBAMS Scientific committee, ACCOBAMS-SC7/2011/Doc06

Foskolos, I., K. C. Gkikopoulou, and A. Frantzis. 2020. Current state of knowledge and conservation perspectives on the cetaceans of the Aegean Sea. In: Anagnostou, C.L., Kostianoy, A.G., Mariolakos, I.D., Panayotidis, P., Soilemezidou, M., Tsaltas, G. (eds) The Aegean Sea Environment. The Handbook of Environmental Chemistry, vol 129. Springer, Cham. https://doi.org/10.1007/698_2020_653

Frantzis, A., P. Alexiadou, and K. C. Gkikopoulou. 2014. Sperm whale occurrence, site fidelity and population structure along the Hellenic Trench (Greece, Mediterranean Sea). Aquatic Conservation: Marine and Freshwater Ecosystems 24(SUPPL.1): 83–102.

Frantzis, A., S. Airoldi, G. Notarbartolo-di-Sciara, C. Johnson, and S. Mazzariol. 2011. Inter-basin movements of Mediterranean sperm whales provide insight into their population structure and conservation. Deep Sea Research Part I: Oceanographic Research Papers 58(4): 454-459.

Frantzis, A., P. Alexiadou, G. Paximadis, E. Politi, A. Gannier, and M. Corsini-Foka. 2003. Current knowledge of the cetacean fauna of the Greek Seas. Journal of Cetacean Research and Management 5(3): 219–232.

Galili, O., O. Goffman, M. Roditi-Elasar, Y. Mevorach, E. Bigal, Y. Zuriel, and A. Scheinin. 2023. Two decades of coastal dolphin population surveys in Israel, Eastern Mediterranean. Biology 12(2): 328.

Gauffier, P., P. Verborgh, J. Giménez, R. Esteban, JMS Sierra, and R. de Stephanis. 2018. Contemporary migration of fin whales through the Strait of Gibraltar. Marine Ecology Progress Series 588:215–228.

Genov, T., P. Kotnjek, and T. Centrih. 2021. Occurrence of common dolphins (*Delphinus delphis*) in the Gulf of Trieste and the northern Adriatic Sea. Aquatic Conservation: Marine and Freshwater Ecosystems 31: 69-75.

Giannoulaki, M., E. Markoglou, V. D. Valavanis, P. Alexiadou, A. Cucknell, and A. Frantzis. 2016. Linking small pelagic fish and cetacean distribution to model suitable habitat for coastal dolphin species, *Delphinus delphis* and *Tursiops truncatus*, in the Greek Seas (Eastern Mediterranean). Aquatic Conservation: Marine and Freshwater Ecosystems 27(2): 436-451.

Gkikopoulou, K-C. 2012. Distribution and abundance estimation of sperm whales (*Physeter macrocephalus*) along the Hellenic Trench in Eastern Mediterranean. M.Phil Thesis. University of St Andrews.

Gnone, G., M. Bellingeri, S. Airoldi, J. Gonzalvo, L. David, N. Di-Méglio, A. M. Cañadas, A. Akkaya, T. Awbery, and B. Mussi. 2023. Cetaceans in the Mediterranean Sea: Encounter Rate, Dominant Species, and Diversity Hotspots. Diversity 15: 321. https://doi.org/10.3390/d15030321

Gómez de Segura, A., E. A. Crespo, S. N. Pedraza, P. S. Hammond, and J. A. Raga. 2006. Abundance of small cetaceans in waters of the central Spanish Mediterranean. Marine Biology 150: 149–160. doi: 10.1007/s00227-006-0334-0.

Gómez de Segura, A., P. S. Hammond, and J. A. Raga. 2008. Influence of environmental factors on small cetacean distribution in the Spanish Mediterranean. Journal of the Marine Biological Association of the United Kingdom 88: 1185–1192. doi: 10.1017/S0025315408000386.

Gonzalvo, J., G. Lauriano, P. S. Hammond, K. A. Viaud-Martinez, M. C. Fossi, A. Natoli, and L. Marsili. 2016. The Gulf of Ambracia's common bottlenose dolphins, *Tursiops truncatus*: a highly dense and yet threatened population. Advances in Marine Biology 75: 259-296.

Holcer, D., G. Notarbartolo Di Sciara, C. M. Fortuna, B. Lazar, and V. Onofri. 2007. Occurrence of Cuvier's beaked whales in the southern Adriatic Sea: evidence of an important Mediterranean habitat. Journal of the Marine Biological Association of the United Kingdom 87(1): 359-362.

IUCN MMPATF. 2024. Global dataset of important marine mammal areas (IUCN IMMA). Downloaded on September 2024. Made available under agreement on terms and conditions of use by the IUCN Joint SSC/WCPA Marine Mammal Protected Areas Task Force and accessible via the IMMA e-Atlas https://marinemammalhabitat.org/imma-eatlas/

Jahoda, M., C. L. Lafortuna, N. Biassoni, C. Almirante, A. Azzellino, S. Panigada, and G. Notarbartolo Di Sciara. 2003. Mediterranean fin whale's (*Balaenoptera physalus*) response to small vessels and biopsy sampling assessed through passive tracking and timing of respiration. Marine Mammal Science 19(1): 96-110.

Karamanlidis, A. A., S. Adamantopoulou, E. Tounta, and D. Dendrinos. 2019. *Monachus monachus* (Eastern Mediterranean subpopulation). The IUCN red list of threatened species 2019: e.T120868935A120869697. https://dx.doi.org/10.2305/IUCN.UK.2019-1.RLTS.T120868935A120869697.en

Karamanlidis, A. A., P. Dendrinos, P. Fernandez de Larrinoa, C. O. Kıraç, H. Nicolaou, and R. Pires. 2023. *Monachus monachus*. The IUCN Red List of Threatened Species 2023: e.T13653A238637039. https://dx.doi.org/10.2305/IUCN.UK.2023-1.RLTS.T13653A238637039.en

Kaschner, K., R. Watson, A. W. Trites, and D. Pauly. 2006. Mapping world-wide distributions of marine mammal species using a relative environmental suitability (RES) model. Marine Ecology Progress Series 316: 285–310.

Krivokhizhin, S. V. 2021. The status of the Kerch-Taman herd of bottlenose dolphins (*Tursiops truncatus ponticus*). Editorial Board 43.

Laake, J., J. Calambokidis, S. Osmek, and D. Rugh. 1997. Probability of detecting harbor porpoise from aerial surveys: estimating g(0). The Journal of Wildlife Management 61(1): 63–75.

Laran, S., E. Pettex, M. Authier, A. Blanck, L. David, G. Dorémus, H. Falchetto, P. Monestiez, O. Van Canneyt, and V. Ridoux. 2017. Seasonal distribution and abundance of cetaceans within French waters- Part I: The North-Western Mediterranean, including the Pelagos sanctuary. Deep Sea Research Part II: Topical Studies in Oceanography 141: 20–30.

Lauriano, G. 2022. *Stenella coeruleoalba* (Mediterranean subpopulation). The IUCN Red List of Threatened Species 2022, e.T16674437A210833690.

Lewis, T., O. Boisseau, M. Danbolt, D. Gillespie, C. Lacey, R. Leaper, J. Matthews, R. McLanaghan, and A. Moscrop. 2018. Abundance estimates for sperm whales in the Mediterranean Sea from acoustic line-transect surveys. J. Cetacean Research and Management 18: 103-117.

Longhurst, A.R. 2007. Ecological geography of the sea. Academic Press, Oxford.

Luna, A., P. Sánchez, C. Chicote, and M. Gazo. 2022. Cephalopods in the diet of Risso's dolphin (*Grampus griseus*) from the Mediterranean Sea: A review. Marine Mammal Science 38: 725–741. doi: 10.1111/mms.12869.

Mannocci, L., P. Monestiez, J. Spitz, and V. Ridoux. 2015. Extrapolating cetacean densities beyond surveyed regions: habitat-based predictions in the circumtropical belt. Journal of Biogeography 42(7): 1267–1280.

Mannocci, L., J.J. Roberts, and P.N. Halpin. 2016. Data gap analysis and data collection for marine species density models in the Mediterranean Sea. Submitted to Naval Facilities Engineering Command Atlantic, prepared for U.S. Fleet Forces Command, prepared by

the Duke University Marine Geospatial Ecology Lab, Durham, North Carolina, under Contract N62470-15-D-8006 (TO21) issued to HDR, San Diego, California. August 2016.

Mannocci, L., J. J. Roberts, and P. N. Halpin. 2018. Development of Exploratory Marine Species Density Models in the Mediterranean Sea. Durham, North Carolina: Duke University Marine Geospatial Ecology Lab.

Mannocci, L., J. J. Roberts, E. J. Pedersen, and P. N. Halpin. 2020. Geographical differences in habitat relationships of cetaceans across an ocean basin. Ecography 43(8): 1250–1259.

Marques, F.F.C., and S. T. Buckland. 2004. Covariate models for the detection function. In Advanced Distance Sampling, Oxford, New York, pp. 31–47.

Meli, M., C. M. Camargo, M. Olivieri, A. B. Slangen, and C. Romagnoli. 2023. Sea-level trend variability in the Mediterranean during the 1993–2019 period. Frontiers in Marine Science 10: 1150488.

Mesgaran, M. B., R. D. Cousens, and B. L. Webber. 2014. Here be dragons: a tool for quantifying novelty due to covariate range and correlation change when projecting species distribution models. Diversity and Distributions 20(10): 1147–1159.

Miller, D. L., E. A. Becker, K. A. Forney, J. J. Roberts, A. Cañadas, and R. S. Schick. 2022. Estimating uncertainty in density surface models. PeerJ 10: e13950. doi: 10.7717/peerj.13950.

Miller, D. L., M. L. Burt, E. A. Rexstad, and L. Thomas. 2013. Spatial models for distance sampling data: recent developments and future directions. Methods in Ecology and Evolution 4(11): 1001–1010.

Minoia, L., G. Consales, S. Mazzariol, C. Mancusi, G. Terracciano, I. Ceciarini, et al. 2023. Preliminary assessment of persistent organic pollutants (POPs) in tissues of Risso's dolphin (*Grampus griseus*) specimens stranded along the Italian coasts. Marine Pollution Bulletin 186: 114470. doi: 10.1016/j.marpolbul.2022.114470.

Mussi, B., A. Miragliuolo, A. Zucchini, and D. S. Pace. 2014. Occurrence and spatio-temporal distribution of sperm whale (*Physeter macrocephalus*) in the submarine canyon of Cuma (Tyrrhenian Sea, Italy). Aquatic Conservation: Marine and Freshwater Ecosystems 24(S1): 59–70.

Nacef, L., N. E. İ. Bachari, A. Bouda, and R. Boubnia. 2016. Variability and decadal evolution of temperature and salinity in the Mediterranean Sea surface. International Journal of Engineering and Geosciences 1(1): 24-33. https://doi.org/10.26833/ijeg.285222

Naceur, L.L.B., M. Gannier, M. N. Bradai, V. Drouot, S. Bourreau, S. Laran, N. Khalfallah, R. Mrabet, and M. Bdioui. 2004. Recensement du grand dauphin *Tursiops truncatus* dans les eaux tunisiennes. INSTM Bulletin: Marine and Freshwater Sciences 31: 75-81.

Natoli, A., A. Birkun, A. Aguilar, A. Lopez, and A. R. Hoelzel. 2005. Habitat structure and the dispersal of male and female bottlenose dolphins (*Tursiops truncatus*). Proceedings of the Royal Society B: Biological Sciences 272(1569): 1217–1226.

Natoli, A., A. Cañadas, C. Vaquero, E. Politi, P. Fernandez-Navarro, and A. R. Hoelzel. 2008. Conservation genetics of the short-beaked common dolphin (*Delphinus delphis*) in the Mediterranean Sea and in the eastern North Atlantic Ocean. Conservation Genetics 9: 1479.

Natoli, A., T. Genov, D. Kerem, J. Gonzalvo, G. Lauriano, D. Holcer, H. Labach, L. Marsili, S. Mazzariol, A. E. Moura, A. A. Öztürk, A. Pardalou, A. M. Tonay, P. Verborgh, and C. Fortuna. 2021. *Tursiops truncatus* (Mediterranean subpopulation) (errata version published in 2022). The IUCN Red List of Threatened Species 2021: e.T16369383A215248781. Accessed on 07 October 2024.

Notarbartolo di Sciara, G. 2016. Marine mammals in the Mediterranean Sea: an overview. Advances in Marine Biology 75: 1–36.

Notarbartolo di Sciara, G., M. Castellote, J.-N. Druon, and S. Panigada. 2016. “Chapter Three - fin whales, *Balaenoptera physalus*: at home in a changing mediterranean sea?” in Advances in marine biology mediterranean marine mammal ecology and conservation, eds. G. Notarbartolo Di Sciara, M. Podestà, and B.E. Curry, Academic Press, 75–101. doi: 10.1016/bs.amb.2016.08.002.

Notarbartolo di Sciara, G., M. Zanardelli, M. Jahoda, S. Panigada, and S. Airoldi. 2003. The fin whale *Balaenoptera physalus* (L. 1758) in the Mediterranean Sea: Fin whales in the Mediterranean. Mammal Review 33: 105–150. doi: 10.1046/j.1365-2907.2003.00005.x.

Ouled-Cheikh, J., J. Giménez, P. Verborgh, C. Jiménez-Torres, P. Gauffier, R. Esteban, and R. de Stephanis. 2023. The non-consumptive economic value of wildlife: the case of three cetacean species. Scientia Marina 87(4): e077-e077.

Özsoy, E., and Ü. Ünlüata. 1997. Oceanography of the Black Sea: a review of some recent results. Earth-Science Reviews 42(4): 231-272.

Öztürk, B., H. A. Ergül, A. C. Yalçıner, H. Öztürk, and B. Salihoğlu. (Eds) 2022. Marmara Denizi 2022 Sempozyumu Bildiriler Kitabı. Türk Deniz Araştırmaları Vakfı (TÜDAV), Yayın no: 63, İstanbul, Türkiye, 461s.

Pace, D. S., A. Miragliuolo, M. Mariani, C. Vivaldi, and B. Mussi. 2014. Sociality of sperm whale off Ischia Island (Tyrrhenian Sea, Italy). Aquatic Conservation: Marine and Freshwater Ecosystems 24(S1): 71-82.

Painter, S. C., M. N. Tsimplis. 2003. Temperature and salinity trends in the upper waters of the Mediterranean Sea as determined from the MEDATLAS dataset. Continental Shelf Research 23(16): 1507-1522.

Paiu, R-M., A. Cañadas, A. Dede, G. Meshkova, D. Murariu, A. Amaha Öztürk, D. Popov, A. M. Tonay, C. Timofte, N. Kopaliani, P. Gol'din, and S. Panigada. 2024. Density and abundance estimates of cetaceans in the Black Sea through aerial surveys (ASI/CeNoBS). Frontiers in Marine Science 11: 1248950. doi: 10.3389/fmars.2024.1248950.

Panigada, S., P. Gauffier, and G. Notarbartolo di Sciara. 2021. *Balaenoptera physalus* (Mediterranean subpopulation). The IUCN red list of threatened species 2021: e.T16208224A50387979. https://dx.doi.org/10.2305/IUCN.UK.2021-3.RLTS.T16208224A50387979.en.

Panigada, S., G. Lauriano, L. Burt, N. Pierantonio, and G. Donovan. 2011. Monitoring winter and summer abundance of cetaceans in the Pelagos Sanctuary (Northwestern Mediterranean Sea) Through Aerial Surveys. PLOS ONE 6: e22878. doi: 10.1371/journal.pone.0022878.

Panigada, S., G. Lauriano, G. Donovan, N. Pierantonio, A. Cañadas, J. A. Vázquez, et al. 2017. Estimating cetacean density and abundance in the Central and Western Mediterranean Sea through aerial surveys: Implications for management. Deep Sea Research Part II: Topical Studies in Oceanography 141: 41–58. doi: 10.1016/j.dsr2.2017.04.018.

Panigada, S., Pierantonio, N., Araújo, H., David, L., Di-Méglio, N., Dorémus, G., Gonzalvo, J., Holcer, D., Laran, S., Lauriano, G. and Paiu, R.M., 2024. The ACCOBAMS Survey Initiative: the first synoptic assessment of cetacean abundance in the Mediterranean Sea through aerial surveys. Frontiers in Marine Science, 10, p.1270513.

Pavlov V., Artov A., Zhuravleva T. 1996. Impact of fishing on Black Sea dolphins off the Crimea coasts. Pp. 41-43. *In*: B. Öztürk (Ed.), Proceedings of the First International Symposium on the Marine Mammals of the Black Sea (Istanbul, Turkey, 27-30 June 1994). ACAR Matbaacilik A.S., Istanbul, 120 p.

Pedersen, E. J., D. L. Miller, G. L., Simpson, and N. Ross. 2019. Hierarchical generalized additive models in ecology: an introduction with mgcv. PeerJ 7: e6876.

Pierantonio, N., G. Paximadis, A. Cañadas, A. Foutsi, and S. Panigada. 2018. Occurrence and abundance of delphinids in the Northern Aegean Sea from aerial surveys. Abstract book of the 32nd Annual Conference of the European Cetacean Society, La Spezia, Italy, p. 83.

Pinardi, N., and E. Masetti. 2000. Variability of the large scale general circulation of the Mediterranean Sea from observations and modelling: a review. Palaeogeography, Palaeoclimatology, Palaeoecology 158(3–4): 153–173.

Pirotta, E., J. M. Brotons, M. Cerdà, S. Bakkers, and L. E. Rendell. 2020. Multi-scale analysis reveals changing distribution patterns and the influence of social structure on the habitat use of an endangered marine predator, the sperm whale *Physeter macrocephalus* in the

Western Mediterranean Sea. Deep Sea Research Part I: Oceanographic Research Papers 155: 103169.

Pirotta, E., J. Matthiopoulos, M. MacKenzie, L. Scott-Hayward, and L. Rendell. 2011. Modelling sperm whale habitat preference: a novel approach combining transect and follow data. Marine Ecology Progress Series 436: 257–272. doi: 10.3354/meps09236.

Pirotta, E., M. Vighi, J. M. Brotons, E. Dillane, M. Cerdà, and L. Rendell. 2020. Stable isotopes suggest fine-scale sexual segregation in an isolated, endangered sperm whale population. Marine Ecology Progress Series 654: 209–218. doi: 10.3354/meps13502.

Pirounakis, K., S. Kaloupi, S. Moschonas, Y. Mourelatos, L. Tselentis, N. Voutsinas, V. Votsinas, and A. Panou, A. 1999. Cetaceans in the eastern Ionian Sea: results of an observers' network. Contributions to the Zoogeography and Ecology of the Eastern Mediterranean Region 1: 429-434.

Podestà, M., and A. Bortolotto. 2001. Il Progetto Spiaggiamenti del Centro Studi Cetacei: analisi dei risultati di 11 anni di attività. Natura—Società Italiana di Scienze Naturali Museo Civico di Storia Naturale di Milano 90: 145-158.

Podestà, M., A. Azzellino, A. Cañadas, A. Frantzis, A. Moulins, M. Rosso, P. Tepsich, and C. Lanfredi. 2016. Cuvier's beaked whale, *Ziphius cavirostris*, distribution and occurrence in the Mediterranean Sea: high-use areas and conservation threats. Advances in Marine Biology 75: 103–140.

Pollock, K .H., H. D. Marsh, I. R. Lawler, and M. W. Allderdge. 2006. Estimating animal abundance in heterogeneous environments: an application to aerial surveys for dugongs. Journal of Wildlife Management 70(1): 255–262.

Praca, E., and A. Gannier. 2008. Ecological niches of three teuthophageous odontocetes in the northwestern Mediterranean Sea. Ocean Science 4(1): 49–59.

R Core Team. 2022. R: A language and environment for statistical computing. R Foundation for Statistical Computing, Vienna, Austria. URL https://www.R-project.org/.

Rendell, L., S. Simião, J. M. Brotons, S. Airoldi, D. Fasano, and A. Gannier. 2014. Abundance and movements of sperm whales in the western Mediterranean basin. Aquatic Conservation: Marine and Freshwater Ecosystems 24(S1): 31-40.

Roberts, J. J., B. D. Best, D. C. Dunn, E. A. Treml, and P. N. Halpin. 2010. Marine geospatial ecology tools: An integrated framework for ecological geoprocessing with ArcGIS, Python, R, MATLAB, and C++. Environmental Modelling & Software 25:1197–1207.

Roberts, J. J., B. D. Best, L. Mannocci, E. Fujioka, P. N. Halpin, D. L. Palka, L. P. Garrison, K. D. Mullin, T. V. N. Cole, C. B. Khan, W. M. McLellan, D. A. Pabst, and G. G. Lockhart. 2016. Habitat-based cetacean density models for the U.S. Atlantic and Gulf of Mexico. Scientific Reports 6: 22615.

Roberts, J.J., Schick, R.S., and Halpin, P.N. 2021. Final Project Report: Marine Species Density Data Gap Assessments and Update for the AFTT Study Area, 2020 (Option Year 4). Document version 2.0. Report prepared for Naval Facilities Engineering Command, Atlantic by the Duke University Marine Geospatial Ecology Lab, Durham, NC.

Roberts, J. J., T. M. Yack, and P. N. Halpin. 2023. Marine mammal density models for the U.S. Navy Atlantic Fleet Training and Testing (AFTT) study area for the Phase IV Navy Marine Species Density Database (NMSDD), Document Version 1.3. Duke University Marine Geospatial Ecology Laboratory, Durham, NC.

Rosso, M., M. Aurelie, and M. Wurtz. 2009. Population size and residence patterns of Cuvier's beaked whale (*Ziphius cavirostris*) in the Genova canyon, north-western Mediterranean Sea. In 18th Biennial Conference on the Biology of Marine Mammals, Society for Marine Mammalogy. Quebec City, Canada.

Salmona, J., J. Dayon, E. Lecompte, A. A. Karamanlidis, A. Aguilar, P. F. de Larrinoa, R. Pires, G. L. Mo, A. Panou, S. Agnesi, A. Borrell, E. Danyer, B. Oeztuerk, A. M. Tonay, K. A. Anestis, L. M. Gonzalez, P. Dendrinos, and P. Gaubert. 2022. The antique genetic plight of the Mediterranean monk seal (*Monachus monachus*). Proceedings of the Royal Society B-Biological Sciences 289: 20220846.

Severtsov Institute of Ecology and Evolution, Russian Academy of Sciences (Moscow) and Bram Laboratory Cooperative Enterprise (Simferopol). (2003). Aerial survey of the distribution, abundance, and species composition of dolphins in the Russian and Ukrainian Waters of the Black and Azov Seas: Russian-Ukrainian Scientific and Conservation Project "Azovka-2002". Moscow: Ministry of Natural Resources of the Russian Federation, Ministry of Ecology and Natural Resources of Ukraine, and Uttrish Dolphinarium LLC.

Shapiro, G. I. 2009. Black Sea circulation. Ocean Currents 2(8).

Stephens, G., A. Akkaya Bas, J. Hardy, N. Araç, and P. Lyne. 2021. Sightings and stranding reports of fin whales (*Balaenoptera physalus*) in the Levantine Sea, with recent sightings from Turkey. Journal of Cetacean Research and Management 22: 55–60. doi: 10.47536/jcrm.v22i1.212.

Tenan, S., N. Hernández, H. Fearnbach, R. de Stephanis, P. Verborgh, and D. Oro. 2020. Impact of maritime traffic and whale-watching on apparent survival of bottlenose dolphins in the Strait of Gibraltar. Aquatic Conservation: Marine and Freshwater Ecosystems 30(5): 949-958.

Tepsich, P., M. Rosso, P. N. Halpin, and A. Moulins. 2014. Habitat preferences of two deep-diving cetacean species in the northern Ligurian Sea. Marine Ecology Progress Series 508: 247–260.

Toderascu, R., and Rusu, E. 2014. "Implementation of a Joint System for Waves and Currents in the Black Sea." International Journal of Ocean System Engineering 4.1: 28-41.

Tsagarakis, K., S. Panigada, A. Machias, M. Giannoulaki, A. Foutsi, N. Pierantonio, and G. Paximadis. 2021. Trophic interactions in the "small pelagic fish-dolphins-fisheries" triangle: Outputs of a modelling approach in the North Aegean Sea (Eastern Mediterranean, Greece). Ocean & Coastal Management 204: 105474.

Verborgh, P., P. Gauffier, C. Brévart, J. Giménez, R. Esteban, M. Carbou, E. Debons, and R. de Stephanis. 2019. Epizootic effect and aftermath in a pilot whale population. Aquatic Conservation: Marine and Freshwater Ecosystems 2019: 1–9. doi: 10.1002/aqc.3082.

Verborgh, P., P. Gauffier, R. Esteban, J. Giménez, A. Cañadas, J. M. Salazar-Sierra, et al. 2016. Conservation status of long-finned pilot whales, *Globicephala melas*, in the Mediterranean Sea. Advances in Marine Biology 75: 173–203. doi: 10.1016/bs.amb.2016.07.004.

Vespremeanu, E. 2007. Geografia Mării Negre. București: Universitară Bucureşti, 225.

Viaud-Martínez, K. A., M. M. Vergara, P. E. Gol'din, et al. 2007. Morphological and genetic differentiation of the Black Sea harbour porpoise *Phocoena phocoena*. Marine Ecology Progress Series 338: 281–294. https://doi.org/10.3354/meps338281.

Vishnyakova, K. O. 2017. The harbor porpoise (*Phocoena phocoena*) in the Sea of Azov and the north-eastern Black Sea: population morphology and demography. Dissertation submitted for the completion of the degree of Candidate of Sciences in Biology. Schmalhausen Institute of Zoology, National Academy of Sciences of Ukraine, Kiev.

Wenger, S. J., and J. D. Olden. 2012. Assessing transferability of ecological models: an underappreciated aspect of statistical validation. Methods in Ecology and Evolution 3(2): 260–267.

Wickham, H. 2016. ggplot2: Elegant Graphics for Data Analysis. Springer-Verlag, New York.

Wood, S. 2014. Mixed GAM Computation Vehicle with GCV/AIC/REML smoothness estimation (mgcv) package Version 1.8-4.

Wood, S. N. 2011. Fast stable restricted maximum likelihood and marginal likelihood estimation of semiparametric generalized linear models. Journal of the Royal Statistical Society: Series B (Statistical Methodology) 73(1): 3–36.

Zaitsev, Y., and V. Mamaev. 1997. Marine biological diversity in the Black Sea.

Zemsky, V. A. 1975. How many dolphins are in the Black Sea. Priroda 6: 113–114.

Zemsky, V. A. 1996. "History of the Russian fishery of dolphins in the Black Sea." In Proceedings of the First International Symposium on the Marine Mammals of the Black Sea, Istanbul, Turkiye, 27–30 June 1994, pp. 46–48. Istanbul: ACAR Matbaacilik AS.

Zemsky, V. A., and A. V. Yablokov. 1974. "Catch statistics, short history of exploitation and present status of *Delphinus delphis*, *Tursiops truncatus*, and *Phocoena phocoena* in the

Black Sea.” In FAO/ACMRR Group II Meeting, La Jolla, USA, 16–19 December 1974. FAO, Rome.